Cranfield UNIVERSITY

CENTRE FOR PHOTONICS & OPTICAL ENGINEERING

SCHOOL OF MECHANICAL ENGINEERING

PhD Thesis

1994

OMER SHAHAB KHAN

OPTICAL FREQUENCY SHIFTER USING STIMULATED BRILLOUIN SCATTERING IN FIBRE OPTIC RING RESONATORS

The thesis is submitted in partial fulfilment of the requirements for the Degree of Doctor of Philosophy

Supervisor Dr R P Tatam

February 1994

ORIGINAL COPY TIGHTLY BOUND

ABSTRACT

A fibre optic frequency shifter has been developed which generates a heterodyne frequency that is used to facilitate electronic demodulation of optical information. The operation of this device is analogous to an acousto-optic device such as a Bragg cell. This frequency shifter works on the principle of mixing two stimulated Brillouin scattering signals (generated in optical fibre ring resonators) which have slightly different frequencies. Dual ring resonator and single ring resonator topologies have been used. For the former system a conversion efficiency of 16% was obtained. The beat frequency was tunable between 218.4 MHz and 414.6 MHz for a 40°C change in temperature. A temperature coefficient of 5 ± 0.2 $MHzK^{-1}$ was measured. The later configuration provides a highly stable carrier frequency (11MHz) with a temperature coefficient of 6.7 ± 0.5 $kHzK^{-1}$. A 20% conversion efficiency was obtained. This demonstrates that this technique offers a practical, fibre efficient, low optical power requirement method for producing a frequency shifter. One of the main advantages of the system is that no electrical power is required to produce the travelling acoustic wave.

A novel technique to characterize the frequency response of optical detector-amplifier combinations, used in this project to detect these high frequencies, is also demonstrated. The technique is based on the wavelength modulation of a laser diode source in a path length imbalanced two-beam interferometer. A robust configuration using a low finesse Fabry-Perot interferometer made from birefringent optical fibre has been implemented. Measurements for several detector circuits are presented for the frequency range DC to about 30 MHz. Results are compared with direct modulation of the laser intensity and also with a circuit simulation programme (*PSpice*) and found to be in close agreement.

ACKNOWLEDGEMENTS

It is difficult to find proper words to thank my honourable parents, Mr. Aslam Khan and Mrs. Birjees Fatima. I am grateful to them for their massive support of me; assisting me out of the cradle and on the road to the PhD.

I am greatly indebted to Dr. Ralph Tatam for his expert supervision and advice throughout the course of this work.

Financial support of the Committee of Vice Chancellors & Principles of the United Kingdom (CVCP) and British Technology group (BTG) is gratefully acknowledged.

I also owe thanks to Helen, Sohail and John for useful discussions and friendship.

Finally, special thanks to my wife Asma (Jana) for her understanding, encouragement and support, not only during my study at Cranfield but in every aspect of my life.

Omer Shahab Khan

19 February 1994

Cranfield.

Dedicated to

Asma

CONTENTS

LIST OF FIGURES

NOTATIONS

a	core radius
A	gain of the amplifier
A_{eff}	effective core area
B	modal birefringence
c	velocity of light in vacuum
d	inter-mirror spacing
E_i	electric field at the ith port
F	finesse of the ring resonator
$G_B(\upsilon_B)$	Brillouin gain coefficient
h	polarization maintaining parameter
h_o	separation between fibre cores in a directional coupler
I_o	laser intensity
I_{input}	power coupled into the fibre
I_{ring}	power circulating in the ring
K	coupling constant
K_A	wave vector of the acoustic wave
K_S	wave vector of the Stokes wave
Kr	coupling constant at resonance
L	fibre length
L_B	beat length
L_{coh}	coherence length
L_i	effective interaction length
L_{eff}	effective length
m	fringe order
n	effective refractive index
N	number of modes

P_{12}	elasto-optic coefficient
P_c	cross-coupled power
P_i	optical power at the *ith* port
$P_{straight}$	threshold power for straight length of the fibre
P_{onset}	threshold power for the onset of SBS
P_t	transmitted power
$P(t)$	polarization of a material system
r_c	splitting ratio or coupling ratio
T	phonon lifetime
R	fibre bend radius
V	visibility
V_a	acoustic velocity
α_o	attenuation coefficient
α_{dB}	fibre attenuation
β	propagation constant
τ_c	cavity decay time
γ_o	intensity loss coefficient
γ_{rt}	fractional intensity loss per round trip
Δf	full width at half maximum of a resonance notch
ΔL	increase in fibre length
Δn	change in refractive index
κ	wavenumber of the perturbation
λ_p	wavelength of the input (pump) light in vacuum
υ_{SBS}	SBS frequency shift
$\Delta\upsilon_B$	beat frequency
$\Delta\upsilon_l$	spectral width of laser diode
$\Delta\upsilon_r$	full width at half maximum point of the resonance notch
ρ_o	material density
ρ_1, ρ_2	radii of the two core fibre
ϕ	phase retardation
$\Delta\phi$	phase shift

χ	susceptibility
Ω_l	spectral density of laser diode
ω	optical frequency
ω_o	$1/e^2$ intensity radius
ϖ	angular frequency of the acoustic wave
Υ	wavelength of the applied perturbation

CHAPTER ONE

INTRODUCTION

Optical fibre technology holds many exciting new possibilities for communications and sensing systems particularly because of their high processing speed and a bandwidth or information capacity thousands of times greater than that of copper circuits. By the year 2000, as much as 10^{10} kilometres of fibre could be installed worldwide [1]. A recent trend towards the use of single mode fibres in all areas of the instrumentation and communications has heightened interest in all fibre devices.

The light guiding properties of optical fibres can be fully exploited by the development of in-line fibre devices, which could obviate the requirement to remove the light from the fibre for processing purposes. There has been a reasonable success in designing and implementing various in-line fibre devices such as directional couplers [2] and fibre amplifiers [3]. They offer high efficiency and good performance over a limited wavelength and frequency range. However, there is still considerable research interest in a wide range of in-fibre devices including fibre ***frequency shifters*** which are at present commercially unavailable.

A frequency shifter is a device that produces a heterodyne carrier at a frequency suitable for electronic signal processing techniques. An optical frequency shifter, in fibre form, is a highly desirable component and is of great importance in interferometric fibre sensors and communications.

In order to understand the function of a frequency shifter and to realise its importance, consider a basic optical sensor configuration, shown in figure 1.1. In this arrangement optical processing transduces phase change, $\Delta\Phi$, to a detectable intensity change, ΔI. Light from a laser is coupled to an input fibre that transfers the beam to the optical system where a measurand, e.g. temperature, strain etc., modulates one or more of the properties of the optical beam. This modulated signal is then transferred to a suitable optical detector for signal processing. The purpose of the signal processing in fibre optic sensors is to transform the optical output of the sensor into an electrical signal as a true representation of the measurand signal.

In practice the modulated carrier, generated by the optical system is too high, i.e. ~10^{14} to 10^{15} Hz for any currently available detector. For over fifteen years a variety of optical processing techniques have therefore been developed generally by mixing optical signals of the same or very slightly different frequency on a photodetector to produce a relatively low frequency optical carrier, but without commercial realization of a device. As a result conventional acousto-optic components (Bragg cells) are used for this purpose. An obvious limitation with this technique is the very high optomechanical alignment stability required to maintain stable low loss coupling of light through the Bragg cell into single mode fibre with core diameters in the range 3-10 μm. This approach is therefore usually limited to relatively complex, high cost sensors.

As a consequence there has been a variety of techniques investigated to produce an all-fibre frequency shifter (reviewed in chapter 3). All these optical

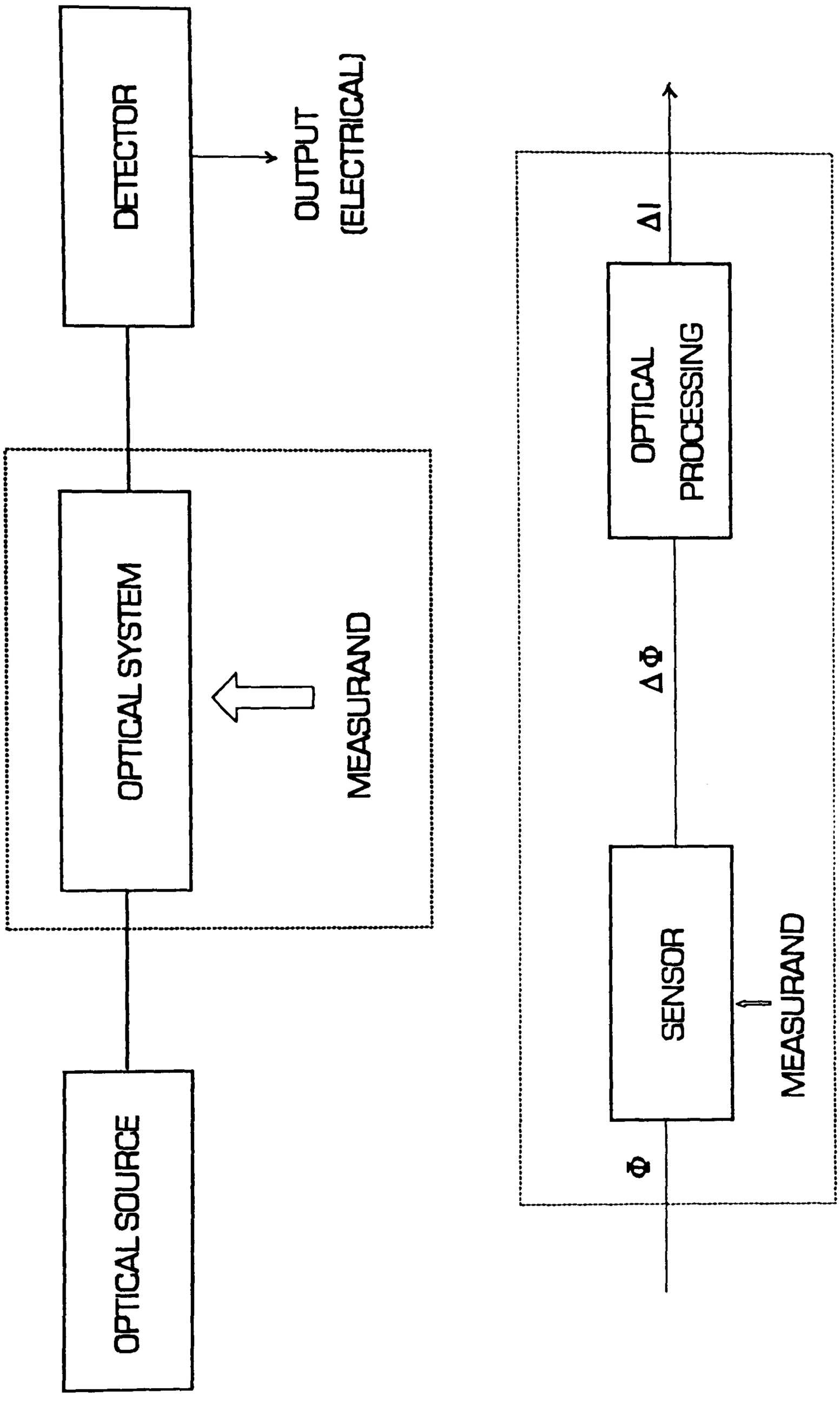

Figure 1.1 Basic elements of an optical sensor system

techniques utilise a similar principle, that is, the periodic coupling of optical power from one eigenmode in an optical fibre to an orthogonal mode using a travelling acoustic wave to produce the frequency shift in an analogous manner to the travelling acoustic wave in a Bragg cell generating a moving diffraction grating.

All of these techniques suffer from the difficulty of efficiently coupling an external generated acoustic wave to the optical fibre. In practice hundreds of milliwatts to several Watts of electrical power are required to generate acoustic waves.

This dissertation demonstrates a new technique to produce a frequency shifter based on mixing the stimulated Brillouin scattering (SBS) light generated from optical fibre ring resonators. The first configuration mixes the SBS generated from two separate resonators to produce a carrier in the 200-400 MHz region. The second technique mixes the two SBS signals produced from the orthogonal polarization eigenmodes of a ring resonator constructed from highly birefringent fibre that gives an optical carrier at ~11 MHz.

Stimulated Brillouin scattering is a non-linear process and can be described classically as the optical input beam (the pump) generating an acoustic phonon (sound wave) and a backscattered frequency downshifted optical beam (Stokes wave). The process can be considered as the optical beam creating a travelling acoustic wave, via the process of electrostriction, and subsequently scattering the pump light. Unlike all previous techniques no external modulator is required and therefore a more robust frequency shifter is, in principle, possible.

A ***fibre optic ring resonator*** is a unidirectional multiple beam interferometer formed by placing two polished fibre sections from the same piece of fibre in

intimate contact. When the total phase delay around the loop is an integral multiple of 2π radians constructive interference takes place within the loop. At resonance there is zero transmitted power and all the optical power circulates in the ring consequently generating high optical intensity within a length of fibre. The output is then a series of resonance dips, and the behaviour is similar to that of a Fabry-Perot etalon except the fibre resonator has sharp output minima (not maxima) reaching zero at resonance similar to the back reflected output from a Fabry-Perot.

In order to observe the response of the frequency shifter without any ambiguity, the detectors/amplifiers, developed to detect high frequency signals in this research programme, are characterized. Previously available techniques [4] used a Michelson interferometer configuration constructed using conventional bulk optic components that place severe restrictions on the optomechanical stability and therefore the optical path imbalance that can be stably achieved. We have demonstrated a new technique that is simpler to implement, is more optomechanically robust and offers the potential for greater flexibility in the frequency range that can be covered. The technique uses wavelength modulation of a laser diode source via modulation of the injection current in a two-beam interferometer configuration. Results are compared with two other methods i.e. direct modulation of the laser output intensity and from a circuit simulation using a computer package.

Chapter 2 gives an introduction to different types of fibre components, optical sources, and detectors used in this project. The principle of operation and a comparison between different types, their advantages and limitations are discussed. Some of the important terms that will be helpful to describe the basic concepts of the system, in the following chapters, are explained.

A review of the fibre optic frequency shifters, basic classification, principle of

operation and their shortcomings are discussed in chapter 3.

Chapter 4 is divided into two parts. The first describes the construction and theory of operation of optical fibre ring resonators. An expression for the transfer function of the resonator is derived. The second part of the chapter deals with nonlinear effects in the fibre with particular emphasis on stimulated Brillouin scattering in ring resonators. Continued improvements in the quality of optical fibre components have led to the availability of optical fibre ring resonators with higher finesse, bringing the onset of stimulated Brillouin scattering to even lower input power thresholds.

Experimental details to characterize the optical detector-amplifier combinations, as mentioned earlier, are explained in chapter 5. A low finesse Fabry-Perot interferometer constructed from high birefringence fibre is used to measure the detector-amplifier response. The results from this method are compared with measurements obtained by direct modulation of the laser and from an electronic circuit simulation programme.

In chapter 6 a fibre optic frequency shifter based on stimulated Brillouin scattering in optical fibre ring resonators is presented using a single frequency Helium Neon pump source. A carrier frequency is generated using two different configurations. The first is a *dual resonator* system and the other is based on a *single resonator.* A frequency shifter based on a laser diode pump source is also described in this chapter. In this connection dependence of threshold power, to generate SBS, on laser linewidth is discussed.

Finally chapter 7 reviews the main results of this research work, draws general conclusions and suggests possible future directions for performance improvements of the frequency shifter.

CHAPTER TWO

SYSTEM COMPONENTS

2.1 INTRODUCTION

The intention of this chapter is to provide a description of the different types of fibre optic components, optical sources, and detectors used in this project. Principle of operation and a comparison between different types, their advantages and limitations are presented. Some key terms are explained which will be used later in the thesis.

2.2 OPTICAL SOURCES

The generation of stimulated Brillouin scattering is highly dependent upon the pump (i.e. light source) linewidth. The Brillouin gain is substantially reduced if the source spectral width exceeds the Brillouin linewidth. It will be explained in Chapter 4 that the Brillouin scattering depends on the relative magnitudes of the pump coherence length and the SBS interaction length. Therefore, narrow linewidth and long coherence length are among the most important

requirements for this project. Two types of lasers, i.e. Helium Neon and semiconductor diode lasers were used.

2.2.1 HELIUM NEON LASER

The Helium Neon (He-Ne) laser is a gas-filled tube (a mixture of Helium and Neon), with internal electrodes exciting the gas to emit light. Mirrors on each end of the tube define the cavity. Structural and operational details can be found in several text books [5].

The frequency stability of single-frequency lasers is of the order of $\pm$1 MHz during a minute interval when operated at constant temperature. However, temperature induced variations in the cavity length can cause the fundamental frequency to vary by around 5 MHz/C° change in ambient temperature, so temperature stability is required for stable frequency output. For the laser used in this project, warm up times of half an hour to an hour are needed to obtain a stable single frequency output.

Table 2.1 shows the specifications of the He-Ne laser used in this project. A single frequency He-Ne laser has a well-defined Gaussian beam of circular cross section that allows more than 50% of the light to be coupled easily into a single mode fibre. The frequency stability of He-Ne laser provides a long coherence length of more than 1000 metres.

Wavelength	632.8 nm
Coherence Length	> 1000 m
Output power	2.2 mW *
Frequency stability	$\leq \pm$ 1 MHz/5 min interval
	< 5 MHz/°,C change in ambient temp.

Table 2.1 Specifications of single frequency HeNe laser, *Coherent 200*.
* Without output polarizer.

Wavelength	827 nm
Output Power	100 mW
Linewidth	4 -12 MHz *
Temperature Sesitivity	0.067 nm/°C
Beam Divergrence ($\theta_{\perp}$, $\theta_{\parallel}$)	30, 10 (deg)

Table 2.2 Specifications of Spectra Physics SDL-5410 laser diode.
*Linewidth is affected by temperature stability and current noise. Current source and the laser were not under any form of temperature control [6] [SDL data sheet].

2.2.2 LASER DIODE

Although the single frequency He-Ne laser provides a very stable output with long coherence length making it an ideal choice as a light source for the *frequency shifter*, laser diodes will provide more versatile rugged pump sources in the long term. Characteristics of a 100 mW Spectra Physics laser diode are shown in table 2.2. One of the important advantages of the laser diode over other optical sources is that their amplitude and frequency can be modulated very easily and rapidly by changing the injection current.

The basic physics of diode lasers is presented in many references [7-8] and will not be repeated here. However, it is important to highlight the features that are relevant to much of the later discussion. The construction of a typical semiconductor diode laser is shown in figure 2.1. A layer of undopped semiconductor material, called the active layer, is sandwiched between two layers of *n*-doped and *p*-doped materials. In this way a waveguiding structure is formed, with optical power confined within the active layer. The laser light is generated by sending a current, called the injection current through the active region of the diode between *n*- and *p*-type cladding layers. This produces electrons and holes, which in turn combine and emit photons. Cleaved facets of the semiconductor serve as the laser's mirror. The output power of a typical semiconductor laser as a function of the injection current and temperature is shown in figure 2.2 [9]. This shows the abrupt onset of laser action at the threshold current and the increase in the threshold with temperature. Alternatively, for a fixed injection current, the laser's output increases rapidly as the temperature is lowered. The lasers used in the experimental work are in the near infrared region (750-890 nm) and are based on AlGaAs (Aluminum Gallium Arsenide). Because the light is emitted from a small rectangular region (on the order of 0.1μm by 0.3μm) the output of a

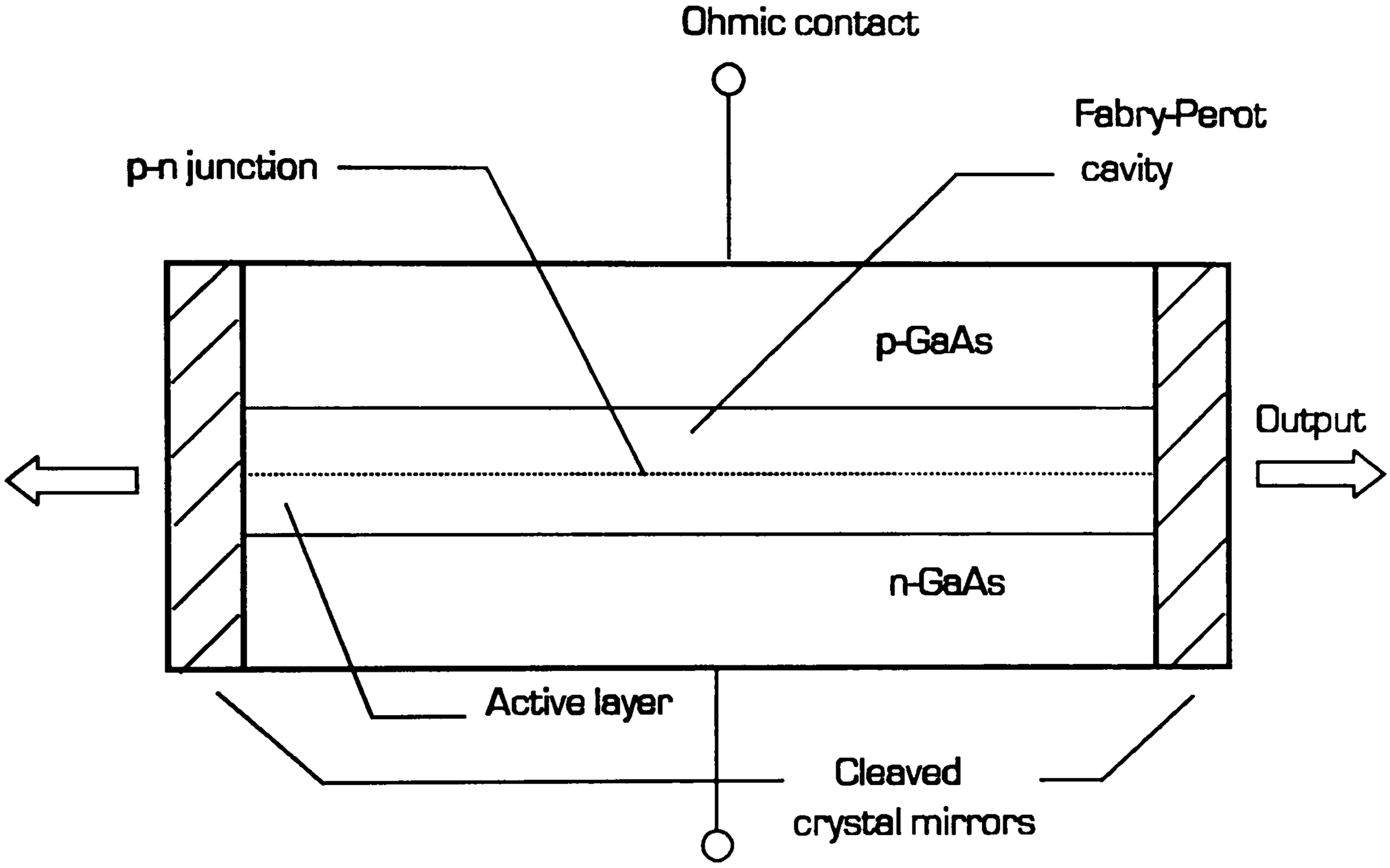

Fig. 2.1 Schematic diagram of a GaAs homojunction injection laser

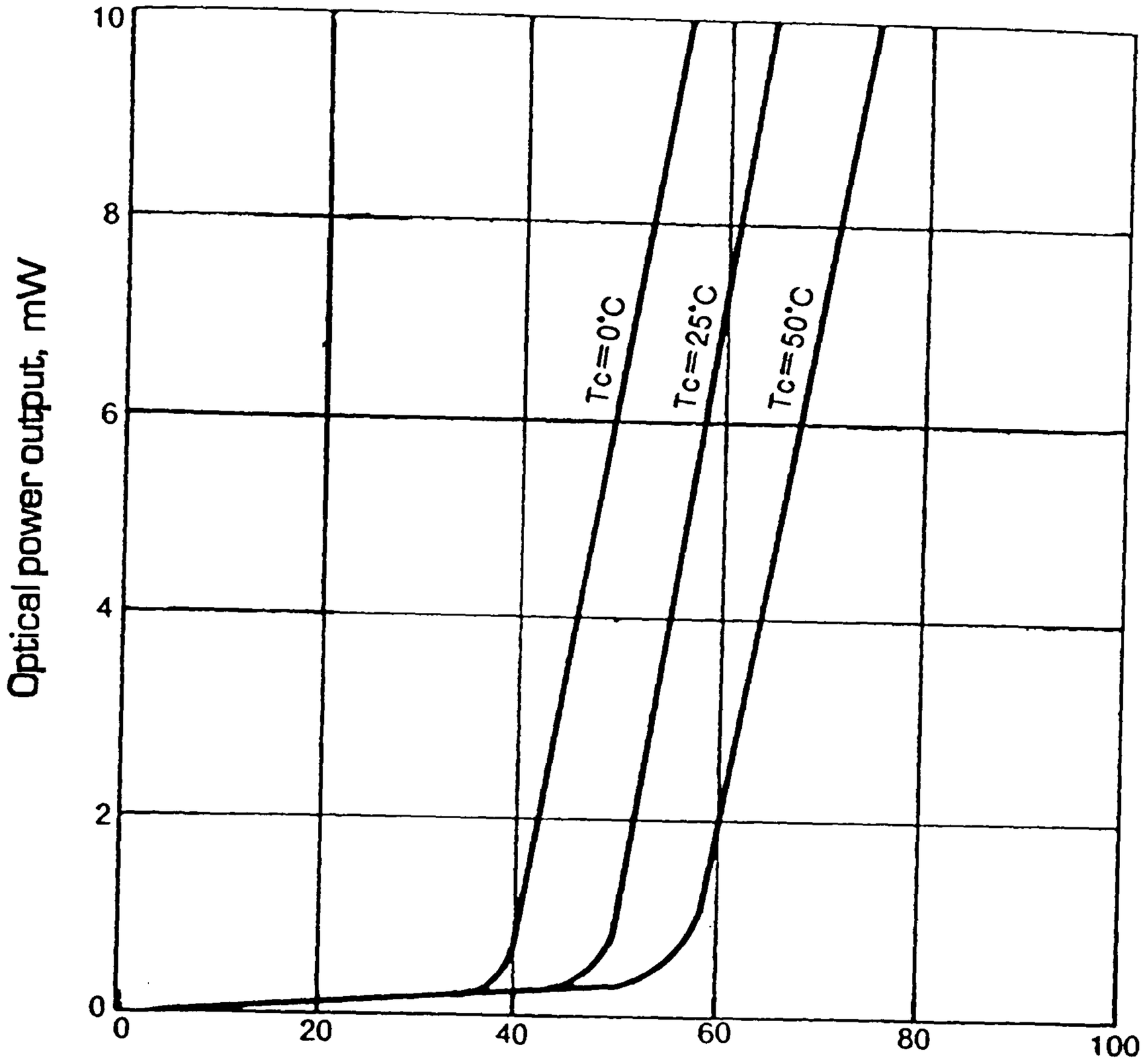

Fig. 2.2 Optical power output of a typical laser diode as a function of the injection current and temperature

diode laser has a large divergence. A typical output beam will have a divergence angle (full width at 50% intensity) of 30° in the direction perpendicular to the junction, and 10° in the parallel direction. To launch the beam into a small core single mode fibre the beam is collimated and focused using a lens.

The sensitivity to optical feedback is one of the important features of diode lasers, to be taken into account, relative to most other lasers. When light is returned to the laser it acts as a photodetector, generating more carriers in the junction and affecting the net laser gain [10].

These effects can be both beneficial and a disadvantage. Let us first consider the disadvantage. External feedback effects, caused primarily by reflections at the fibre air interface on launching and by secondary effects from other optical elements in the system, cause unstable operation of the diode output and in general result in a broadening in the laser linewidth. The broadening of the laser linewidth can be explained as follows. Consider the reflection of light from the fibre end. In this case there are now two different cavities formed. One is the laser internal cavity and the other is between the fibre endface and the far end of the laser cavity. In this situation more laser modes will be generated and the coherence might collapse. This causes two potential problems in our experimental work. Firstly, to maintain maximum stimulated Brillouin scattering (SBS) gain the pump linewidth needs to be less than the SBS linewidth. This can be seen by considering the peak value of the Brillouin gain, g_{peak}, which is described by [11]:

$$g_{peak} = \frac{\Delta \upsilon_B}{\Delta \upsilon_B + \Delta \upsilon_p} G_B(\nu_B) \qquad (2.1)$$

where $\Delta\upsilon_p$, $\Delta\upsilon_B$ are the pump and SBS linewidths, $G_B(\upsilon_B)$ is the Brillouin gain coefficient, and thus feedback induced broadening of the pump linewidth can

reduce the effective gain.

Secondly, to obtain optimum finesse from a ring resonator the number of coherently recombining beams must be at least equal to the finesse; recent modelling work indicates that the number of interfering beams must be approximately twice the finesse [12]. Thus for a 1m loop length and a finesse of 100 the coherence length needs to be ~200m. It will be explained in chapter 6 that the effective finesse of the fibre ring resonator depends strongly on the laser spectral linewidth.

2.2.3 AVOIDING OPTICAL FEEDBACK

Fibre input face was cleaved at an angle to reduce the feedback to some extent. For effective and reliable isolation a Faraday isolator was used. It comprises a magneto-optic rod placed in a strong axial magnetic field between two polarizers. Light, linearly polarized by the input polarizer, undergoes a 45° rotation of the polarization azimuth as it passes through the rod. The output polarizer is set for maximum transmission. The light, which is reflected back from the optical components/fibre end, undergoes an additional 45° azimuth rotation and is therefore not transmitted by the input polarizer. Unfortunately these isolators usually cost several times as much as the laser itself.

2.2.4 TECHNIQUES TO NARROW THE LASER LINEWIDTH

Reduction in laser linewidth can be achieved by suppression of all except one of the modes, so that the power in the remaining modes exceeds that in all other modes by a large factor. To achieve this, the gain of the dominant mode must be greatly enhanced with respect to the gain of the other modes. In practice, the laser linewidth dependence on the external feedback can be used to achieve this goal. The essence of the optical feedback methods is the simple idea that by increasing the quality factor (Q) of the laser's resonator, the linewidth will be reduced.

SIMPLE FEEDBACK

The simplest implementation of the optical method for spectral narrowing is just to reflect back to the laser a small fraction of its output power. Some limited success has been achieved in this way by using simple optical elements. Among the optical elements that have been used for feedback are mirrors [13], etalons [14], fibre cavities [15]. The resulting systems must be described as lasers with complex resonators where the diode's facets and the external optical elements all play a role in creating the net resonator structure as seen by the semiconductor gain medium. By providing optical feedback from a small mirror or glass plate placed close to one of the lasers facets, a multimode laser can be forced to oscillate on a single mode. It is quite difficult to achieve long term stable performance with such systems.

EXTERNAL CAVITY LASERS

The method of the *external cavity laser* uses antireflection (AR) coatings on the diode laser chips, and some external optics to provide the laser resonator. The external optics may contain frequency selective elements such as a grating [16,17]. In one of the laser diodes used in the experimental work, a

grating is used to narrow the linewidth of the laser. Its operation will be discussed in more detail in chapter 6.

2.2.5 LASER DIODE MODULATION

One of the unique aspect of semiconductor diode lasers is the ease with which their output optical frequency and amplitude can be modulated. The amount of modulation can be both large and very fast. For common diode lasers the modulation response extends out to a few gigahertz. A few special lasers are capable of modulation rates of more than 10 GHz. The modulation properties of laser diodes are fully exploited in this project for the characterization of optical detectors as we will see in Chapter 5.

These modulation capabilities arise from the fact that the output wavelength of semiconductor laser diodes depends on both temperature and injection current.The temperature dependence arises because both the refractive index of the cavity and the energy gap are temperature dependent. Typically the wavelength of each laser mode shifts by ~0.06 nm K^{-1} .

A change in the injection current causes a wavelength shift due to the dependence of the laser temperature on injection current; the magnitude of this is typically 0.04 $K(mA)^{-1}$. However, the injection current also controls the charge carrier concentration and consequently affects the refractive index of the cavity. This effect may be utilized to modulate the laser output frequency via the injection current. The two effects outlined above are dominant for different regimes; at low frequencies the thermal effect dominates whilst at high frequency the variation in charge carrier concentration dominates.

2.2.6 LASER DIODE WAVELENGTH TUNING

The band gap of the semiconductor material, the junction's temperature and current density determine the laser diode's wavelength [18]. The band gap is not under the control of the laser user. The dependency of the optical path length of the cavity on temperature can be exploited to tune the laser frequency. Commercial diode lasers are typically rated to operate in a range of $\pm$30K about room temperature. This provides a tuning range of about 21nm for AlGaAs lasers. The elevated temperatures generally cause noticeable degradation in the laser's lifetime. For example, the data sheets indicate that a typical lifetime of about 10^5 h is reduced by a factor of 5 when the temperature is increased by 10K [10]. Other performance characteristics may also be degraded at higher temperatures. Lasers can actually be cooled far more than 30K; the lower temperatures bring some additional complications such as the need to protect the laser from water condensation and mechanical stresses due to large temperature changes.

2.3 OPTICAL FIBRE

The optical fibre wave guide is a two component coaxial transparent medium. The central core which guides the light has a larger refractive index than that of the outer cladding. D. Gloge [19] analyzed cylindrical symmetric optical fibre waveguides and showed that in general there is not a single optical path for the injected light to follow as it propagates through the fibre, but a large number of paths, called modes which have different propagation constants. This constant β for any guided mode in the fibre is defined by:

$$\beta = 2\frac{\pi n}{\lambda} \tag{2.2}$$

where n is the effective refractive index of the medium and λ is the free space wavelength of the light propagating through the waveguide. The number of modes in the fibre is given by

$$N = \frac{4V^2}{\pi} \tag{2.3}$$

where

$$V = \left(\frac{2\pi a}{\lambda}\right)(n_1^2 - n_2^2)^{1/2} \tag{2.4}$$

is the normalized frequency of the fibre, n_1 and n_2 are the refractive indices of core and cladding respectively and a is the core radius. When V<2.405 only the lowest order spatial mode i.e, the LP_{01} mode, can propagate. The LP_{01} mode comprises two orthogonal linearly polarized modes with propagation constants β_x and β_y . Ideally fibre is assumed to be perfectly circular with a circularly symmetric refractive index distribution and hence there is a perfect degeneracy of the two LP_{01} modes i,e., the x-polarized and y-polarized LP_{01} modes have the same propagation constant. However, actual fibres generally exhibit some elipticity of the core and/or some anisotropy in the refractive index distribution due to asymmetric stresses. This results in two different propagation constants for the two orthogonal modes. Thus the fibre behaves as a birefringent medium due to the difference in the effective refractive indices, and hence phase velocities , for these two orthogonally polarized modes.

Single mode optical fibres do not generally maintain the polarization state of the light input for more than few meters. Their polarization properties are also easily modified by environmental factors such as pressure, twists and bends

which in practical installation vary in an unpredictable manner. These factors will cause random coupling between the orthogonal modes of the single mode fibre. The overall fibre birefringence, and thus the output polarization state can not be predetermined and, moreover, will vary with time and temperature. While this can be exploited in a number of fibre sensor devices, it can be troublesome in applications where a stable output polarization state is required. Fibres with both low and high birefringence have been developed to enhance or diminish their environmental sensitivity.

2.3.1 HIGH & LOW BIREFRINGENT FIBRES

Polarization maintaining fibres permit light to pass through whilst retaining its state of polarization. Polarization maintaining fibres can be classified into two major groups, namely, highly birefringent and low birefringent fibres. The birefringence of a conventional single mode fibre is in the range $B = 10^{-6}$ to 10^{-5} [20]. A hi-bi fibre requires $B>10^{-5}$.

Highly birefringent fibres offer the attractive feature of preserving a specific polarization state of light over significant distances. These fibres exhibit a strong intrinsic birefringence which creates two well defined orthogonal polarization modes having significantly different propagation constants. Such strong mismatched modes remain relatively uncoupled through out the waveguide; an input state of polarization identical to one of the polarization modes is therefore preserved along the fibre.

To maintain a stable state of linear polarization in the fibre, it is necessary to reduce the amount of coupling between the two mode components by introducing strong linear birefringence into the fibre. One method of doing this

is to make the core noncircular in shape so that the refractive index distributions in the two principal directions are different. Earlier fibres used highly elliptical cores [21]. The stress in the fibre of the second category is created by an elliptical cladding [22], elliptical jacket [23] or stress inducing members which are embedded close to the core. Such stress-inducing members can have the form of asymmetric refractive index pits [24], rods as in Panda fibres [25-28] or bows as in Bow-Tie fibres [29]. Cross sections of different types of birefringent fibres are shown in figure 2.3. There is a slight temperature dependence of the birefringence, as the applied stress will vary with temperature. The polarization maintaining fibres used in this project are stress induced birefringent of the PANDA type manufactured by Fujikura.

2.3.2 BEAT LENGTH & CROSS TALK

In all highly birefringent fibres, light polarized along one of the principal axes will retain its polarization for all length of the fibre, say z. Light polarized at an angle θ with respect to one of the fibre axis, say the x-axis will pass through various states of elliptical polarization as the phase retardation

$$\phi(x) = (\beta_x - \beta_y)z \qquad (2.5)$$

varies with length, provided the two normal components maintain their phase coherence.The degree of birefringence can easily be assessed by observing the light scattered sideways from the fibre when the input (from a He-Ne laser for example) is linearly polarized at an angle of 45° to the principal transverse axis. Because of their different phase constants the two propagating polarization modes run into and out of phase at a rate determined by the birefringence, thus producing a periodic variation in the transmitted polarization state from linear to circular and back again. For incident linear polarization

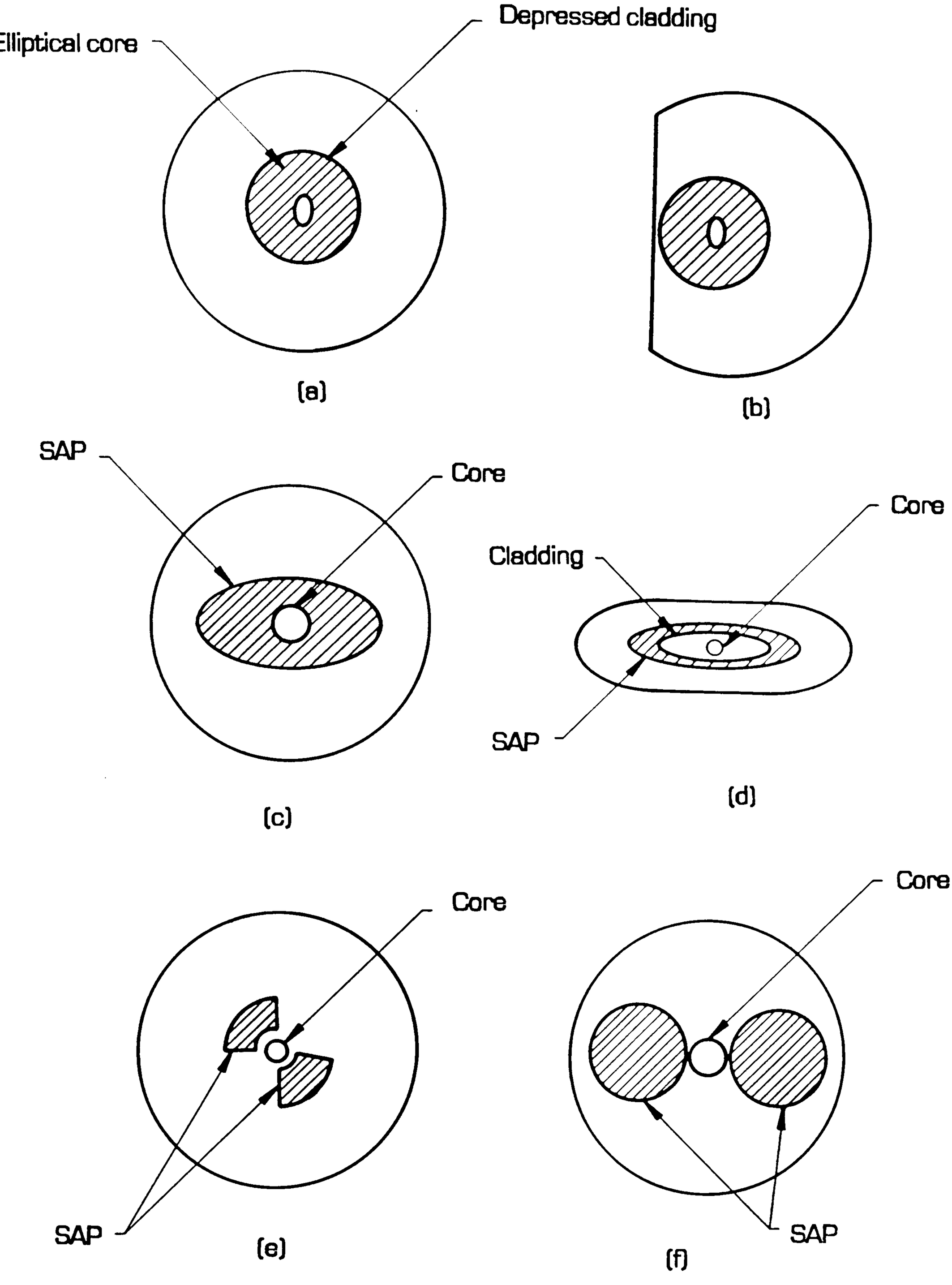

Fig. 2.3 Polarization maintaining fibre structure; (a) elliptical core; (b) D-Shaped elliptical core; (c) elliptical stressed cladding; (d) rectangular stressed cladding; (e) bow-tie; (f) circular stressed. SAP: Stress applying parts.

with $\theta = 45°$ at z =0, the polarization becomes circular for $\Phi = \pi/2$, linear with $\theta = -45°$ for $\Phi = \pi$, circular for $\Phi = 3\pi/2$, and linear with $\theta = 45°$ for 2π as shown in figure 2.4(a). The length L_B is called the *beat length*. The beat length was observed directly by means of dipole (Rayleigh) scattering from the fibre. A fibre, illuminated with a He-Ne laser, viewed along the direction of the incident polarization exhibits a series of dark and bright bands with period L_B. In this case the length, along the fibre, at which a random state of polarization is repeated is called *beat length* of the fibre, as shown in figure 2.4(b). The radially scattered intensity, which depends on the polarization of the transmitted light, therefore fluctuates with the same periodicity.

The beat length L_B measured in this way is given by:

$$L_B = \frac{2\pi}{\beta_x - \beta_y} = \frac{\lambda}{B} \qquad (2.6)$$

where B is the modal birefringence which is related to the refractive indices by the formula:

$$B = n_x - n_y = \frac{\lambda}{2\pi}(\beta_x - \beta_y) \qquad (2.7)$$

A large modal birefringence, B, or equivalently a small beat length is required in Hi-Bi fibres. It is well known from standard coupled-mode theory [30] that maximum power transfer between modes occurs when the period of external perturbations matches that of the beat length. The natural stiffness of the fibre prevents external perturbations with very short periods (less than 1mm) and thus submillimeter beat lengths are desirable for high performance operations. Indeed, this requirement is met in today's state of the art stress-induced hi-bi fibres. Such fibres can exhibit crosstalk levels of the order of -40 dB/Km or less [31], if care is taken to avoid strong perturbations. The beat length and the modal birefringence are the two parameters among the three important

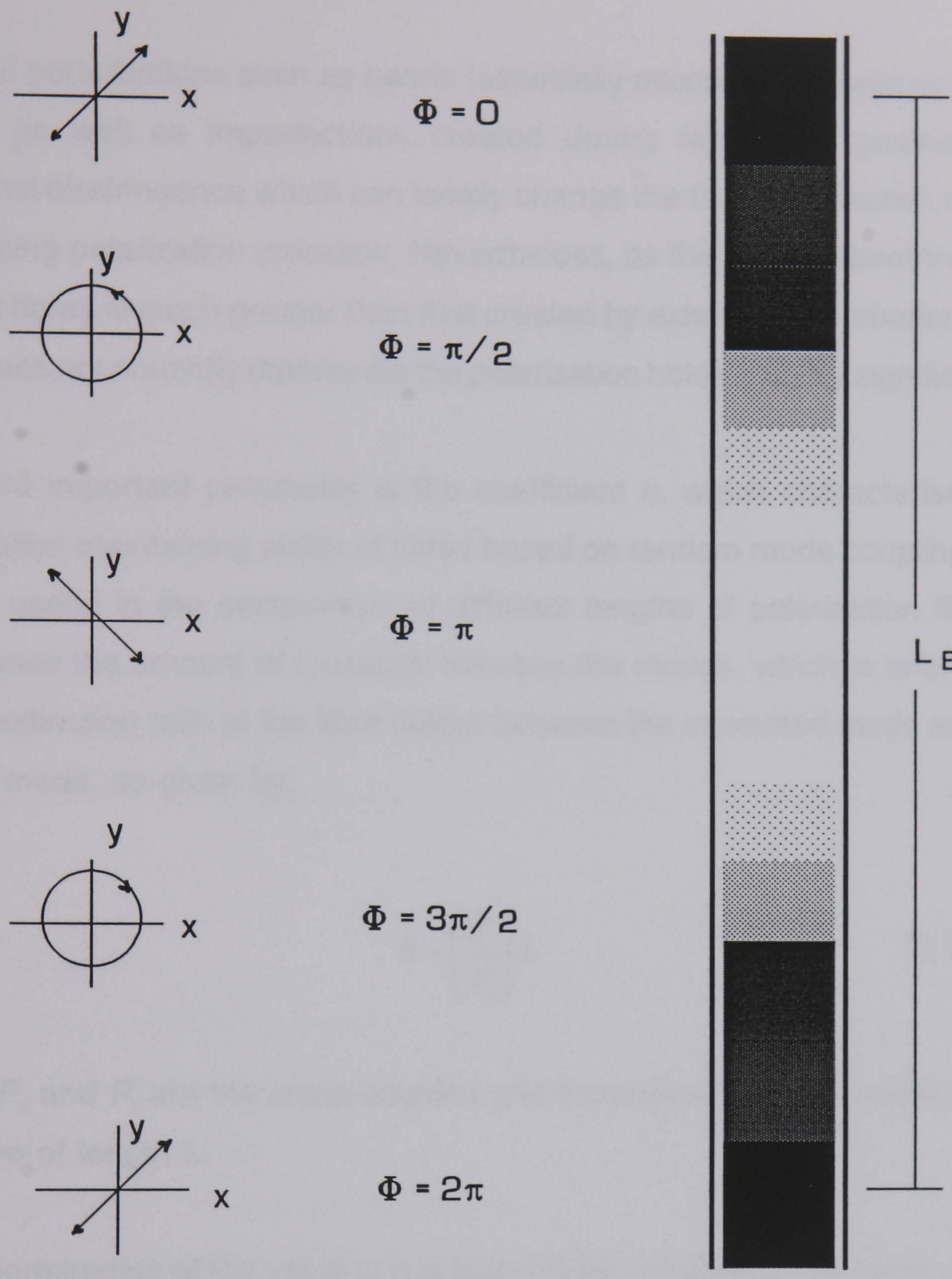

(a) (b)

Fig. 2.4 Beat length: (a) states of polarization versus Φ(z)
(b) scattered intensity observed normal to fibre at angle θ=45°

ones used to describe the polarization holding ability of hi-bi fibres.

External perturbations such as bends (especially microbends), twist or lateral stress, as well as imperfections created during fabrication generate an additional birefringence which can locally change the fibre polarization modes introducing polarization crosstalk. Nevertheless, as the intrinsic birefringence of Hi-Bi fibres is much greater than that created by external perturbations, the latter does not normally deteriorate the polarization holding ability significantly.

The third important parameter is the coefficient *h*, which characterises the polarization maintaining ability of fibres based on random mode coupling, and proves useful in the comparison of different lengths of polarization fibre. It determines the amount of crosstalk between the modes, which is referred to as the extinction ratio at the fibre output between the unwanted mode and the launch mode, as given by:

$$h = \left(\frac{P_c}{P_t}\right) L \qquad (2.8)$$

where P_c and P_t are the cross-coupled and transmitted powers respectively, in a fibre of length L.

The determination of the value of *h* is found to be sensitive to the quality of the fibre coating, external stresses and bends. For *PANDA* fibre its value is ~$1.6\times10^{-7}m^{-1}$, corresponding to an output extinction ratio of -38dB after 1km. Note, however, that this figure is dependent on the fibre configuration and packaging and will be worse when the fibre is wound in tight coils or sheathed in badly designed cables.

2.3.3 PANDA FIBRE

PANDA is an acronym for **p**olarization maintaining **and** **a**bsorption reducing fibre. The sectional structure of the fibre is shown in figure 2.5.

DESIGN

The core part, with diameter *2a*, consists of GeO_2 doped silica glass. The major parts of the cladding consist of pure silica glass. Hatched regions on both sides of the core indicate stress-applying parts. These parts consist of $B_2O_3GeO_2SiO_2$ glass. In order to reduce the transmission loss, the stress applying parts must be sufficiently separated from the core. On the other hand, it is necessary that the stress applying parts be as close to the core as possible to exert high birefringence. Anisotropic stress induced birefringence in the core is produced by the thermal-expansion difference between the fused silica cladding and the stress applying parts. The x and y-axis are defined in figure 2.5.

FABRICATION

PANDA fibre is fabricated using a technique called the pit-in-jacket method [32]. In this method a VAD (vapour axial deposition) [33] preform, which was jacketed into a silica tube with a 50 mm outer diameter, was used as the core-cladding preform. The core and cladding consisted of GeO_2-doped silica glass and pure silica glass, respectively. The germanium doping in the core of the fibre used in this project is of the order of 3 mol% [34]. Two approximately 10 mm diameter pits are then bored into this core-cladding preform with an ultrasonic machine. The MCVD (modified chemical vapour deposition) stress-applying preforms, are then inserted into the pits, producing the final preform. In order to avoid the scattering loss due to refractive index mismatch in the stress-applying parts, the B_2O_3 and GeO_2 concentration ratio is set to correct

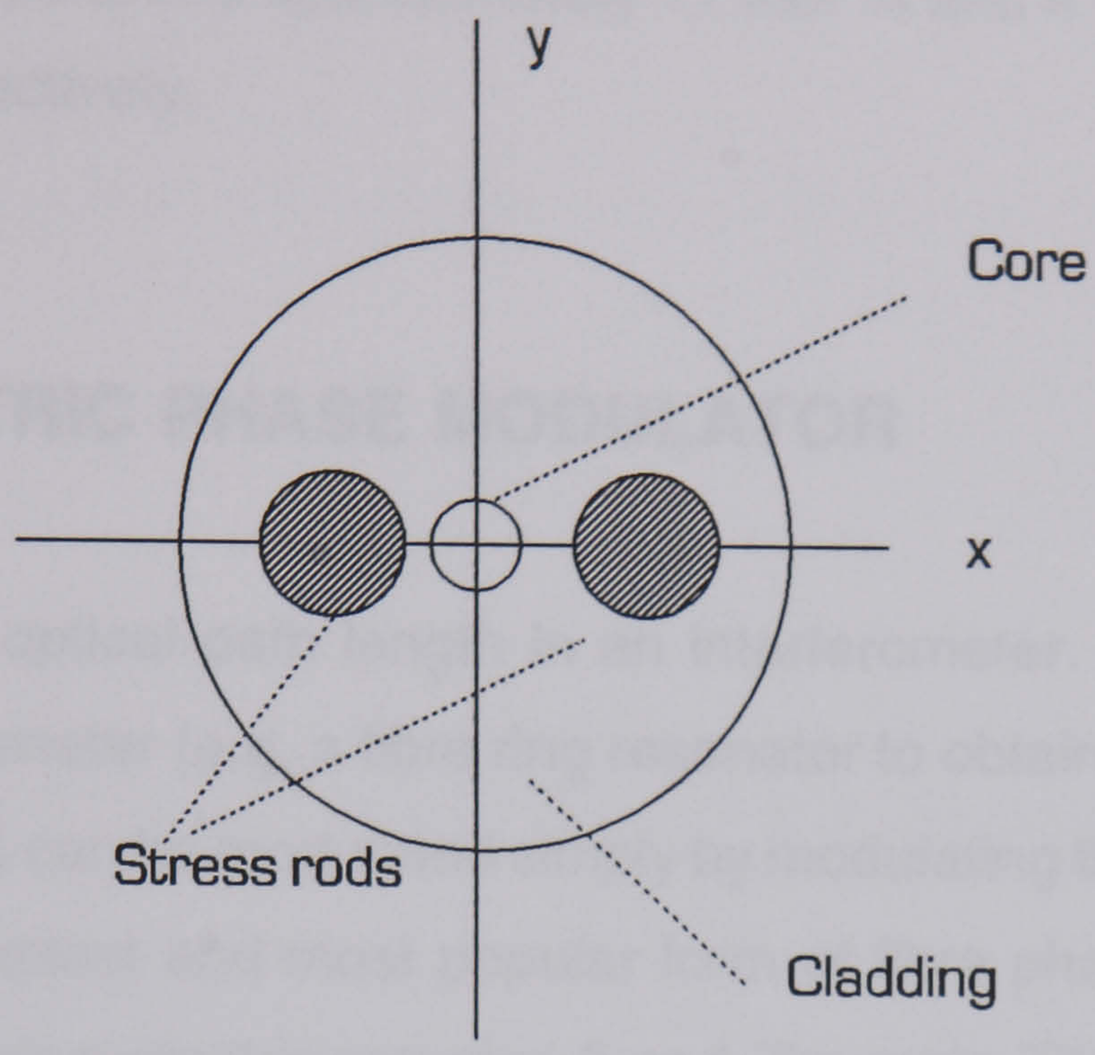

Fig. 2.5 Schematic diagram of cross section of PANDA fibre.

the refractive index of pure silica glass. The diameter of the cladding is set to be large to avoid the influence of ambient fluctuations. Dopant concentrations of the stress-applying parts are approximately 11 mol % and 4 mol % [27] for B_2O_3 and GeO_2, respectively.

2.4 PIEZOELECTRIC PHASE MODULATOR

It is used to vary the optical path length in an interferometer. The phase of light in a fibre interferometer (e.g. a fibre ring resonator to obtain and maintain a resonance condition) can be modulated simply by modulating the fibre length mechanically. The simplest and most popular form of fibre phase modulator for laboratory use is a piezoelectric actuator (Lead-Zirconate-Titanate, or PZT) with several turns of fibre wrapped around it under a small tension, as shown in figure 2.6.

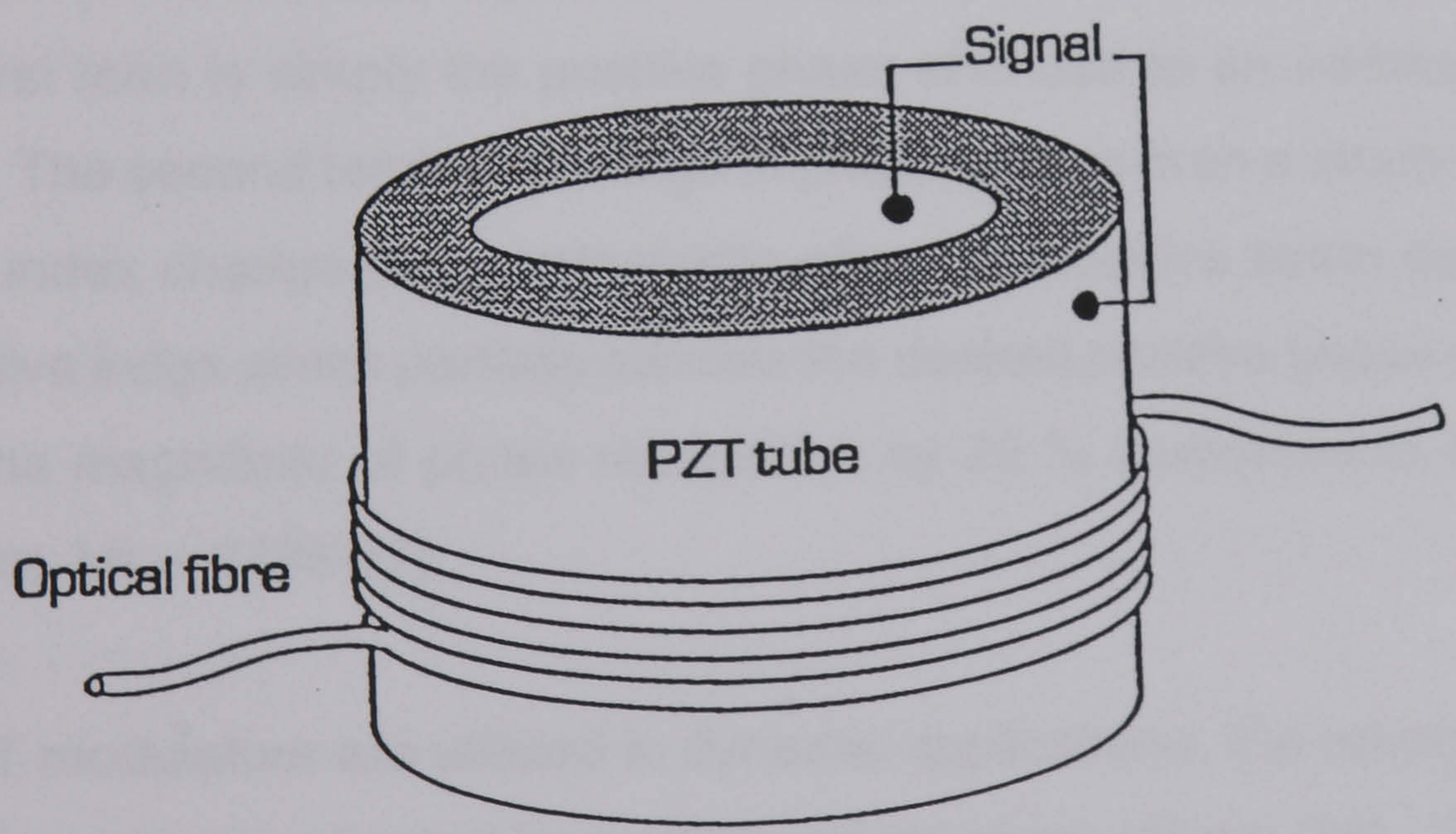

Fig. 2.6 Piezoelectric phase modulator.

When a voltage is applied across the wall of a PZT plate or cylinder its dimensions change owing to the strain induced in its wall thickness and height, resulting in a change in the fibre length.

If ΔL is the increase in actual fibre length L, the induced phase shift is given by [35]:

$$\Delta\phi = \frac{2\pi}{\lambda} n\Delta L \tag{2.9}$$

where λ is the free space optical wavelength and n is the refractive index.

If Δn is the change in refractive index, the induced phase shift of the light travelling in the fibre is given by:

$$\Delta\phi = \frac{2\pi}{\lambda}(n\Delta L + L\Delta n) \tag{2.10}$$

The two terms in the above equation have opposite effects on the phase shift $\Delta\phi$. The first term is simply the positive phase shift due to an additional path length ΔL. The second term is a change in phase arising from a strain-induced refractive index change (the photoelastic effect). A positive strain decreases the refractive index which partially cancels the desired positive phase shift and reduces the magnitude of phase modulation by 22 % compared to the ideal case where $\Delta n = 0$ [36-37].

When PZT modulators are utilized in dynamic applications, the response to a driving voltage is complicated by inertial and resonant effects [38]. Therefore for a given PZT, the frequency bandwidth is limited. Although these undesirable characteristics are not detrimental for most applications, care has to be taken for extremely sensitive phase measurements.

Despite such shortcomings and the relatively large size, this type of phase modulator is by far the most popular for low frequency laboratory and experimental field applications because of its structural simplicity and the large phase modulation that can be achieved by wrapping many turns of fibre around the PZT.

2.5 DIRECTIONAL COUPLER

A prerequisite for most fibre optic systems is the ability to transfer optical power between two optical fibres. A great effort has been made by different researchers using either multimode or monomode fibres to achieve this. Figure 2.7 represents the basic idea behind the operation of a directional coupler. This is a four port device which ideally splits the input signal (port 1) into two channels (the throughput port 3 and the coupled port 4).

2.5.1 OPERATION

The basic principle of operation of a fibre coupler is that under appropriate conditions light transfer can occur between adjacent fibre cores via a mechanism called evanescent wave coupling. As represented in figure 2.8 (location A), when two fibre cores are in close proximity the evanescent field of the signal travelling in the throughput fibre reaches into and excites the guided mode of the coupled fibre. When the modes of the two fibres exhibit the same phase velocity, resonant interaction takes place and total energy transfer occurs after some interaction length referred to as the coupling length (distance AB). If the interaction is allowed to continue beyond this point, the fibre roles are reversed and the signal is coupled back into the throughput fibre

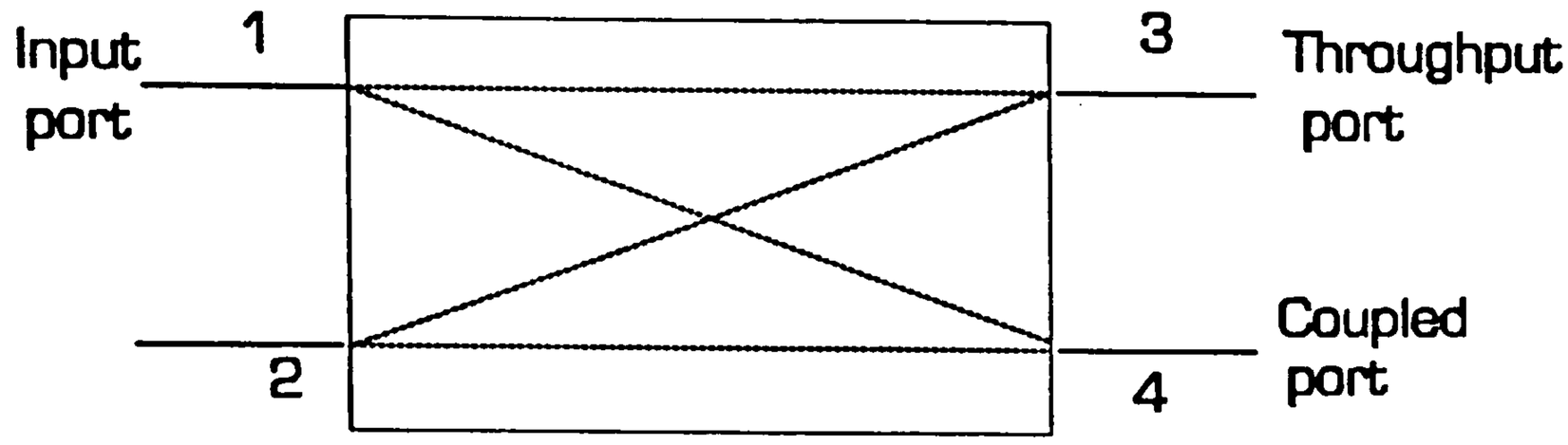

Fig. 2.7 Conceptual diagram of a directional couple

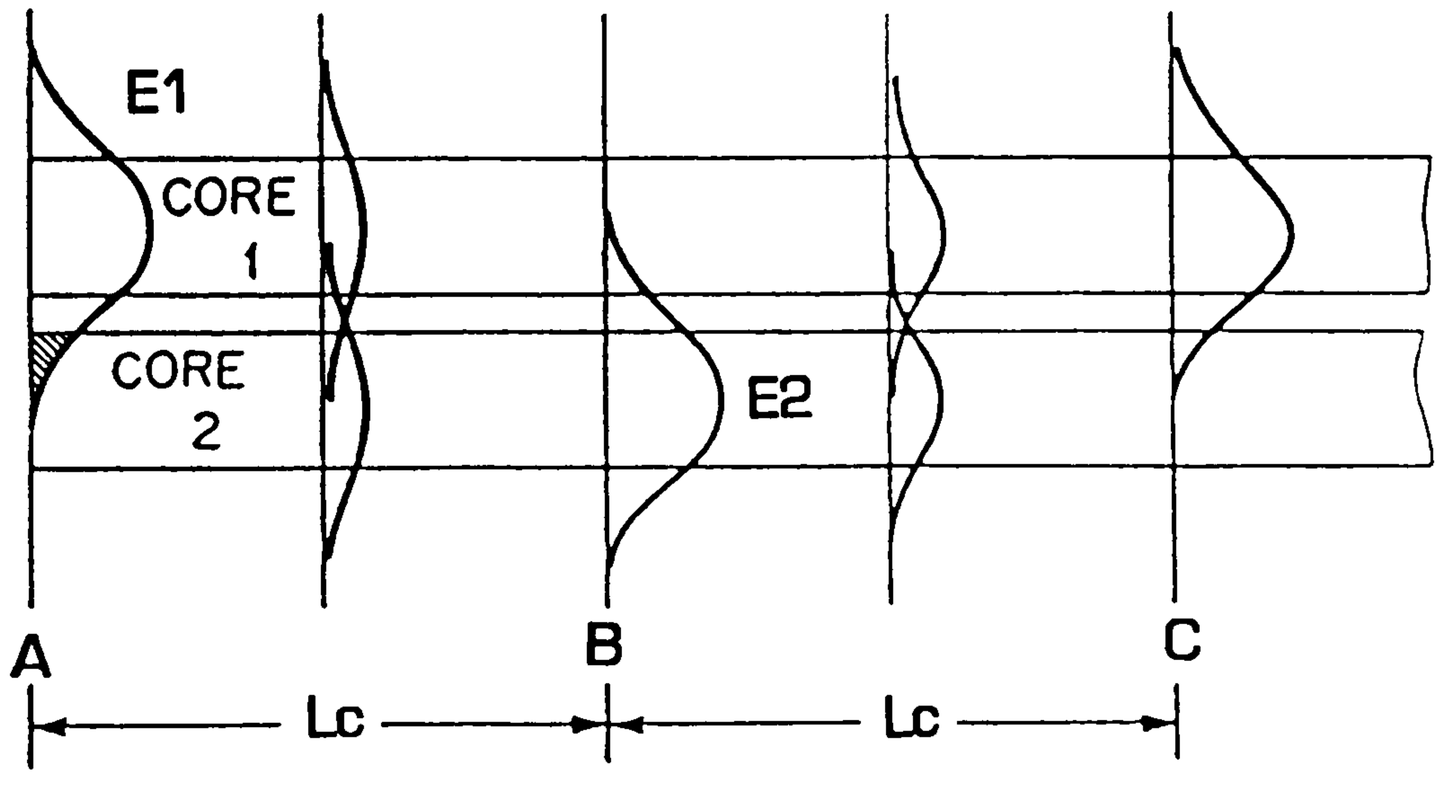

Fig. 2.8 Evolution of the energy distribution along two parallel coupled fibre cores according to the coupled mode concept.

until the entire signal resides in the throughput fibre after two coupling lengths (location C). This situation is generally referred to as "over coupling". If the length of the coupling region is sufficient, the process repeats itself in a cyclic manner along the length of the coupler.

2.5.2 FABRICATION

The optical signal travelling inside a single mode fibre is confined to a very narrow core region surrounded by a thick cladding. Light transfer from one fibre to another therefore requires a physical modification of this situation to bring the core regions within a short distance of each other, typically of the order of one signal wavelength. To this end three basic methods have been developed; etching, fusing and mechanical polishing techniques.

For this research work polished fibre couplers were used. These couplers rely on partial removal of the fibre cladding by controlled mechanical polishing along one side of the fibre. The fibres are first mounted individually in a fused silica substrate where they are bonded in a curved grove as shown in the figure 2.9. The substrate and fibre are then ground and polished until the desired cladding thickness remains at the apex of the fibre curve. Two such fibre substrates are then placed on top of each other with a layer of index matching oil between them to form a coupler. One of the merits of this scheme is that the relative lateral position of the mated fibres can be adjusted using a micrometer to control the coupling ratio. This tunability greatly reduces the fabrication tolerance on h_o as shown in figure 2.10.

Because the polishing method minimizes physical perturbation of the fibre, polished fibre couplers can exhibit very low backscattering in the second port

(-70 dB directivity)[39] and their insertion loss may be as low as 0.005 dB [40].

The suitability of a coupler type to sensor application depends strongly on the particular sensor requirements. For fibre gyroscopes, attention is generally given to directivity and stability to environmental parameters where as in all fibre resonator sensors the insertion loss is also a critical parameter. Other considerations include ease of manufacturing. In this respect, fused couplers have taken the lead in popularity because of their relative simplicity and mechanical stability, while polished couplers continue to exhibit superior properties on most counts.

From a polarization point of view both low birefringence and high birefringence fibre couplers were used in our experimental work.

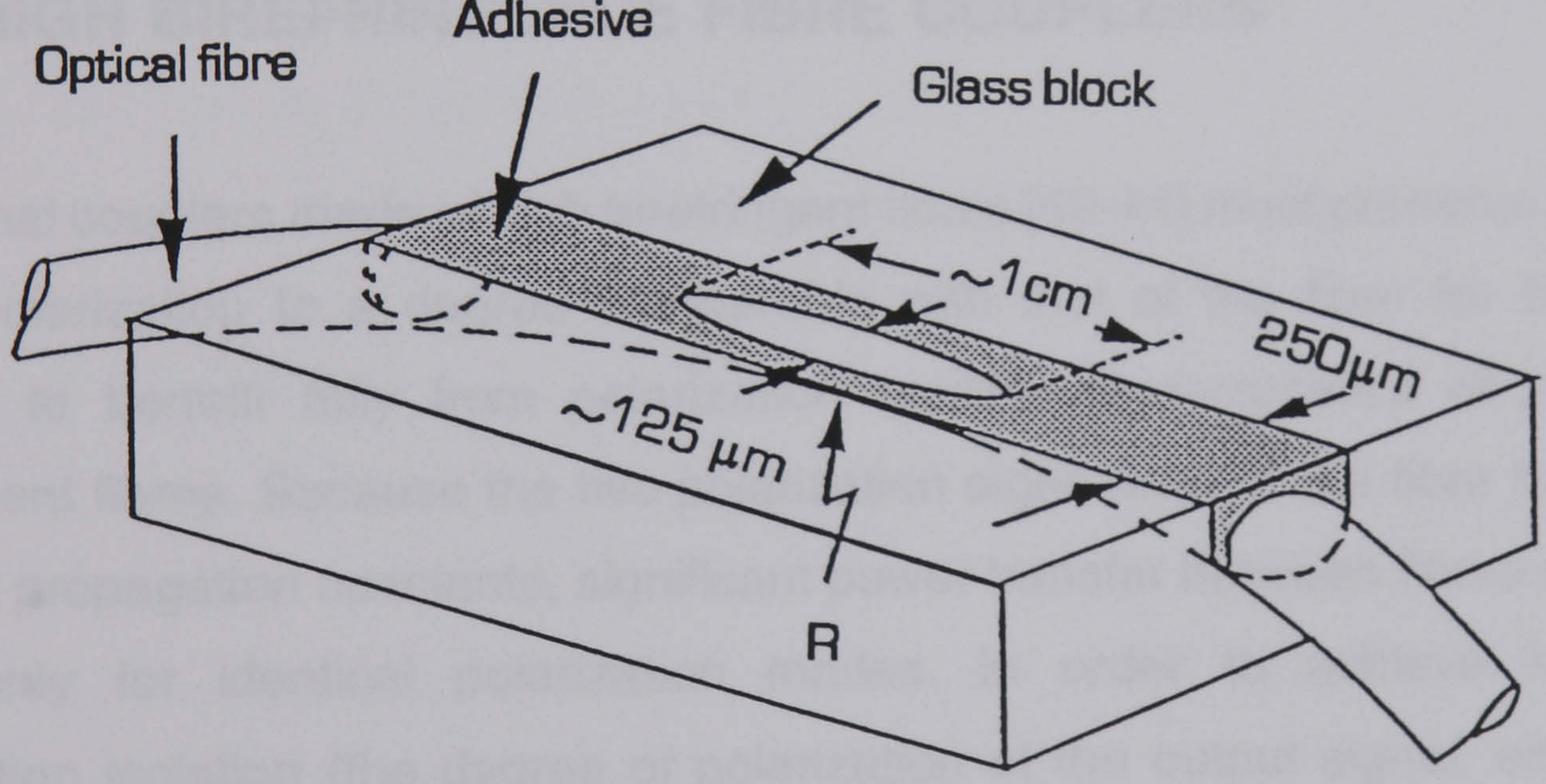

Fig. 2.9 Schematic diagram of a polished block (not to scale).

2.5.3 LOW BIREFRINGENCE FIBRE COUPLERS

The dependence of the coupling ratio on the signal polarization and the effect of the coupling region on the state of polarization of the signal are two types of polarization effects which are of interest in fibre directional couplers. In a coupler made of perfectly nonbirefringent fibres, the coupling ratio is approximately the same for an input signal with polarization parallel or perpendicular to the polished surface [41].

The polarization dependence of the coupling ratio was measured to be 0.1% in a polished coupler tuned anywhere between 50% and 100% coupling, in accord with theory [2].

2.5.4 HIGH BIREFRINGENCE FIBRE COUPLERS

Directional couplers made of high birefringent fibres [42-44] must preserve the signal polarization to a degree comparable with that of the fibre for fibre sensors to benefit fully from polarization holding characteristics of high birefringent fibres. Because the two polarization eigen axes of the fibre have different propagation constants, significant power transfer between fibres can occur only for identical polarization modes. In order to achieve high polarization isolation (the degree of polarization of the output signal, either throughput or coupled, relative to a linear input polarization) and high coupling, the birefringence axis of the two fibres must be well aligned to better than 0.5 degree for an isolation of -35dB [43]. Reproducible alignment is the most significant difficulty in the fabrication of high birefringent fibre couplers. The polishing method can be used in combination with visual alignment of the fibre axis with respect to the polishing surface.

THEORY

The effective interaction length is related to the fibre parameters and bend radius *R* as [2]:

$$L_i = \left(\frac{R\lambda}{2\sqrt{n_{eff} - n_{cl}}} \right)^{1/2} \qquad (2.11)$$

where n_{eff} and n_{cl} are effective core and cladding refractive indices respectively.

The coupling mechanism can be described by coupled mode theory [41,45-46].

Light enters the coupler from ports 1 and 2 and exits from ports 3 and 4 (fig. 2.10.a) after having interacted in the coupling region. When the fibre guides are evanescently coupled, the z-dependence of the coupler fields in fibre 1 and 2 follows standard coupled mode relations [46]:

$$\frac{dE_1(z)}{dz} = jKE_2(z) \qquad (2.12.a)$$

$$\frac{dE_2(z)}{dz} = jKE_1(z) \qquad (2.12.b)$$

where *K* expresses the power fraction coupled to fibre 2, therefore *K* is the normalized intensity coupling constant, or simply the coupling constant as it will be called for short.

The complex electric field amplitudes at the coupler ports are interrelated as [47]:

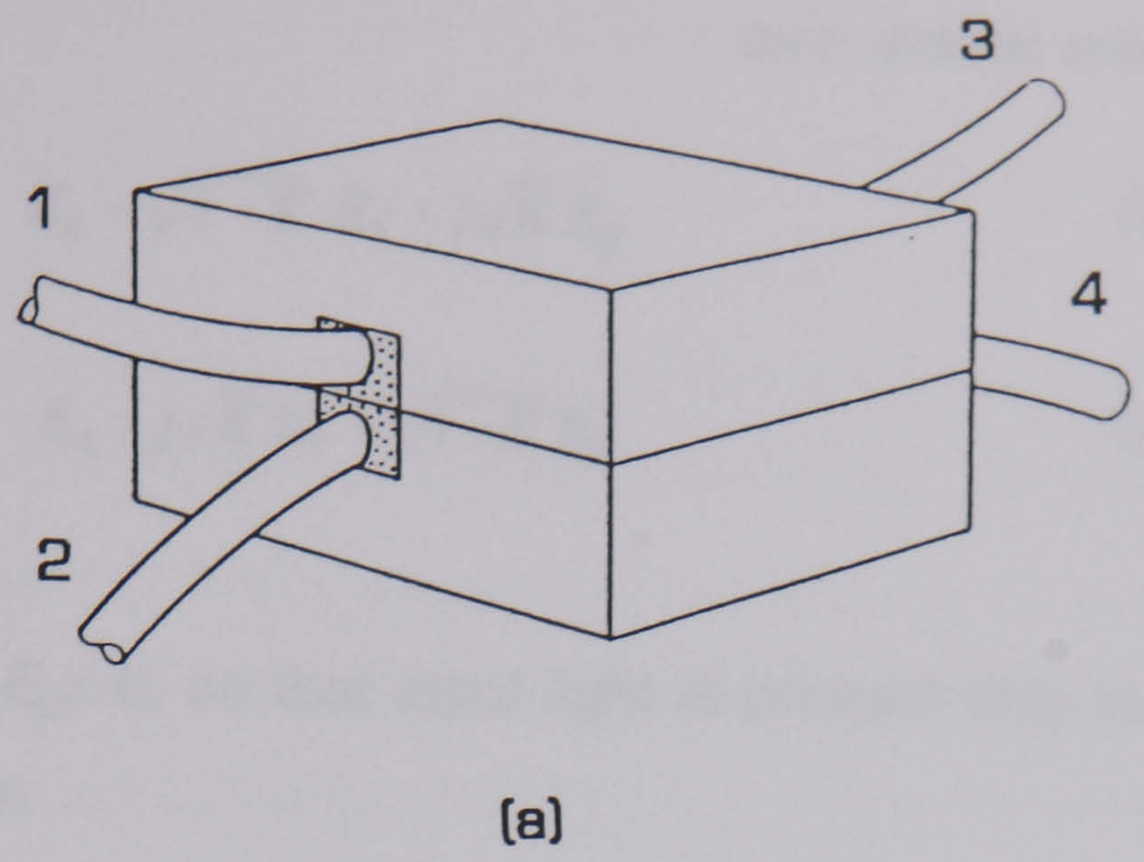

(a)

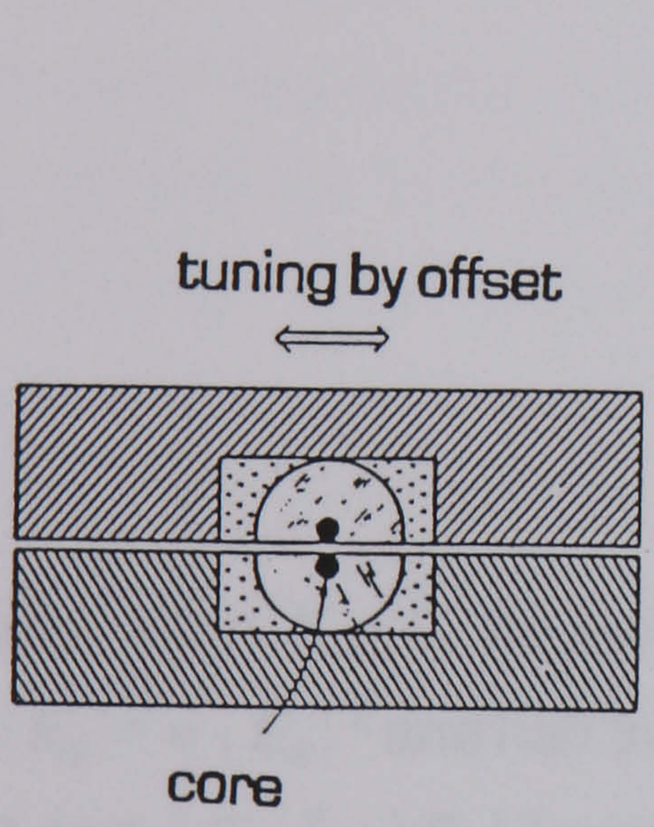

(b)

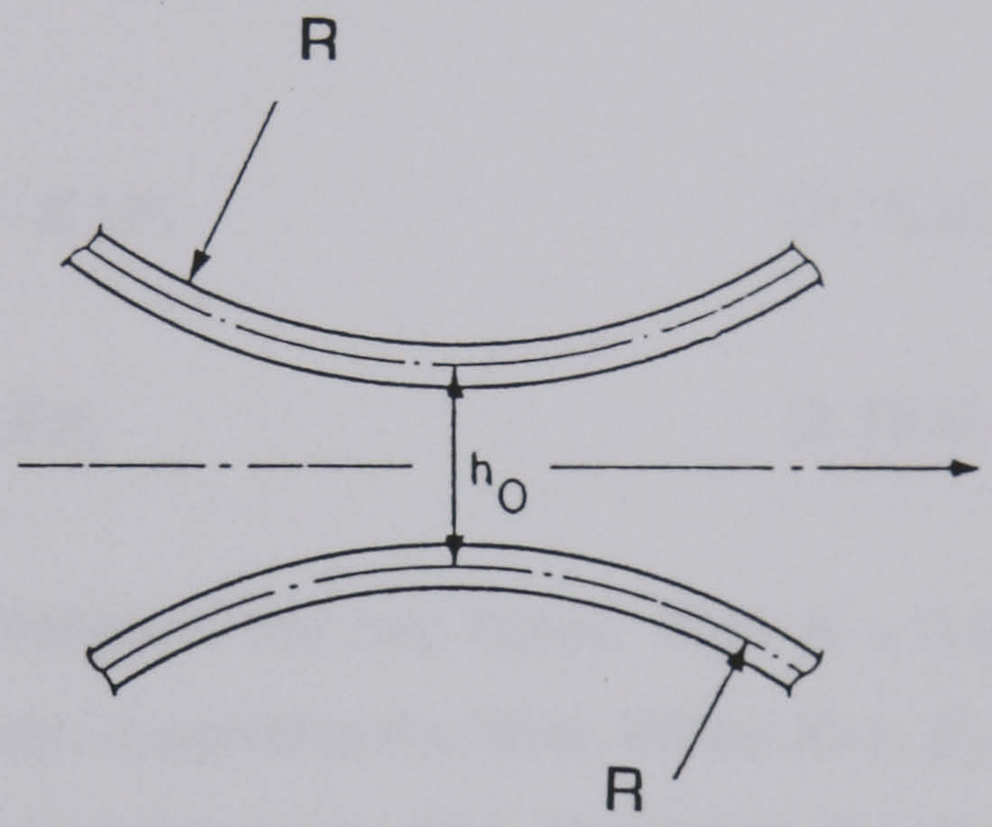

(c)

Fig. 2.10 Polished fibre coupler: (a) Directional coupler formed by mating two polished substrates; (b) cross-section of the coupler at the centre of the coupling region; (c) fibre geometry in the vicinity of the coupling region.

$$E_3 = \sqrt{1-K}\, E_1 + j\sqrt{K}\, E_2 \qquad (2.13.a)$$

$$E_4 = j\sqrt{K}\, E_1 + \sqrt{1-K}\, E_2 \qquad (2.13.b)$$

Consider the case where $E_2 = 0$, so that input light is present only in fibre 1, equation (2.13) reduces to:

$$E_3 = \sqrt{1-K}\, E_1 \qquad (2.14.a)$$

$$E_4 = j\sqrt{K}\, E_1 \qquad (2.14.b)$$

which in terms of optical powers are expressed as:

$$P_3 = (1-K)\, P_1 \qquad (2.15.a)$$

$$P_4 = K P_1 \qquad (2.15.b)$$

and when $K = 0$, no coupling occurs between the two fibres. With $K = 0.5$, $|E_3|^2 = |E_4|^2$ and half the power has been coupled to the fibre. When $K=1$, $E_3 = 0$ and $|E_4|^2 = |E_1|^2$ and all the power has been coupled. Therefore K is the intensity coupling constant.

The phase of light in port 4 (figure 2.10) is greater than in port 3 by $\pi/2$ radians as indicated by the j factor in the expression for E_4. Thus E_4 lags E_3 in time. Physically, the coupling of power from guide 1 to guide 2 occurs because the evanescent electric field in guide 1 induces a linear polarization in guide 2 at the optical frequency in phase with that field in guide 1.

Ideal fibre couplers should distribute light among the waveguides with no

scattering loss or the generation of noise, and they should function with complete insensitivity to the state of polarization of the light. In practice passive polarization couplers do not display all of the above properties and hence the characteristics of the device affect the performance of optical fibre systems. The power insertion loss of these couplers is low, ranging from 2% to 10%. The directivity is high (more than 60dB) and the coupling ratio is nearly independent of the input state of polarization.

2.6 OPTICAL DETECTION & AMPLIFICATION

The detector in an optical system takes an optical signal from the transmission channel (waveguide or free space), converts it into electrical form, and then amplifies this electrical signal in order to prepare it for further processing functions. The detector thus provides an interface between the optical and electronic domains. In this thesis the term detector will be used for a combination of a photodetector (a semiconductor junction diode) and an electronic amplifier and will be discussed in detail in Chapter 5.

2.7 FABRY-PÉROT INTERFEROMETER

A Fabry-Pérot is a multiple-beam interferometer frequently used to examine the detailed structure of spectral lines. In principle, the device consists of two plane (or confocal), parallel, highly reflecting surfaces separated by some distance *d*.

OPERATION: Fabry-Pérot (FP) interferometers are essentially ultra-narrow linewidth filters which produce a series of sharp transmission peaks as the

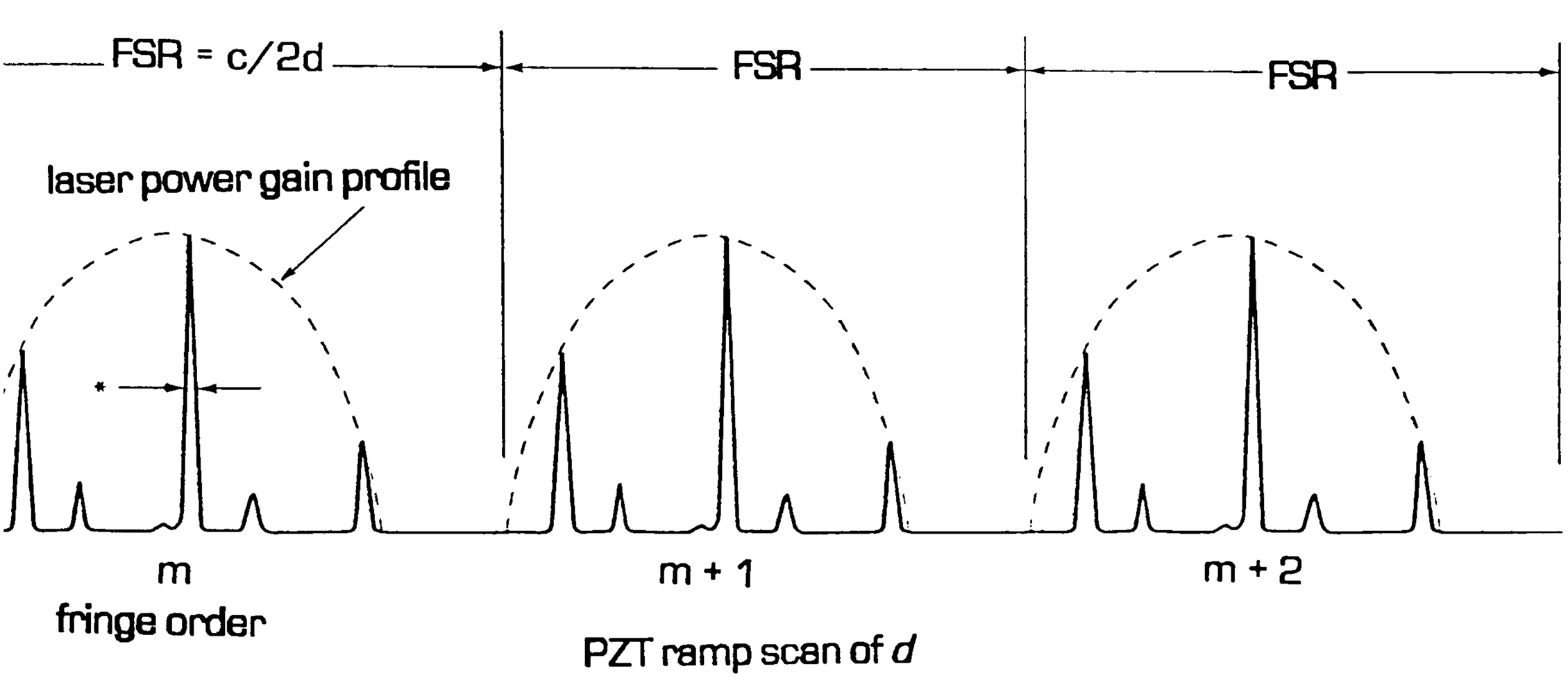

Fig. 2.11 A typical laser spectrum repeated over a scan of three free spectral ranges (FSR) together with the outline of the laser power-gain profile. * FWHM linewidth; Finesse = FSR/FWHM.

mirror separation is slightly varied with the scanning of the piezoelectric ramp voltage. These peaks occur when the multi-reflected beams within the interferometer cavity are additive in phase at the exit surface. The small percentages transmitted at each reflection (<1%) reinforce and produce the bright transmission peaks which are detected by a silicon or a germanium detector.

Each spectral component of the incoming radiation produces a transmission peak when the optical path d matches the spectral wavelength λ as $d \approx m\lambda/2$ ($d \approx m\lambda/4$ for a confocal FP), where m is a large integer called the fringe order. Thus for any wavelength there will be a transmission peak every time the scanning mirror separation gives an integral value of m for that wavelength.

There will be a comb of transmission peaks corresponding to different integral values of m if the ramp scan voltage (signal applied to the PZT) is large enough as shown in figure 2.11. For each and every spectral line or mode in the incoming beam there will be a similar comb of peaks and thus a sequence of identical spectra will be displayed across the screen as the mirror separation is ramped through a succession of mirror orders m.

Adjacent fringe orders are separated by the *Free Spectral Range* (FSR), where the FSR is given by $c/2d$ (or $c/4d$ for confocal FP) Hz and the separation between peaks is linear in frequency.

The sharpness of individual peaks is limited by the *Finesse* of the interferometer which is defined as the ratio of *FSR* to the full width at half maximum of the resonance peak. The value of the finesse is controlled by the reflectance of the mirrors and the quality of the interferometer construction.

2.8 CONCLUSIONS

In this chapter different fibre optic components, i.e., optical sources, low & high birefringent optical fibres, directional couplers, a phase modulator, and detectors, used in this project were discussed. The principle of operation of system components and a comparison between different types, their advantages and limitations were presented. Basic terminology was explained which will be used later in this thesis.

CHAPTER THREE

REVIEW OF FIBRE OPTIC FREQUENCY SHIFTERS

3.1 INTRODUCTION

Many frequency shifter techniques have been investigated. All these devices operate in essentially the same manner, i.e., the interaction of acoustic waves with the guided optical beam. The propagation medium of the acoustic wave can either be the unsupported fibre or a substrate with which the fibre is in contact. Non-birefringent single mode fibre supports two degenerate modes each with the same propagation constant but with orthogonal polarizations. In practice there will be some small degree of birefringence due to residual stress induced in manufacture and further stresses induced by bending and twisting. As a result the polarisation state of the guided light is not maintained. On the other hand in highly birefringent fibres (Chapter 2) additional birefringence is induced in the manufacturing process, thus creating a fast and slow axis.

Linearly polarized light launched into one axis will not couple into the orthogonal axis which has a different propagation constant. Externally imposed stress can cause coupling between the modes. This is most effective if the stress acts at 45° to the fibre axis [48].

The principle of operation of fibre frequency shifters is based on mode coupling within the waveguide, either polarization mode coupling between the eigenmodes in highly birefringent fibre or spatial mode coupling between the LP_{01} and LP_{11} modes in single mode fibre produced by a travelling acoustic wave.

In an unperturbed straight fibre, the two lowest order modes (LP_{O1} and LP_{11} with propagation constants β_{O1} and β_{11}), are orthogonal to each other, and they do not exchange optical power as they propagate along the fibre. An efficient coupling between these modes can be obtained by introducing periodic microbending whose spatial period matches the beat length between them. The beat length is given by equation 2.1. When the periodic microbending is a travelling wave an optical signal that is coupled from one mode to the other by this wave is frequency shifted. For a fibre with propagation constants β_1 and β_2 for the two modes, we can write:

$$\Delta\beta = \beta_1 - \beta_2 - \kappa \qquad (3.1)$$

where κ is the angular wavenumber of the perturbation, which in this case takes the form of a travelling acoustic wave.

For the case of a travelling acoustic wave producing mode coupling, if ω_1 and ω_2 are the optical frequencies associated with modes 1 and 2 of the fibre

respectively, then [49]:

$$\omega_2 = \omega_1 + \frac{\beta_2 - \beta_1}{|\beta_1 - \beta_2|}\varpi \qquad (3.2)$$

where ϖ is the angular frequency of the acoustic wave. If $\beta_2 > \beta_1$, i.e., β_1 is a fast mode, then $\omega_2 > \omega_1$ and the mode coupling produces an upshift in the frequency. therefore:

fast mode $\rightarrow$ *slow mode* $\Rightarrow$ *upshift*

slow mode $\rightarrow$ fast mode $\Rightarrow$ downshift

The above condition will be reversed if the acoustic and optical waves are travelling in the opposite direction.

The amount of power transferred from mode 1 to mode 2 after a distance z is defined as [49]:

$$P(z) = \left|\frac{A_2(z)}{A_1(0)}\right|^2 = \frac{|K|^2}{|K|^2 + (\Delta\beta/2)^2}\sin^2[|K| + (\Delta\beta/2)^2]^{1/2} \qquad (3.4)$$

where K is the coupling coefficient. The above equation shows that as $\Delta\beta$ varies, the fraction of the coupled power varies periodically and unless $\Delta\beta = 0$ (i.e., the phase matching condition) complete power transfer will not occur.

For $\Delta\beta = 0$ equation 3.1 gives the condition for complete power transfer as:

$$\Upsilon = \frac{2\pi}{|\beta_1 - \beta_2|} \qquad (3.5)$$

where Υ is the wavelength of the applied perturbation. It is important to note here that the right-hand side of the equation, by definition, is the fibre beat

length. Hence for maximum power coupling the wavelength of the external perturbation should be equal to the beat length.

Figure 3.1 shows schematically the basic operation of frequency shifters previously developed by different researchers. The optical wave excited in mode 1 interacts with the travelling acoustic wave and is coupled to mode 2. As the coupled wave is frequency shifted by the travelling wave. The first modal filter ensures that any initial energy in mode 2 does not enter the interaction region. Further down the fibre, the frequency shifted component resides in mode 2 and is separated from mode 1, which carries the original unshifted frequency component, by the second modal filter.

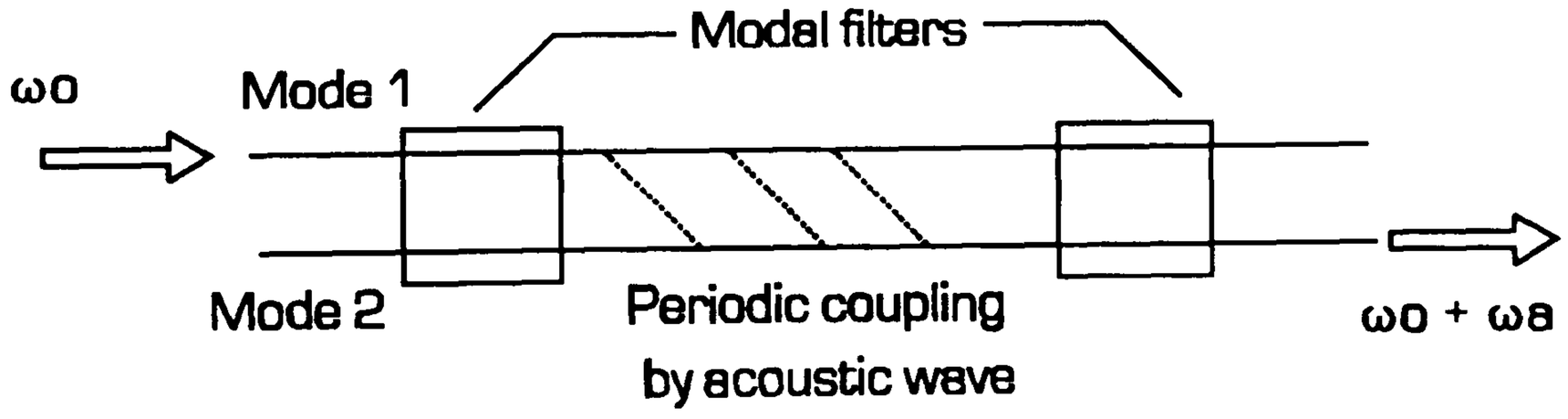

Figure 3.1 Basic principle of acousto-optic frequency shifting in an optical fibre.

The parameters of importance for frequency shifters are high suppression of the carrier and sideband, frequency tuning range and a high conversion efficiency defined as the fraction of optical power initially in one mode that is converted to the other mode. Sideband suppression and carrier suppression are defined as the inverse ratio of the optical power at these spurious frequencies to the optical power of the main output signal. Figure 3.2 , taken from reference [49] shows the output spectrum of a frequency shifter when the frequency shifted beam was mixed with the output from a Bragg cell. The mixing with a carrier from Bragg cell allows the upshifted and downshifted frequency components to be displayed separately.

In high birefringence fibre at integral multiples of the beat length (Chapter 2), light guided in one axis has the same relative phase relationship to the light guided in the other axis. The phase matched, modal coupling is generated through an acoustic travelling wave that has a wavelength equal to the beat length between the polarization or spatial modes in the fibre. These devices differ from each other in terms of the method used to generate the travelling acoustic wave in the fibre. In order to couple the acoustic wave onto the optical fibre a piezoelectric modulator or interdigital transducer is generally employed. These devices fall into two main categories; integrated optic waveguide [50-51] and dual mode i.e., high birefringence optical fibre. Integrated optical devices were demonstrated with better than 30dB sideband suppression, but reduction of the relatively high insertion loss of the devices, especially when coupling to the fibre, and further suppression of unwanted sidebands has yet to be seen. For practical devices it is very important to produce single sideband (SSB) operation, i.e., one in which there is no residual carrier and no image sideband, as this maximises the optical efficiency of the device and simplifies subsequent electronic demodulation.

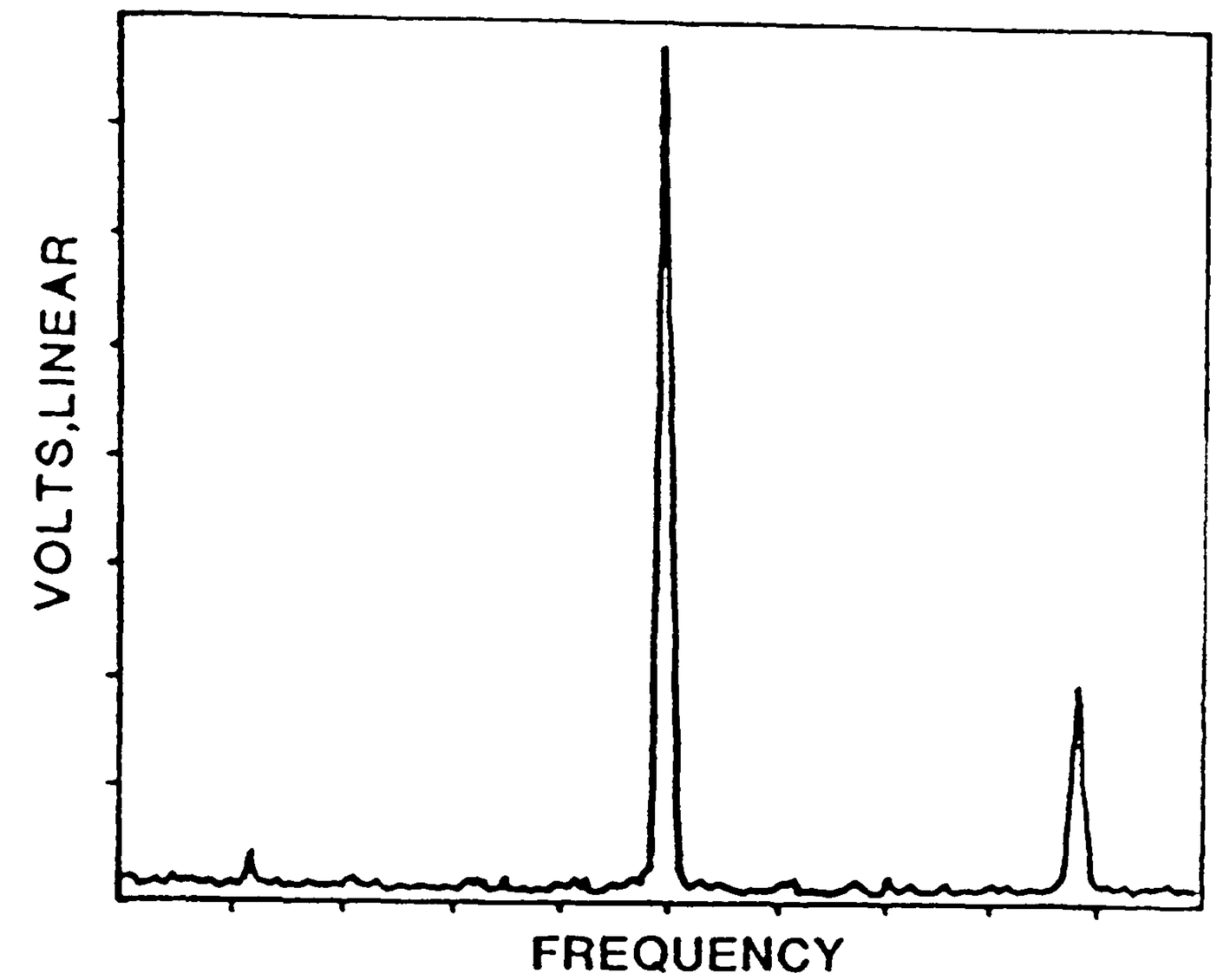

(a)

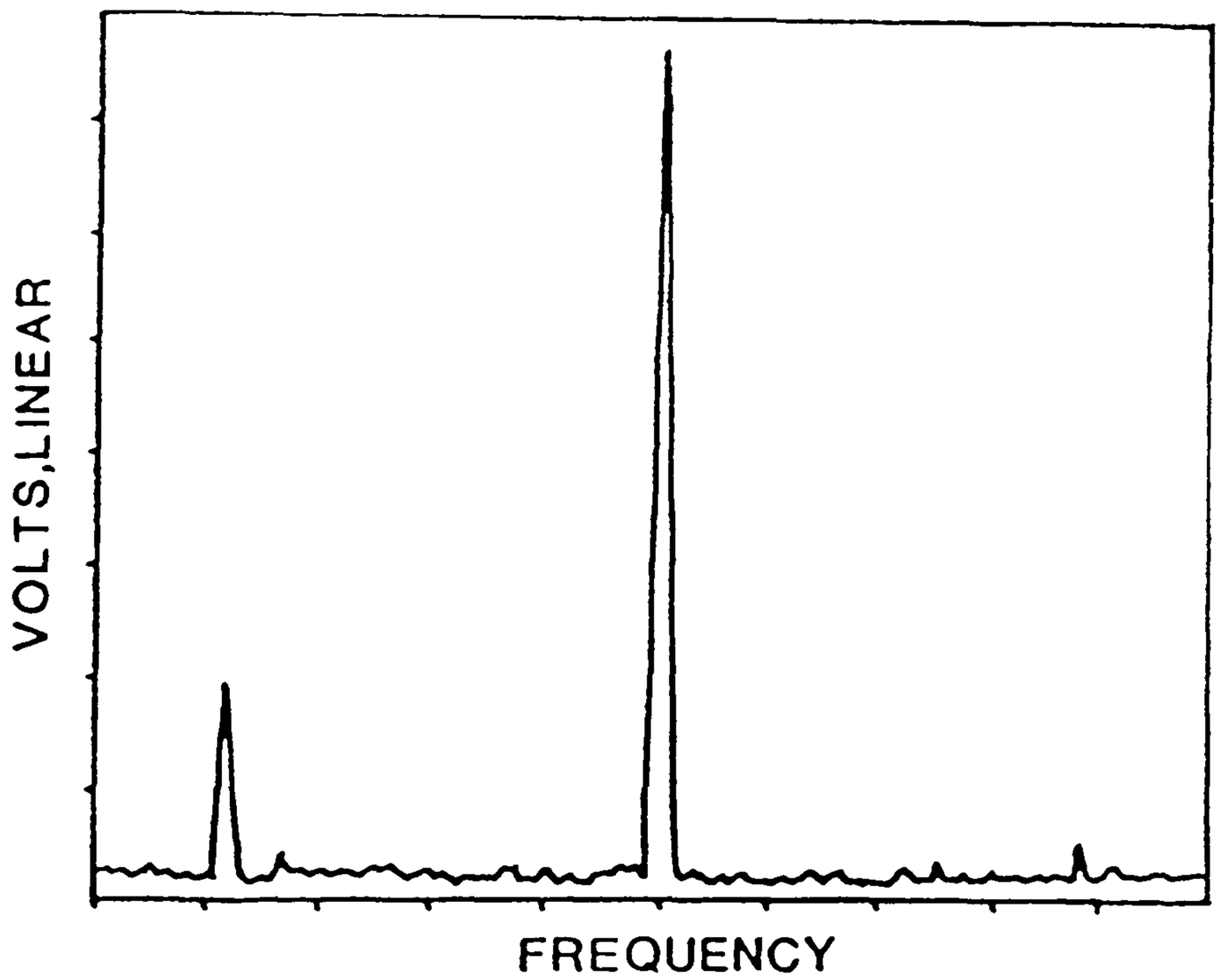

(b)

gure 3.2 The effect of interfering the reference beam (from Bragg cell) with the frequency shifted beam. (a) Upshift (b) Downshift.

3.2 CLASSIFICATION

The acoustic wave can be generated either externally to the fibre and then coupled to it (extrinsic devices) or internally within the fibre (intrinsic devices); this is the basis of major classification in frequency shifters [52].

3.3 SURFACE ACOUSTIC WAVE (SAW) DEVICES

SAWs are the waves that propagate on the free surface of a solid. Particle displacements occur both normal to the surface and also in the direction of wave propagation. Displacements decay rapidly below the surface and consequently over 90% of the wave's energy is contained within one acoustic wavelength of the substrate surface. This concentration of acoustic energy, where it is accessible, is very convenient and SAW technology is well developed. Unwanted acoustic energy can easily be absorbed without significant reflection by placing putty-like materials on the surface.

One of the first approaches was from Risk *et al* [53]. They introduced a kind of frequency shifters based on the coupling of two orthogonally polarised modes of a birefringent fibre induced by travelling acoustic waves excited on a substrate with which the fibre is held in contact. The idea behind their approach was that a spatially periodic stress pattern can induce coupling between the two orthogonally polarised modes of single mode birefringent fibre, leading to power transfer from one mode to the other and vice-versa. This power transfer will be cumulative only if the spatial period of the stress pattern is equal to the beat length of the fibre. This principle was

demonstrated for a static stress pattern elsewhere [54]. In this technique, a single mode birefringent fibre was squeezed between a flat base and a plastic block with ridges $L_B/2$ long and spaced by $L_B/2$ gaps. The power transfer between the two polarisation modes was more than 30 dB.

If the stress pattern moves along the fibre, coupling still take place, but now the light coupled from one polarisation to the other is shifted in frequency because of the motion of the coupling region. By inducing such a moving stress pattern in the fibre by a travelling acoustic wave, a shifted frequency can be obtained. Hence a frequency shifter can be constructed by using a polarizer to launch light into only one of the polarization modes. Then a travelling acoustic wave couples some or all of the light to the orthogonal polarisation with a frequency shift, and an analyzer is used to pass only the polarisation containing the shifted frequency.

The first device, described by Risk *et al* [53], uses a surface acoustic wave to induce the required stress pattern in the fibre. An edge bonded PZT transducer launches a surface acoustic wave (SAW) on an aluminium block as shown in figure 3.3. The fibre is pushed into contact with this block by sandwiching it between the block and a flat, rigid base. Pressure is applied to make good acoustic contact between the fibre and the aluminium block. Because surface acoustic waves will travel around bonded corners, damping putty is applied to other faces of the block to extinguish the surface waves before they make a second pass through the interaction region and to eliminate any waves which might be launched in the opposite direction.

Five watts of CW acoustic power at 1.45 MHz was used to drive the transducer in this device. The conversion efficiency was estimated to be 10%. The sideband suppression was ~ 30dB. The carrier was not suppressed in this demonstration because it requires greater care in the adjustment of the

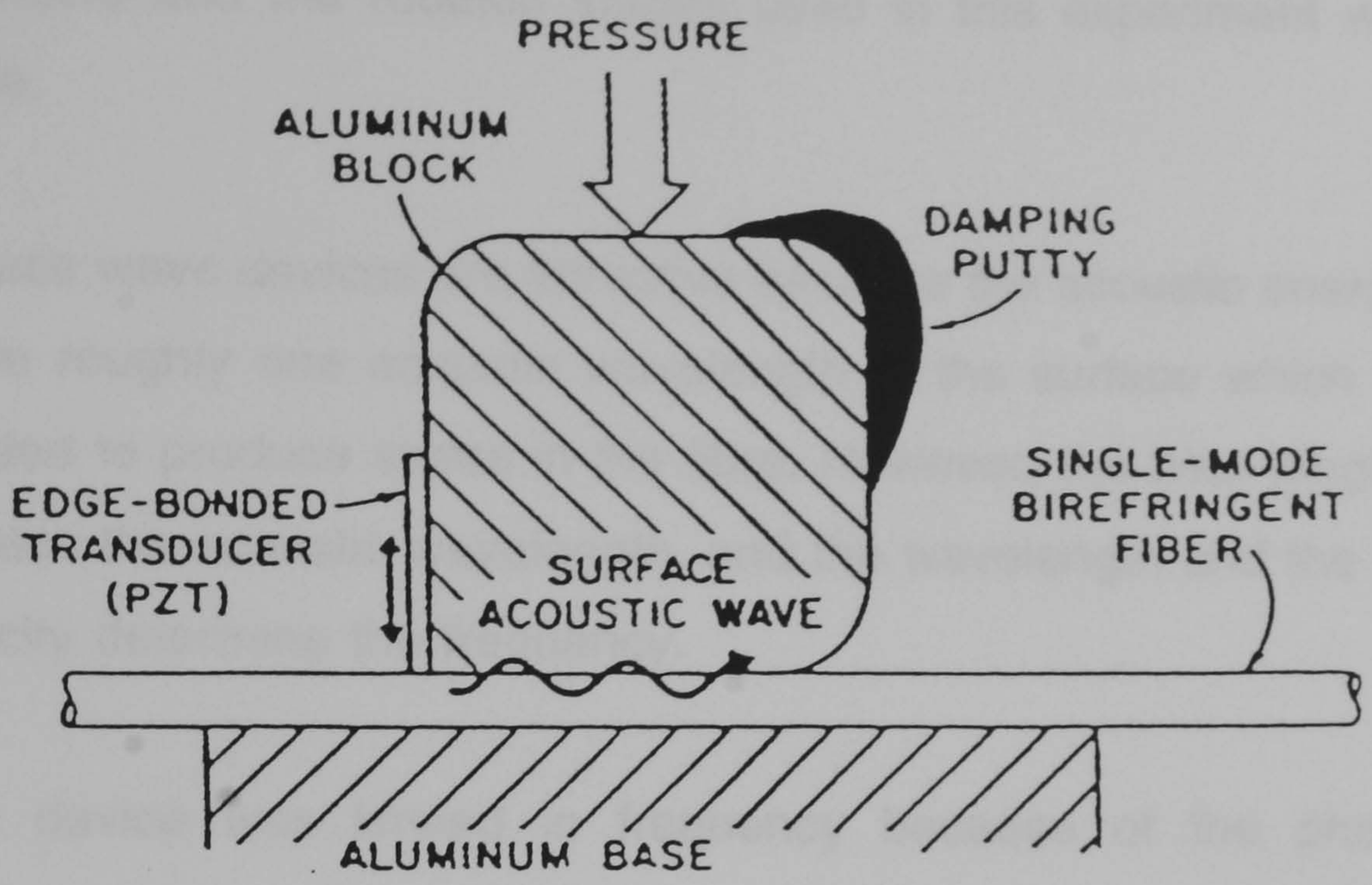

Fig. 3.3. Schematic diagram of the surface-acoustic-wave frequency shifter.

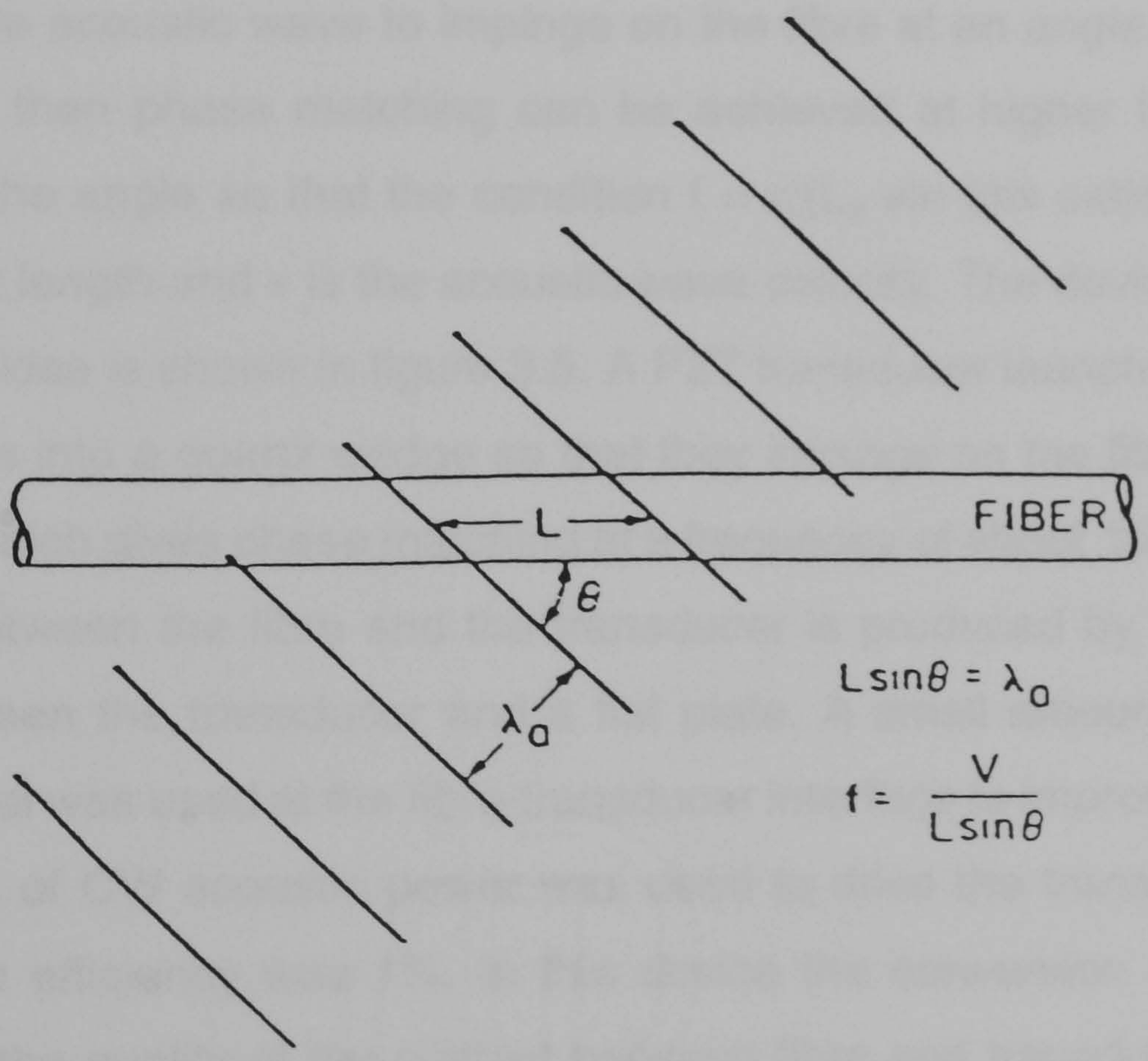

Fig. 3.4. Geometry for phase matching at angle.

polarisers and the rotation stages used in this experiment were relatively crude.

Surface wave devices are attractive because the acoustic energy is confined within roughly one acoustic wavelength of the surface which is where it is needed to produce stress in the fibre. However, the beat length of the fibre dictates the acoustic wavelength, and the wavelength and the surface wave velocity determine the frequency.

This device was limited in frequency because of the phase matching requirement that the acoustic wavelength equals the beat length of the fibre. Given the range of surface wave velocities on common materials, this limits the modulation frequency to a few MHz at best.

A new configuration was presented to overcome this problem. The idea was to allow the acoustic wave to impinge on the fibre at an angle θ as shown in figure 3.4 then phase matching can be achieved at higher frequencies by selecting the angle so that the condition $f = v/(L_B \sin \theta)$is satisfied, where L_B is the beat length and v is the acoustic wave velocity. The device constructed using this idea is shown in figure 3.5. A PZT transducer launches longitudinal bulk waves into a quartz wedge so that they impinge on the fibre at an angle of 13.5°, which gives phase matching at a frequency of about 15MHz. Acoustic contact between the fibre and the transducer is produced by squeezing the fibre between the transducer and a flat plate. A small amount of ultrasonic coupling gel was used at the fibre-transducer interface to improve the contact. 2.25 watts of CW acoustic power was used to drive the transducer and the conversion efficiency was 1%. In this device the conversion efficiency was limited by the quality of the contact between fibre and transducer.

To produce a device with enhanced performance the aluminium pressure plate

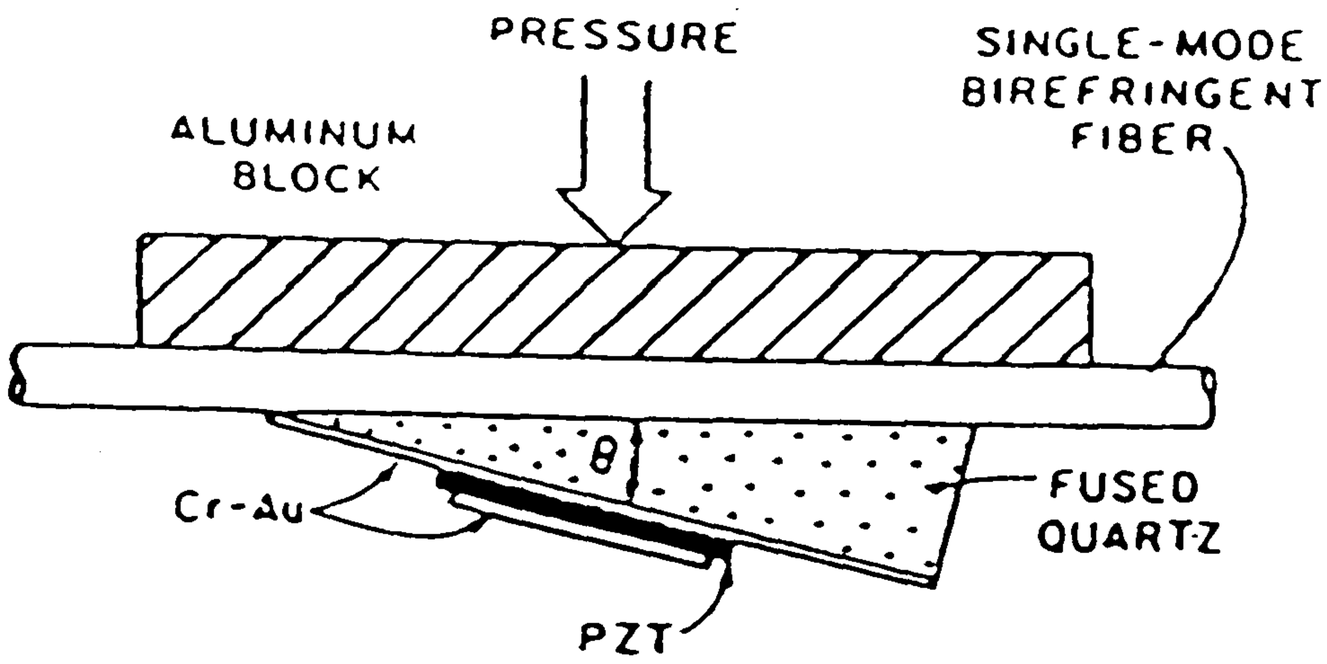

Fig. 3.5. Schematic diagram of the bulk acoustic wave frequency shifter.

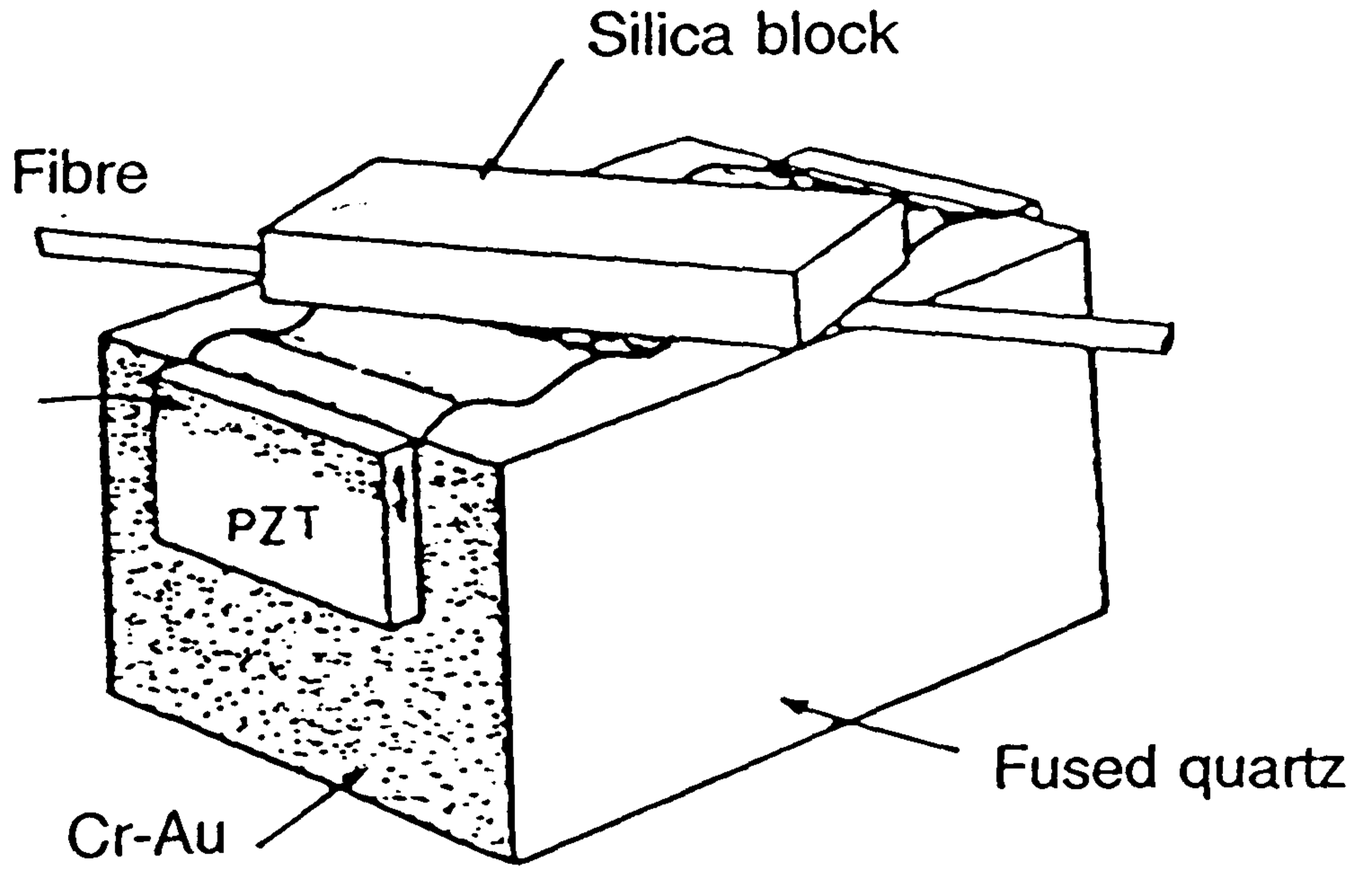

Fig. 3.6. Fibre optic frequency shifter using a surface acoustic wave incident at an oblique angle.

shown in the figure was replaced by a spring loaded fixture holding a quartz block. The quartz block was used to push the fibre up against the quartz wedge and a thin layer of cyanoacrylate adhesive was applied between the blocks and the fibre. The pressure was adjusted until optimum performance was achieved. The cement was allowed to harden, and then the static pressure was removed. This procedure provided good acoustic contact and hence improved performance of the device. It also eliminated some of the undesirable effects of static stress, which can limit the suppression of the carrier and unwanted sidebands.

These devices suffer from two principle limitations. One is the relatively low coupling efficiency, which is probably due to an imperfect contact between the transducer and the fibre. The second is the limitation on sideband and carrier suppression dictated by how well the light is confined to one mode.

In another approach the same group of researchers reported a new kind of frequency shifter in which the acoustic wave is a Rayleigh wave incident upon the fibre at an oblique angle as shown in figure 3.6 [55].

The angle θ between the fibre and the direction of propagation of the acoustic waves is chosen so that the spatial period of the stress exerted on the fibre by the acoustic wave is equal to the beat length of the fibre. This is called the phase matching condition. The device consists of two edge-bonded PZT transducers, either one of which can excite a 2.54 cm wide beam on a quartz substrate. The transducers were electrically impedance matched to 50 Ω with a centre frequency of 4.5 MHZ. The conversion loss from electrical power to acoustic power is 5 dB. Damping putty was applied between the fibre and the transducer to extinguish reflections. The fibre was pressed against the quartz substrate using a polished block of silica. At the frequencies of interest, the angle θ was approximately 27°. Because the coupling efficiency is critically

dependent on the uniformity of the contact between the fibre and the substrate, the substrate was mounted on a tilt platform so that the pressure exerted by the Si block could be adjusted. The static pressure used to produce contact between the fibre and the quartz stresses the fibre and causes the birefringence to change in the stressed region. Single-sideband operation occurs when the light entering the interaction region with the acoustic wave is polarised along one of the principal axes. In the interaction region, light in one principal polarisation is coupled to the other and shifted in frequency. A maximum coupling of 95% was obtained using 25W of electrical input power. Unwanted sideband suppression of approximately 40 dB and carrier suppression of 25 dB were obtained.

Although the angled approach has produced nearly 100% coupling from one polarisation to another, the electrical input power required to achieve this efficiency is quite large (~25 W). Risk *et al* [56] developed a method to achieve phase matching to a high frequency acoustic wave propagation in the direction of the fibre, the acoustic wave could be confined to a waveguide, increasing the acoustic power density in the region of the fibre, and reducing the input power needed to obtain a given degree of coupling. They experimentally demonstrated a technique for phase matching to a collinearly propagating acoustic wave at frequencies above the usual collinear phase matching frequency [56]. Their approach was to permit the acoustic wave to interact with the fibre at periodic intervals along the fibre length. The basic concept behind this approach can be explained as follows.

If a non phase matched collinearly propagating acoustic wave were permitted to interact with the fibre uniformly over the entire length of the interaction region, a small portion of the power initially in one polarisation would be coupled back to the original polarisation further down the device. This build up and decrease of power in the second polarisation is due to the phase

mismatch and is periodic along the length of the interaction region. By shifting off the coupling in those regions where the power couples back to the first polarisation a large amount of power can be cumulatively transferred to the second polarisation. In other words, allowing the acoustic wave to interact with the fibre periodically introduces space harmonic components, one of which has the proper periodicity to restore phase matching. The coupling was turned on and off by pressing the fibre into contact with surface wave using a rigid block, or grating as shown in figure 3.7.

An edge bonded PZT transducer was used to launch a Rayleigh wave on a fused quartz block. The fibre was pressed against the quartz substrate using a polished silicon block into which a series of square grooves had been cut. The maximum coupling efficiency observed was 26% with 32 watts of input electrical power. The efficiency was critically dependant on the quality of the contact between the surface wave substrate and the fibre. The sideband suppression was more than 24 dB.

Most of the frequency shifters, based on SAW devices, have used the edge bonded transducer as the acoustic generator. Greenhalgh *et al* [57] used another technique which employs interdigital transducers on a piezoelectric substrate in a family of devices. One of the main advantages of this technique is the simplicity in the preparation of interdigital transducers as compared to the lengthy and complicated procedures involved in the construction of edge bonded devices.

Figure 3.8 shows the basic device structure. York Bow-tie fibre was used in the experiments. The acoustic substrate was a PZT block with a large electromechanical coupling coefficient. The device was operated at 3MHz and consequently required the fibre to be angled on the surface to achieve the beat length matching condition. A sideband suppression of 38dB and a carrier

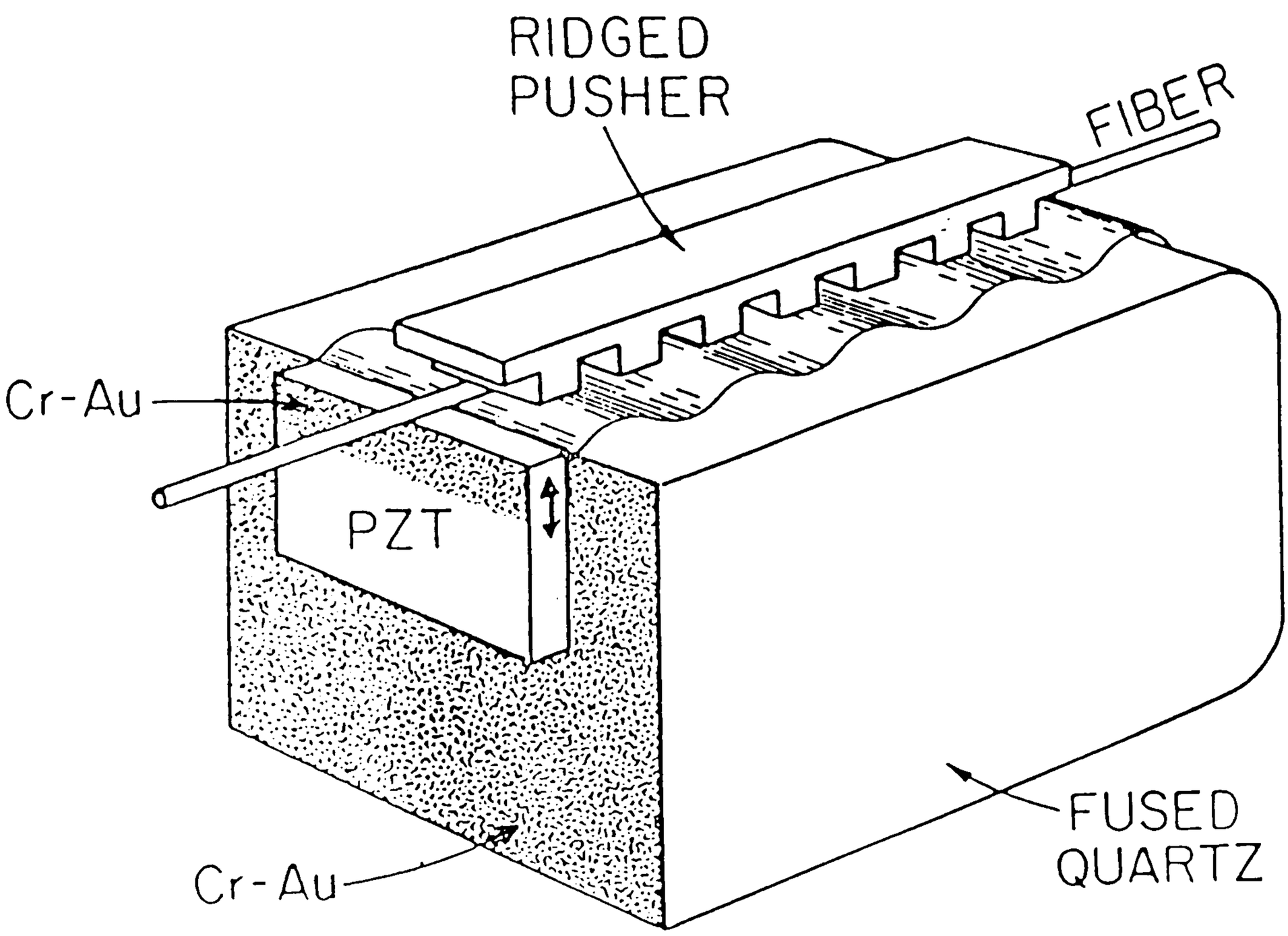

Fig. 3.7. Fibre optic frequency shifter using periodic contact with a co-propagating surface acoustic wave.

suppression of 29dB was obtained. The highest efficiency attained for this device was 4.1% with 1.9W of electrical power.

Theoretical results showed [57] that doubling the interaction length would give a worthwhile increase in efficiency from 4% to 15% for no increase in drive power. A device in which multiple passes of fibre are laid across an acoustic beam could therefore give the advantages of a long interaction length in a more compact form without the need to polish a very long thin substrate. Also more effective use of the relatively wide acoustic beam could be made. It was necessary to maintain the phase matching condition between the two passes to achieve good results. The alignment was achieved by means of a phase modulator in the loop of fibre between the two interaction lengths. The method of phase modulation was to attach the fibre loop to a heated resistor. Thermal modulation of the birefringence of the fibre cycled the overall efficiency of the device between a minimum value and a maximum. The two pass device is shown in figure 3.9.

The best efficiency achieved for this device was 8% with 1.9 W of electrical power. This efficiency is less than the predicted value because it was not possible to optimise the fibre angle and clamping conditions to the same degree as the single pass device. Sideband suppression was not comparable to previous devices due to the inadequate clamping. As the matching of beat length to the acoustic wavelength is extremely important, longer devices would have to operate in temperature stable environments in order to maintain a constant value of efficiency.

One way to increase the amount of mode coupling is to increase the magnitude of the surface displacements. This may be achieved for a given electrical drive by reducing the acoustic aperture and hence increasing acoustic power density. Also for a given input power, surface displacements

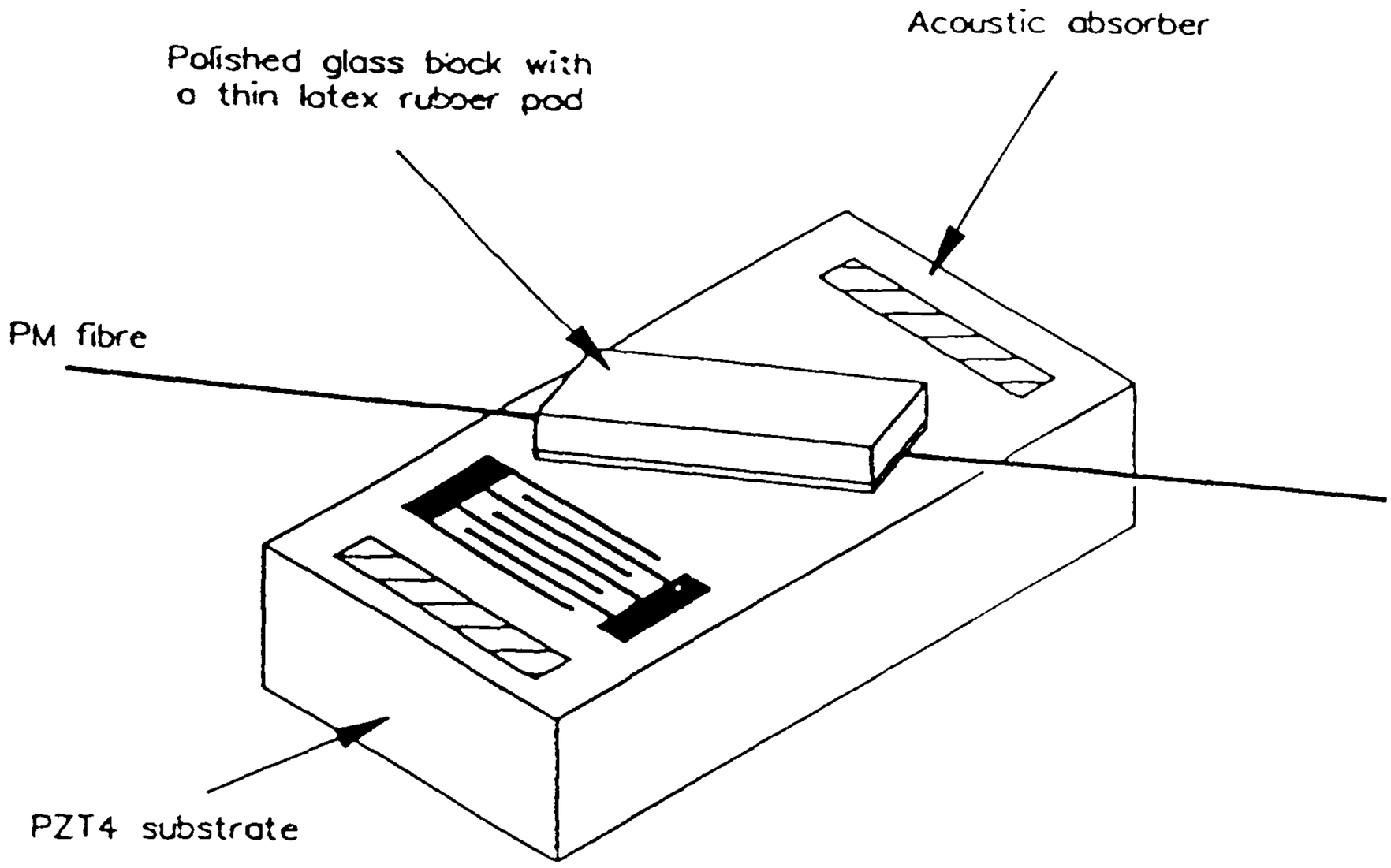

Fig. 3.8. Fibre optic frequency shifter based on interdigital transducers.

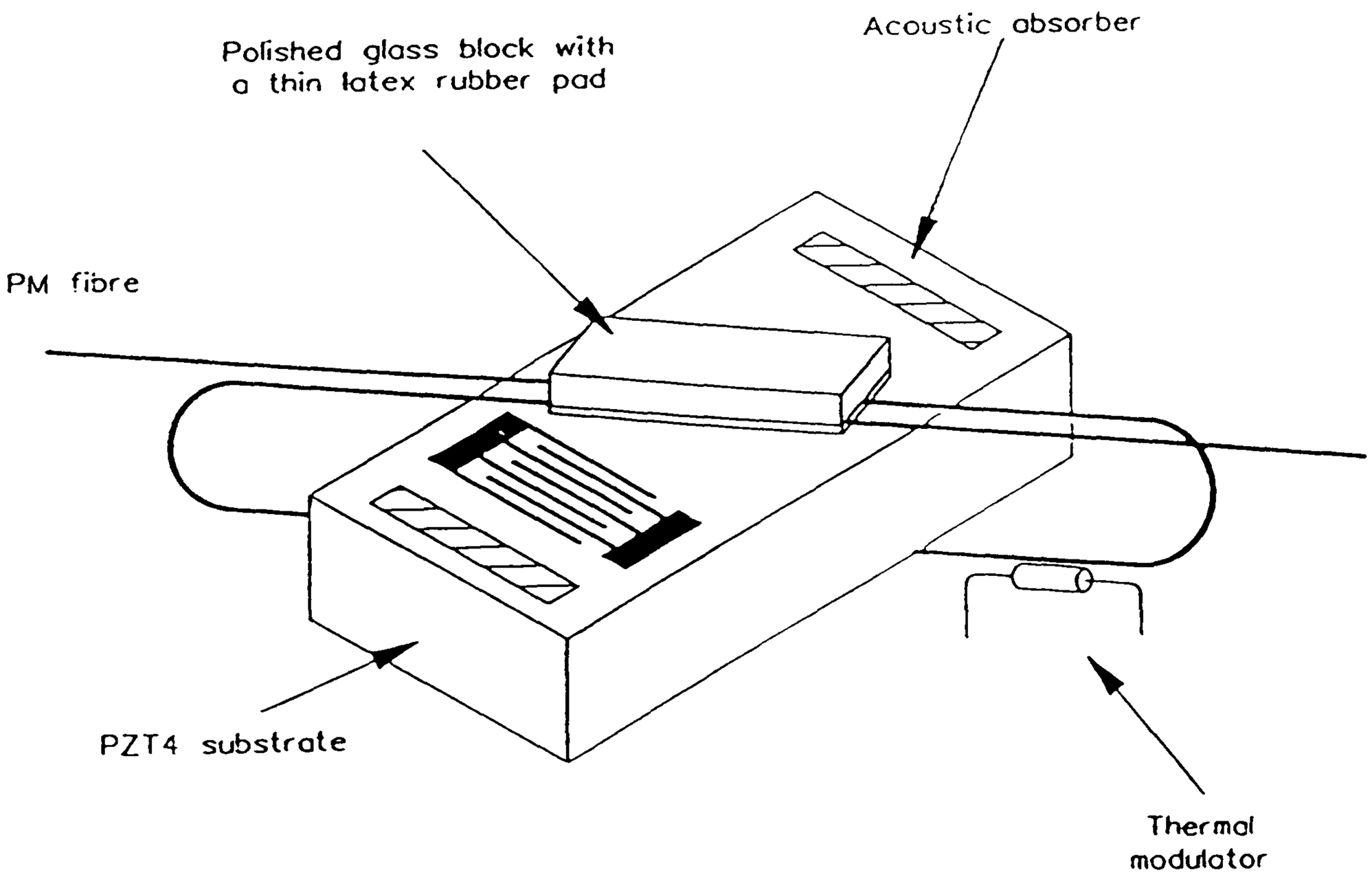

Fig. 3.9. The two pass device.

are greater at lower frequencies. Hence the device should operate at the longest acoustic wavelength possible. In order to increase the acoustic power density the aperture was reduced to 5mm as shown in figure 3.10. No significant improvement was obtained with this device. The best efficiencies achieved were 25% for a 6.5 W electrical power. This is relatively poor compared to the results obtained with the basic and two pass devices. One of the contributing factors to poor efficiency was that the clamping arrangement was inadequate to maintain good contact between the fibre and the substrate over the interaction length of 40mm. Another reason might be that regions of fibre further away from the transducer were being acoustically shadowed by the regions of fibre closer to the transducer.

In 1991 the same group of authors , i.e., Foord *et al* [58] claimed that most of the shortcomings of the frequency shifters previously discussed can be overcome by the use of multiple resonant acoustic transducers positioned along the fibre as shown in figure 3.11. By driving these with correctly phased signals the effective coupling can be made to travel along the fibre. The operating frequency is independent of acoustic velocity and there was no power flow through the device. Power need only be supplied to meet losses in the transducers. The carrier can be suppressed if the transducers are equally spaced over a beat length. In this device three transducers separated by L_B /3 and driven 120° out of phase were used. The fibre used was York Bow-tie. The transducers squeezed the fibre against a glass substrate. At each transducer a series of ridges matched to the beat length ensured effective coupling. These were etched using photolithography to accurately define a separation between each set. It was operated at 54kHz, at which frequency it was capable of producing a frequency shift .

To evaluate the potential performance of such devices a computer model was developed [58]. Devices with two, three, four, six and eight transducers were

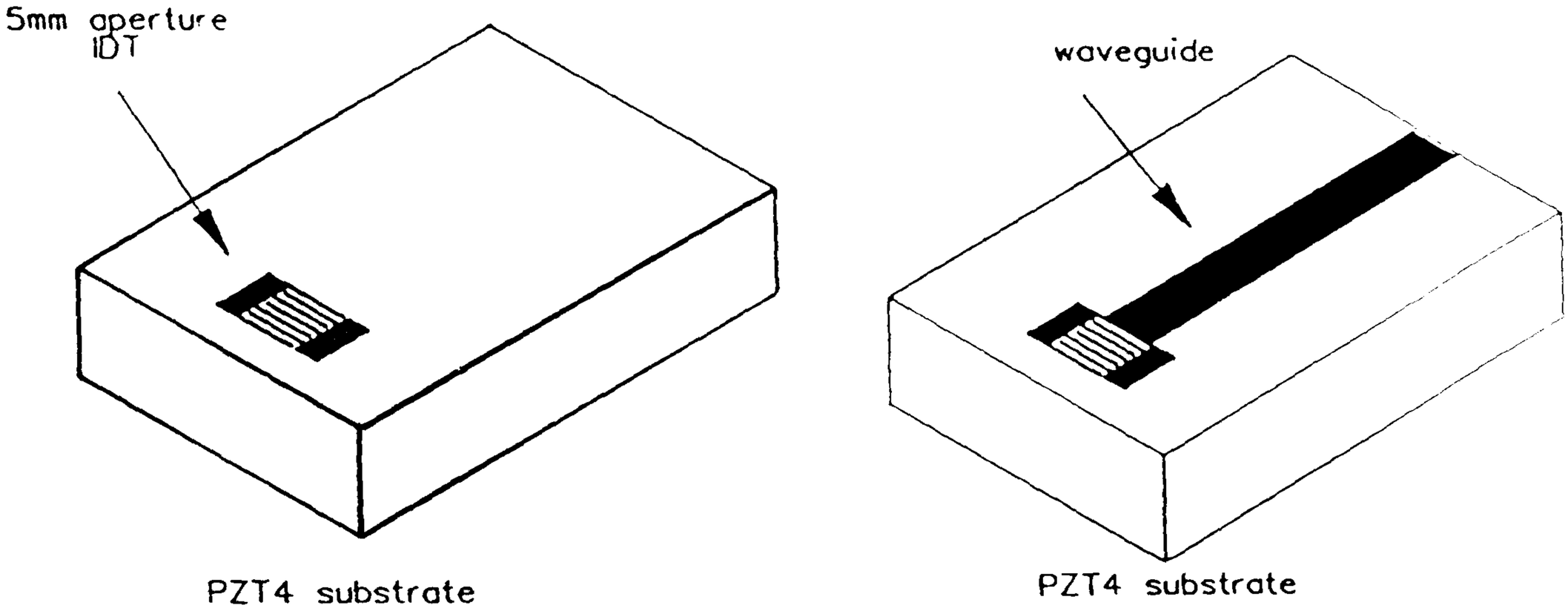

Fig. 3.10. High acoustic power density device.

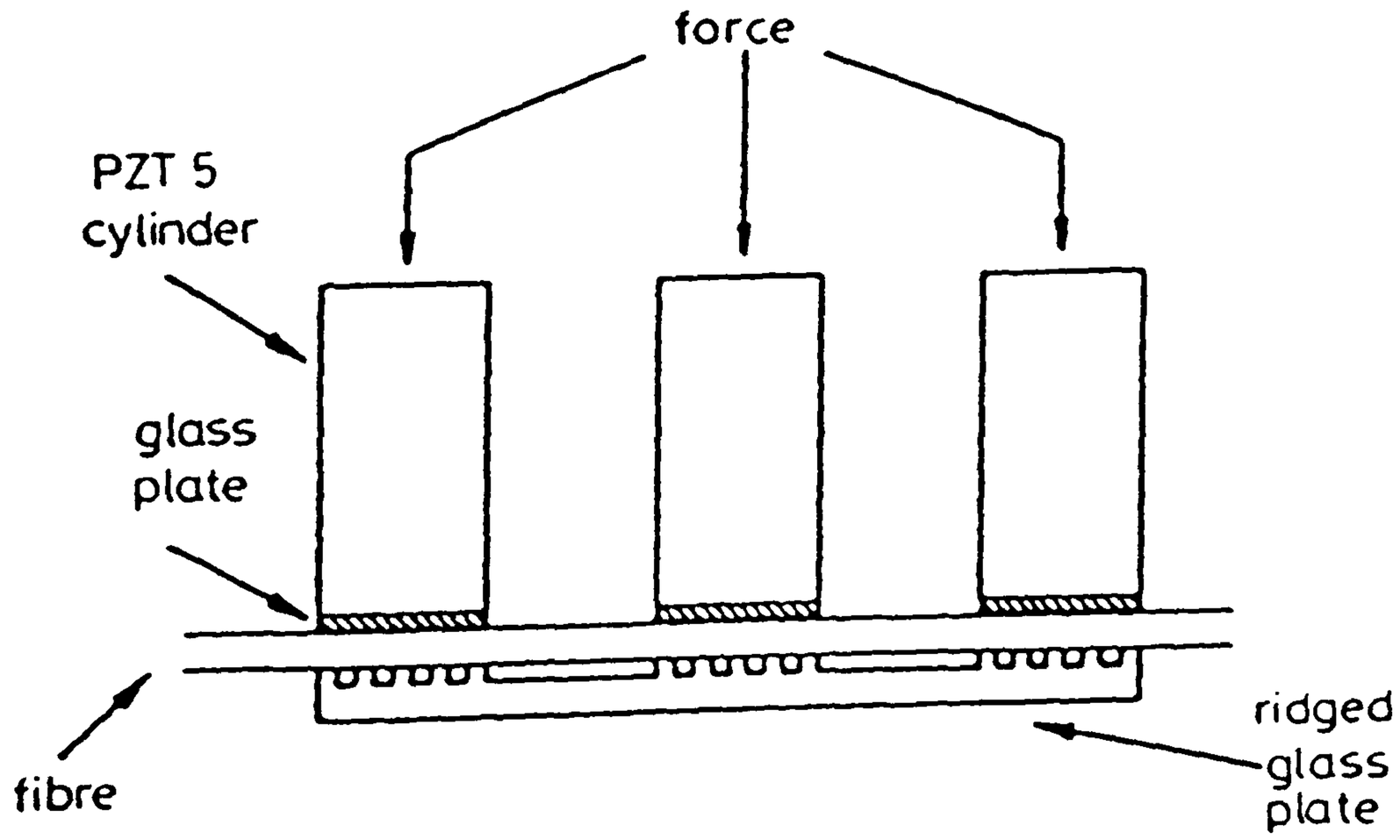

Fig. 3.11. Frequency shifter using three transducers.

simulated. Theoretically a device with eight transducers gave a maximum efficiency of 92% with a carrier suppression of 25dB.

3.4 FLEXURE WAVE DEVICES

In this class of the devices, the refractive index of the fibre is modified by microbending while in SAW devices the mechanism of mode coupling is that of pressure induced changes in refractive index.

In both categories the frequency shift arises due to the travelling nature of the perturbation. The class of device in which the acoustic wave is excited onto the free fibre is inherently more efficient than the substrate type. This is simply a consequence of the more efficient concentration of acoustic energy into the vicinity of the fibre core.

Flexure wave (FW) devices are based on periodic optical coupling between two spatial modes (LP_{O1} and LP_{11}) in circular optical fibres, instead of two polarisation modes. FW devices do not require any critical angular alignments of fibre axes [59]. Also, since the optical fibre actually guides the acoustic wave, the acoustic energy can be more efficiently employed without compromising the carrier and sideband suppression ratios.

Travelling periodic microbending can be generated by exciting an acoustic flexural wave travelling along the optical fibre. The optical signal coupled from the slow mode (LP_{O1}) to the fast mode (LP_{11}) will be downshifted by an amount equal to the acoustic frequency.

Kim *et al* [59] demonstrated a device based on the above concept. The schematic diagram for the frequency shifter is shown in figure 3.12(a). Both the input and output ends of this device are single mode fibres that are connected to a double mode fibre that supports the LP_{01} and LP_{11} modes. The key elements of this frequency shifter are mode filters for the LP_{01} and LP_{11} modes and an acoustic transducer that excites travelling microbends (flexural mode) guided along the optical fibre. A mode filter that strips the LP_{11} modes was realised by wrapping the fibre around the circular cylinder or by adiabatically tapering the core diameter of a section of the fibre. The LP_{01} mode strippers have taken the form of an evanescent field directional coupler constructed with a double mode fibre and a single mode fibre, where only the LP_{11} modes in the double mode fibre can couple to the single mode fibre. In this case, the propagation constant of the guided mode in the single mode fibre matches well with that of the second order mode in the double mode fibre to permit complete optical power transfer between these modes. The propagation constant mismatch and smaller optical field overlap between the two fundamental modes suppress optical power coupling between them.

The acoustic transducer was designed to displace transversely a short section of the fibre perpendicular to its axis such that a flexural acoustic wave is excited, which travels along the fibre. The wavelength of this flexural wave is required to match the beat length between the two optical modes. This was accomplished by using a cylindrical acoustic horn made of silica glass bonded to a PZT on one end and to the fibre on the other end, as shown in fig. 3.12(b). This configuration permits concentration of the acoustic intensity generated by the PZT into a higher acoustic intensity signal at the tip of the horn. Therefore a large excursion of the tip can be obtained with low acoustic power. By making the diameter of the tip of the horn that is bonded to the fibre approximately the same as that of the fibre, a good acoustic energy transfer can be achieved. The bonding between the fibre and the horn was done by

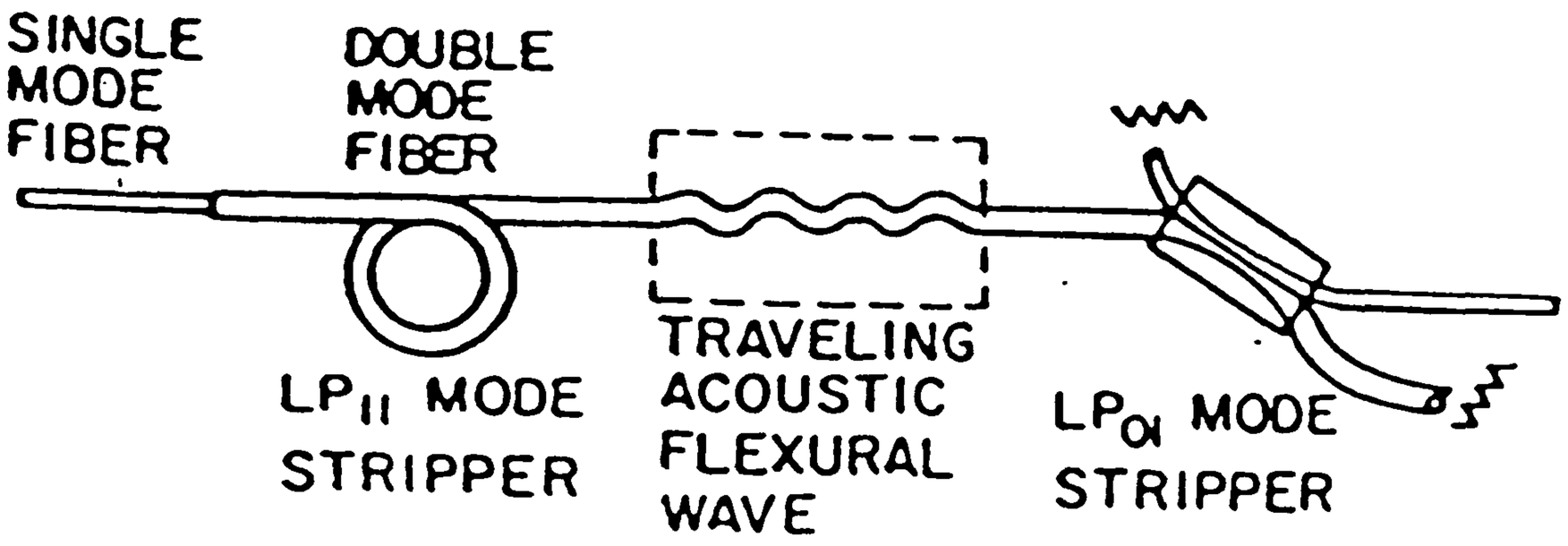

(a)

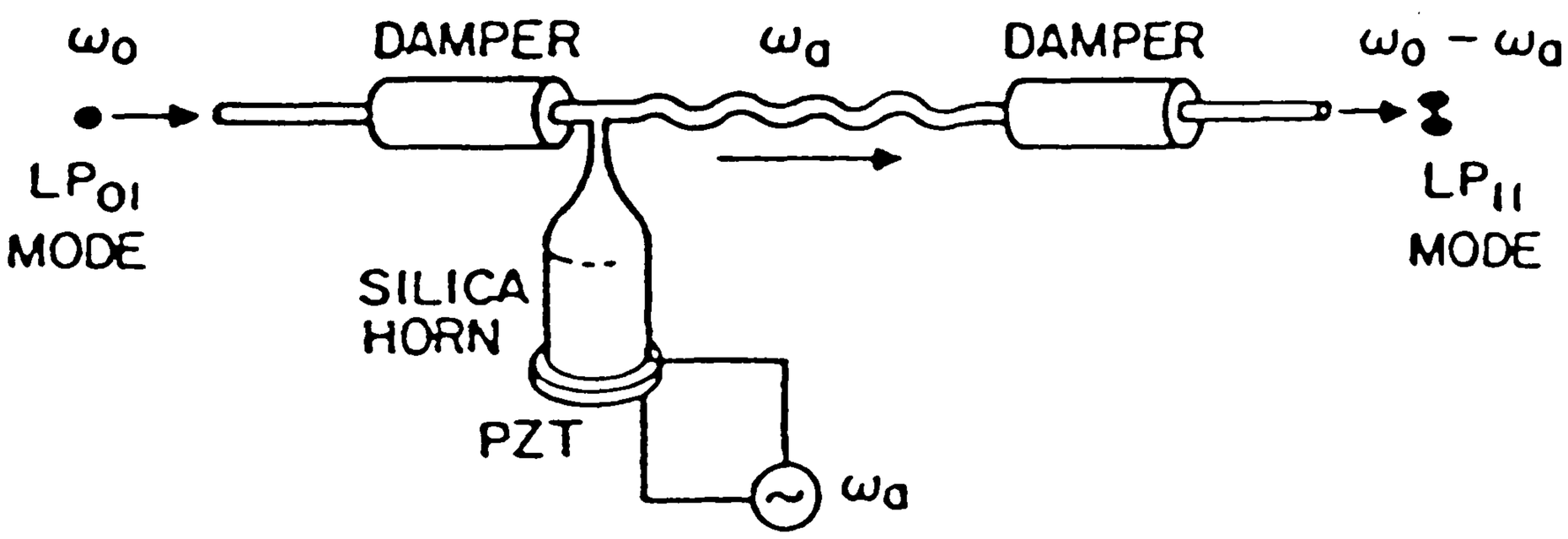

(b)

Fig. 3.12. (a) Schematic diagram of fibre optic frequency shifter with mode filters and a travelling acoustic flexural wave excited by an acoustic horn. (b) Frequency shifting in a double-mode fibre using intermodal coupling by an acoustic flexural wave excited by an acoustic horn.

direct fusion. To prevent the acoustic wave from travelling in both directions and to limit the acousto-optic interaction length, acoustic dampers were used, as shown in figure 3.12(b).

Now consider an optical input from the single mode fibre that is spliced to the double mode fibre (left hand side of figure 3.12(a)). By aligning the centres of the two cores, one can excite mostly the LP_{01} mode in the double mode fibre. The small amount of excited LP_{11} mode will be suppressed further by the mode stripper so that only the LP_{01} mode enters the interaction region. Because of the microbending that is travelling along the fibre in the same direction as the optical wave, optical energy is coupled to the LP_{11} mode and its frequency is downshifted by the acoustic frequency. The optical signal that has not coupled and retains the original frequency will not be coupled to the single mode fibre when it arrives at the directional coupler on the right hand side of figure 3.12(a). Therefore the light that is tapped into the single mode fibre contains only the shifted frequency component. The same effect will be achieved for an optical input from the single mode fibre that is coupled to the double mode fibre through the directional coupler on the right hand side of figure 3.12(a), making this frequency shifter a reciprocal device. Only the LP_{11} mode will be excited in the double mode fibre, and it will be coupled to the LP_{01} mode and downshifted in frequency as it interacts with the acoustic flexural wave that is travelling in the opposite direction to the optical wave. The unshifted frequency component in the LP_{11} mode will be attenuated by the single mode stripper. Therefore the optical signal that is coupled into the single mode fibre at the left contains only the frequency shifted component.

In this experiment the optical source wavelength was 488 nm. The acoustic frequency that produced the maximum inter mode coupling was about 8 MHz. At this frequency, a coupling efficiency of ~100% was achieved with about 0.25 W of electric power applied to the PZT. The LP_{01} mode stripper did not

efficiently discriminate the shifted frequency component from the unshifted one. This resulted in a poor optical carrier suppression because the two modes were mixed at the splice. Sideband suppression of about 35dB and carrier suppression of about 15dB were achieved. Most of the error originated from the imperfect mode filters.

Pannell *et al* [2] developed a frequency shifter using a birefringent fibre, to overcome this problem such that the flexure wave couples between the linear polarisation eigenmodes. A schematic diagram of this frequency shifter is shown in fig. 3.13.

A ceramic disc of resonant frequency 760 kHz was bonded with a thin film of araldite to a silica matching horn. A signal generator was used to drive the PZT. To obtain the most efficient mode coupling, the polarisation plane of the acoustic flexure devices was orientated at 45° to the fibre eigenaxes. The horn tip was bonded at 90° to the fibre. The interaction region was limited in extent at either end by leaving a plastic buffer coat of the fibre in place to act as an absorbing barrier.

The efficiency of the frequency shifter was 2% with an input of 150 mW. At higher powers spurious phase modulation appeared. It seems that in any fibre frequency shifter that relies for its operation on mechanical agitation of the fibre, phase modulation will inevitably be produced. This imposed a fundamental limit on the spectral purity of the output obtainable from such a device.

Patterson *et al* [60] developed a SAW horn which provides a more robust acoustic source. The horn is shown in fig 3.14. It consists of a fused quartz

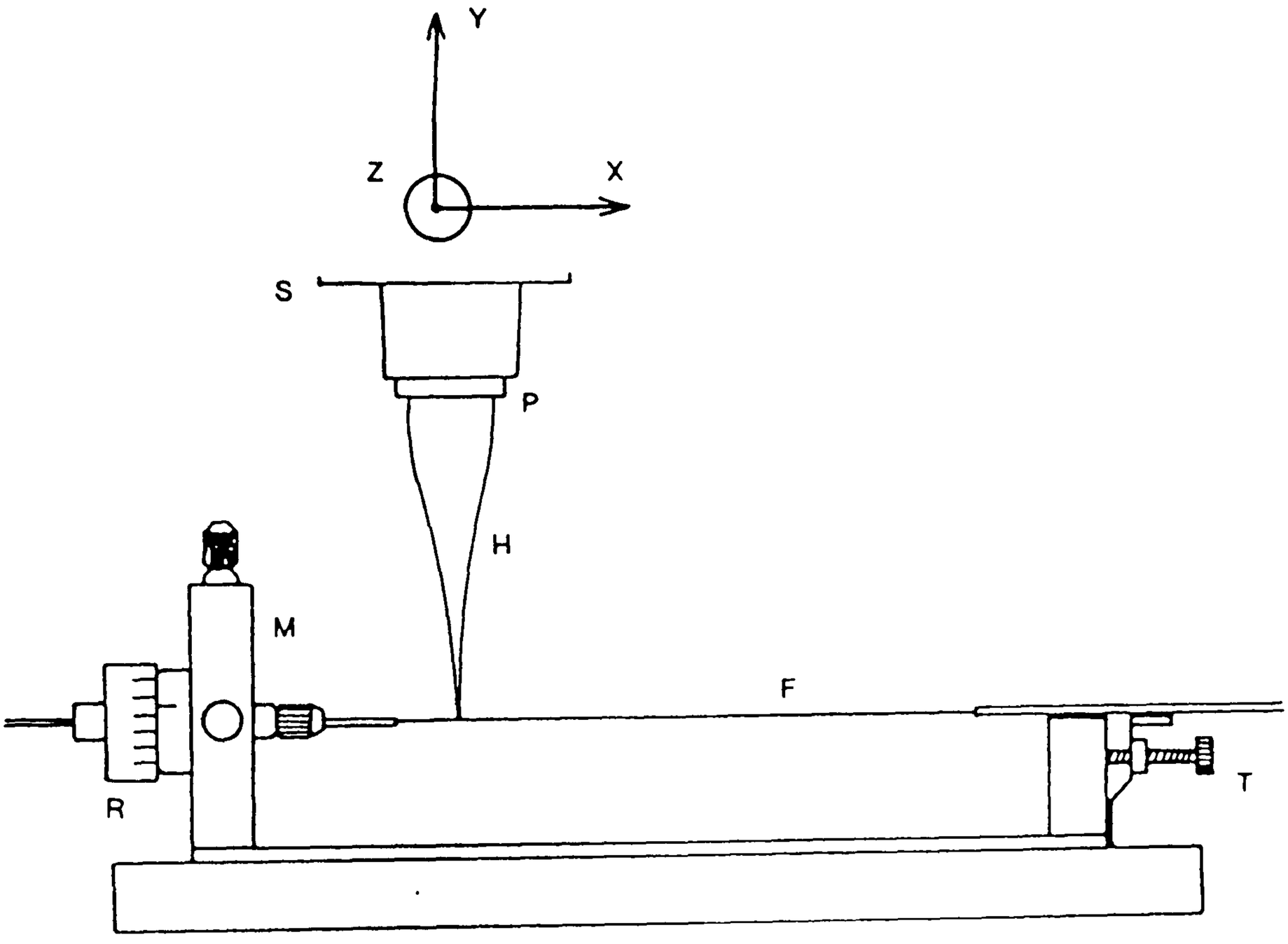

Fig. 3.13. Frequency shifter based on travelling flexure waves.
H: horn; P: PZT; R: rotating fibre chuck; S: x y z translation stage;
T: fibre tensioning screw and spring; F: fibre.

cylinder, which has been lapped and polished to a 150 micron tip with a 45° taper. An edge-bonded PZT transducer excites surface acoustic waves which are focused to the tip, where a dual mode optical fibre was bonded.

A cascaded acoustic configuration was used as demonstrated recently by Askautrud *et al* [61] as shown in fig 3.15. A backward propagating wave was used for LP_{01} to LP_{11} conversion with a frequency upshift. A forward wave, excited by the same acoustic source, subsequently converted LP_{11} to LP_{01}, again with a frequency upshift. In order to obtain a pure frequency shift with high sideband suppression, mode filters were used at the device input and output. These ensured upper and lower sidebands will be produced by either a forward or backward acoustic wave. But if only one mode is present, each acoustic interaction produces either an upshift or a downshift, not both. An output filter was then used to remove any uncoupled power which contains energy at the input carrier frequency.

The cascade interaction simplifies the mode filter requirements, since only an LP_{11} mode stripping filter is needed at both input and output. In frequency shifters previously discussed, LP_{11} mode strippers have been fabricated by simply winding the optical fibre in a tight coil. For a sufficiently small radius of curvature, the more weakly guided LP_{11} mode is radiated into the cladding while the LP_{01} is transmitted with negligible loss.

In the same paper [61] a new type of optical mode filter was presented which provided over 30dB of LP_{11} suppression. This filter consisted of a region of fibre which was etched or polished to very near the fibre core. Here the evanescent cladding fields were appreciable at the interface and interacted with a medium placed at the interface. The refractive index of the material was lower than the effective index of the LP_{01} mode, but higher than the effective

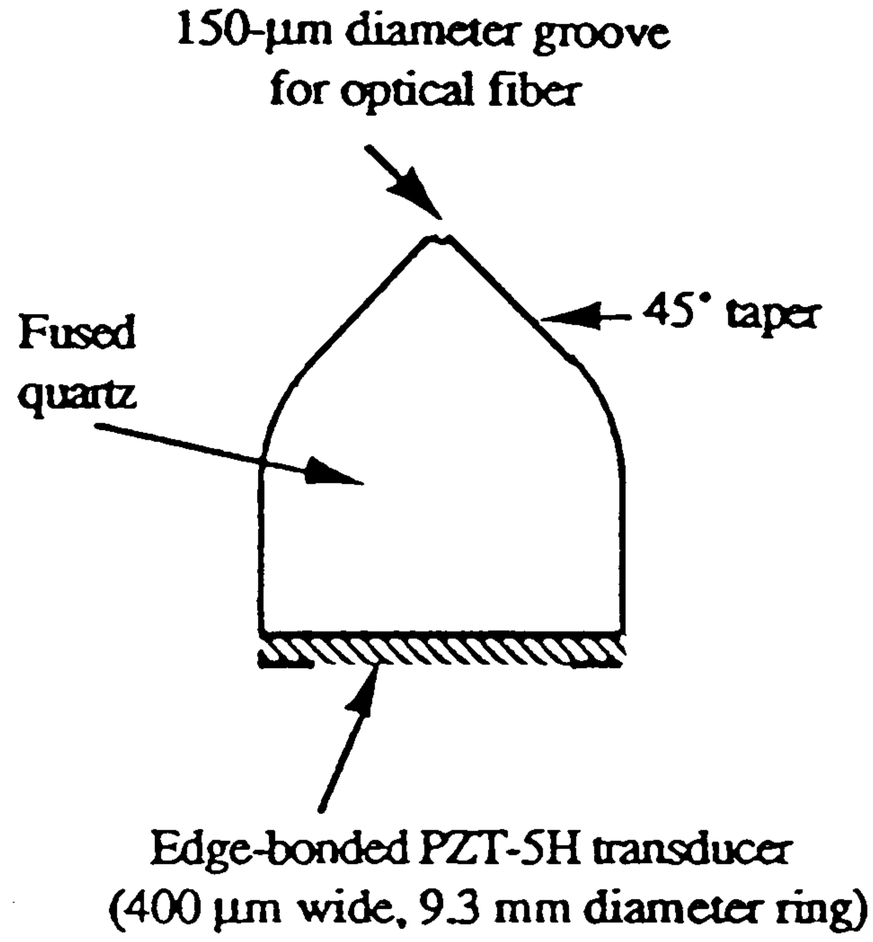

Fig. 3.14. The surface acoustic wave horn.

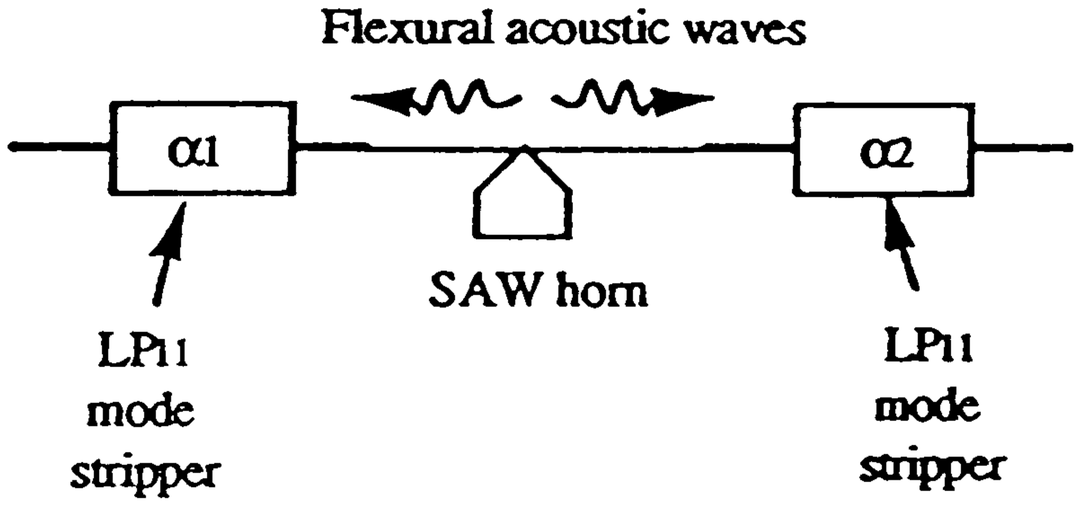

Fig. 3.15. Frequency shifter based on travelling flexural waves.

index of the LP_{11} mode, so that the former remains guided while the latter is radiated into the medium.

The frequency shifter was constructed from an elliptical core dual mode fibre (at 1.3 microns) using the coiled mode strippers as input and output LP_{11} filters 35dB spurious signal suppression was observed. The applied RF power was 250 mW at an acoustic frequency of 3.15 MHz. The evanescent coupled LP_{11} filter as the output filter in the similar experiment, gave 35dB suppression with 400mW of applied power.

3.5 DUAL CORE FIBRE DEVICES

In the group of devices just discussed, most of the time it is difficult to excite just one normal mode, and a frequency shifted signal in the LP_{11} mode is not appropriate for efficient pigtailing to single mode fibre. These problems are compounded by the fact that slight errors in the launching condition produce a mixture of both normal modes resulting in an intermodal interference.

To avoid these problem dual core devices have been developed by permitting low loss fusion splicing of single mode fibres to either core and have negligible intrinsic coupling [62]. This was achieved by designing the fibre such that the phase velocities in the two cores were mimatched.

The dual core fibre was fabricated in such a way that one core was arranged to be eccentric, and the other centrally for ease of splicing to standard single mode fibres. Two different dual core fibres, DC1 and DC2, were designed at $\lambda = 1$ micron. To set up the frequency shifter, a length of dual core fibre was

stripped of its coating and place in rotating clamps to permit elimination of any twist and precise alignment of the two cores in the plane containing the horn axis. The fibre was then bonded to a silica horn, itself mounted on a piezo element designed to be resonant in the desired frequency range.

A matching network was used for efficient coupling conversion of electrical energy into acoustic as shown in fig 3.16. 780 nm light was delivered to the sensing fibre via a 3dB fused coupler, and the reflected signal detected at a Si photodiode.

In this configuration of frequency shifter, two different phenomena contributed to acousto-optic coupling constant; the first was microbending and the second strain optical effects. The intrinsic coupling in DC1 was too small to measure with this setup, and 8.5% acousto-optical coupling was obtained at 4.6MHz and 962.5 nm. DC2's intrinsic coupling was around 3%, and 100% acousto-optical coupling was achieved at 56kHz. The electrical driving power at 100% coupling was around 200mW.

Another type of frequency shifter was proposed by Chu *et al* [63]. They proposed to use a twin core fibre excited by an acoustic wave at frequency ω_2. The incident optical signal of frequency ω_1 is launched into core 1 (see fig. 3.17). The frequency shifted signal at ω_2 will emerge from core 2 after a length *L*. In this paper, the theory of the frequency shifter was explained and an approximate design formula for the required shifter length was given. The approach adopted for a frequency shifter design is summarised below. Consider a fibre consisting of two pulled cores as shown in figure 3.17. These cores couple power among themselves owing to the presence of an evanescent field. However, the amount of power transfer is negligible when the cores differ only slightly from each other in the refractive indices. The theory of this is discussed elsewhere [30]. This property was used to remove any

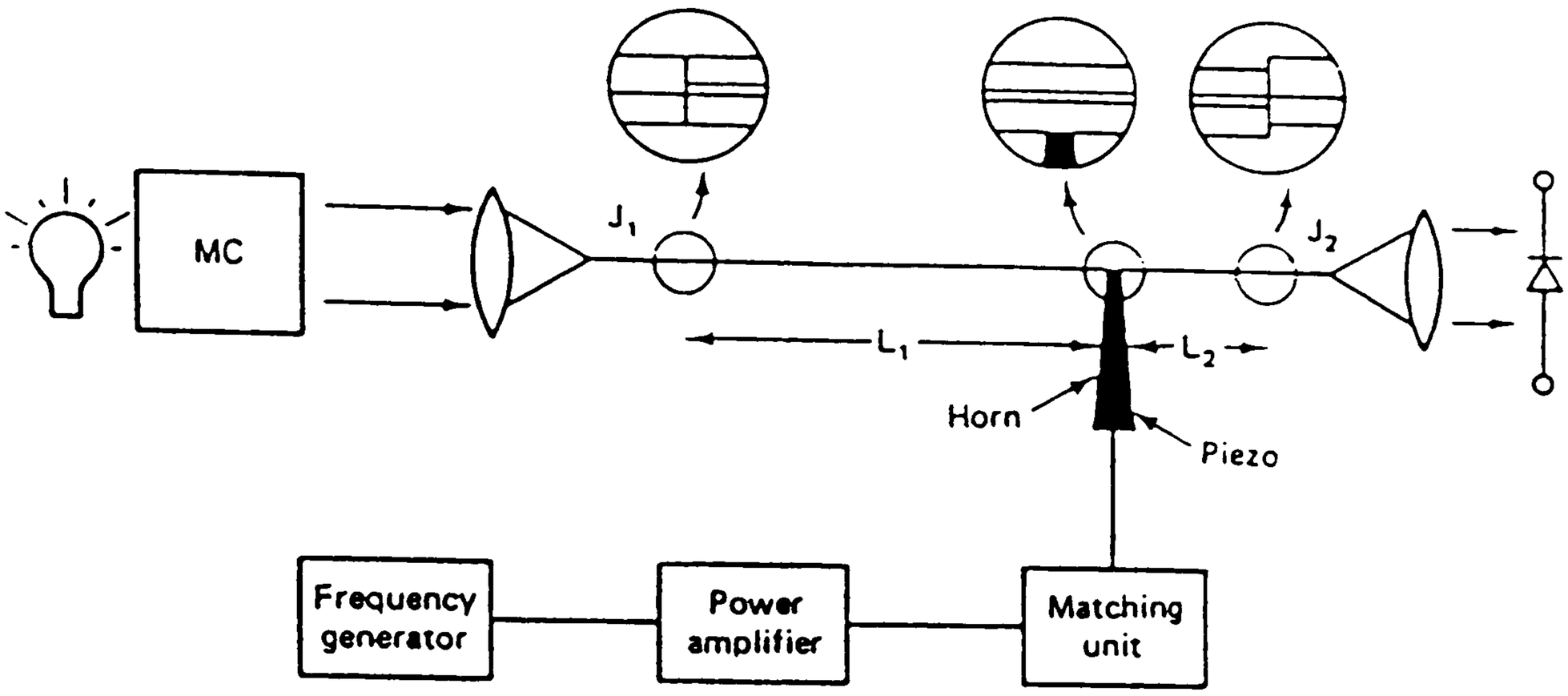

Fig. 3. 16. Experimental set-up for a dual core fibre frequency shifter. A lamp plus monochromator (MC) are used to supply wavelength tunable light. The dual core fibre is spliced to single core fibre at joints J1 & J2.

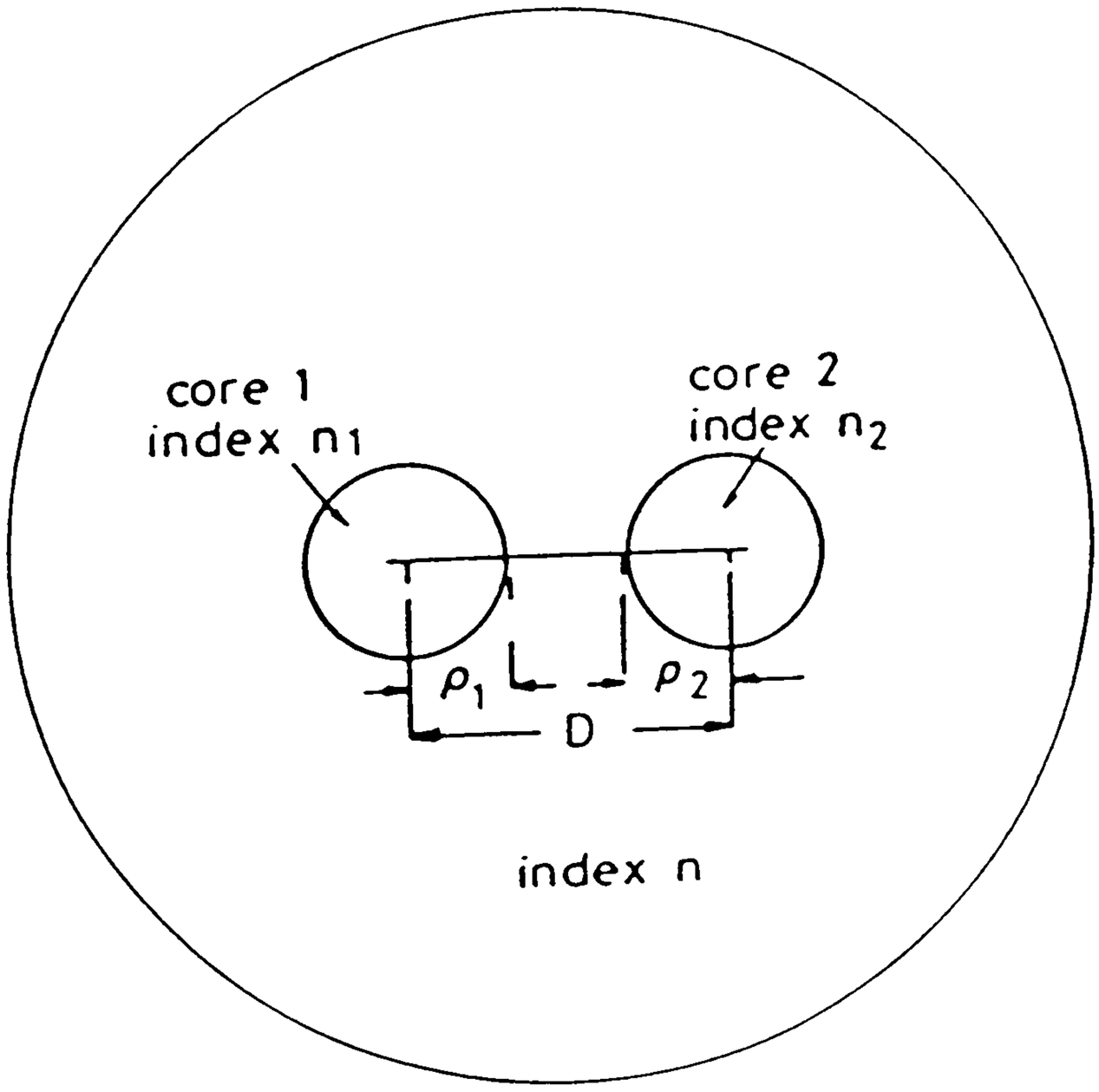

Fig. 3.17. Cross-section of a twin-core fibre. Cores differ from each other in their refractive indices (n_1 , n_2) and radii (ρ_1 , ρ_2).

coupling so that the cores act as independent channels.

The light in core 1 has propagation constant β and frequency ω_1 and light in core 2 has β_2 and ω_2. Now an acoustic wave of longitudinal LP_{01} mode can be launched into the fibre by a cylindrical PZT resonator sleeved on to the fibre. Provided that the acoustic wavelength is larger than the overall diameter of the fibre, the acoustic wave creates a periodic perturbation in the refractive index along the length of the fibre and throughout the fibre cross section.

3.6 FREQUENCY SHIFTERS BASED ON STIMULATED BRILLOUIN SCATTERING

Theoretically the devices discussed in the previous sections offer promise, but in practice it is quite difficult to produce a device that operates with reasonable efficiency, good sideband suppression, low power consumption and is mechanically rugged; these devices generally require several Watts or hundreds of milli Watts of electrical input power. Situation can be improved if the acoustic wave is generated within the fibre as we have seen that in previously discussed devices the main problem comes from the difficulty to efficiently couple acoustic wave to the optical fibre and produce a travelling wave. Difficulty is experienced in preventing reflections of the acoustic wave along the fibre which results in a standing wave and as a result both upshifted and down shifted sidebands. Suppression of unshifted light (see figure 3.2) is also generally difficult. About twenty years ago it was realised that higher input powers launched into the fibre can cause strong frequency conversion, optical gain, and many other nonlinear effects, generally associated with strong optical intensities and highly nonlinear materials. One of these effects is stimulated

Brillouin scattering (SBS) [64-66] which is the basis of recently reported frequency shifters. The main advantage of this technique is that the acoustic waves are produced within the fibre. SBS can be described as a parametric interaction among the pump wave, the backscattered Stokes wave, and an acoustic wave. The pump wave generates an acoustic wave through the process of electrostriction [67] (the electric field induced mechanical strain on a medium) which in turn causes a periodic modulation of the refractive index. The pump induced refractive index grating scatters the pump light through Bragg diffraction. This scattered light wave is Doppler shifted to a frequency which is slightly different from pump frequency since the acoustic wave acts as a moving diffraction grating. SBS will be discussed in more detail in chapter 4.

It is important to note here that unlike all other previously discussed techniques in this chapter, no external modulator is required to generate acoustic waves and therefore a more robust frequency shifter is, in principle, possible. Theoretical analysis regarding the rate of growth of SBS along the fibre, given by C. L. Tang [68] shows that the SBS frequency shift is inversely proportional to the pump wavelength. This assumption is in good agreement with experimental results with frequency of the shifted beam υ_{SBS} ~ 13GHz for λ_p = 1.3μm [69], υ_{SBS} ~ 27GHz for λ_p= 632.8nm [70] and υ_{SBS} ~ 34GHz for λ_p= 514.5nm [71], where λ_p is the wavelength of the input (pump) light. Although in principle this frequency shift could be used directly for heterodyne signal processing in practice it is still too high for relatively simple electronic demodulation techniques, generally required in fibre optic sensor technology. A lower frequency, in the vicinity of 15MHz can be obtained by mixing two, slightly different frequencies.

Initial approaches used long lengths of fibre, typically hundreds of meters, and Argon ion laser sources as pump with tens to hundred of milliwatts to produce significant conversion. D. Culverhouse *et al* [72] used two 500m reels of single mode fibre with slightly different refractive indices. The beat frequency was dependent on the refractive index difference between the two different optical fibres used in the experiment. The light source was a single frequency Argon ion laser operating at 514.5nm. The SBS produced from the two fibres was mixed on a high speed detector and analyzed with an electronic spectrum analyzer. A beat frequency at 754MHz was obtained. As two separate fibres were used the beat frequency is very dependent on the relative temperature of the two reels; the beat frequency was found to vary by ~4MHzK^{-1}. This temperature dependency can cause problems. If a stable carrier, independent of the environmental perturbations, is required then the temperature difference between the two fibres would have to be maintained to better than $\pm$ 0.1K.

A single fibre frequency shifter that reduces the frequency shift to ~10MHz and offers simpler implementation and greater stability of the carrier frequency to environmental disturbances was demonstrated by C. Duffy *et al* [73-75]. The beat frequency is obtained by mixing two SBS signals generated along the fast and slow eigenmodes of highly birefringent optical fibre.

In this configuration using an 800m reel of EOTec elliptical clad birefringent fibre, with loss 14.3dBkm^{-1}, an SBS onset threshold of 24mW for 514.5nm pump light from a single frequency Argon ion laser was obtained. The maximum conversion efficiency was 41% for 110mW of launched optical power. The beat frequency was observed on a spectrum analyzer. When two signals were mixed together a beat frequency at 10.6MHz was obtained. The carrier was modulated about its mean value by $\pm$ 8MHz.

3.6.1 LIMITATIONS

Techniques discussed in this section offer some obvious advantages over devices discussed in sections 2.3-2.5. For example no electrical power is required to produce the acoustic wave. Still there are some limitations in using these techniques. In addition to the unstable nature of the output, long lengths of the fibre and relatively high input optical powers to generate SBS (i.e., higher cost and large bulky equipment), are two major problems. These factors severely affect the commercial and industrial feasibility of the devices. The necessity of cooling high power lasers and the requirement for three phase high electrical input powers further complicate the situation.

Table 3.1 summarises some of the important results of the research work done to date, in an effort to develop a fibre optic frequency shifter.

3.6.2 THE SOLUTION

These problems can be overcome by using fibre ring resonator configuration [76] where at resonance all the optical power recirculates in the ring. Submilliwatts of SBS thresholds have been demonstrated for these systems [77, 78]. The ring resonator will be discussed in detail in chapter in chapter 4.

Reference	Classification	Applied Power	Efficiency	Sideband Supp..	Carrier Supp.
Risk *et al*	SAW	5 W	10%	30 dB	
Risk *et al*	SAW	2.25 W	1%		
Risk *et al*	SAW	25 W	95%	40 dB	25 dB
Risk *et al*	SAW	32 W	26%	24 dB	
Greenhal-gh *et al*	SAW	1.9 W	4.1 %	38 dB	29 dB
Greenhal-gh *et al*	SAW	1.9 W	4-15% *		
Greenhal-gh *et al*	SAW	6.5 W	25%		
Foord *et al*	SAW		92% *		25 dB
Kim *et al*	FW	0.25 W	100%	35 dB	15 dB
Pannell *et al*	FW	150 mW	2%		
Duffy *et al*	SBS	110mW (optical) †	41%		

Table 3.1 Summary of the results of research on frequency shifters.
* Theoretical. † Zero electrical power

3.7 CONCLUSIONS

A brief review of fibre optic frequency shifters developed to date has been presented. After describing the basic principle of operation and theory behind these devices, different configurations, i.e., SAW devices, flexure wave devices, dual core fibre devices, and devices based on SBS and their advantages and limitations were discussed.

The technique that we have developed is based on the principle of mixing two SBS signals which have slightly different frequencies generated in optical fibre ring resonators. The advantage of using a ring resonator is that SBS can be generated using optical input powers less than 10 μW in short lengths of fibre.

CHAPTER FOUR

STIMULATED BRILLOUIN SCATTERING IN OPTICAL FIBRE RING RESONATORS

4.1 INTRODUCTION

This chapter discusses the generation of stimulated Brillouin scattering in optical fibre ring resonators. It can be divided into two major sections. The first section describes the constrution, properties and theory behind the operation of the ring resonator. The relation between the input and output intensities is derived. The second part of the chapter explains the production of stimulated Brillouin scattering, first in straight lengths of the fibre and then in ring resonators incorporating dependence of SBS threshold on resonator finesse.

4.2 OPTICAL FIBRE RING RESONATOR

The optical fibre ring resonator is a multiple beam interferometer. It consists

of a length of fibre forming a ring through a polished coupler as shown in figure 4.1.The device is a resonant ring cavity in which an optical signal traverses a closed fibre loop. When the round trip path length of this interferometer equals an integer number of optical wavelengths, constructive interference leads to a build up of the optical intensity inside the optical cavity, and a concurrent decrease in the intensity at the output port. Under appropriate conditions there is zero transmitted power at the output and all the optical power circulates in the ring; this is called the resonance condition.

Although Shupe [79] was the first to describe the optical fibre ring resonator the first comprehensive theoretical and experimental analysis was presented by Stokes *et al* [80]. There are many features of the ring resonator, e.g., high finesse and ease of operation, that have attracted a large number of researchers but the one which is the most important in this project is the large enhancement of circulating power at resonance that makes the resonator appealing for the study and applications of nonlinear phenomena. These effects can be created in the ring at submilliwatt input powers [78]. The power enhancement allows the onset of stimulated Brillouin scattering at input power levels as low as 3 μW [81].

4.2.1 FABRICATION

Single mode optical fibre can be used to make a high-finesse optical resonator by forming a short piece of fibre into a closed ring to constitute a low loss cavity. The choice of fibre for the fabrication of the ring resonator is typically determined by the fibre loss and system application. The coupler used to fabricate the resonator can be either polished, fused, or etched. Whilst fused couplers are quick to make and have good stability, polished fibre couplers are

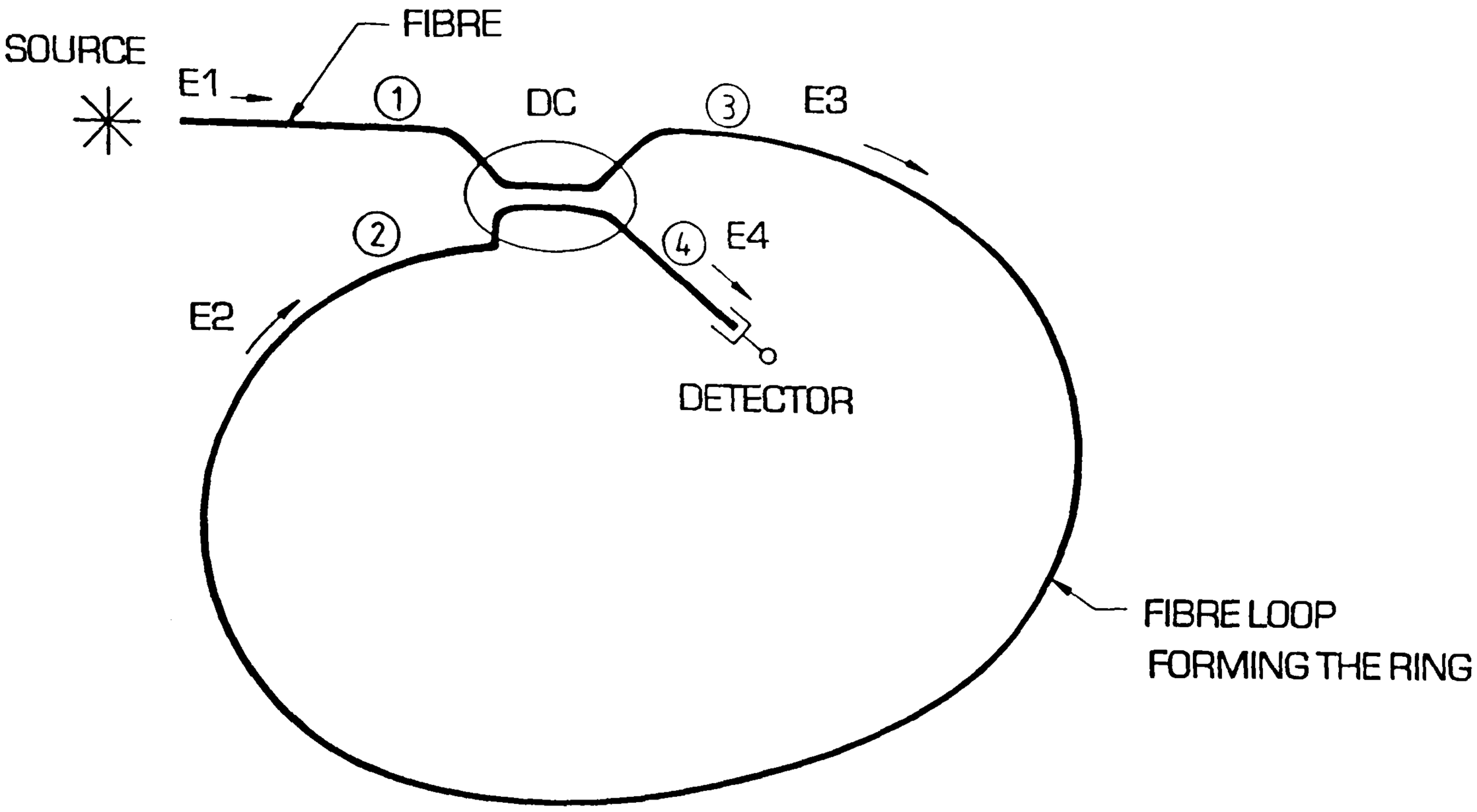

FIG. 4.1 THE FIBRE OPTIC RING RESONATOR

DC: DIRECTIONAL COUPLER

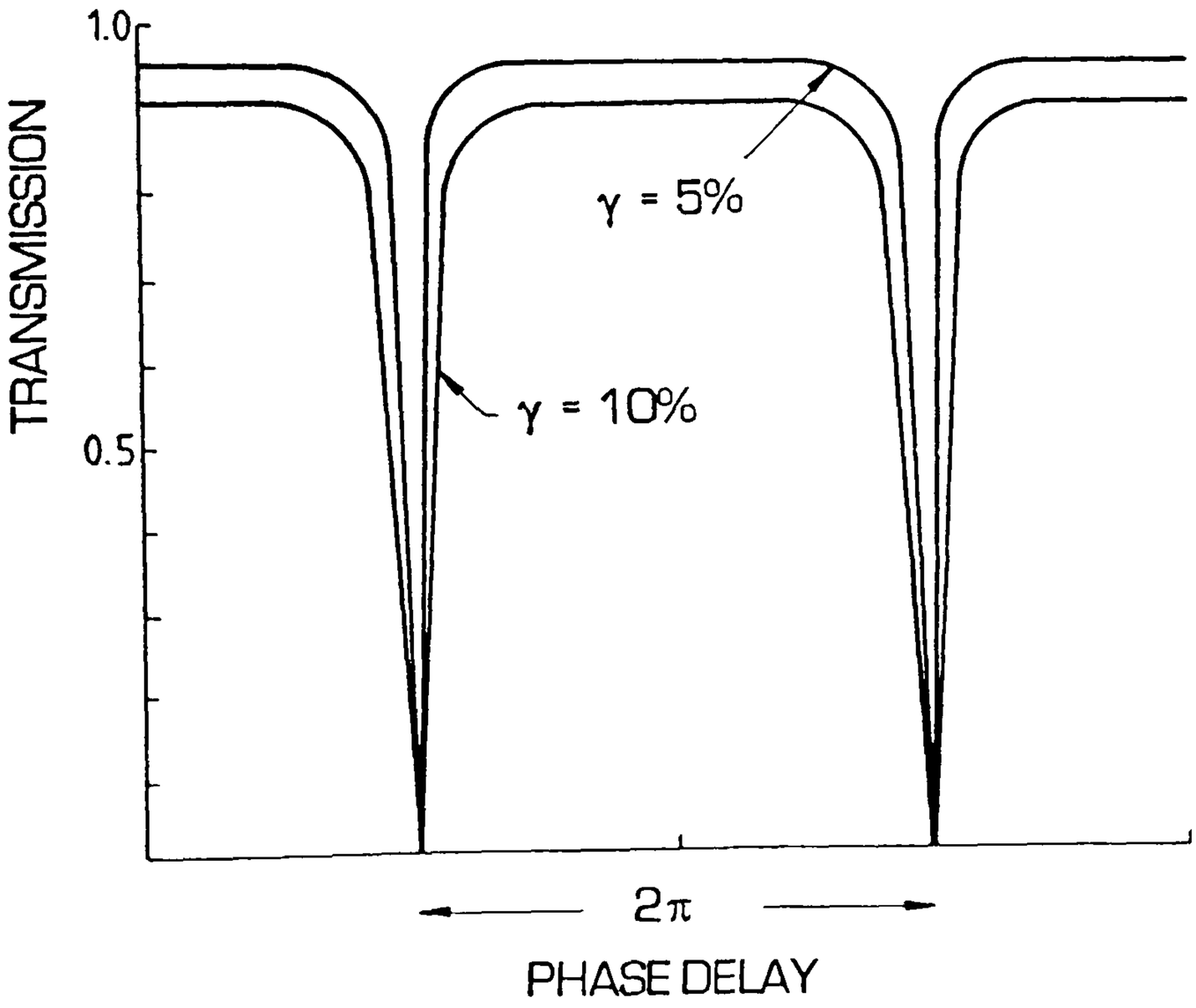

FIG. 4.2 TRANSFER FUNCTION OF RING RESONATOR

preferable in fibre resonators because of their variable coupling constant, and to date better polarization isolation [82]. Each half of the directional coupler (Chapter 2) is fabricated on the same strand of optical fibre, spaced a distance *L* apart. Placing the two halves together to form a coupler, with the polarization axes perfectly aligned along the interaction region, produces a ring resonator. Two different types of ring resonator, fabricated from low and high birefringent fibre, are used for this research work. Polarization axes alignment for the formation of the high birefringent fibre directional coupler is one of the important tasks, as slight misalignment can affect the polarization isolation.

4.2.2 OPERATION

When the ring resonator is illuminated by a laser, light entering the coupler at port 1 propagates partially to the output port, port 4, and partially to port 3, circulates in the ring, and reenters the coupler at port 2. It once again splits to port 3 and 4 and recirculates in the loop.

In the hi-bi fibre ring, the resonant eigenstates correspond to the two orthogonal (fast and slow) polarization axes of the fibre. The incident polarized light is projected onto these two linearly polarized eigenstates, and each eigenstate independently generates its own resonance characteristics. The phase separation between the resonances formed is a direct function of the fibre birefringence. In an ideal situation, by launching into only one fibre axis a stable resonance response corresponding only to that eigenstate is formed. In practice ring resonator performance deviates significantly from that of the ideal case. A finite amount of cross coupling always occurs, primarily due to the unavoidable slight misalignment of the fibre axes at the coupler and also

to a much lesser extent because of deformations and scattering in the fibre loop. The intensity coupling and attenuation constant may also in general be slightly different for each birefringent axes. Coupler tuning is accomplished by sliding one block over the other to vary the core-to-core separation and interaction length and thus optimise the coupling coefficient as shown in figure 2.10

PHASE MODULATION: The operation of the optical fibre ring resonator is related to phase modulation in the fibre ring, which is used to control its phase delay and consequently its transmission characteristics. A small length of the fibre forming the ring is wrapped around a piezoelectric modulator and a ramp voltage signal is induced to vary the phase of the light in the ring. Figure 4.2 shows a typical intensity transmission of the ring resonator as a function of the fibre ring phase delay, βL, for different values of intensity loss coefficient γ_o. Whenever this phase delay attains the value of $2m\pi$, where m is an integer, a sharp minima occurs which is due to all the circulating beams mixing in phase in the ring. This gives rise to the build up of a high circulating intensity in the cavity, while destructive interference takes place in the output port 4 producing the characteristic resonance notch. Consider the case when the fibre loop length is adjusted for constructive interference between coherent components entering port 3 from port 1 and 2. The small fraction of light from port 2 to port 4 will destructively interfere with the light coupling from port 1 and to port 4. With an optimum value of coupling which depends on losses, the two destructively interfering components exiting port 4 are equal in amplitude and completely cancel. The reason for this destructive interference is the differential phase shift of $\pi/2$ (induced when light couples from one waveguide to the other) between the circulating and directly coupled components.

From an energy conservation point of view, the circulating power grows until

the power dissipated by losses in the loop equals the input power at port 1. With the PZT connected to a signal generator, the power emerging from port 4 will show a series of sharp minima whenever the input optical frequency matches the resonant condition. The behaviour is similar to a Fabry-Perot type resonator with the difference that the transfer function consists of a series of transmission dips instead of peaks, as shown in figure 4.2. When used for non-linear applications, the operating point of the ring resonator is locked on the point of maximum slope or (as in our case) the resonant point. A feedback control system is used to compensate for ring phase variations created by unwanted perturbations such as thermal drifts. A long coherence length laser source must excite the ring (as explained in chapter 2) in order to produce the interference effects.

FINESSE: One of the most important parameters which provides a direct measure of the quality of the ring resonator is the finesse, *F*, which depends on the cavity loss and coupler coupling constant, defined as:

$$F = \frac{FSR}{\Delta f} = \frac{c}{nL\Delta f} \tag{4.1}$$

where *FSR* is the free spectral range of the cavity (i.e. the frequency spacing between two adjacent resonant modes), Δf is measured as the full width at half minimum of a resonance notch, c is the velocity of light and n is the effective refractive index of the fibre.

4.3 THEORETICAL CONSIDERATION

Let us consider a resonator having a fibre loop length L, characterized by an amplitude attenuation coefficient, α_o. Let K be the intensity coupling coefficient between the two fibres in the coupler and γ_o, the intensity loss coefficient. In order to get an expression for ring resonator response we apply the

conservation of energy principle to the coupler to obtain the following relation [78]:

$$|E_3|^2 + |E_4|^2 = (1-\gamma_o)\ (\ |E_1|^2 + |E_2|^2\ ) \qquad (4.2)$$

where E_i is the electric field at *ith* port. The output electric field amplitudes in the fibre, after the coupled-mode interaction are related to incident fields by:

$$E_3 = (1-\gamma_o)^{1/2}\ [\ (1-K)^{1/2} E_1 + j\sqrt{K}\, E_2] \qquad (4.3)$$

$$E_4 = (1-\gamma_o)^{1/2}\ [j\sqrt{K}\, E_1 + (1-K)^{1/2} E_2] \qquad (4.4)$$

The phase of the light in port 4 is greater than in port 3 by $\pi/2$ rad as indicated by the *j* factor in the expression for E_4 . E_4 is lagging E_3 in time. Physically, the coupling of power from guide 1 to guide 2 occurs because the evanescent electric field in guide 1 induces a linear polarization in guide 2 at the optical frequency in phase with that field in guide 1. This polarization generates an electromagnetic wave in guide 2 that lags this polarization in time. The driving polarization and driven field in guide 2 have the proper phase relationship for power exchange from the induced polarization to the field.

If we take account of the attenuation loss in the fibre, E_2 and E_3 can be related as :

$$E_2 = E_3\, e^{j\beta L} e^{-\alpha_o L} \qquad , \beta = n\frac{\omega}{c} \qquad (4.5)$$

where α_o is the amplitude attenuation constant of the fibre, L is the length of fibre ring and ω is the optical frequency.

Putting the value of E_2 in eq. 4.3:

$$E_3 = \sqrt{1-\gamma_o}\,[\sqrt{1-K}E_1 + j\sqrt{K}E_3\, e^{-\alpha_o L} e^{j\beta L}] \tag{4.6}$$

$$E_3 - E_3\sqrt{1-\gamma_o}\, j\sqrt{K}\, e^{-\alpha_o L} e^{j\beta L} = \sqrt{1-\gamma_o}\sqrt{1-K}\; E_1 \tag{4.7}$$

$$\frac{E_3}{E_1} = \frac{\sqrt{1-\gamma_o}\sqrt{1-K}}{1-\sqrt{1-\gamma_o}\, j\sqrt{K}\, e^{-\alpha_o L} e^{j\beta L}} \tag{4.8}$$

The above equation gives the output intensity relative to the input field E_1.

Now squaring both sides of the equation and using some complex number identities (see appendix A):

$$\left|\frac{E_3}{E_1}\right|^2 = \frac{(1-\gamma_o)\,(1-K)}{1+K(1-\gamma_o)\, e^{-2\alpha_o L} + 2\sqrt{K}\,\sqrt{1-\gamma_o}\, e^{-\alpha_o L} \sin\beta L} \tag{4.9}$$

Eq.(4.9) gives the circulating intensity in the ring.

As $\sin\beta L = -\cos(\beta L + \pi/2) = 2\sin^2(\beta L/2 + \pi/4) - 1$

therefore:

$$\left|\frac{E_3}{E_1}\right|^2 = \frac{(1-\gamma_o)\,(1-K)}{(\sqrt{K}\sqrt{1-\gamma_o}\, e^{-2\alpha_o L})^2 + 4\sqrt{K}\,\sqrt{1-\gamma_o}\, e^{-\alpha_o L} Sin^2\left(\frac{\beta L}{2} + \frac{\pi}{4}\right)} \tag{4.10}$$

Now we can calculate the transfer function of the ring resonator for resonant

coupling. Putting the value of E_2 from eq. (4.5) into eq. (4.4) gives the output field at port 4 as:

$$E_4 = \sqrt{1-\gamma_o}\,[\,j\sqrt{K}\,E_1 + \sqrt{1-K}\,E_3\,e^{-\alpha_o L}\,e^{j\beta L}] \qquad (4.11)$$

Now from eq.(4.8) and eq(4.11):

$$\frac{E_4}{E_1} = \sqrt{1-\gamma_o}\,[j\sqrt{K} + \frac{\sqrt{1-K}\sqrt{1-\gamma_o}\,e^{-\alpha_o L}e^{j\beta L}}{1-j\sqrt{K}\sqrt{1-\gamma_o}\,e^{-\alpha_o L}e^{j\beta L}}] \qquad (4.12)$$

At resonance i.e. when all the optical power is circulating in the ring the output field E_4 will be zero:

$$0 = j\sqrt{K} + \frac{(1-K)\sqrt{1-\gamma_o}\,e^{-\alpha_o L}e^{j\beta L}}{1-j\sqrt{K}\sqrt{1-\gamma_o}\,e^{-\alpha_o L}e^{j\beta L}} \qquad (4.13)$$

$$j\sqrt{K}+K\sqrt{1-\gamma_o}e^{-\alpha_o L}Cos\beta L+jK\sqrt{1-\gamma_o}Sin\beta L e^{-\alpha_o L}+(1-K)\sqrt{1-\gamma_o}e^{-\alpha_o L}Cos\beta L$$

$$+j(1-K)\sqrt{1-\gamma_o}e^{-\alpha_o L}Sin\beta L=0 \qquad (4.14)$$

The real part gives $Cos\ \beta L = 0$, or $Sin\ \beta L = \pm 1$.

The imaginary part gives:

$$\sqrt{K}+K\sqrt{1-\gamma_o}e^{-\alpha_o L}Sin\beta L=0 \qquad (4.14.a)$$

Because K, γ_o, and $e^{-\alpha oL}$ are all positive quantities, the imaginary part of eq.(4.14) only allows $Sin\ \beta L = -1$

Using $Sin\beta L = -1$ the imaginary part of eq.(4.14) requires that the coupling constant has a certain value for resonance (at $E_4 = 0$) denoted by K_r (i.e. at resonance $K = K_r$).

∴ Eq. 4.14(a) can be written as:

$$\sqrt{K_r} + K_r\sqrt{1-\gamma_o}\, e^{-\alpha_o L} Sin\beta L = 0 \qquad (4.14.b)$$

Putting the value of *Sin* βl gives:

$$K_r = (1-\gamma_o)\, e^{-2\alpha_o L} \qquad (4.15)$$

It is important to mention here that for a low-loss cavity (i.e. round trip loss of few percent) the value of K_r is close to unity. For coupling constant values different than the above the resonance depth decreases together with the circulating power.

Replacing *K* with resonant value of coupling the circulating intensity (eq.14.10) becomes:

$$\left|\frac{E_3}{E_1}\right|^2 = \frac{(1-\gamma_o)\,(1-K_r)}{(1-K_r)^2 + 4K_r Sin^2(\beta L/2 + \pi/4)} \qquad (4.16)$$

which is the ratio of the circulating intensity to the input intensity.

OUTPUT INTENSITY: Squaring both sides of eq.(4.12) and using eqs.(4.2), (4.5), (4.15) and (4.16) give the output intensity with resonant coupling constant K_r (see appendix A):

$$\left|\frac{E_4}{E_1}\right|^2 = (1-\gamma_o)\left[1 - \frac{(1-K_r)^2}{(1-K_r)^2 + 4K_r\, Sin^2\left(\frac{\beta L}{2} + \frac{\pi}{4}\right)}\right] \qquad (4.17)$$

$$\left|\frac{E_4}{E_1}\right|^2 = \frac{(1-\gamma_o)\, 4K_r\, Sin^2\left(\frac{\beta L}{2} + \frac{\pi}{4}\right)}{(1-Kr)^2 + 4K_r\, Sin^2\left(\frac{\beta L}{2} + \frac{\pi}{4}\right)} \qquad (4.18)$$

CAVITY FINESSE: An expression for the cavity finesse incorporating the resonator coupling coefficient is given by [78]:

$$F = \pi \frac{\sqrt{K_r}}{1 - K_r} \tag{4.19}$$

In practice there are situations when the coupling constant is not adjusted to its resonant value. In this case the output power will not be zero at the output port. When the coupling constant is less than K_r , the finesse decreases. As K approaches 1 light cross-couples to port 4, and no light enters the fibre loop. For $K>K_r$ it remains almost constant.

CAVITY DECAY TIME: The last important parameter of the ring resonator to be discussed is its cavity decay time given as [83]:

$$\tau_c = \frac{nL/C}{\gamma_{rt}} \tag{4.20}$$

where nL/c is the cavity round-trip decay time and γ_{rt} is the fractional intensity loss per round trip. If the input optical power is cut off, the circulating power will decay via the coupler loss, γ_o , the fibre attenuation, $2\alpha_o L$, and the output port itself $(1-K_r)$. From eq.(4.15) the first two loss mechanisms contribute $1-K_r$ to γ_{rt}. Thus:

$$\tau_c \approx \frac{nL/C}{2(1-K_r)} \approx \frac{1}{2\pi\Delta f} \tag{4.21}$$

To produce resonant effect in the optical fibre ring resonator, a laser source with a coherence length greater than $c\tau_c$ must be used. For a resonator made from 15 m of fibre with refractive index 1.47, attenuation 12 $dBkm^{-1}$ and a finesse of 100, i.e., $K_r = 0.9$ (using eq. 4.19), the cavity decay time would be ~0.367 μs. Therefore a laser souce with a coherence length greater than 110 m ($c\tau$) is reqiured.

4.4 NONLINEAR EFFECTS

Nonlinear optics is the study of phenomena that occur as a consequence of the modification of the optical properties of a material system by the presence of light. These phenomena are *nonlinear* in the sense that they occur when the response of a material system to an applied optical field depends in a nonlinear manner upon the strength of the optical field.

Fibres are usually considered to be completely passive or linear media. As the input power is increased, one expects only a proportional increase in output power. However at higher input powers dramatic nonlinear effects can occur. These are manifested as strong frequency conversion, optical gain, and many other effects, generally associated with strong optical intensities and highly nonlinear materials.

Before 1960 the study ofnonlinear processes was the exception and conventional optical systems were analyzed using a linear theory. The neglect of nonlinear effects was due to the fact that large optical fields could not be easily produced. After the invention of the laser, a source became available that enabled the production of nonlinear optical behaviour.

About twenty years ago it was realised that optical nonlinearity could place an ultimate practical limitation on the power levels used in fibre transmission systems [64, 65]. Over the past decade a wide range of interesting nonlinear effects have been studied extensively and have found useful application in optical frequency converters and amplifiers [84]. The study of stimulated scattering in optical fibres has become important for several reasons. First, the long interaction length that can be achieved with fibres can lead to the observation of different dynamic behaviour. Second, the power levels at which

one can observe nonlinear effects in fibres are greatly reduced because the light is guided by the fibre. Since fibre losses are highly reduced in modern manufacturing techniques (<0.2dBkm^{-1} at 1550nm)[85], the light is guided over very long distances up to tens of kilometres. Nonlinear effects also have great importance to optical fibre communication systems, since they severely limit the power levels that can be transferred through the fibre.

4.5 THEORETICAL BACKGROUND

On a fundamental level, the origin of the nonlinear response is related to the anharmonic motion of the bound electrons under the influence of an applied field. In order to describe more precisely what is meant by an optical nonlinearity, let us consider how the dipole moment per unit volume, or polarization *P(t)* of a material system depends upon the strength *E(t)* of the applied optical field. In the case of conventional i.e., linear optics, the induced polarization depends linearly upon the electric field strength in a manner that can often be described by the relationship:

$$P(t) = \chi^{(1)} E(t) \tag{4.22}$$

where the constant of proportionality $\chi^{(1)}$ is known as the linear susceptibility. In nonlinear optics, the nonlinear optical response can often be described by generalizing eq.(4.22) by expressing the polarization *P(t)* as a power series in the field strength *E(t)* as:

$$\begin{aligned} P(t) &= \chi^{(1)} E(t) + \chi^{(2)} E^2(t) + \chi^{(3)} E^3(t) \ldots . \\ &\equiv P^{(1)}(t) + P^{(2)}(t) + P^{(3)}(t) + \ldots . \end{aligned} \tag{4.23}$$

This equation is only valid for a medium which is lossless and dispersionless. The quantities $\chi^{(2)}$ and $\chi^{(3)}$ are known as second- and third-order nonlinear susceptibilities , respectively. We shall refer to $P^{(2)}(t) = \chi^{(2)} E^2(t)$ as the second-order nonlinear polarization and to $P^{(3)}(t) = \chi^{(3)} E^3(t)$ as the third-order nonlinear polarization.

The physical processes that occur as a result of the second-order polarization $P^{(2)}$ are distinct from those that occur as a result of the third-order polarization $P^{(3)}$. Second-order nonlinear optical interaction can occur only in *noncentrosymmetric* crystals, that is, in crystals that do **not** display inversion symmetry. Since liquids, gases, amorphous solids (such as glass) do display inversion symmetry, $\chi^{(2)}$ vanishes for such media, and consequently they cannot produce second-order nonlinear optical interactions. On the other hand, third-order nonlinear optical interactions i.e., those described by a $\chi^{(3)}$ susceptibility , can occur both for centrosymmetric and noncentrosymmetric media.

The third order nonlinearity $\chi^{(3)}$ is responsible for a number of effects such as:

1- Stimulated Raman Scattering (SRS).
2- Stimulated Brillouin Scattering (SBS).
3- Four wave mixing.

Both SRS and SBS are inelastic processes (because the scattered wave does not have the same frequency as the incident wave) where the scattered radiation is shifted with respect to the incident radiation, and the energy difference of the two quanta is retained by the scatterer as *internal energy*. In the case of SRS, this internal energy is electronic excitation of the atom or more usually vibrational excitation of the molecule. Whereas in SBS, the

energy difference of the two quanta is taken up by an acoustic phonon i.e., classically, an acoustic wave is generated. The down shifted scattered wave is known as the *Stokes* component whereas the upshifted is referred to as the *anti-Stokes*. As far as this research programme is concerned, we will confine our discussion to Stimulated Brillouin Scattering only, which is described in the following section.

4.6 STIMULATED BRILLOUIN SCATTERING

The nonlinear process in fibres with the largest gain and hence the lowest threshold in some important instances is SBS. It can be described as an interaction among the input light wave (the pump), the Stokes wave (backscattered frequency downshifted optical beam), and an acoustic wave. In terms of *quantum mechanics*, the destruction of a pump photon creates simultaneously a Stokes photon and an acoustic phonon.

The basic concept behind SBS process is illustrated schematically in figure 4.3. The pump wave (ω_P) generates an acoustic wave through the process of electrostriction [86] (the electric field induced strain on a medium) which in turn causes a periodic modulation of the refractive index. The pump induced refractive index grating scatters the pump light through Bragg diffraction. This scattered light wave is Doppler shifted to a frequency ω_S which is slightly different from ω_P since the acoustic wave acts as a moving diffraction grating. Since the acoustic wavefronts (fig. 4.3) move away from the incident laser wave, the scattered light is shifted downwards in frequency to the Stokes frequency $\omega_s = \omega_p - \omega_A$. The process is analogous to that used in conventional Bragg cells.

GAIN: This spatially periodic, moving structure of alternate high and low

density coincides with the acoustic wave from which the initial scattering started, so a positive feedback situation exists and hence stronger scattering occurs and so on.

SBS can be initiated by the acoustic waves which are always present in the medium due simply to thermal excitation. It is found that the process occurs most strongly for a scattered light wave travelling in the opposite direction to the pump wave. Thus a significant proportion e.g., 65% [84] of the optical power travelling in the fibre may be converted into the scattered wave which travels backwards towards the transmitter. Conditions, such as a narrow excitation linewidth and long interaction length are precisely those which favour the nonlinear process of Stimulated Brillouin Scattering.

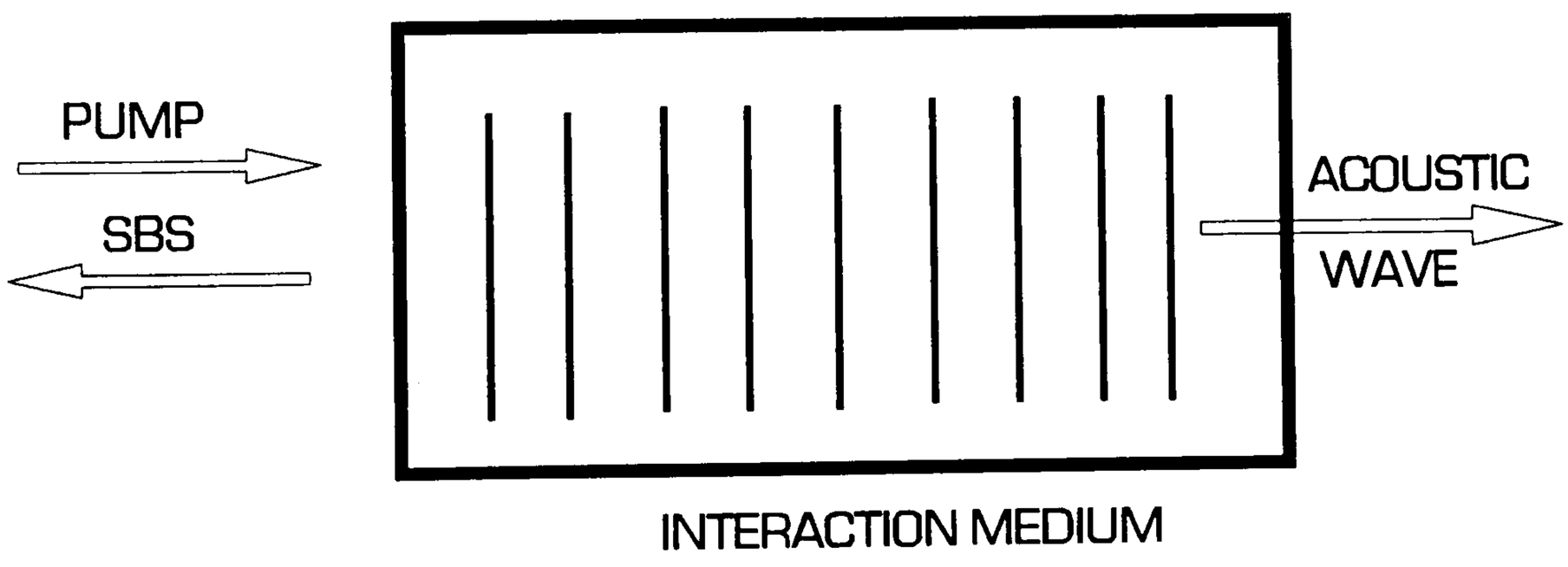

FIG. 4.3 GENERATION OF SBS IN OPTICAL FIBRE

The frequencies and the wave vectors of the three waves are related by law of conservation of energy:

$$\omega_p = \omega_A + \omega_S \tag{4.24}$$

$$K_P = K_A + K_S \tag{4.25}$$

where ω_P, ω_S, ω_A are frequencies and K_P, K_S, K_A are wave vectors of the *pump, Stokes,* and *acoustic waves* respectively.

As

$$K_p = 2\frac{\pi}{\lambda_p} n(\lambda_p) \tag{4.26}$$

and

$$K_S = 2\frac{\pi}{\lambda_S} n(\lambda_S) \tag{4.27}$$

then

$$|K_P| \simeq |K_S| \tag{4.28}$$

because the pump and the shifted wavelengths are approximately equal, i.e., they differ by only 1 part in 10^4.

The frequency ω_A and the wave vector K_A satisfy the dispersion relation [87]:

$$\omega_A = |K_A| v_A = 2v_A |K_P| \sin(\theta/2) \tag{4.29}$$

In the above equation θ plays a very vital role since it is the angle between the pump and Stokes waves. It is quite obvious that the frequency shift of the Stokes wave depends on the scattering angle. In a fibre only two directions exist (i.e., θ can only be 0°or 180°) and it is therefore seen to be a maximum in the backward direction ($\theta=\pi$) and vanishes in the forward direction ($\theta=0$). The Stokes shift (or frequency shift) is given by [84]:

$$\nu_B = 2\frac{nV_A}{\lambda} \tag{4.30}$$

where V_A is the acoustic velocity, n is the refractive index of fibre core and λ is the optical pump wavelength. Experimentally υ_B has been found to be ~34 GHz and ~10 GHz for pump wavelengths of 514 nm and 1300 nm, respectively.

4.6.1 BRILLOUIN GAIN COEFFICIENT & GAIN

The Brillouin gain coefficient $G_B(\nu_B)$ characterizes the growth of the Stokes

wave. It is related to the damping time of the acoustic waves i.e., the phonon life time *T*:

$$\Delta\nu_B = \frac{1}{\pi T} \tag{4.31}$$

Brillouin gain coefficient is given by the relation:

$$G_B(\nu_B) = \frac{2\pi n^7 P_{12}^2}{c\lambda_p^2 \rho_0 V_A \Delta\nu_B} \tag{4.32}$$

where λ_p is the pump wavelength, ρ_0 is the material density P_{12} is the longitudinal elasto-optic coefficient and *c* is the velocity of light.

In order to calculate the Brillouin gain let us assume that the laser light be injected at $z = o$, in the fibre, travelling in the +ve *z* direction with a pump power P_p . In the absence of any nonlinear interaction the pump propagates as [64]:

$$P_p(z) = P_p(0) \exp(-2\alpha_o z) \tag{4.33}$$

where α_o is the fibre (amplitude) attenuation coefficient. The Stokes wave of initial power P_{st} an exponential gain after travelling along the fibre, corresponding to the pump power, given by [88]:

$$\frac{P_{st}(z)}{P_{st}(0)} = \exp\left[G_B(\nu_B)\, P_{input} \frac{z}{A_{eff}}\right] \tag{4.34}$$

where P_p / A_{eff} is the pump intensity, A_{eff} is the effective mode cross-sectional area given as [89]:

$$A_{eff} = \pi \omega_o^2 \tag{4.35}$$

where ω_o is the $1/e^2$ intensity radius.

An empirical formula which allows A_{eff} to be calculated from a core radius a and the normalised frequency parameter V, is given as [90]:

$$A_{eff} = \pi \left[a \left(0.632 + \frac{1.478}{V^{3/2}} + \frac{4.76}{V^6} \right) \right]^2 \tag{4.36}$$

where

$$V = \frac{2\pi a}{\lambda_p} (n_1^2 - n_2^2)^{1/2} \tag{4.37}$$

n_1 and n_2 are the refractive indices of core and cladding respectively.

Assuming that α_o is same for the pump and Stokes waves, the differential equation for stimulated scattering is given by [64]:

$$\frac{dP_{st}(z)}{dz} = \left(\frac{G_B(\nu_B)}{A_{eff}} P_p(z) \right) P_{st}(z) \tag{4.38}$$

Integrating along the fibre of length L and putting the value of $P_p(z)$ from eq.(4.33) we get:

$$\log \left(\frac{P_{st}(L)}{P_{st}(0)} \right) = \frac{G_B(\nu_B)}{A_{eff}} P_{input}(0) \left(\frac{1 - e^{-2\alpha_o L}}{2\alpha_o} \right) \tag{4.39}$$

where $[(1-e^{-2\alpha oL})/2\alpha_o]$ is the effective length L_{eff} [91] of the fibre. The effective length is less than L due to fibre linear attenuation of the pump. For a short fibre ($2\alpha_o L << 1$), $L_{eff} \approx L$, while for a long fibre ($2\alpha_o L >> 1$), $L_{eff} \approx 1/2\alpha_o$. The

backscattered SBS wave experiences the usual fibre attenuation of $e^{-2\alpha_o L}$ in travelling a length *L*. It is assumed that α_o is the same for both the pump and Stokes wave, as the frequency difference between pump and Stokes is small compared to the pump frequency. Now the SBS gain of the system is given as follows:

$$Gain = \frac{P_{st}(L)}{P_{st}(0)} = Exp\left(\frac{G_B(\nu_B)}{A_{eff}} P_p(0)\, L_{eff}\right) \qquad (4.40)$$

The optical power of the laser source will decide which stimulated scattering process will occur. If the optical intensity is higher than the threshold level the SBS with its peak gain coefficient of [89] ~3×10^{-9} cm/W will dominate. As the gain coefficient of the Raman scattering is smaller [88], i.e., ~2×10^{-11} cm/W, more pump power will be needed to achieve gain for the Raman process than for the Brillouin scattering.

4.6.2 THRESHOLD POWER

Stimulated Brillouin scattering is only significant above a certain power level called the *threshold* . The threshold power for SBS is defined as the input power for which the backward stimulated Stokes power equals the input power at $z = 0$, where z is the distance travelled along the fibre [65]. For the limiting case $\alpha_o L >> 1$, it can be shown that the gain required for amplified spontaneous scattering up to the threshold level for straight length of fibre is

≈20. More generally, the threshold power can be approximated as [89]:

$$P_{straight} = A_{eff} I_{straight} \simeq 20 \frac{A}{G_B(\nu_B)\, L_{eff}} \qquad (4.41)$$

where $I_{straight}$ is the optical intensity in straight length of fibre. An expression for the threshold power for the *onset* of SBS is given as [91]:

$$P_{onset} = 4.4 \times 10^{-3} d^2 \lambda_p^2 \alpha_{dB} \nu_p \qquad (4.42)$$

where λ_p and d are the pump wavelength and fibre core diameter respectively, both measured in micrometers, α_{dB} is the fibre attenuation in deciBels per kilometre and υ_p is the source bandwidth in gigahertz. Eq.(4.42) allows the determination of the threshold optical power which must be launched into a single mode fibre before SBS occurs.

4.7 SBS IN OPTICAL FIBRE RING RESONATORS

With the use of a low insertion loss directional coupler and high quality low loss single mode fibre, a ring resonator with high finesse may be constructed and a relatively low power laser can cause Stimulated Brillouin Scattering to occur. The threshold input pump power levels for SBS are greatly reduced for three main reasons. First, the ring resonator geometry offers a significant circulating pump power enhancement factor. Second, the polarization maintaining nature of the fibre ensures that both the pump wave and the scattered wave have the same polarization state, thus maximizing the SBS gain factor. Third, because of the low loss nature of the device the round trip non-linear gain need be only a few percent. Circulating loop powers can thus often be above SBS threshold, even for very low input powers.

4.7.1 ENHANCEMENT OF OPTICAL POWER

As it has been mentioned earlier in this chapter that at resonance the output intensity is zero and the optical power circulating in the ring is given by eq.4.16:

$$\frac{I_{ring}}{I_{input}} = \frac{(1-\gamma_o)}{(1-K_r)} \qquad (4.43)$$

as at resonance $Sin^2\,[\beta L/2 + \pi/4]=0$, where I_{input} is the power coupled into the fibre, I_{ring} is the circulating power. Equation 4.43 provides the value of the enhancement of the circulating power at resonance. As an example, a finesse of 80 and γ_o = 3% implies a circulating intensity enhancement of ~25 (using eq. 4.43 and 4.19).

The backward scattered Brillouin frequency shifted wave is amplified by a factor given from eq.(4.34) by $exp[G_B(\upsilon_B)P_{input}L/A_{eff}]$ (SBS gain). A small fraction of the backward travelling Stokes wave is tapped out at port (1) and adds coherently on each circulation to give an output power from port (1).

4.7.2 THRESHOLD POWER

For a ring resonator configuration a relation between the input threshold power, length of the fibre, finesse, and Brillouin gain coefficient is given by

[78]:

$$P_{ring} = \frac{2A_{eff}(\gamma_o + 2\alpha_o L)^2}{G_B(\nu_B)\,L(1-\gamma_o)} \simeq \frac{2A_{eff}\pi^2}{G_B(\nu)\,LF^2} \qquad (4.44)$$

This relation shows that threshold power to produce SBS is highly dependent upon the finesse of the ring resonator. Figure 4.4 shows the theoretical variation of threshold power and the finesse for several loop lengths; the parameters used are for Fujikura *PANDA* fibre with $A_{eff} = 16.46\ \mu m^2$ and $G_B = 4.2\times10^{-11}$. It can be seen that SBS can occur at very low input power levels even in the range of few hundred micro Watts for a finesse of larger than 50. For same values of gain and effective area, figure 4.5 shows the dependence of the SBS threshold power on the ring resonator loop length. It can be seen that to generate SBS at low threshold powers, long loop lengths are advantageous.

4.8 CONCLUSIONS

The construction, properties and the theory behind the operation of ring resonator were discussed. The relation between the input and output intensities was derived. Generation of stimulated Brillouin scattering was discussed; first in straight lengths of the fibre and then in ring resonators. Theoretical modeling showed that the threshold power required to generate SBS is highly dependent on the finesse of the ring resonator.

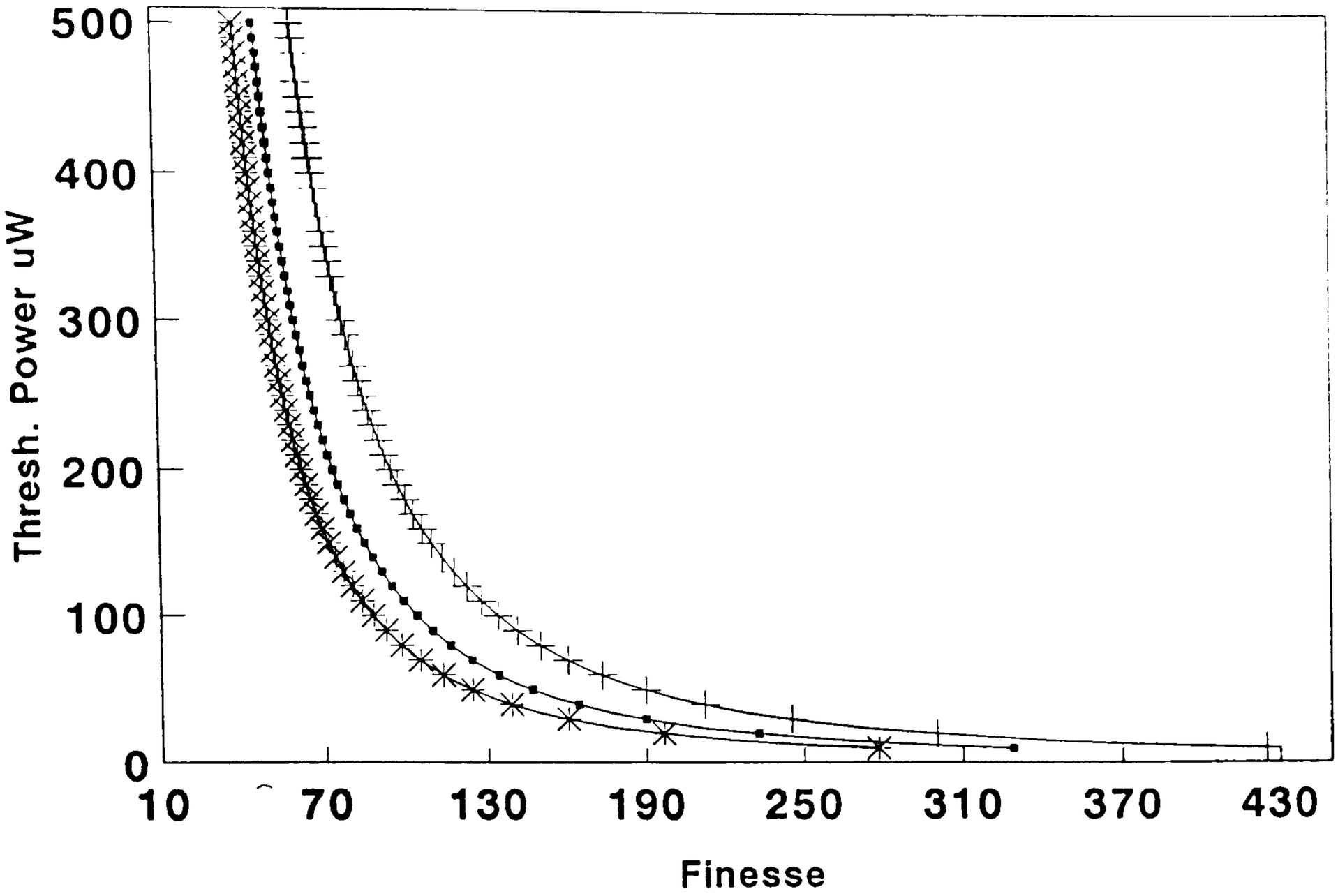

Fig. 4.4 Threshold power vs Finesse
for different loop lengths

4.2X10 m/W A=16.462um Finesse= 100

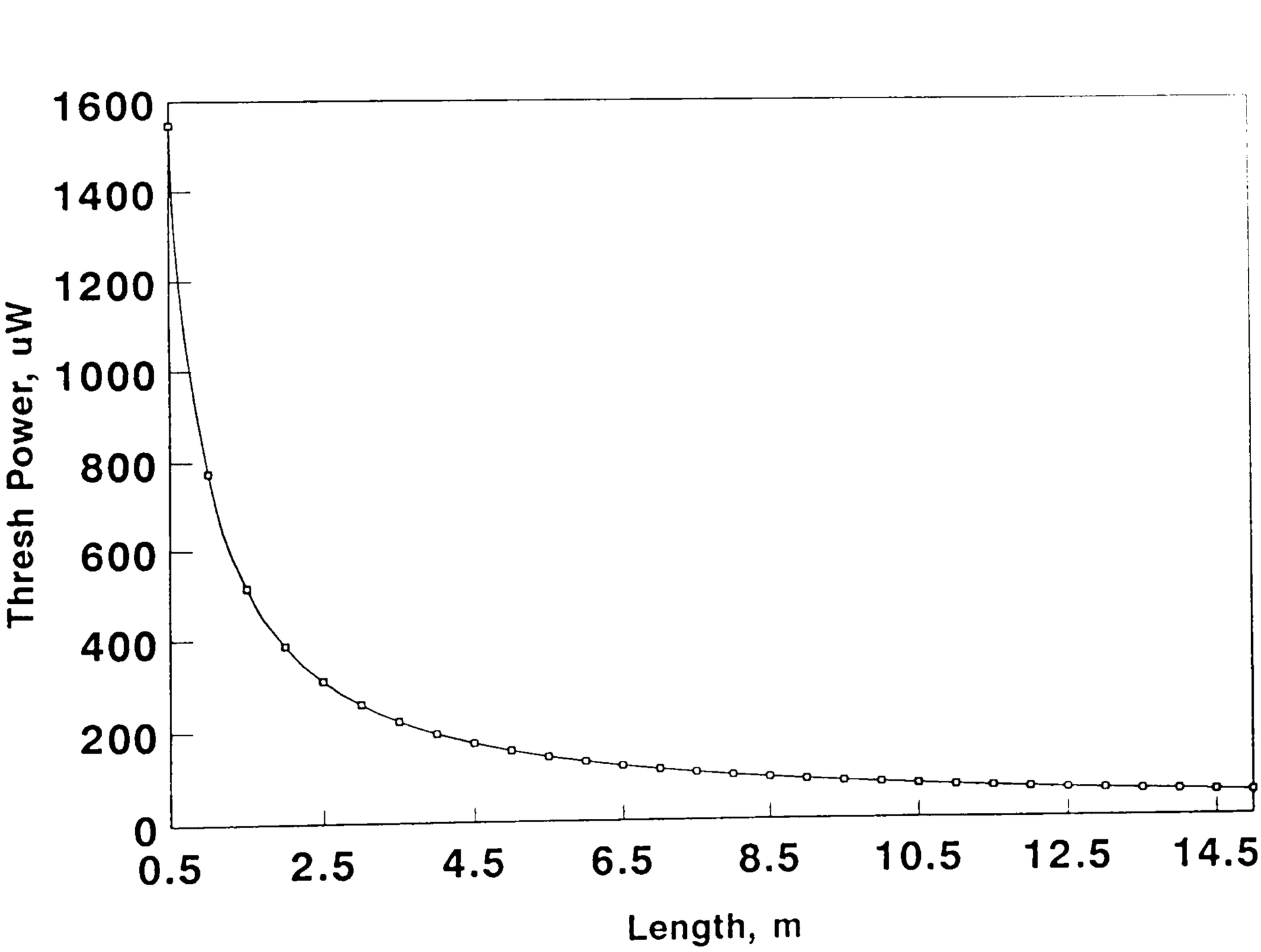

Fig. 4.5 Threshold Power vs Length

CHAPTER FIVE

CHARACTERIZATION TECHNIQUE FOR OPTICAL DETECTOR-AMPLIFIER COMBINATIONS

5.1 INTRODUCTION

The characterization of high frequency optical detector-amplifier combinations is essential for most optical signal processing and sensing applications. There are two main reasons for the experimental determination of the frequency-response characteristics. Firstly, to ensure that any observed signal is real and not due to overshoot at a particular frequency in the amplifier. Secondly, if the signal of interest is not within the flat frequency region (e.g. after roll off), measurements could be uncaliberated and potentially misleading.

High speed detector-amplifier combinations, developed to detect signals in the

range from kilohertz to megahertz, for this project, are characterized using a new technique that requires low frequency source modulation but provides detector characterization over a much wider frequency range. The frequency response has been measured by transducing low frequency wavelength modulation of the source to a higher frequency intensity modulation using an interferometer with unbalanced optical paths. In this chapter, measurements for several detector circuits are presented using both a bulk optic Michelson interferometer and a Fabry-Perot interferometer constructed from highly birefringent optical fibre. Experimental results are compared with simulation using *PSpice* and direct intensity modulation of the source.

5.2 PREVIOUS TECHNIQUES

Recently optical techniques have been reported that make measurement from d.c. to approximately 50 MHz. Khalil *et al* [4] used a Michelson interferometer configuration constructed using conventional bulk optic components that places severe restrictions on the optomechanical stability and therefore the path length imbalance that can be stably achieved. The technique presented by Andres [92] uses a fibre optic interferometer configuration with intensity modulation at the interferometer output, generated by modulating the phase of the interferometer with a piezoelectric modulator. A low frequency electrical signal applied to the piezoelectric modulator produces a modulation of the light beam at a frequency determined by the frequency of the electrical signal multiplied by the number of interferometric fringes swept out during one period of the electrical signal. Thus a low frequency electrical signal applied to the piezoelectric modulator can produce higher frequency modulation of the optical beam. This method, which used a helium neon laser (λ = 632.8 nm) as a source, was demonstrated over the frequency range 1kHz to 45 MHz.

However a major disadvantage of using piezoelectric modulators is the non-linear response of the dimensional change of the ceramic to the applied voltage and their complex frequency response characteristics [38] which are very dependent on the dimensions and thickness of the piezoelectric modulators.

In this chapter we present a technique that is simpler to implement, is more optomechanically robust and offers the potential for greater flexibility in the frequency range that can be covered. The technique uses interferometric modulation of an optical beam produced by modulating the wavelength of a laser diode in an unbalanced interferometer. This technique enables high frequency modulation of the optical beam for a low frequency modulation signal applied to the laser diode injection current and thus offers significant advantages to direct modulation of the laser diode particularly at higher frequencies. Optical fibre interferometers are employed to increase the mechanical robustness and simplify the implementation.

5.3 THEORETICAL BACKGROUND

The technique described here uses the dependence of the diode laser output optical frequency on the injection current [18] combined with a two beam interferometer with unequal path lengths for the two beams. The output intensity, *I*, for a two beam interferometer is:

$$\frac{I(\phi)}{I_o} = K_o(1+V\ Cos\phi) \qquad (5.1)$$

where I_o is the laser intensity, K_o is a constant, V is the visibility, and ϕ a phase term which may be written

$$\phi = \frac{2\pi n}{\lambda} \Delta L = \frac{2\pi \nu n}{c} \Delta L \qquad (5.2)$$

where n is the refractive index, λ is the free space wavelength of the source and ΔL the path length difference in the interferometer. A change in optical wavelength $\delta\lambda$ produces a change in phase, $\delta\phi$, given by

$$|\delta\phi| = \frac{2\pi n}{c} \delta\nu \ \Delta L \qquad (5.3)$$

where $\Delta\upsilon$ is the change in optical frequency. Hence the change in phase is directly proportional to both the path length difference and the wavelength change.

5. 4 EXPERIMENTAL

The initial experimental arrangement used to demonstrate the technique is shown in figure 5.1. The configuration consists of a Michelson interferometer constructed from conventional optical components illuminated with a 30 mW Sharp LTO24MD laser diode operating at 785 nm. The optical isolator was used to prevent feedback into the laser cavity and thus maintain the intrinsic linewidth of the laser. The linewidth was measured on a confocal Fabry-Perot interferometer, with a free spectral range of 2 GHz and finesse of ~150, to be approximately 30 MHz although this measurement is on the resolution limit of the Fabry-Perot. This implies that the coherence length of the diode is ≥10m.

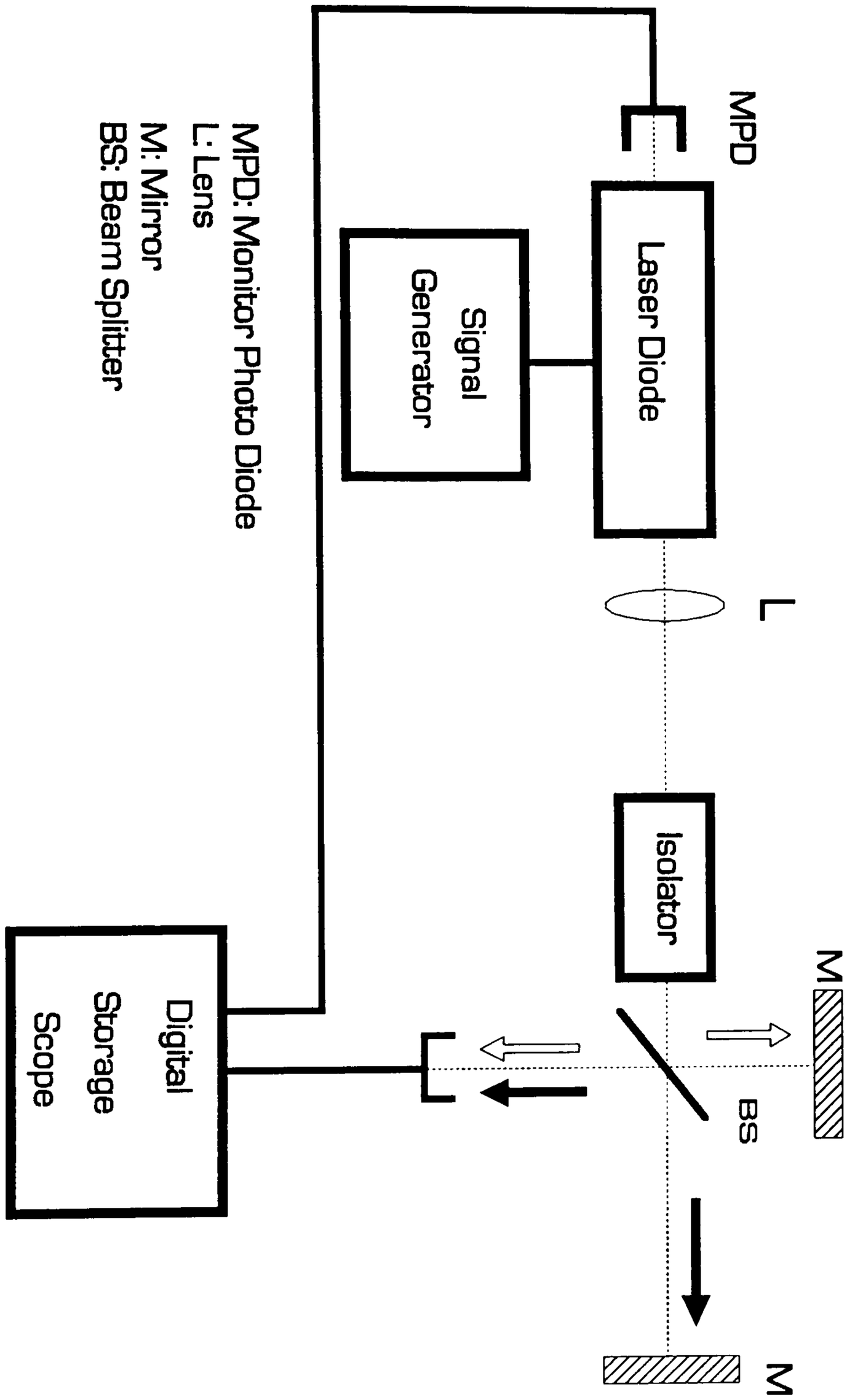

MPD: Monitor Photo Diode
L: Lens
M: Mirror
BS: Beam Splitter

Figure 5.1 Experimental arrangement: Optical Detector characterisation.

Bulk optic configuration.

The path length imbalance was arranged to be 15 cm and the laser injection current sinusoidally modulated. The frequency response characteristics were then recovered by measuring the amplitude and frequency of the interferometric fringes using a digital storage scope (DSO)(LECROY 9400). Details are discussed below in conjunction with fibre optic interferometer.

Figure 5.2 shows the experimental arrangement for a fibre optic interferometric deployment. A low-finesse Fabry-Perot interferometer is formed between the input and distal fibre-air interfaces. A length of high birefringence optical fibre (York HB800, N.A = 0.11, cut-off wavelength = 565 nm) was used to form the Fabry-Perot interferometer. This interferometer arrangement is much more rugged than that of figure 5.1. The polarisation state, and hence the fringe visibility, is maintained independent of environmental perturbations by coupling the linearly polarised output from the isolator into a single polarisation eigenmode of the fibre using the half-wave plate. A much greater path length imbalance can now be easily and stably achieved as the two 'mirrors' always remain parallel. The path length imbalance is now restricted by the coherence length of the source and not mechanical alignment stability. In this experiment an imbalance of approximately 150 cm (~50 cm length of fibre) was used to demonstrate the technique with the higher speed detector-amplifier combination.

Figure 5.3(a) shows the output from the detector-amplifier combination at relatively low frequency. The low frequency modulation envelope superimposed on the higher frequency interferometric fringe modulation is caused by the concomitant output intensity modulation of the laser diode when the injection current is modulated in addition to the optical frequency modulation [93]. The frequency response of the detector-amplifier combination is recovered from the amplitude of the interferometric fringes and therefore the additional intensity modulation complicates the measurement and causes large

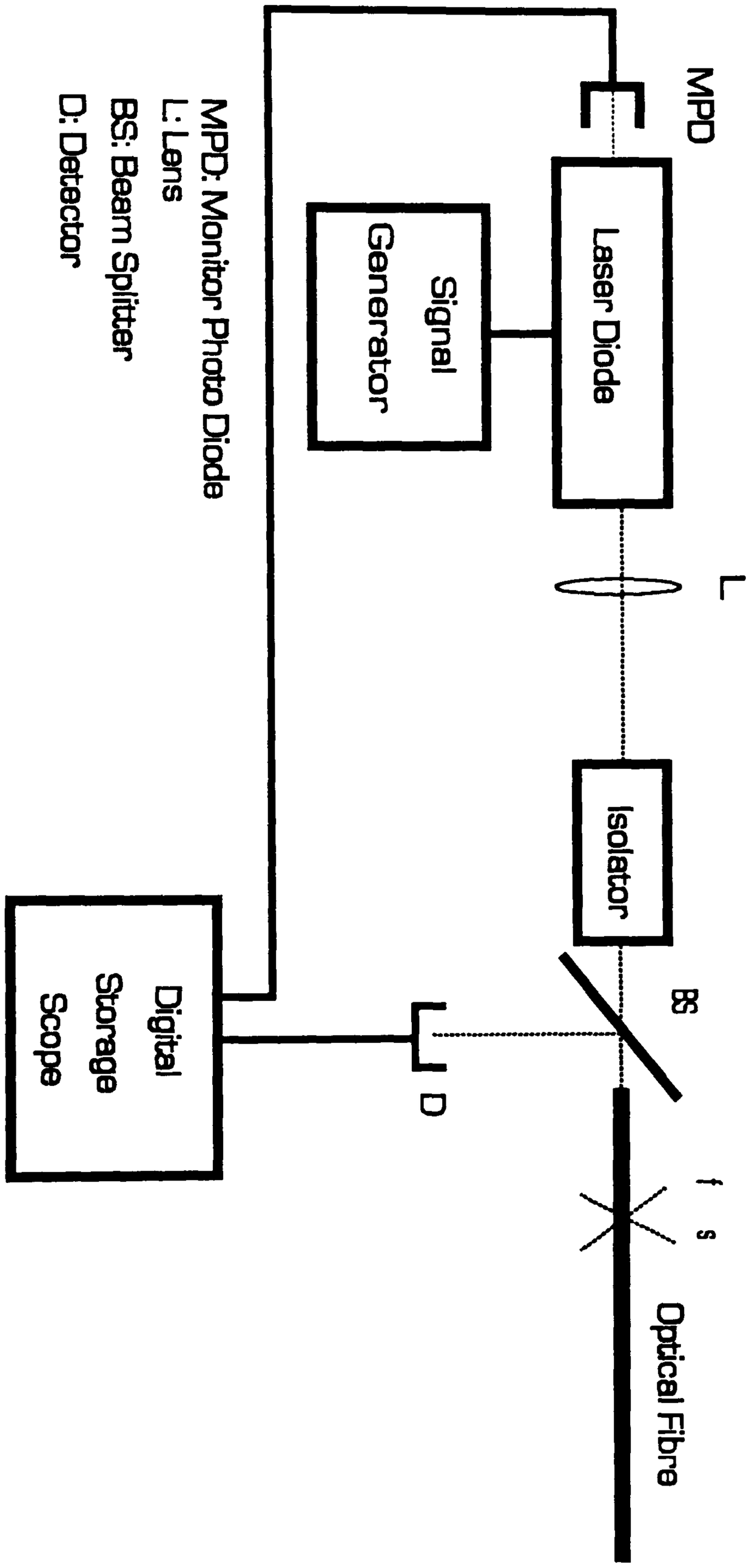

Figure 5.2 Experimental arrangement: Optical detector characterization; optical fibre interferometer

errors particularly at high modulation indices if not removed. The effect was removed from the fringes by dividing the detector output by the output from the monitor-photodetector built into the back of the laser. In these experiments the division was achieved using the DSO. Figure 5.3(b) shows the output from the monitor-photodetector and figure 5.3(c) the division of 5.3(a) by 5.3(b).

Figure 5.4(a) depicts the detector-amplifier output at higher frequency with the modulation signal applied to the injection current. As the rate of change of the drive signal increases the detector-amplifier output decreases. Figure 5.4(b) shows, on an expanded timescale, the output obtained during the linear portion (maximum rate of change) of the applied signal. The detector-amplifier response characteristics were obtained by measuring the amplitude of the fringes during this period and ratioing this with the amplitude obtained for low frequency operation, i.e. well within the detector-amplifier bandwidth. The frequency was measured by counting the number of fringes generated during a small time period of the linear part of the sine wave modulation signal and dividing by the time period.

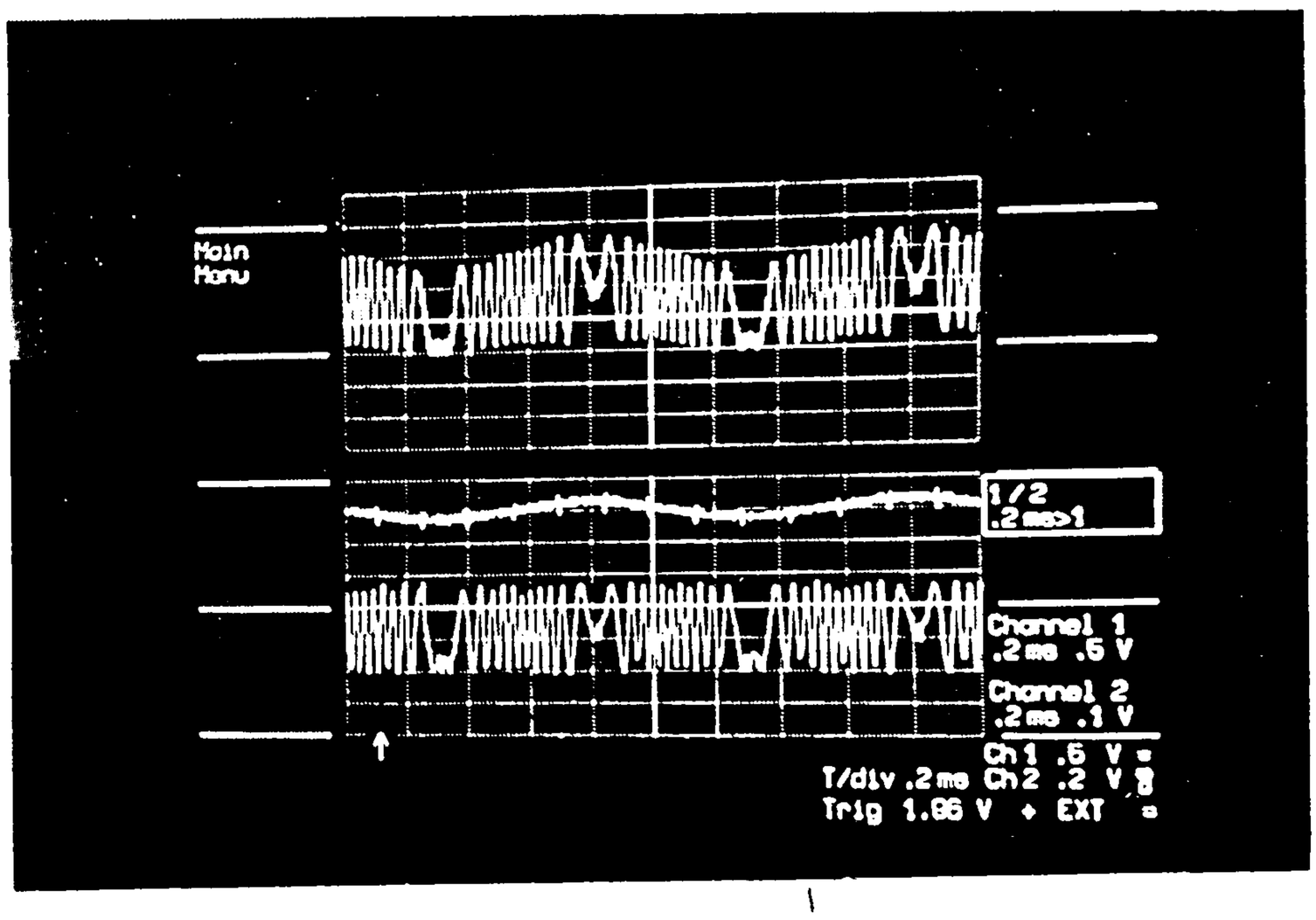

Figure 5.3 (a) Upper Trace: Detector-amplifier combination output
(b) Middle Trace: Monitor Photodiode Output
(c) Bottom Trace: Upper trace divided by middle trace

(a)

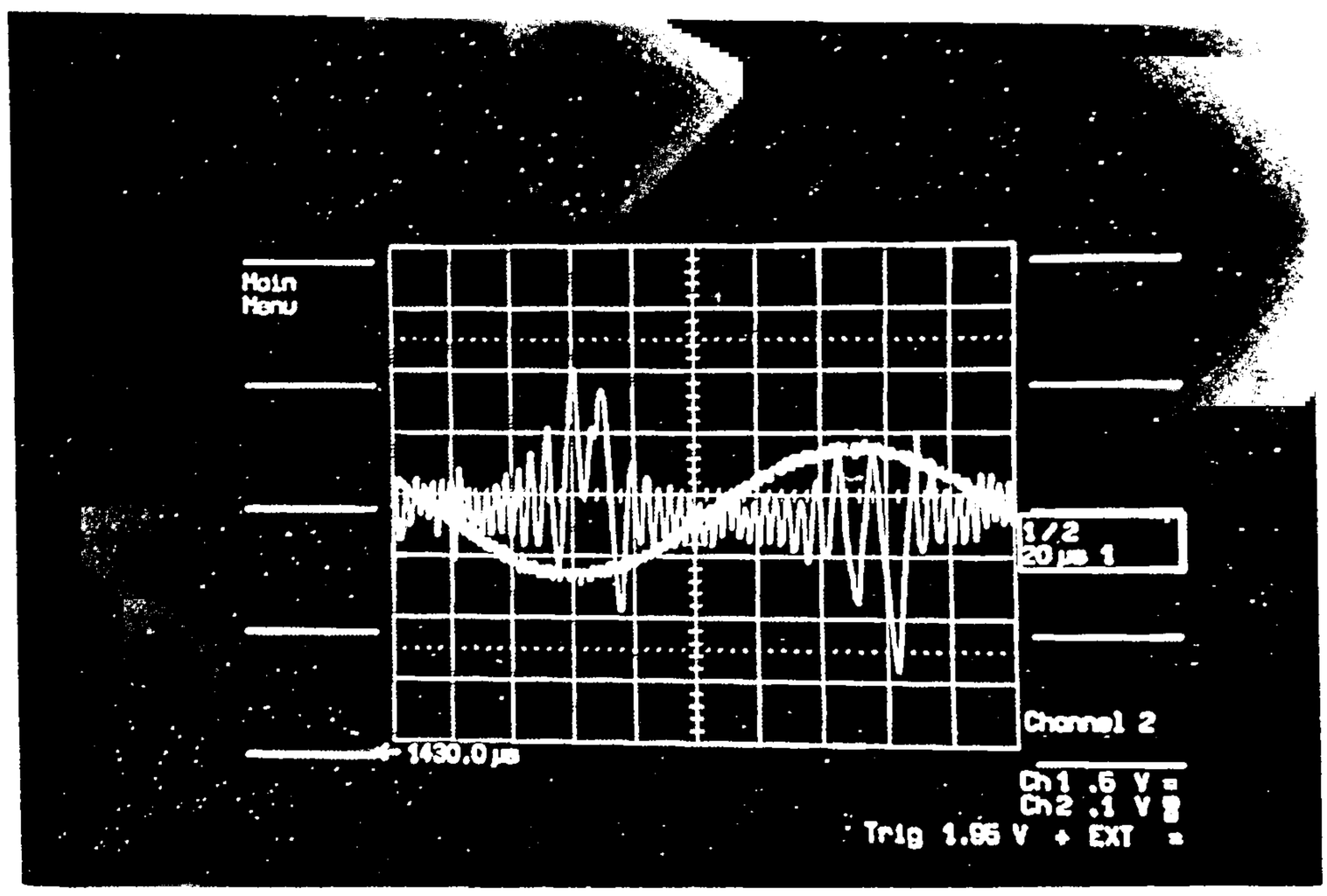

(b)

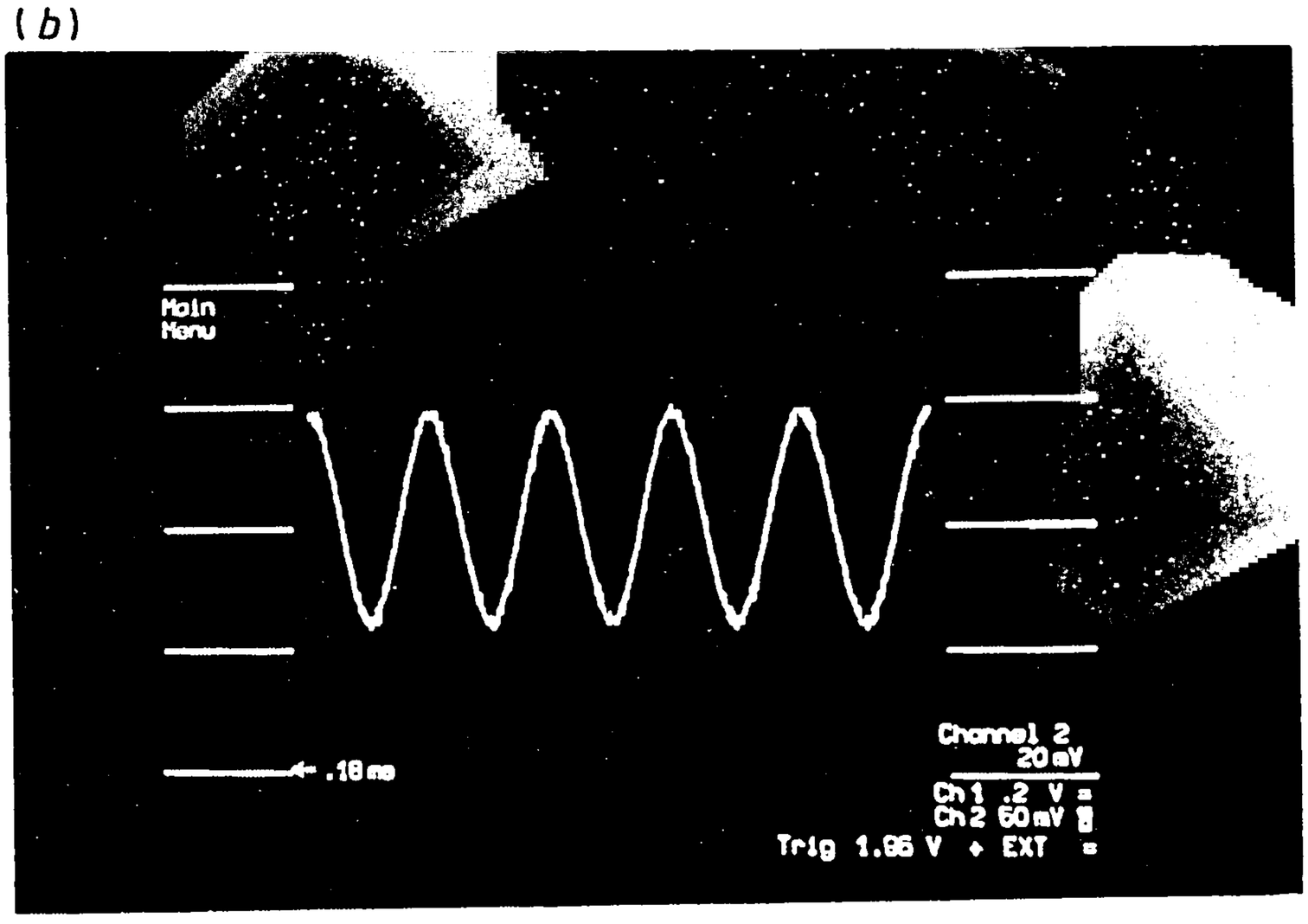

Figure 5.4 (a) Higher frequency modulation. The amplitude of the fringes decreases during the most rapidly varying portion of the modulation signal

(b) Expanded portion of trace a for the linearly changing part of the modulation signal

Measurements made using the interferometric method were compared to those obtained by directly modulating the laser diode output intensity.This was achieved by modulating the laser injection current by a sine wave. Modulation for both sets of experiments was provided by a synthesised function generator (Stanford DS345) with a maximum frequency modulation capability of 30 MHz.

5.4.1 PSpice SIMULATION

Spice stands for *Simulation Program with Integrated Circuit Emphasis*. Spice is used to simulate the operation of various electronic circuits and devices. Its *PSpice* [94] version is designed to operate on PCs. This package has models of basic semiconductor devices such as diodes, transistors etc. It also has a library of several predefined electronic circuits. Its *SUBKT* function allows the user to redefine the model. Although the PC version is limited by the number of predefined circuits, it is quick and easy to use for the state of the art electronic circuits whereas the VAX version has the disadvantage of old design. This program was used in this experiment to obtain the theoretical response of the detector-amplifier combinations which are under investigation.

5. 5. RESULTS

A number of detector-amplifier combinations were used to assess the viability of the technique. The experimental results are compared with the results from simulations using PSpice.

Figure 5.7 shows the results for two circuits based on BPX65 photodetectors and OP07 amplifiers. The higher frequency response combination uses a

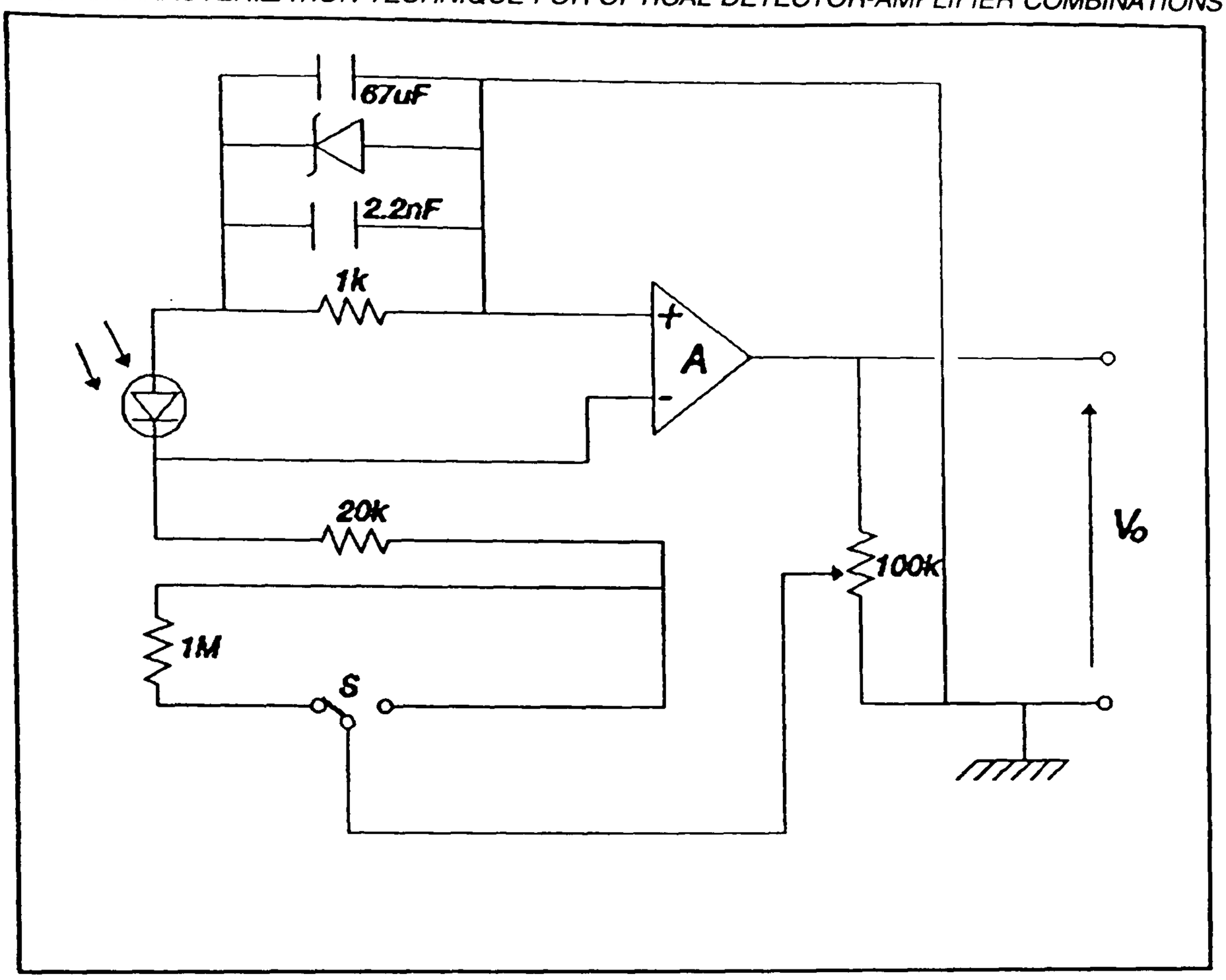

Figure 5.5 Circuit diagram of detector-amplifier using single OP-07

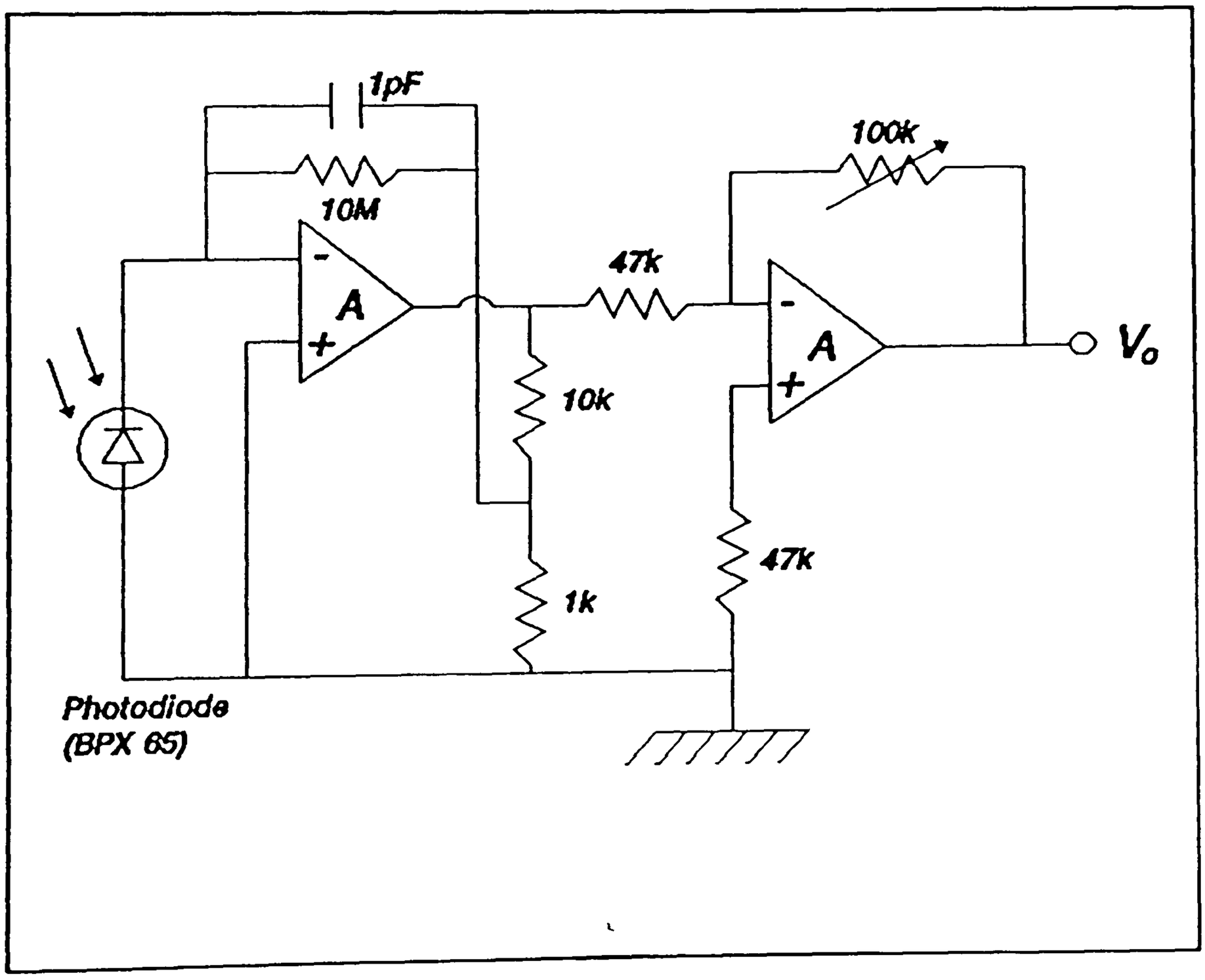

Figure 5.6 Circuit diagram of detector-amplifier using two OP-07s

single OP07 amplifier whilst the lower frequency combination uses two OP07s. Circuit diagrams are shown in figures 5.5 and 5.6 respectively. Agreement between the two experimental methods and the simulation are within a few percent during the linear response regime. As the response rolls off there is greater deviation between the experimental and simulation results due to approximations in the simulation software which lead to deviations between actual and theoretical circuit performance. However, the experimental results presented are the average of many readings resulting in a standard deviation of 6%. Figure 5.9 presents the frequency response characteristics of a Photops UDT455HS hybrid photodetector-amplifier combination (fig.5.8).

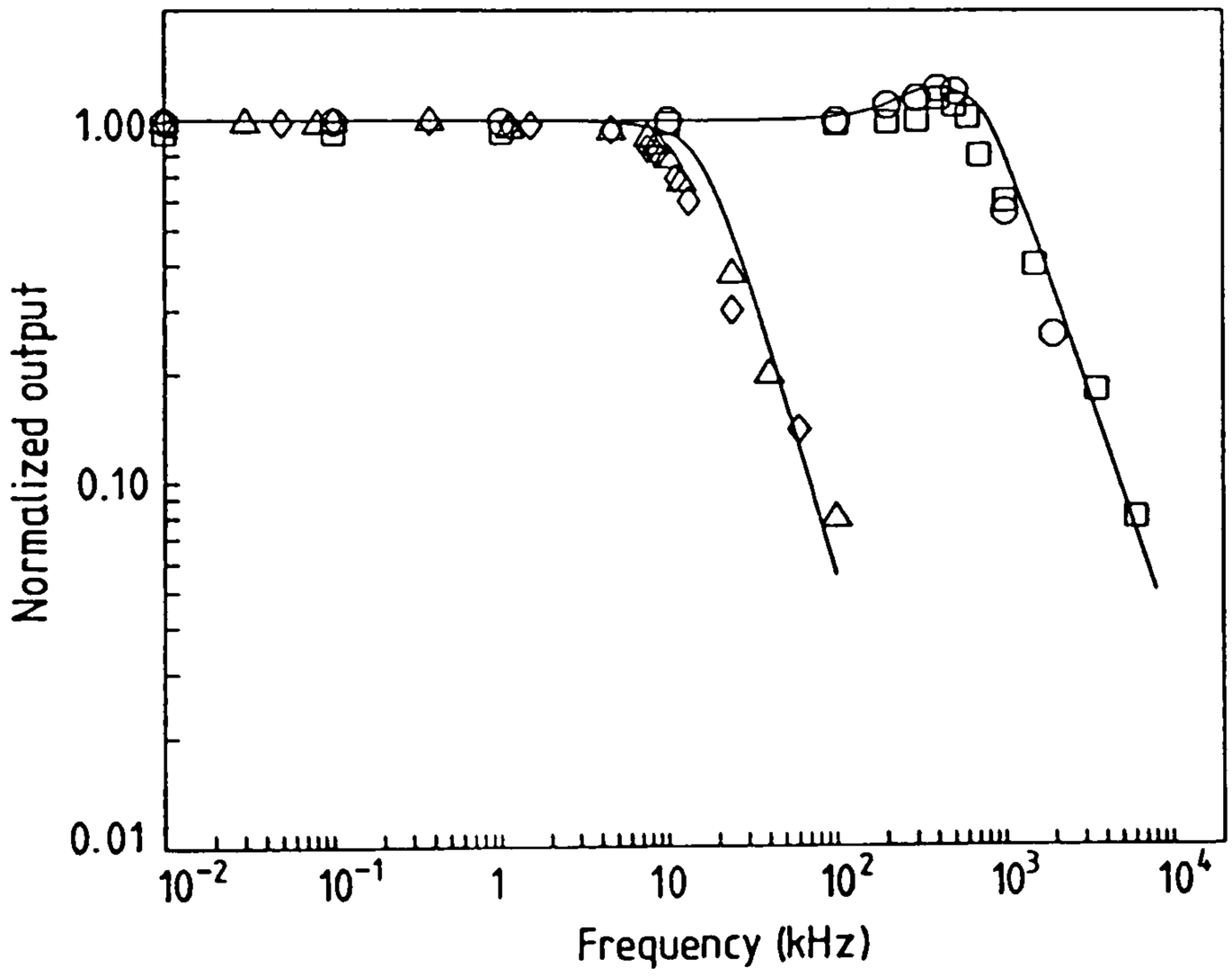

Figure 5.7 Frequency-response characteristics of two detector–amplifier combinations using BPX65 photodetectors. ○ and □ are the interferometric and direct modulations results respectively for a circuit using a single operational amplifier OP07. ◇ and △ are the interferometric and direct modulation results respectively for a circuit based on two OP07 operational amplifiers. In both cases the full line represents simulation results using PSpice.

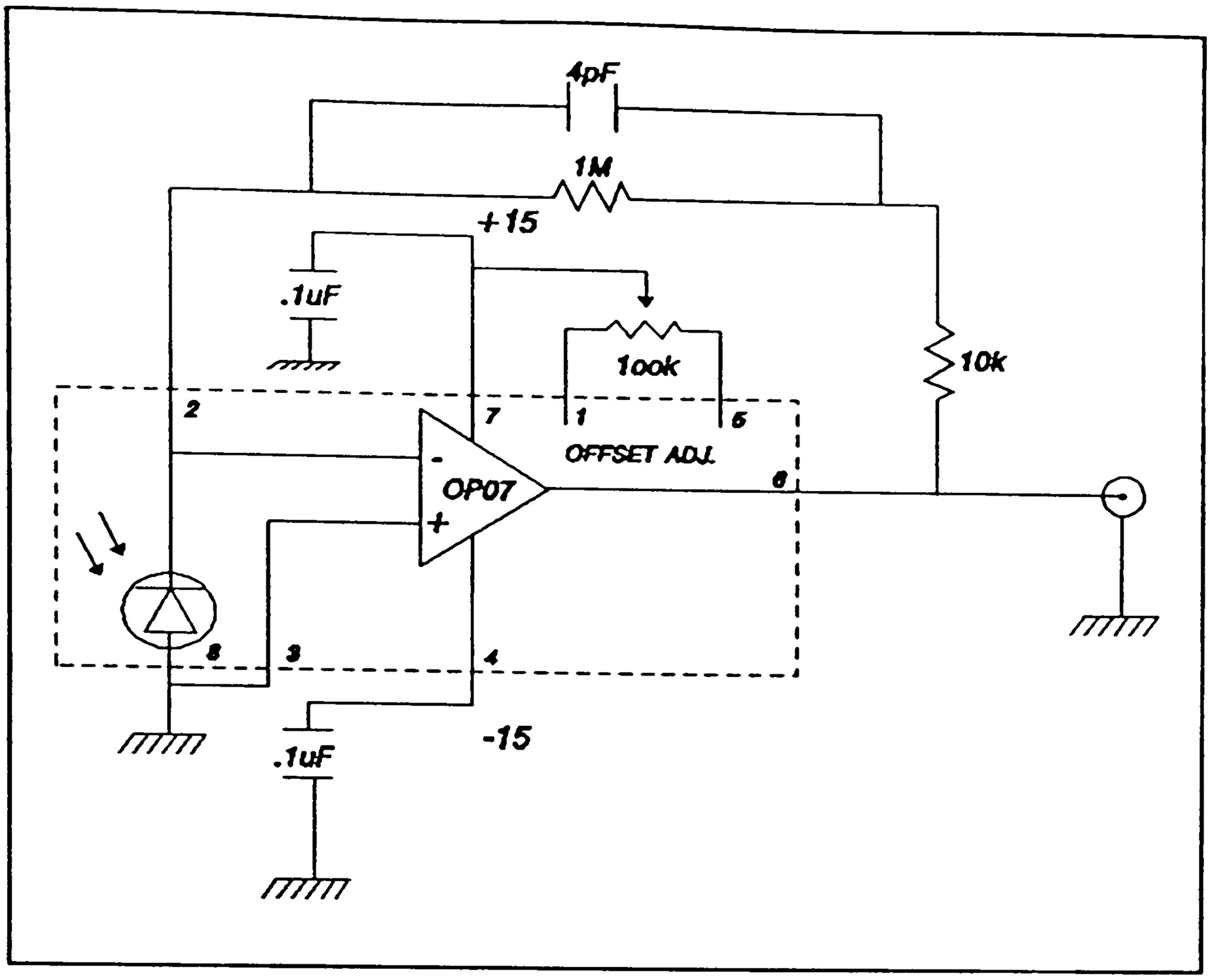

Figure 5.8 Circuit diagram of detector-amplifier using Photops UDT455HS

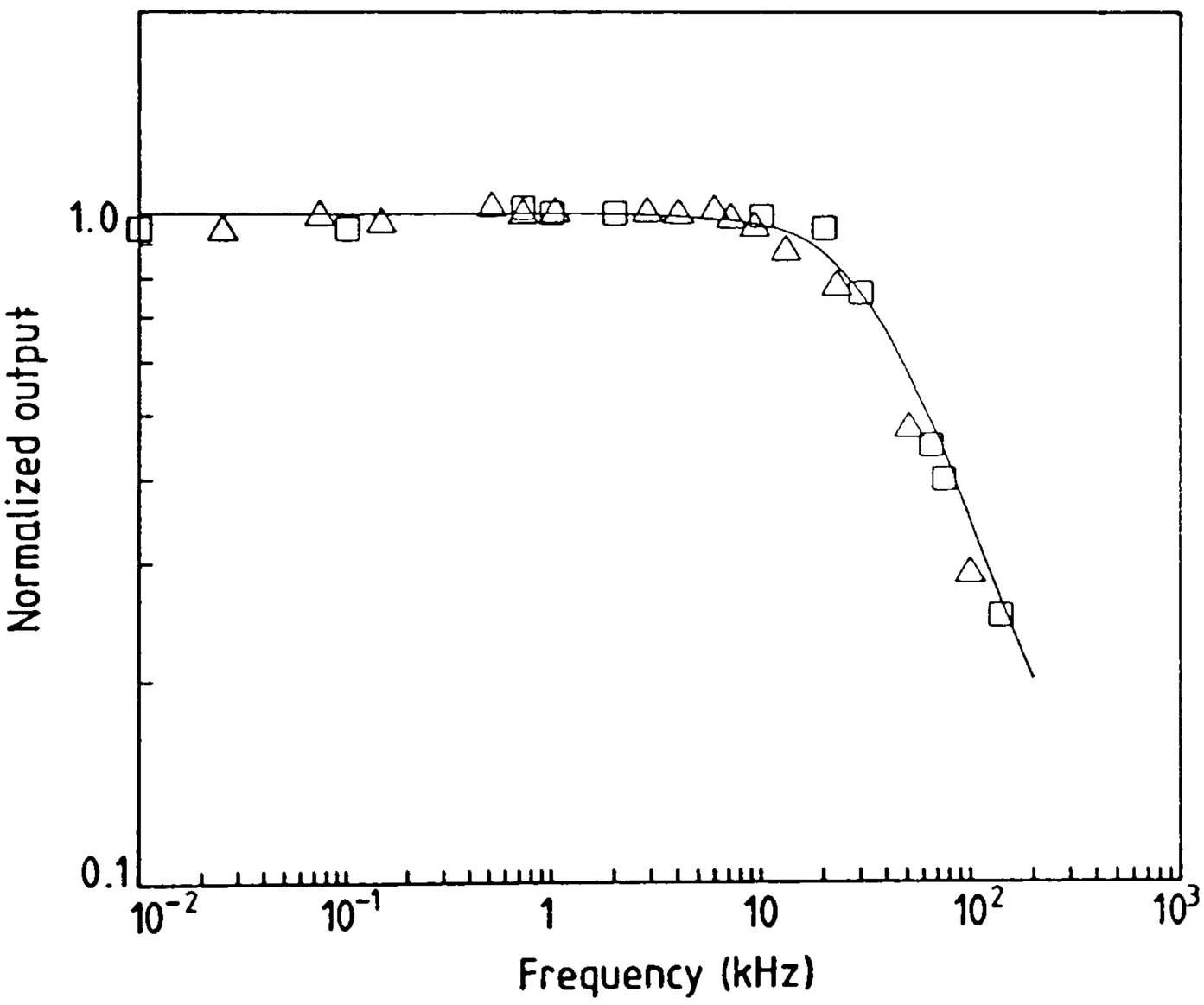

Figure 5.9 Frequency-response characteristics for a detector–amplifier combination using a Photops UDT455HS hybrid detector–amplifier combination. △ and □ represent the interferometric and direct modulation results respectively. The full line represents simulation results using PSpice.

Figure 5.11 shows the response of a BPX65 photodetector and an SL560 (Plessey) high frequency amplifier combination (fig.5.10) obtained using the fibre optic interferometric configuration. For this circuit a response modelled using PSpice is not shown because there was insufficient information on the exact parameters of the amplifier to enable incorporation into the program. However, comparison with the direct intensity modulation technique demonstrates agreement within a few percent up to ~30 MHz, limited by the range of the function generator.

5.6 DISCUSSION

The upper limit on the frequency range that can be achieved is determined by the path length imbalance that can be used, i.e. the coherence length of the source and the modulation frequency bandwidth of the source. The maximum continuously tunable frequency range of single mode laser diodes is approximately 50GHz and the coherence length typically lies in the range 1 to 10m. If we assume that a path length imbalance of approximately half the coherence length is required to provide an adequate signal to noise ratio then, using equation 5.3, a maximum phase change of approximately 10^3 to 10^4 radians, equivalent to approximately 160 to 1600 fringes, can be produced. To ensure a simple relationship between the modulation frequency and the measured frequency the delay time due to the optical path length imbalance must be much less than the time period of the modulation signal. Hence the upper frequency response measurement lie in the tens of gigahertz region.

At very low frequencies the temperature sensitivity of the fibre interferometer could reduce the accuracy of the measured frequency. For most applications this will not present major problems but for demanding applications the stability

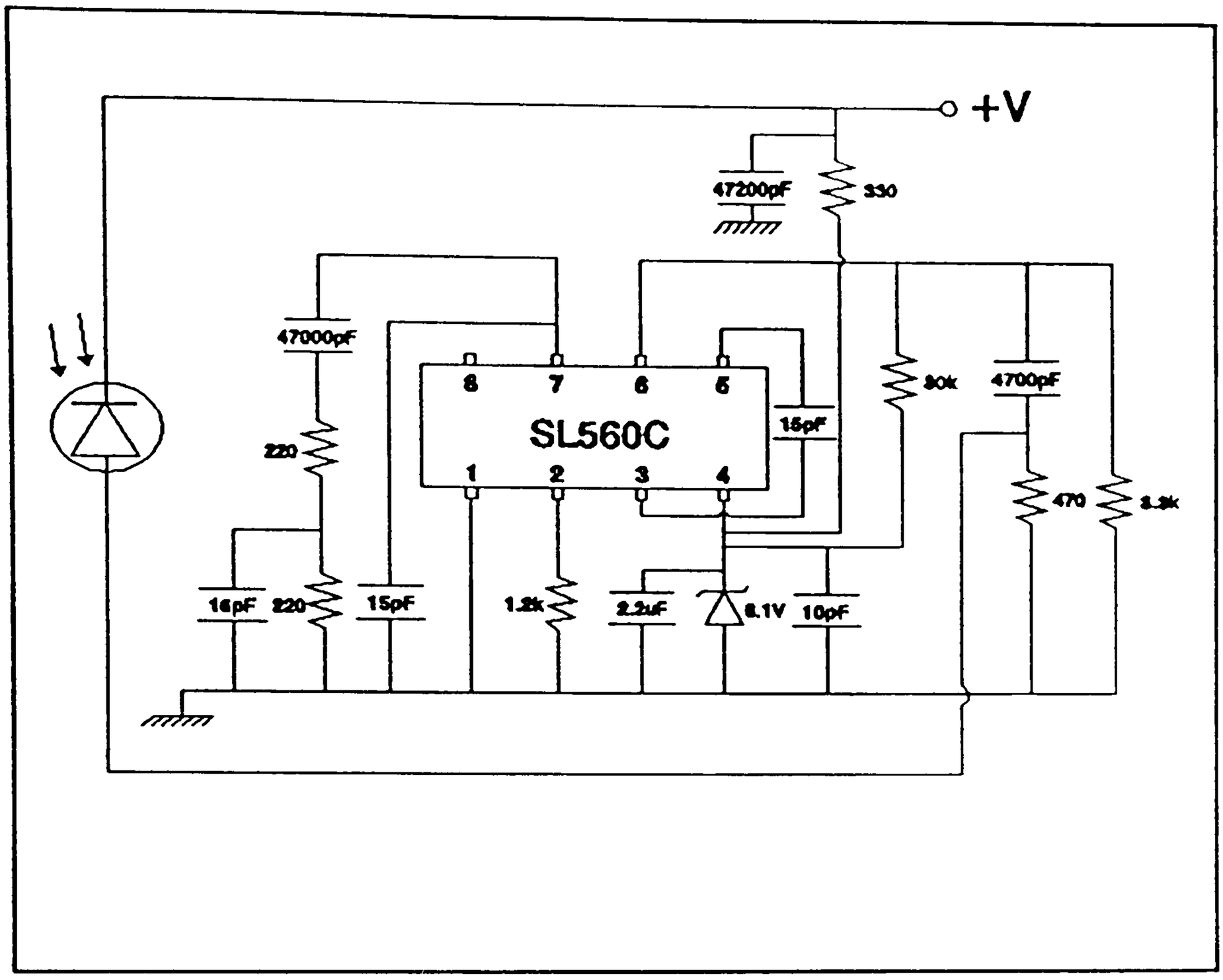

Figure 5.10 Circuit diagram of detector-amplifier using Plessey SL560C

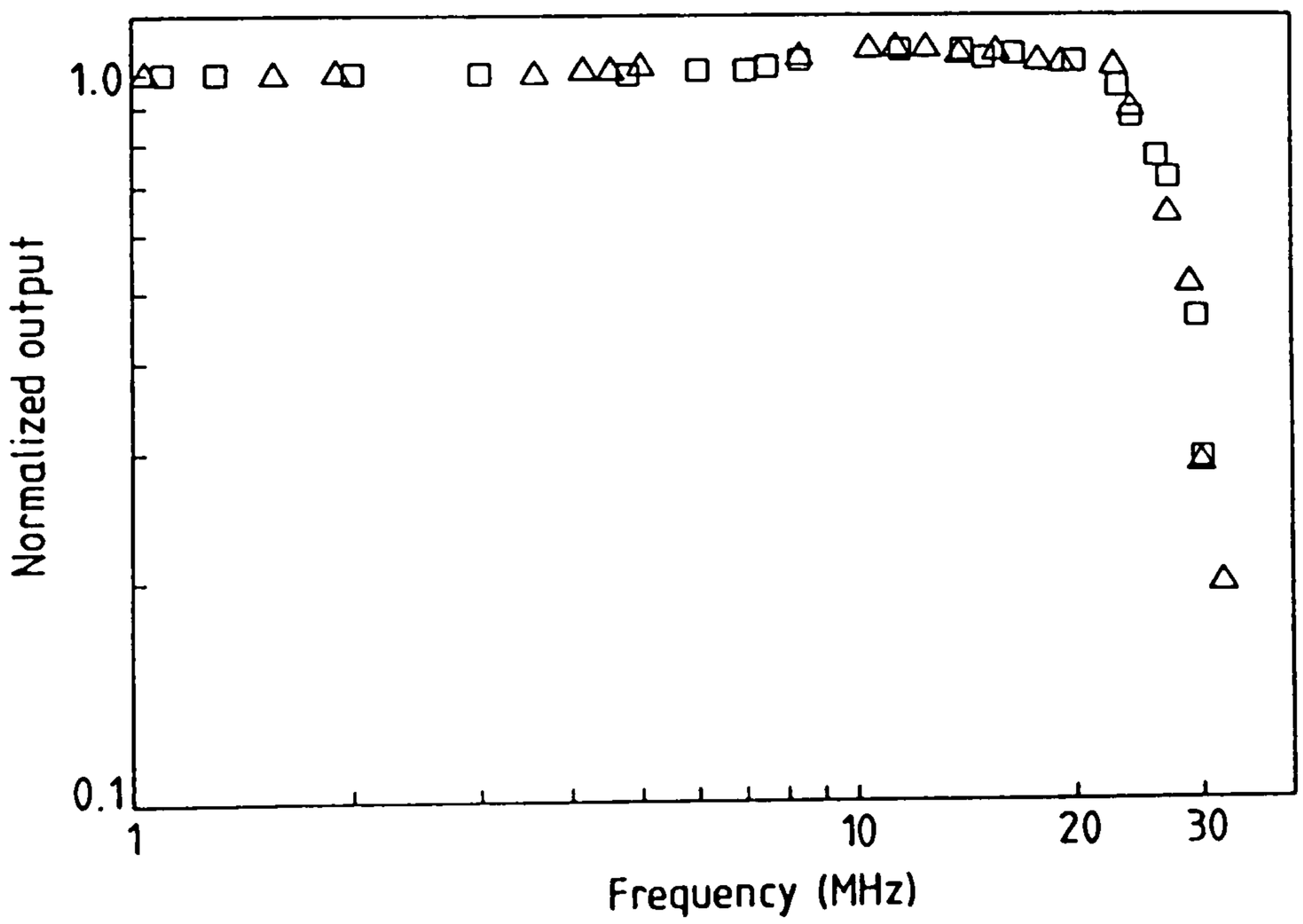

Figure 5.11 Frequency-response characteristics for a BPX65 photodetector and Plessey SL560 amplifier combination. △ and □ represent the interferometric and direct modulation results respectively.

could be improved by incorporating a path length stabilisation scheme by wrapping the fibre on a piezoelectric modulator [95] and locking the system for low frequency thermal fluctuations. Since polarisation preserving fibre is used the state of polarisation of the guided beam will be unaltered and therefore fibre optic polarisation state controllers [96] are not required.

CHAPTER SIX

FIBRE OPTIC FREQUENCY SHIFTER

6.1 INTRODUCTION

In this chapter a fibre optic frequency shifter, based on stimulated Brillouin scattering in optical fibre ring resonators, is demonstrated. First, the experimental performance of the ring resonators, which are the centrepiece of the frequency shifter, are investigated. An optical heterodyne carrier is generated by mixing two stimulated Brillouin scattering signals. Two different configurations are discussed; the first using two separate resonators and the other a single resonator. The dependence of carrier frequency on temperature variations is investigated for both configurations. A comparison between the two techniques is presented with particular emphasis on producing a device with a stable frequency output. Finally, the use of a laser diode in such a system, the effect of its linewidth on the resonator finesse, its advantages and limitations are described. Measurement of laser linewidth, using the self heterodyne technique and using effective finesse is also discussed.

6.1 THE PROPOSED APPROACH

As discussed in chapter 4 SBS generates a backscattered optical beam that is downshifted to a new frequency ν_P-ν_B. The frequency shift (the difference between the input pump wave and the Stokes wave) is 34 GHz to 10 GHz for a pump wavelength in the range 514 nm to 1300 nm respectively. This frequency is too high to be processed using the relatively simple electronic techniques, generally required in fibre optic sensor technology. However, the frequency can be reduced by mixing two slightly different SBS frequencies, generated from optical fibres with different effective refractive indices or from the two orthogonal polarization eigenmodes of a highly birefringrent optical fibre. This is the key idea behind the operation of the frequency shifters demonstrated later in this chapter.

6.2 PRODUCTION OF SBS

It is very important to consider the minimum power, or threshold power, required to produce SBS. In section 4.7.2 it was shown theoretically that SBS can be produced for <1 mW input power for high finesse, >50, devices. Also discussed in chapter 3 was that SBS can be observed at very low levels of pump power, <1 mW if a very large length of fibre is used, in non-interferometric configuration, otherwise the input power requirements will be very high. An alternative and efficient way to produce SBS at very low threshold power is to use an optical fibre ring resonator configuration. The obvious and the most important advantage of SBS based configurations, lacked in all other approaches, is that no external power source is required to provide the travelling acoustic wave; the travelling acoustic wave is generated

6.3 THE BEAT FREQUENCY

When the light of frequency υ is coupled into two different fibres, provided that the light intensity is above the threshold level, SBS will be generated and the frequency shift is given by eq. 4.9. Now, if these two frequencies υ^1_{SBS} and υ^2_{SBS} are mixed together, using eq. 4.9, the beat frequency is given by:

$$\Delta\nu_{SBS} = |\nu^1_{SBS} - \nu^2_{SBS}| = \frac{2}{\lambda_p}\left|\left(n^1 v_a^1 - n^2 V_a^2\right)\right| \qquad (6.1)$$

where $n^{1,2}$ and $v_a^{1,2}$ are the effective refractive indices and the acoustic velocities respectively for two different fibres. For the situation where a single high birefringence fibre is used, equation (6.1) becomes

$$\Delta\nu_{SBS} = |\nu^1_{SBS} - \nu^2_{SBS}| = \frac{2}{\lambda_p}\left|\left(n^f v_a^f - n^s V_a^s\right)\right| \qquad (6.2)$$

where the superscripts f, s refer to the fast and slow orthogonal polarisation eigenmodes respectively.

The absolute difference in refractive indices of different fibre types is generally very small and the difference in refractive index of the fast and slow eigenmodes in high birefringence fibre is also very small (<0.1%) and hence

to a good approximation $V_a^f \approx V_a^s$. Equation 6.1, for two separate fibre system, reduces to

$$\Delta\nu_{SBS} = \frac{2V_a}{\lambda_p}(|n^1 - n^2|) \qquad (6.3)$$

and equation 6.2, for a single high birefringence fibre system reduces to

$$\Delta\nu_{SBS} = \frac{2V_a}{L_B} \qquad (6.4)$$

where L_B is the beat length of the fibre ($= \lambda_p / (|n^f - n^s|)$). From equations 6.1 - 6.4 it can be seen that the heterodyne beat frequency obtained is proportional to the refractive index difference and hence different fibre birefringences can produce different carrier frequencies. Many types of high birefringent fibres are available with very small beat lengths of about 1 mm. It is obvious that the higher the birefringence the larger the frequency shift.

6.4 RING RESONATOR SPECIFICATIONS AND EXPERIMENTAL PERFORMANCE

A single frequency Helium Neon laser was selected as the *pump* as this laser has an extremely long coherence length; required to ensure high finesse operation of the resonator. Dependence of the effective finesse on the coherence length will be discussed later in this chapter in connection with the use of diode laser for this system. The maximum output power available from this HeNe (*Coherent 200*) is ~2.2 mW, after removing the output polarizer from the laser head. The function of this polarizer was to reduce the output power of the laser. Therefore, all calculations to specify the resonator were based on

this maximum power limitation. A maximum coupled power into the fibre of 60% was assumed. Since, to a first approximation for the case of the single high birefringent fibre system, equal amounts of optical power must be coupled into both eigenmodes simultaneously, this is equal to a maximum coupled power of 0.99 mW per eigenmode. The resonator has therefore to be specified such that SBS thresholds (eq. 4.44) are substantially below this figure in order to provide sufficient signal to noise ratio for the SBS beams.

One of the most important parameter from resonator performance point of view is its loop length. From equation 4.44 and figure 4.5 it can be seen that long resonator lengths favour lower values of SBS threshold power and hence improved conversion efficiency. On the other hand longer lengths also tend to increase losses in the resonator system. In addition to the finite coherence length of the pump laser (which places a limit on the resonator length in laser diode based systems), increased sensitivity of the longer lengths to ambient temperature changes, is another significant point to be taken into account, when specifying the length of the resonator.

We have experimentally observed that long loop lengths are better for the generation of stimulated Brillouin scattering, because in this case, although there will be a small decrease in finesse (equations 4.15 and 4.19) there will be an increase in the Brillouin interaction length per round trip leading to approximately the same input threshold pump power. This concept is supported by figure 4.5 which shows a decrease in finesse from 300 to 200 does not make a big difference to the threshold power. However, a decrease in interaction length will lead to a dramatic increase in the threshold power. As an example, considering the theoretical relation shown in figure 4.4, between the length and the threshold power shows that a decrease in length from 5.5m to 0.5 m increases the threshold power from 140 μW to 1547 μW (i.e. a

change of 1407 μW) while an increase of 5 m decreases the threshold power from 140 μW to 73.7 μW (i.e. a difference of 66 μW).

6.4.1 LOW BIREFRINGENT FIBRE RING RESONATOR

The first ring resonator (resonator 1), constructed from York Spun low birefringence fibre. Its specifications are given in table 6.1.

Loop length	2 m
Fibre type	York Spun Low Birefringent, LB600
Fibre loss	8 dB/km
Core diameter	~4 μm
Cladding diameter	~125 μm
Cut-off wavelength	535 nm
Numerical aperture	~0.12

Table 6.1 Specifications of low birefringent fibre ring resonator (resonator 1).

The experimental arrangement used to test the transmission properties of the resonator is illustrated in figure 6.1.

Light from stabilized single mode HeNe laser was launched into the ring resonator using microscope objective L_1 . The light emerging from the ring resonator was collimated by L_2 and detected by a detector *D*. To modulate the ring phase delay and to scan its free spectral range a length of the fibre was

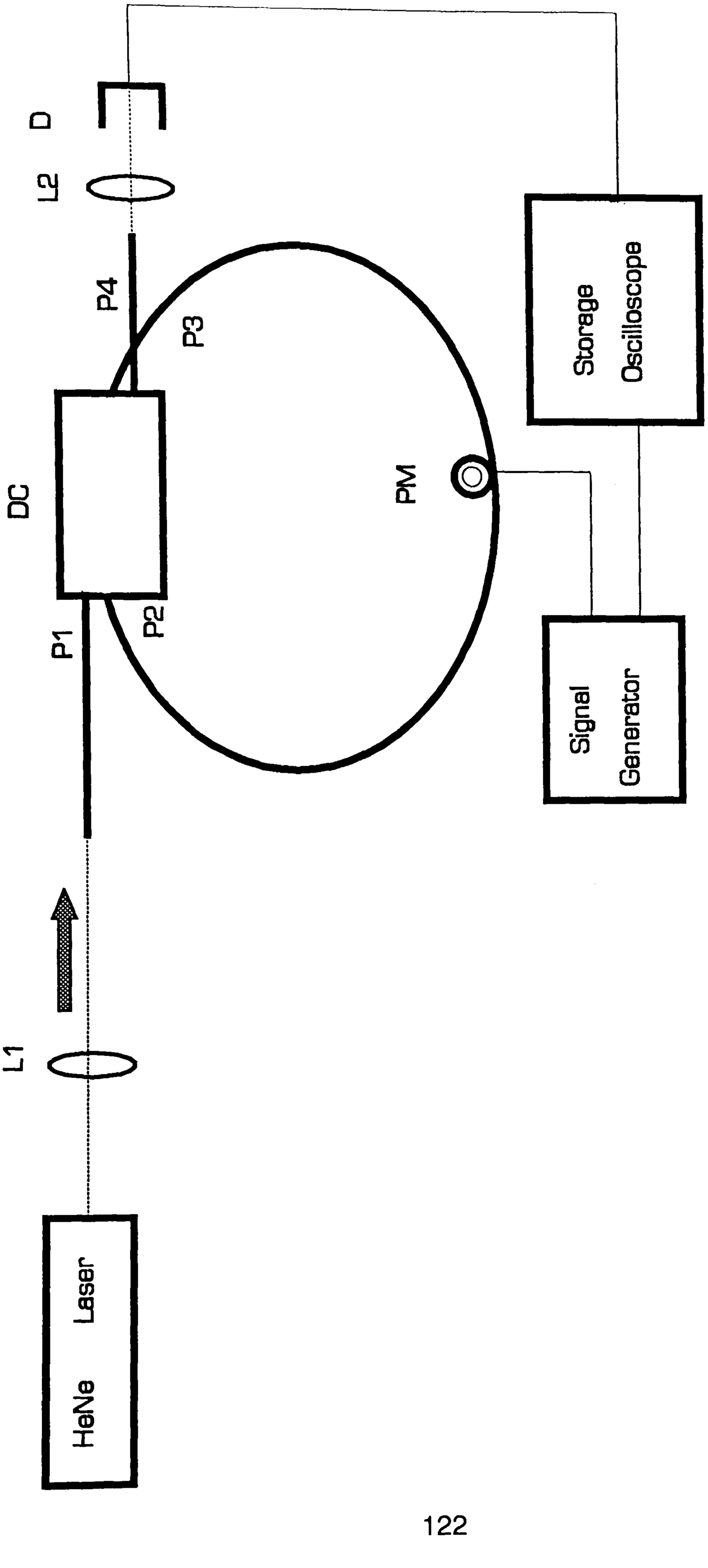

Figure 6.1 Experimental arrangement used to observe the transmission reponse of the ring resonator.
DC: Directional coupler PM : PZT phase modulator D: Detector-amplifier L1 & L2: Microscope objective.

attached with two PZT plates. The piezoelectric modulator was driven by a function generator. Both the transmitted intensity and modulating signal were monitored on a storage oscilloscope. The ring resonator was thermally shielded to prevent ring phase delay variations created by ambient temperature drifts.

The division of the total input power P_1 between the powers P_3 and P_4 leaving the output ports was selected by varying the distance between the fibre axes, i.e., the coupling coefficient K, using the micrometer attached to the coupler assembly for transverse movement,or by varying the coupling length using the longitudinal adjustment precision screws as shown in figure 6.7. The intensity coupling coefficient , K, is optimised when it is adjusted to inject just enough light into the fibre loop to compensate for the round trip cavity loss. At resonance constructive interference leads to the circulating intensity within the loop building up to a level such that the fraction of the circulating intensity that exits from port 2 to port 4 (i.e., $1 - K_r$) is exactly matched by the intensity of light coupled directly from port 1 to port 4. The splitting ratio or coupling ratio is given as:

$$r_c = 100 \frac{P_4}{P_3 + P_4} \quad (\%) \qquad (6.5)$$

The coupler was adjusted for zero transmission at resonance. The transfer function of the ring resonator is shown in figure 6.2. The resonator exhibited a finesse of ~100 which implies a ~4% round trip loss $(1-K_r)$ (eqs.4.1 & 4.19) and K_r ~ 0.96. The free spectral range c/nL of the resonator as 102 MHz. The frequency linewidth is 1 MHz. The maximum finesse of the resonator was in excess of 110.

For tuning and testing ring resonators phase modulation is required. The type of modulation that we have used was the linear ramp. In some instances

additional nonzero resonance dips and ringing effects were observed These spurious resonance dips were removed by decreasing the modulation frequency. The nonlinear response of dimensional change and resonant and ringing characteristics [38] of the piezoelectric modulator are the main reasons for these effects.

The piezoelectric transducer responds linearly, to applied signals, away from its mechanical resonant frequencies. Therefore to avoid these effects either low (<40 Hz) modulation frequencies or transducers with high mechanical resonant frequencies should be used.

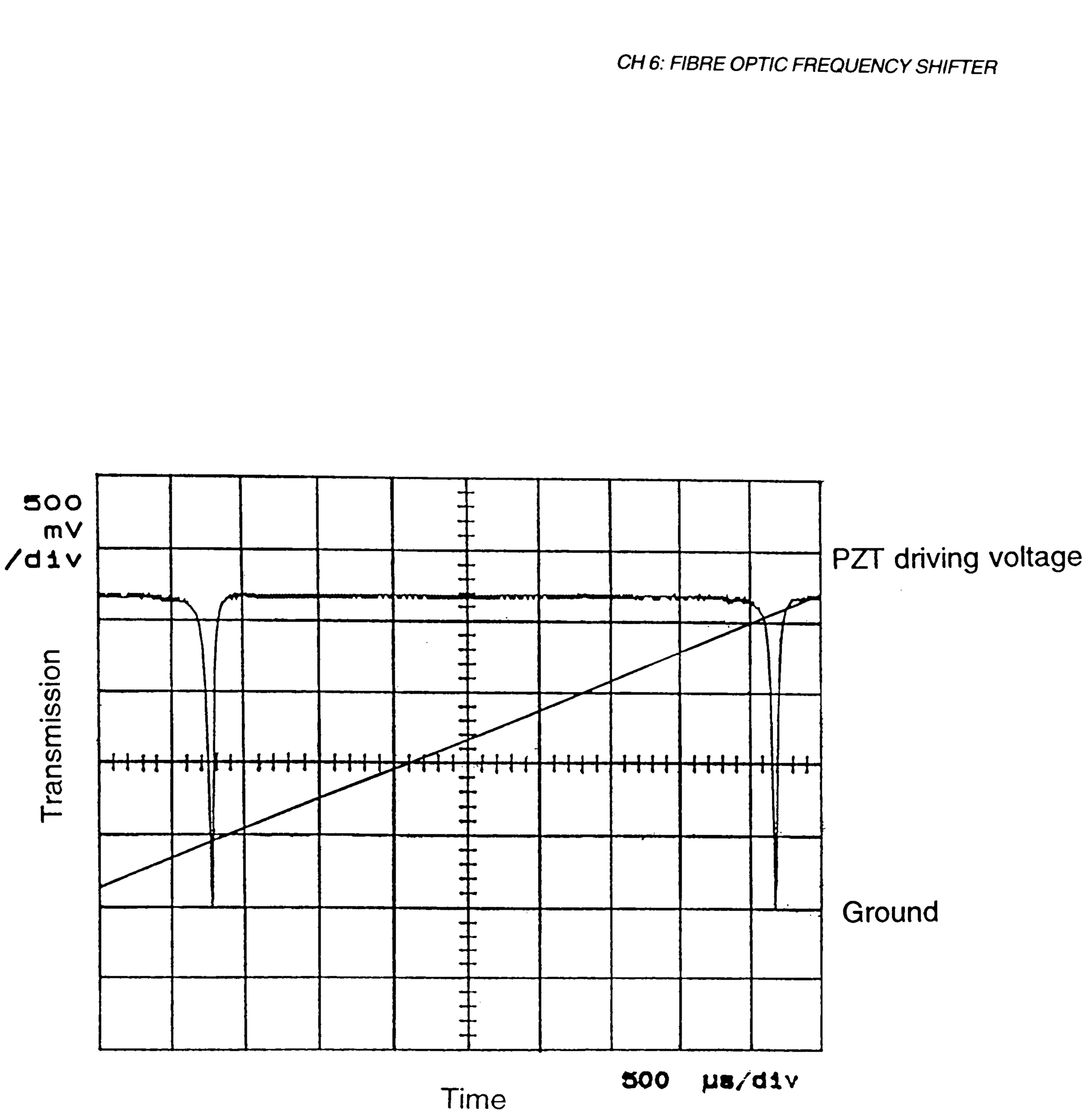

e 6.2 Experimental response of optical fibre ring resonator (resonator 1)

6.4.2 HIGHLY BIREFRINGENT FIBRE RING RESONATOR

The second resonator (resonator 2) was constructed from 15 m of Fujikura *PANDA* fibre (chapter 2). Its specifications are tabulated in table 6.2.

Length	15 m
Fibre type	Fujikura *PANDA*
Fibre loss	12 dB/km
Core diameter	~4 μm
Cladding diameter	~125 μm
Cut-off wavelength	620 nm
Numerical aperture	~0.11
Beat length	~1.1 mm

Table 6.2. Specifications of hi-bi fibre ring resonator (resonator 2).

The beat length of the fibre was measured by observing the polarization state evolution along the fibre from the Rayleigh scattering , as explained in section 2.3.2.

A fibre, illuminated with HeNe laser, viewed along the direction of the incident polarization exhibited a series of dark and bright bands with period L_B as shown in figure 2.4. From this measured value of 1.1$\pm$0.1mm, at λ_p = 632.8 nm, the birefringence of the fibre $B = \lambda/L$ is ~0.6×10^{-4}.

Figure 6.4 shows the experimental configuration used to observe the response of the highly birefringent ring resonator. Again, a single frequency HeNe laser was used as the pump. Before launching the light into the resonator, using a microscope objective, it was passed through a rotatable half wave plate to

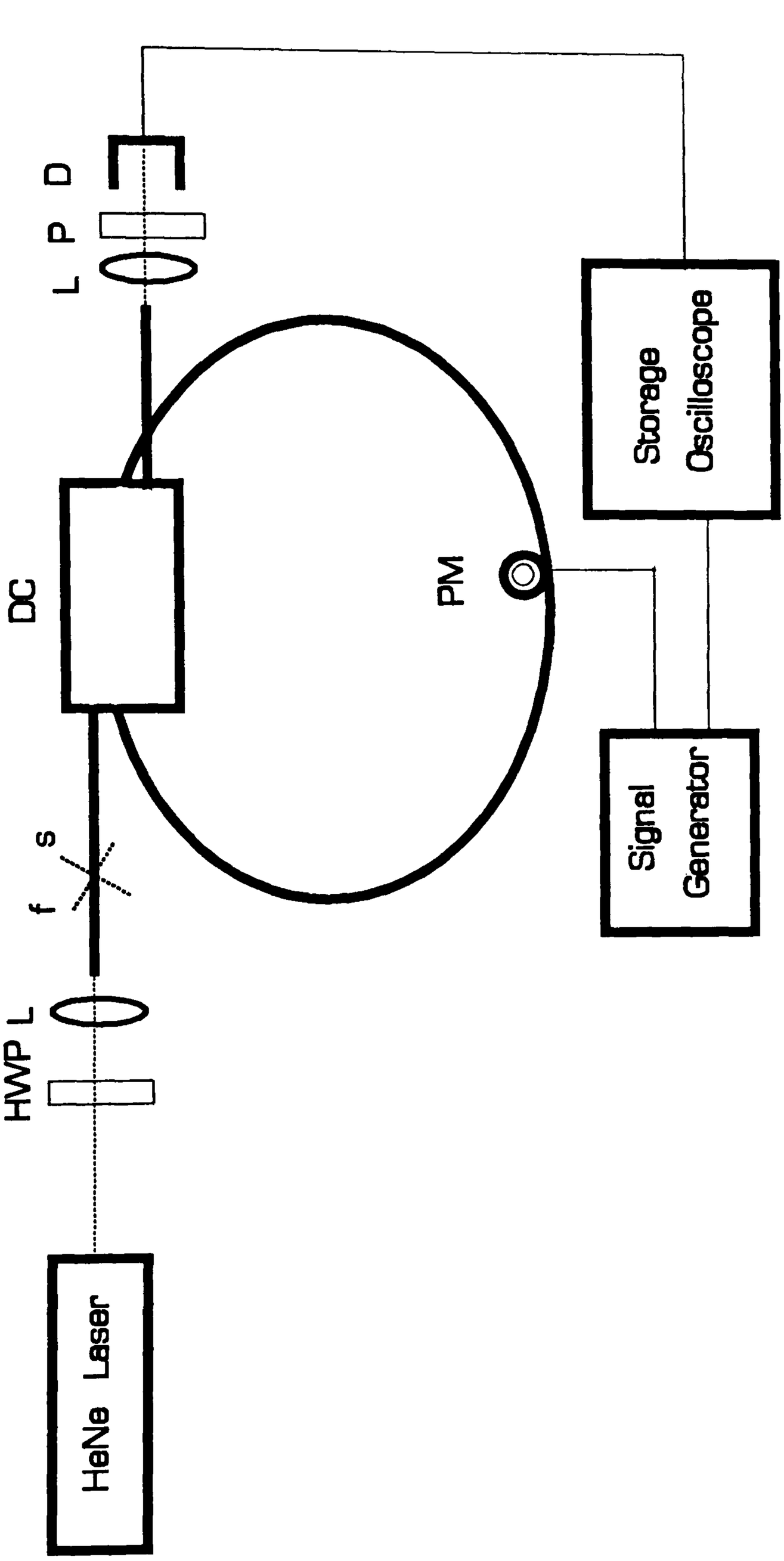

Figure 6.4 Experimental setup to observe the transmission reponse of the hi-bi fibrering resonator.
DC: Directional coupler PM: PZT phase modulator D: Detector-amplifier L: Microscope objective P: Polarizer.
HWP: Half wave plate.

microscope objective, it was passed through a rotatable half wave plate to align the linear state of polarization from the laser with a single eigenaxis or to launch the light at 45° into the orthogonal eigenaxes of the fibre ring resonator. The output of the resonator was collimated and detected by a photodetector amplifier combination. A polarizer was also sometimes used at the output of the resonator so the any light coming out from the axis which is not initially populated, can be extinguished. A small portion of the fibre loop was attached to two piezoelectric plates. The phase modulator was driven by a triangular voltage signal. The intensity transmission of the ring resonator was observed from the oscilloscope connected to the detector.

Figure 6.5(a) shows the output from the ring resonator when light was launched into one of the fibre axis . The finesse was measured as 50. Eq.4.19 gives K_r = 0.78 and round trip loss ($1\text{-}K_r$) of ~22%. The free spectral range c/nl is 13.6 MHz which gives a frequency linewidth Δf of resonator output spectrum ~0.5 MHz. When the coupling constant was changed, using the micrometer attached to the directional coupler, from its resonant value K_r, the output power became nonzero (as discussed in chapter 4). Figure 6.5(b) shows the output for K less than K_r.

When the linear polarization state of the light source is not exactly aligned with one of the fibre axes (this can be achieved by rotating the half wave plate at the input of the ring resonator) each polarization eigenstate produces a distinct resonance effect in the response of the resonator. Figure 6.14(a) shows a typical transfer function of resonator in the presence of birefringence. The transmission exhibits two response dips instead of one. The extent of excitation of each eigenstate depends on the amount of light coupled in each fibre axis. In general these two modes resonate at two different scanned positions due to slightly different propagation velocities of the two polarization modes.

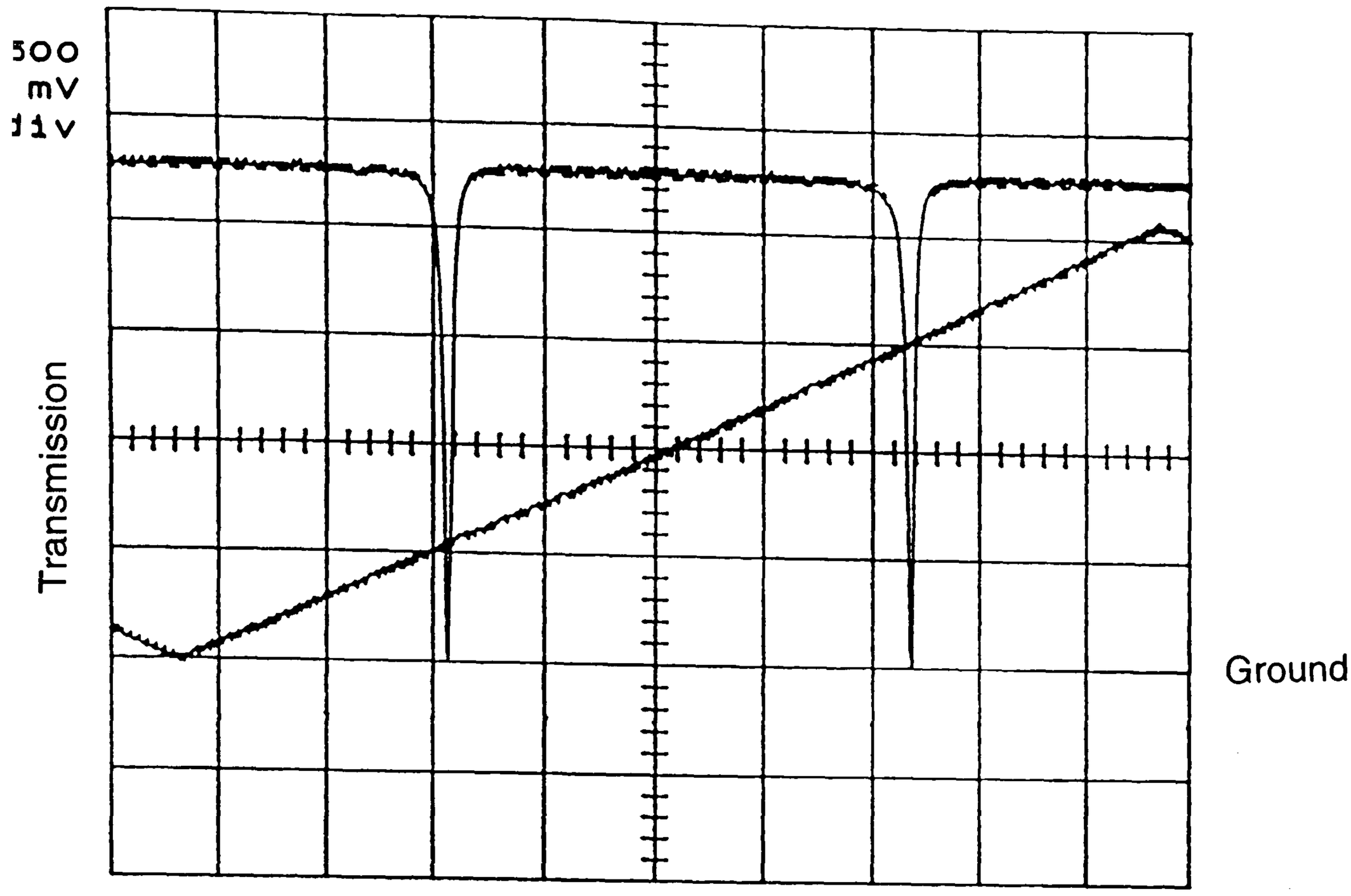

Figure 6.5 (a) Output of the ring resonator with *K* ~*Kr*

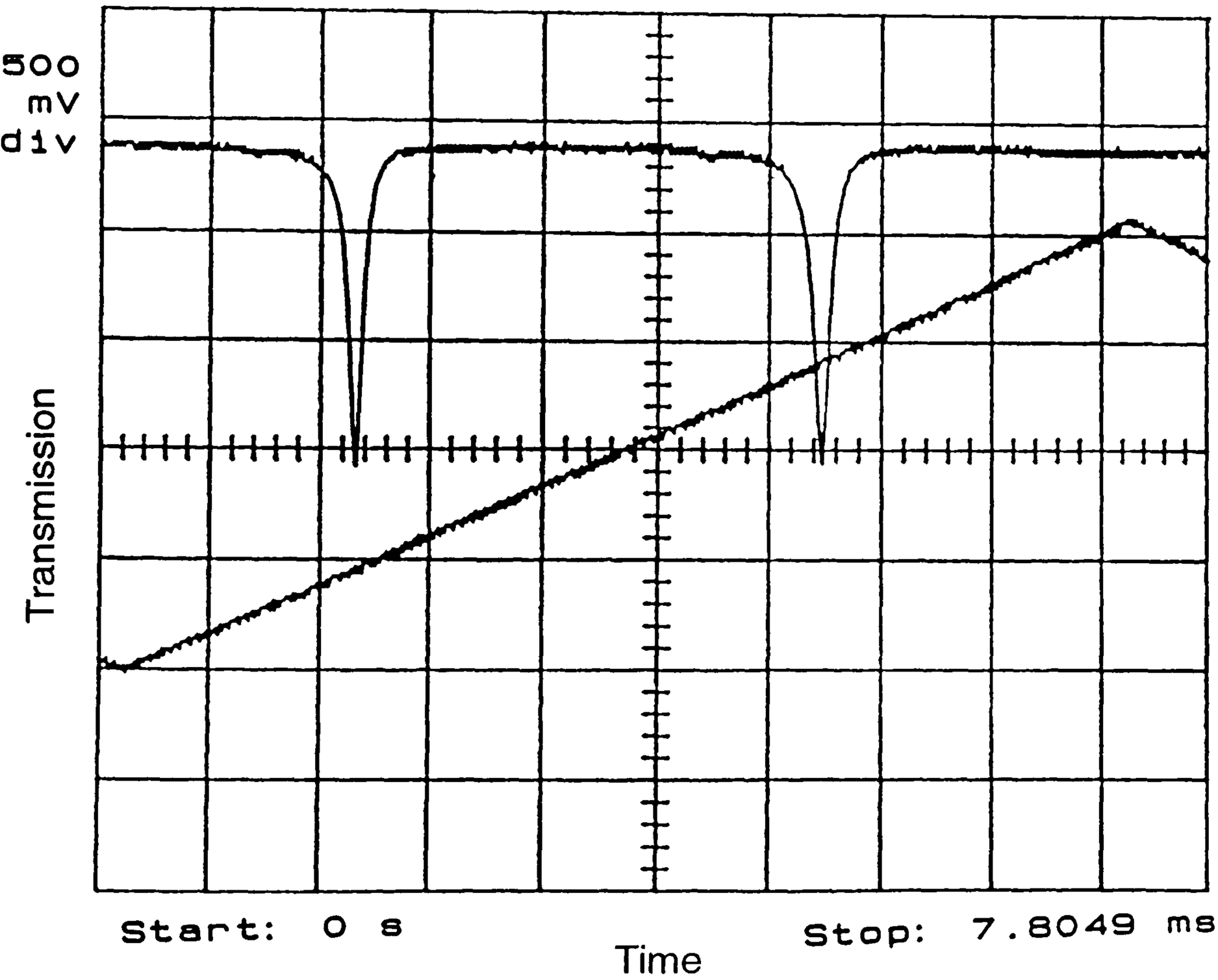

Figure 6.5 (b) Output of the ring resonator with *K* < *Kr*

6.5 IMPROVEMENT OF RESONATOR PERFORMANCE

Initially the resonator exhibited a finesse of ~27. For this value of finesse a large amount (> 1.5 mW) of optical power is required to produce a minimum detectable amount of SBS. In an effort to increase the finesse of the resonator, the two coupler blocks were moved in the longitudinal direction parallel to the fibre. Movement in the direction perpendicular to the fibre axis was controlled by the micrometer as shown in figure 6.6. To obtain the maximum amount of coupling, the polished fibre portions should overlap so that the fibre cores are closest. No resonance dips were observed at this position; the reason being that this situation usually corresponds to a coupling constant greater than the desired K_r , and called *overcoupling*. Therefore the coupler blocks must be transversely offset a few microns to increase the core to core separation, thereby reducing the coupling to the value K_r. If the polished portions of the fibre are offset longitudinally, by sliding one block over the other, using precision screws on both sides of the coupler, in the direction parallel to the fibre axis, the core to core separation increases, yet enough coupling may remain to obtain resonance. This longitudinal offset showed a dramatic effect on the resonator finesse and the coupler insertion loss. Index matching oil also plays an important role in the loss mechanism of the ring resonator. From time to time during the experiments a small amount of the oil was inserted between the blocks using capillary action.

The angle between two fibre polished regions determines the symmetry of the output transfer function. This angle is changed by rotating one coupler half with respect to the other about an axis perpendicular to the polished coupler-half plane. During the experiments the coupler was adjusted quite often to maximize the finesse. It was found that even a small rotation can cause a change in the shape of the output. Figure 6.7 shows the output of the resonator when the two blocks are slightly misaligned. After aligning the blocks and optimizing the coupling constant a maximum finesse of ~125 was

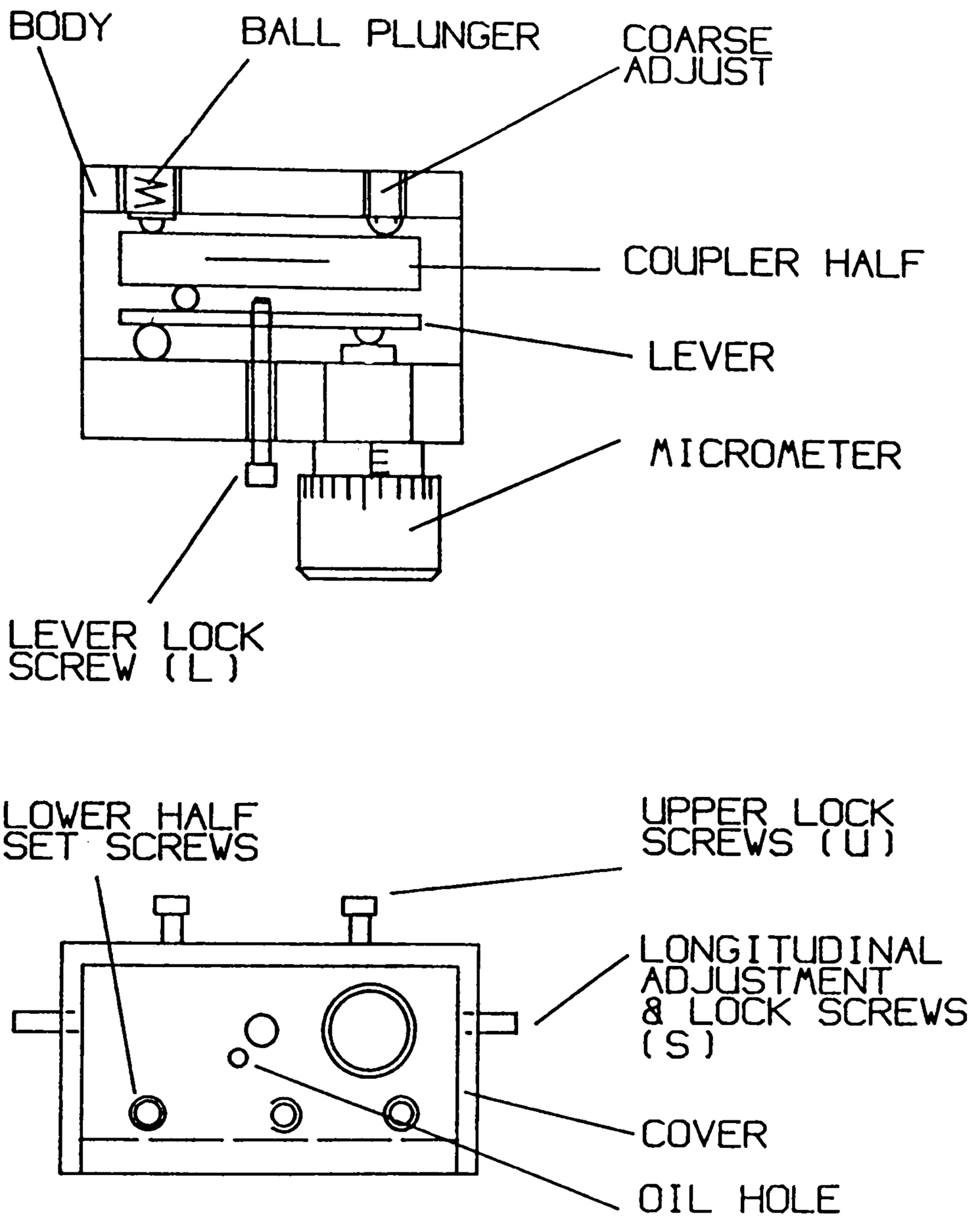

Figure 6.6 Mechanical setup of directional coupler

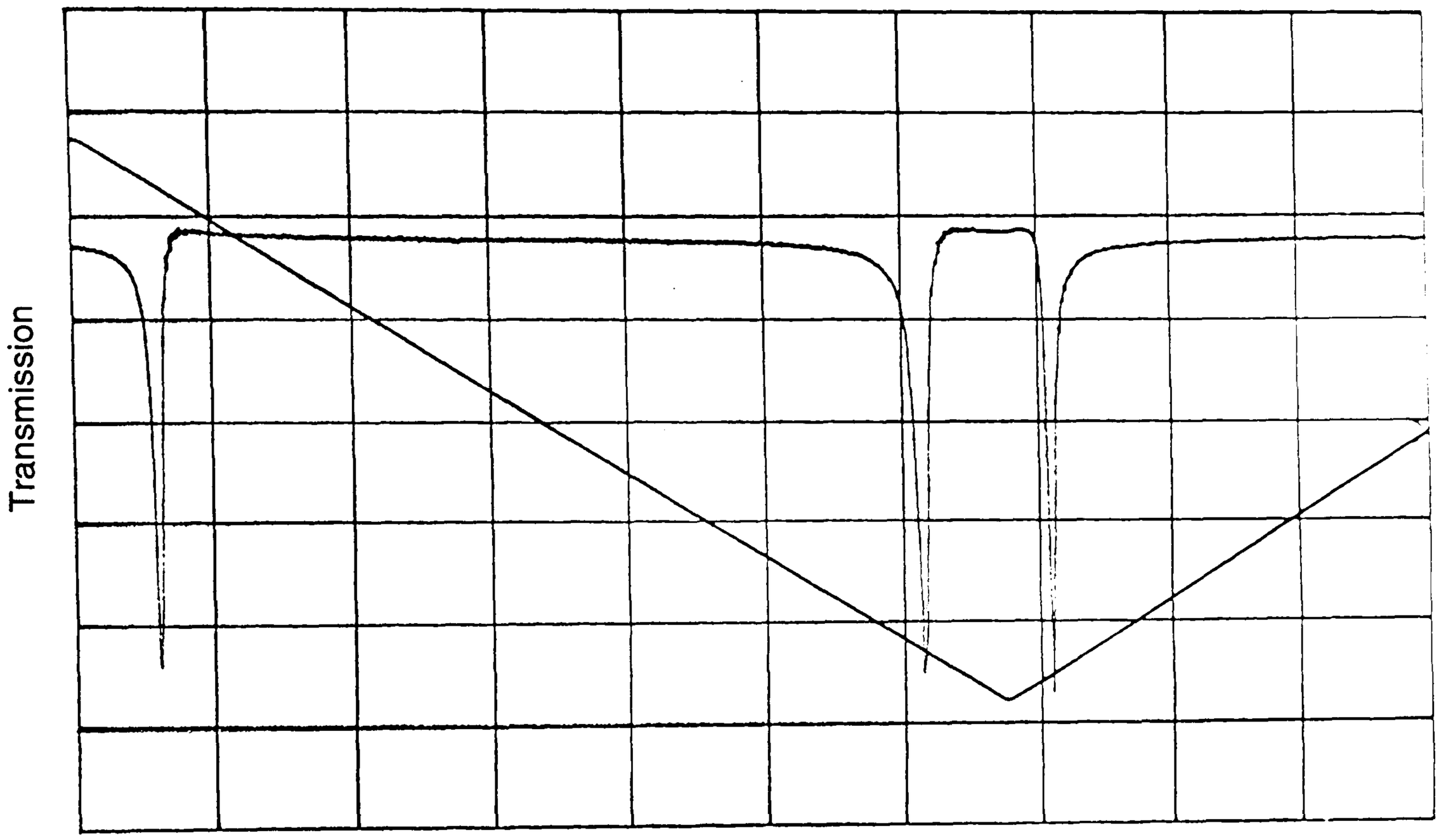

Figure 6.7 Asymmetric resonator output due to misalignment of the coupler blocks

6.6 FREQUENCY SHIFTER BASED ON DUAL RESONATOR SYSTEM

The experimental arrangement for a frequency shifter, based on two resonators, is shown in figure 6.8. A single frequency Helium Neon (632.8 nm) laser with a maximum output power of ~2.2 mW was used as the pump source to ensure sufficient coherence length to obtain maximum finesse, and hence minimum threshold powers. The half wave plate was used to align the linear state of polarisation from the laser with a single eigenaxis of the birefringent resonator. An active length stabilisation technique incorporating a piezoelectric phase modulator and servo control was used to compensate for random environmentally induced phase perturbations and thus maintain the resonance condition and hence maximise the circulating optical power. In this technique, the detected output from the ring resonator is sent via the feedback electronics to the PZT which is used to adjust the loop length. The backscattered SBS from each resonator was mixed on a high speed detector amplifier combination and monitored on an electronic spectrum analyzer HP8591A (9kHz-1.8 GHz). The overall launching efficiency for resonator 1 and 2 was 68% and 48% respectively. The SBS onset was ~15μW and ~6μW respectively for resonator 1 and 2. The heterodyne carrier power was ~200 μW giving an overall conversion efficiency of ~16%. To tune the heterodyne carrier frequency ring resonator 2 was heated to ~40°C in an oven and then cooled to ~1°C in a fridge whilst maintaining resonator 1 at room temperature (~24°C).

6.6.1 RESULTS AND DISCUSSION

For both resonators the SBS shift was measured as 26$\pm$0.4 GHz using a Fabry-Perot interferometer. Figure 6.9 shows the spectrum analyzer output for

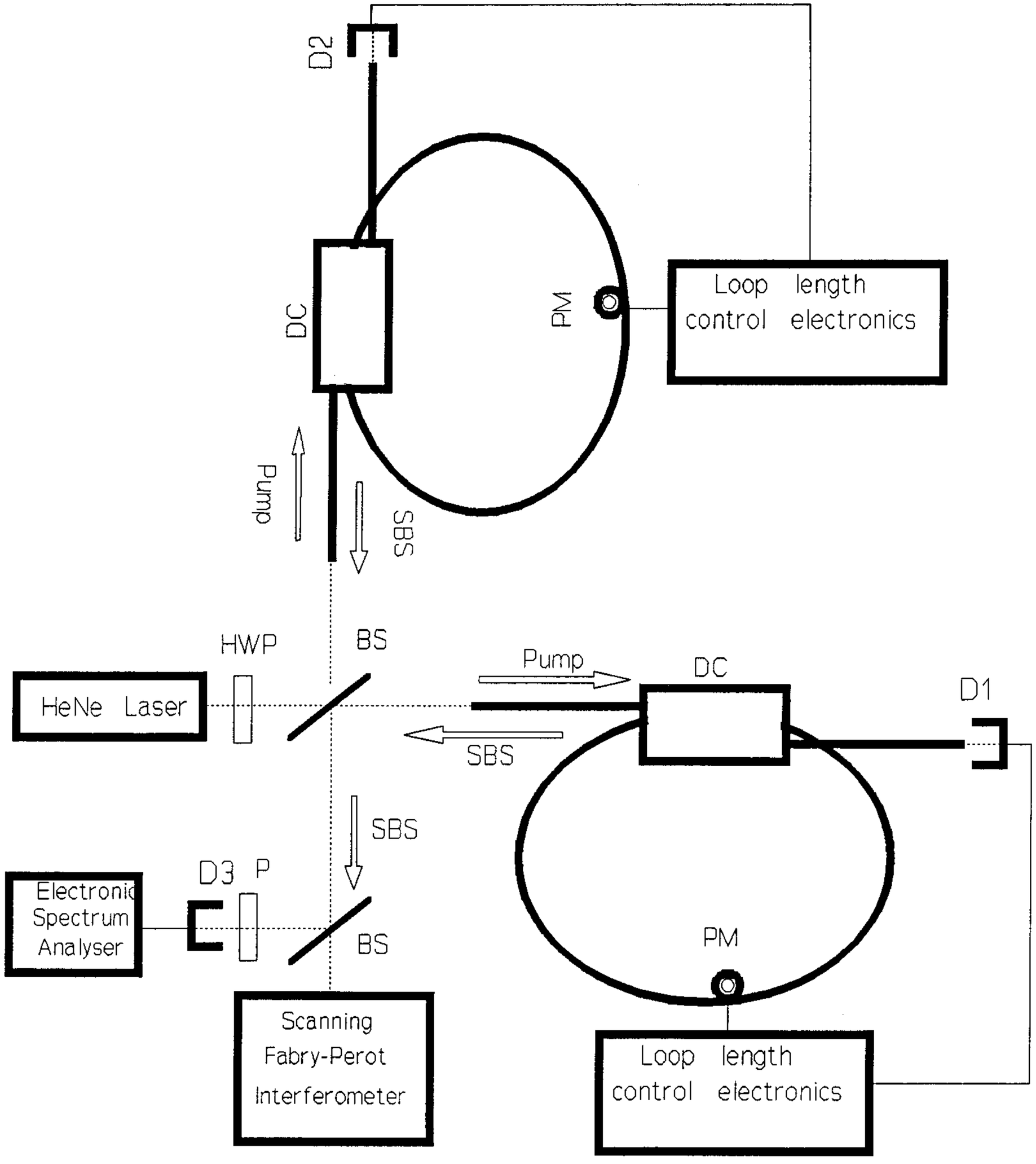

Figure 6.8 Experimental arrangement (dual resonator system). HWP: half wave plate; BS: beamsplitter; DC: directional coupler; PM: PZT phase modulator; P: polarizer; D1, D2, D3: detectors.

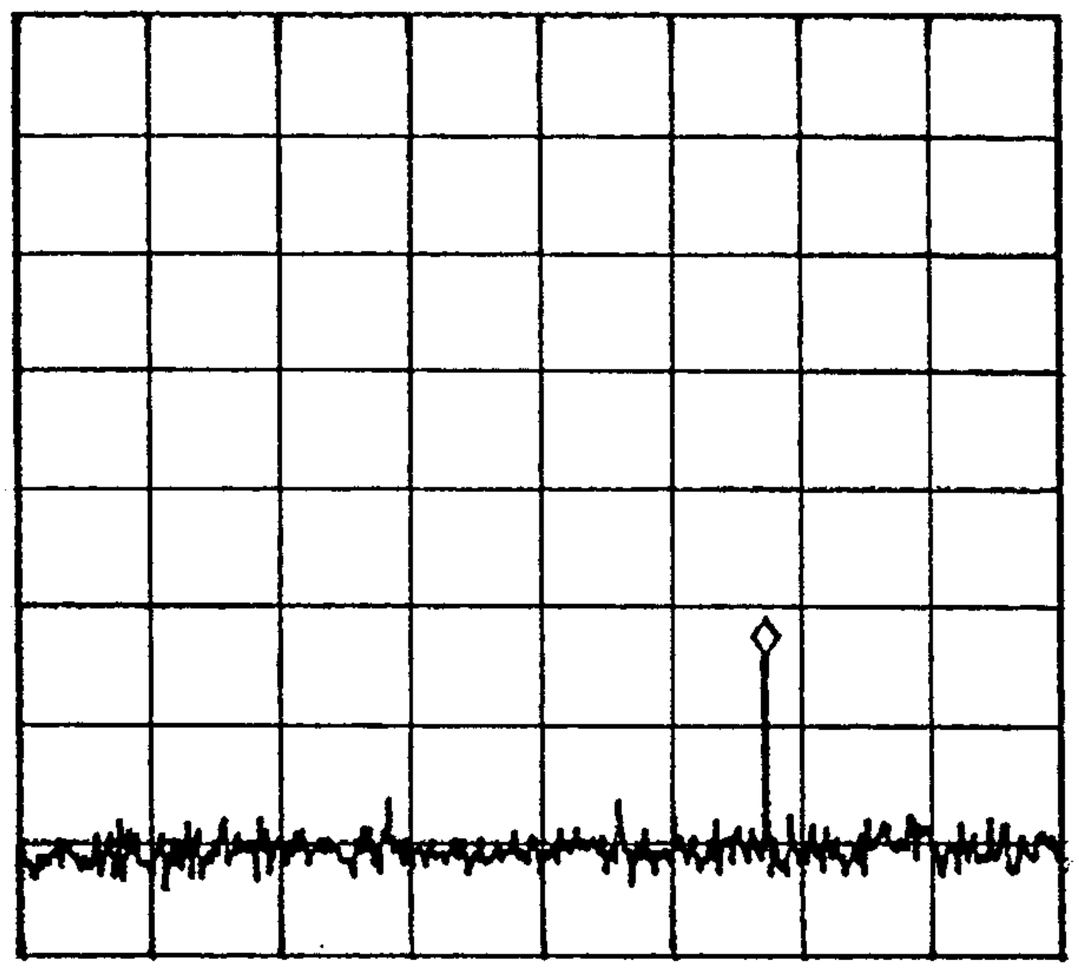

Temperature = 36.5°C Frequency =371MHz

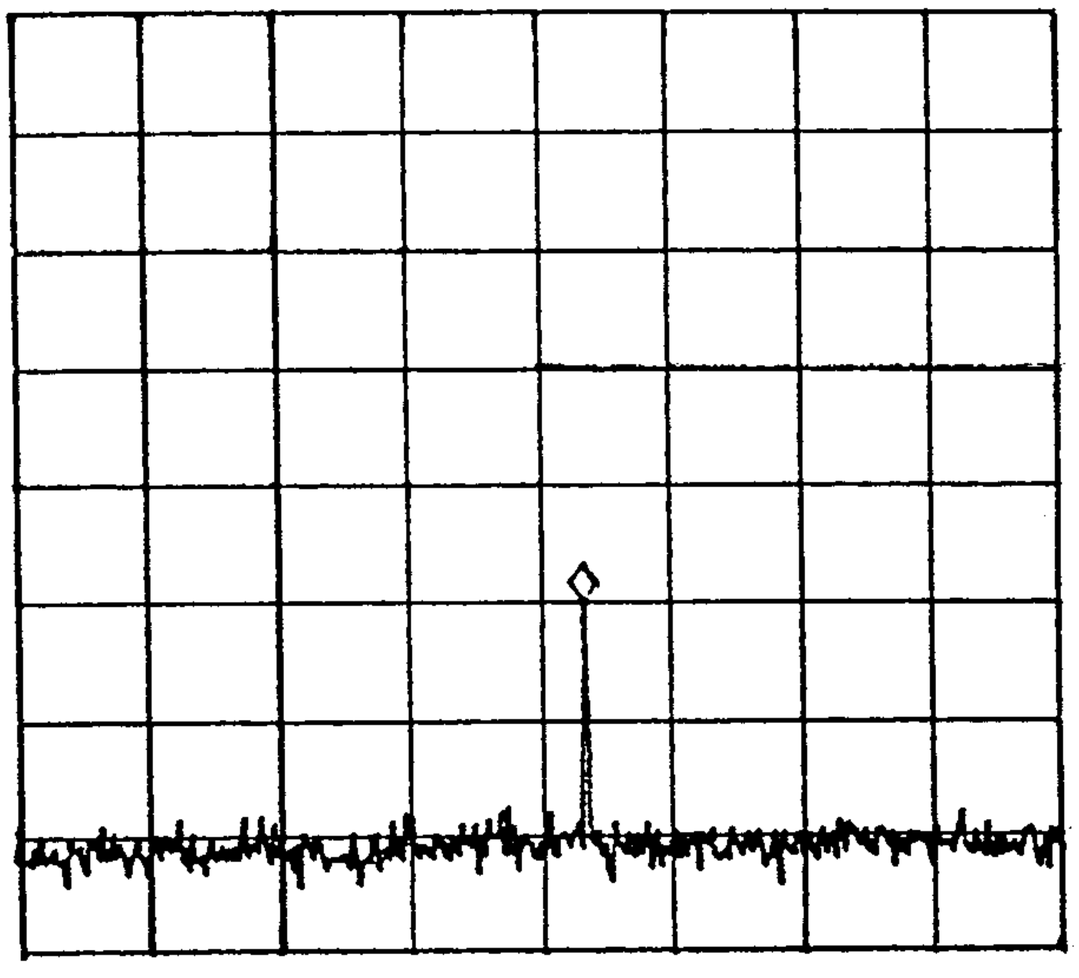

Temperature = 34.4°C Frequency =362MHz

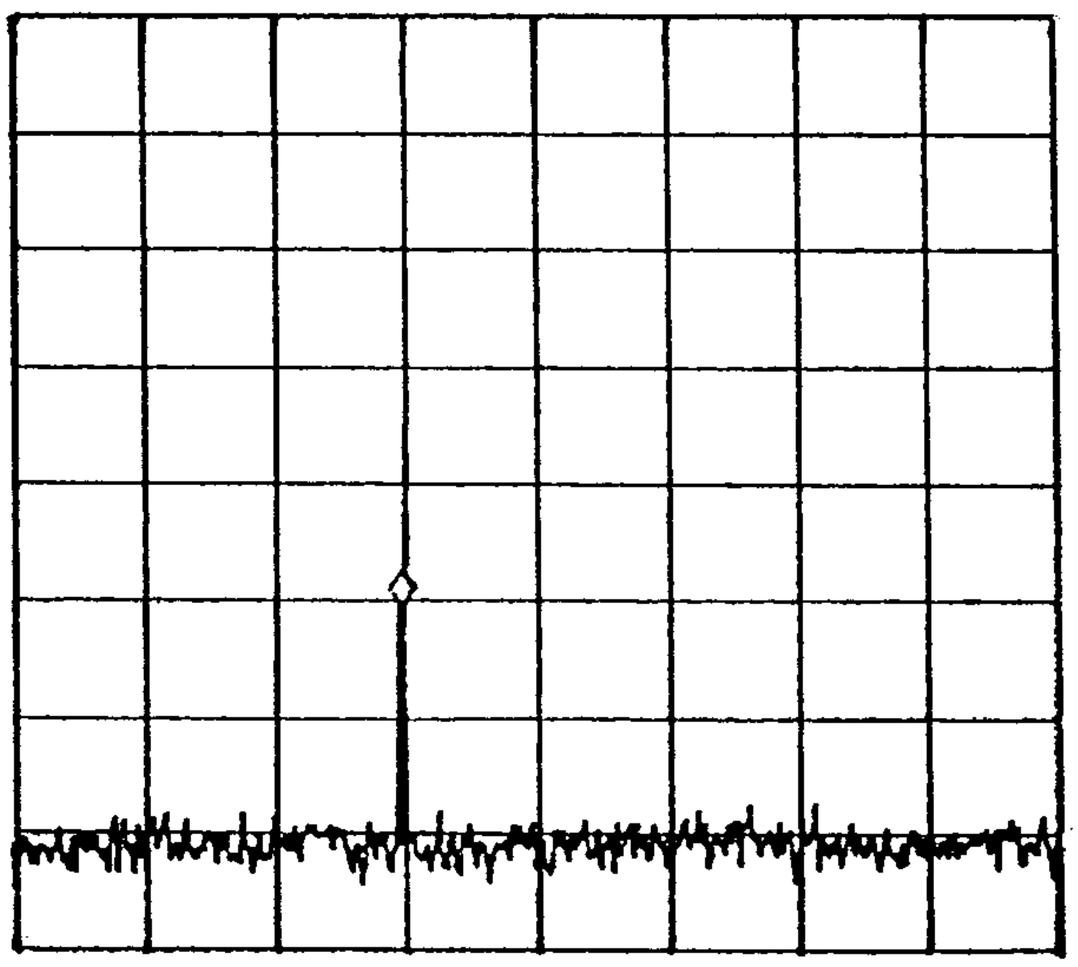

Temperature = 30.5°C Frequency =351MHz

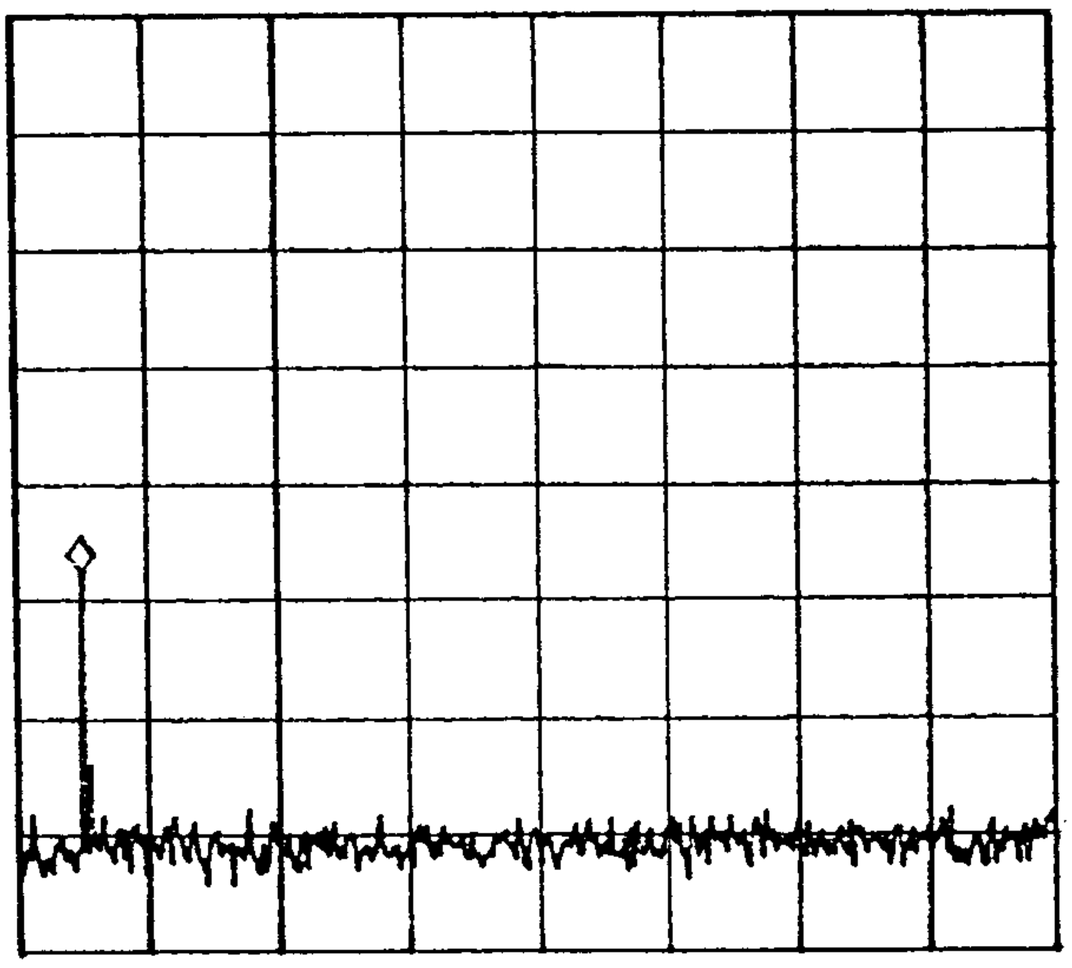

Temperature = 26.3°C Frequency =332MHz

Figure 6.9 Heterodyne beat frequency displayed on electronic spectrum analyzer for four different temperatures of resonator 2; resonator 1 @ 24°C. Resolution bandwidth was 30 kHz.

four different temperatures of resonator 2 (resonator 1 @ 24 °C). The beat frequency is in the region 200-400 MHz for a 40°C change in temperature. A coefficient of $d\Delta\nu_B/dT = 5\pm0.2$ MHz/ °C was measured which is consistent with 3 MHz/ °C reported in reference [100] using different fibre types. The absolute frequency shift can be varied either by changing the relative temperature between the rings or by using rings manufactured from different fibre types such that there is different refractive index difference. However, the $d\Delta\nu_B/dT$ coefficient will stay in the range of 3-5 MHz/ °C for silica based optical fibres. Although the carrier frequency is readily tunable using two rings in order to obtain a carrier frequency stable to ~10 kHz/ °C (comparable to a conventional Bragg cell) requires a temperature stability of ~2×10^{-3} °C between rings which is very difficult to achieve.

6.7 FREQUENCY SHIFTER BASED ON A SINGLE BIREFRINGENT RESONATOR SYSTEM

The technique, for a frequency shifter using single resonator, was demonstrated using the optical configuration of figure 6.10. The resonator was fabricated from 15 m of Fujikura *PANDA* fibre (ring resonator 2) as discussed in section 6.4.2. A single frequency Helium-Neon laser operating at 632.8 nm with an output power of ~2.2 mW was used as the pump source. A half wave plate was used to orientate the input state of polarisation at ~45° to the fast and slow axes of the fibre thus providing approximately equal population of the two orthogonal modes; in practice the threshold power for the two modes is slightly different due to slightly different effective core diameters and different core refractive indices. A 50/50 beam splitter at the input was used to couple a portion of the backscattered SBS onto a high speed detector-amplifier combination (D2) and scanning Fabry-Perot interferometer. Figure 6.11 shows

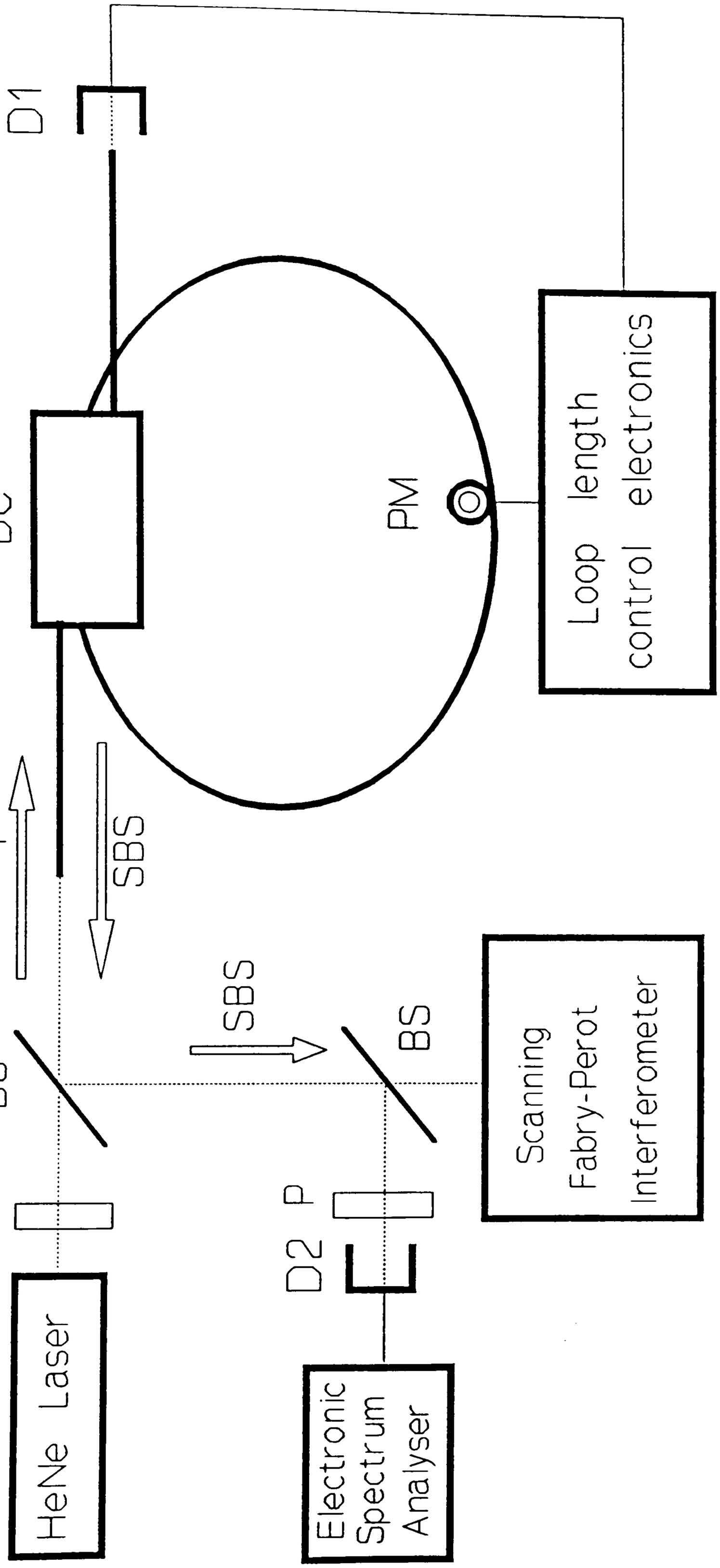

Figure 6.10 Experimental arrangement (single resonator system). HWP: half wave plate; BS: beamsplitter; DC: directional coupler; PM: PZT phase modulator; P: polarizer; D1, D2: detectors.

a photograph of the 15 m resonator locked onto resonance. The resonator loop can be seen glowing clearly, demonstrating the large buildup in circulating pump power that can be achieved. The SBS frequency shift was measured as 26±0.4 GHz using the Fabry-Perot as shown in figure 6.12. The frequency shift was in good agreement with previously reported values for this pump wavelength. The detector D1 is used in the servo locking electronics. The polariser in front of D2 is oriented at 45° to the eigenaxes and thus resolves the two orthogonally polarised SBS beams.

In this configuration there are essentially two resonators, separated by state of polarisation rather than spatially as in the previous technique, and both must be held at resonance simultaneously to produce an SBS mixed frequency. Since the propagation constants are different for the two polarisation eigenmodes they will not in general be at resonance simultaneously. However, the modes can be brought to a simultaneous resonance by changing the relative propagation constants. This can be achieved by either longitudinal strain applied to the fibre or by changing the temperature of the fibre. In this experiment a low frequency triangular waveform was applied to the piezoelectric phase modulator to scan the output of the ring resonator. Figure 6.13(a) shows the general case when the two modes are not resonating together and figure 6.13(b) when the modes are resonating simultaneously. Once the two modes are resonating simultaneously the servo is switched on.

6.7.1 RESULTS AND DISCUSSION

Figure 6.14(a) shows the variation of backscattered optical power as a function of coupled pump power for different finesse values. The percentage error in measuring the SBS power was ±5%. As expected from equation (4.44), P_{ring}

Figure 6.11 Ring resonator at resonance

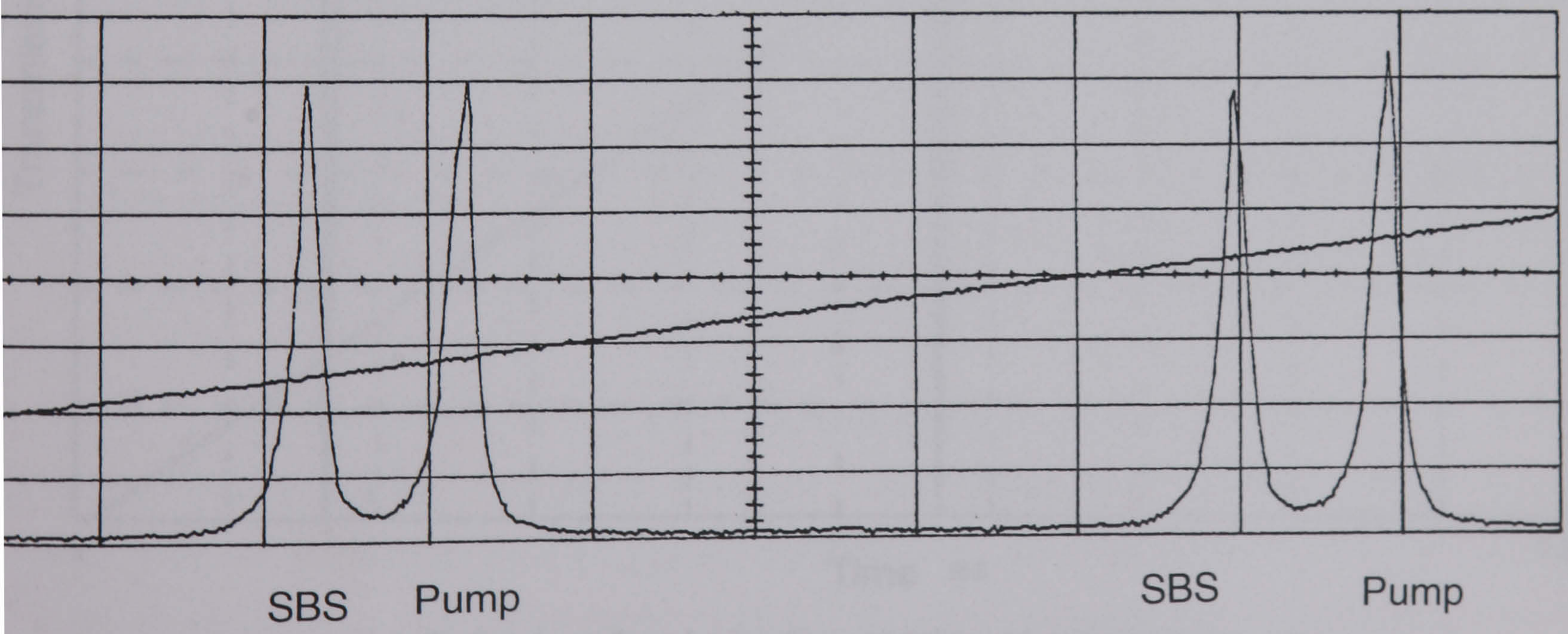

Figure 6.12 Fabry-Perot response showing pump and the frequency shifted peak

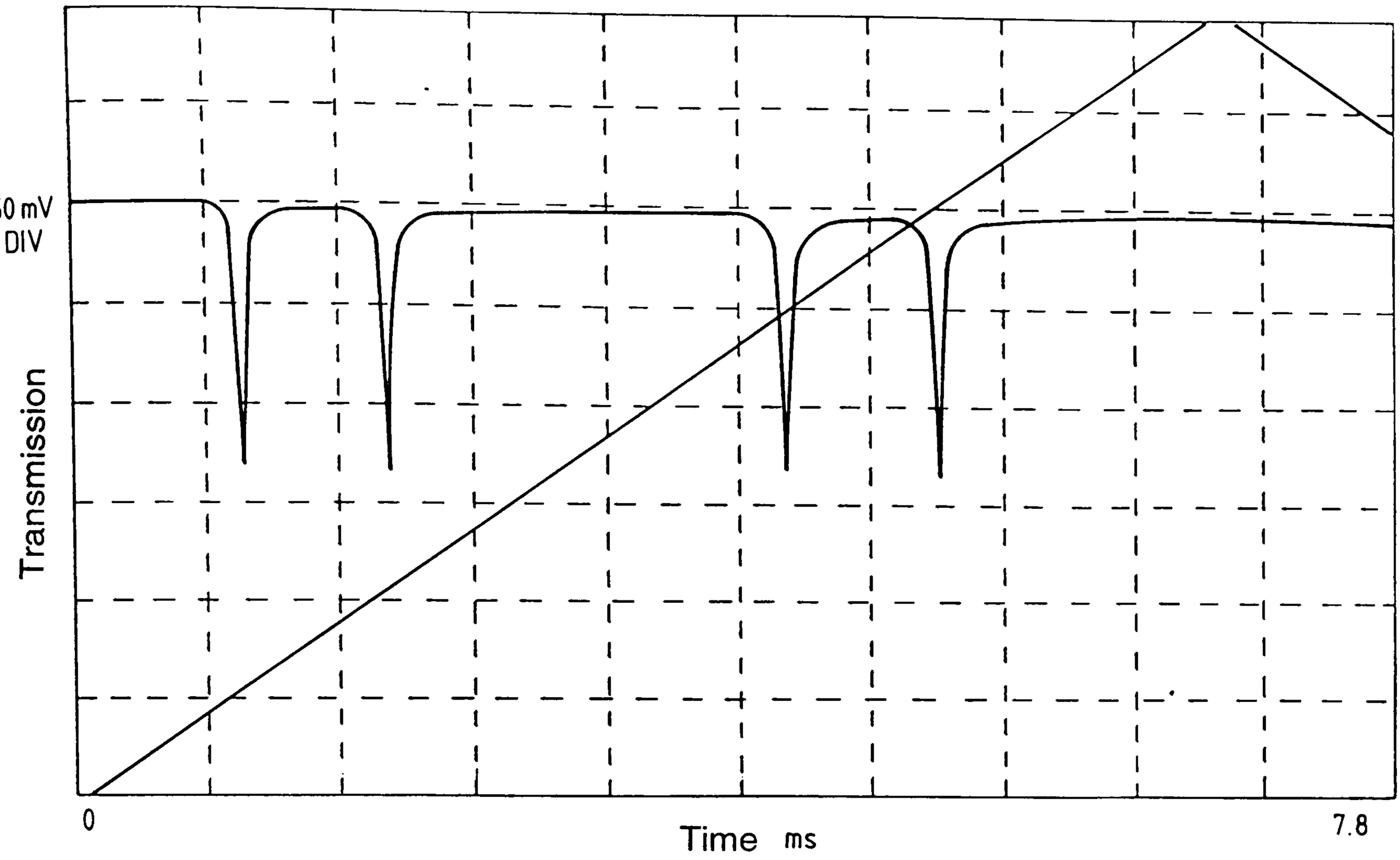

(a) Orthogonal polarization modes not at resonance

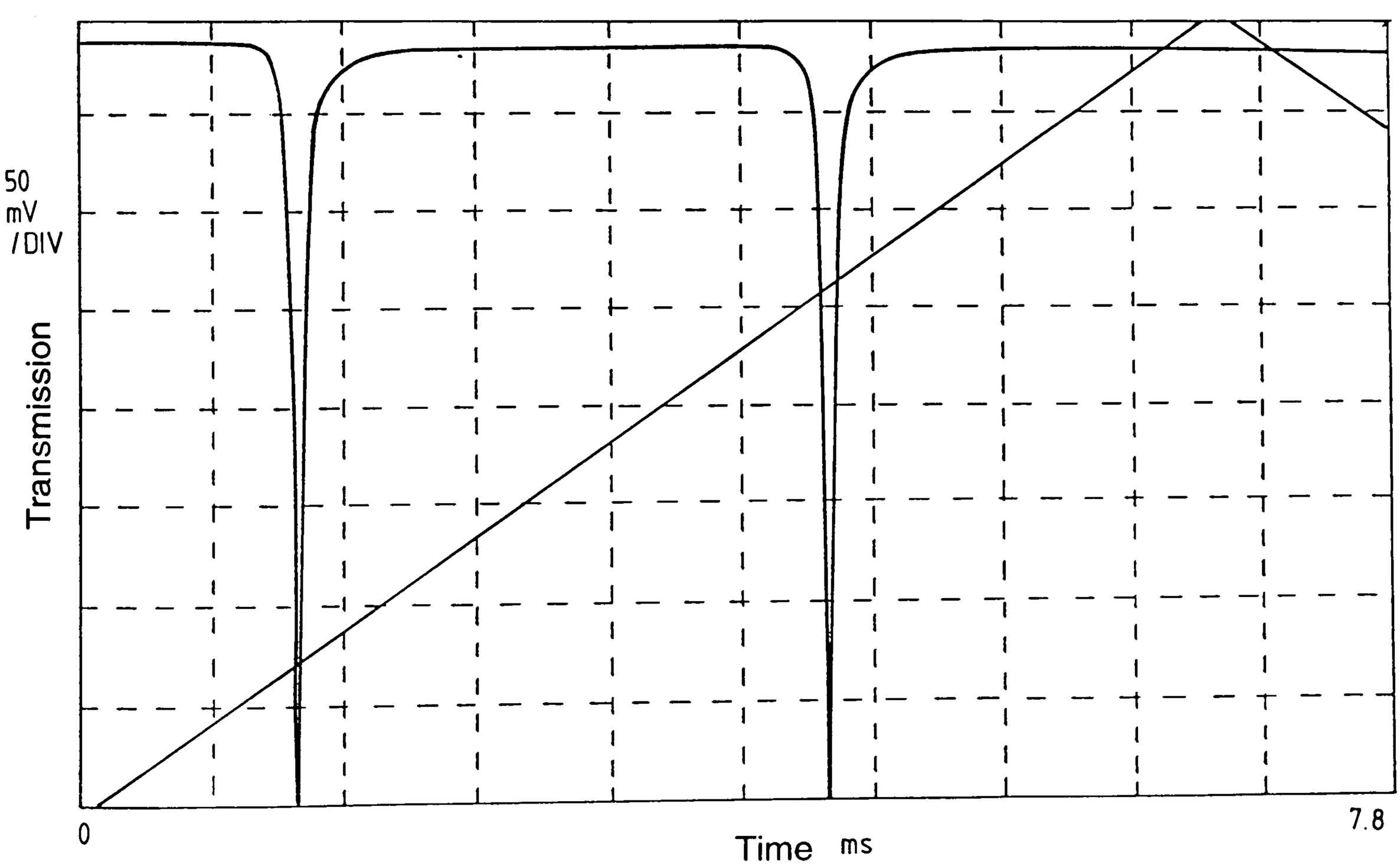

(b) Orthogonal polarization modes at resonance

Figure 6.13 Resonator output scanned using the piezoelectric phase modulator.

measuring the SBS power was ±5%. As expected from equation (4.44), P_{ring} is smaller for higher finesse and hence the conversion efficiency is higher for higher finesse. After threshold is reached a linear increase in SBS power was obtained for pump powers up to 1 mW with a maximum slope efficiency of ~33% for a finesse of 70 and a maximum conversion efficiency of 20%. A similar trend was observed for the low birefringent fibre ring resonator (resonator 1) as shown in figure 6.14 (b). The obvious difference was that of maximum slope efficiency i.e., 40% for a finesse of 100.

An observable SBS onset for pump powers of ~2-3μW was obtained for a finesse of ~125. For this resonator a maximum conversion efficiency of ~20% was obtained with a finesse of ~125 and a pump power of ~1 mW. Figure 6.15 shows the difference in SBS characteristics for the fast and slow eigenaxis arising due to a small difference in mode field diameter and hence pump power density, for the two modes with a measurement error of ±3% . The coupling constant and the coupler loss may also be slightly different for each fibre axis. Figure 6.16 shows the spectrum analyzer trace obtained by mixing the two orthogonally polarised SBS beams, resolved using a linear analyzer on the surface of a high speed detector-amplifier combination. The peak is at 11.68 MHz which is within 13% of the value predicted from equation (6.2) using a value of the acoustic velocity of 5596±86 ms^{-1}, obtained from the measured SBS shift and equation (6.4), of 10.17±0.16 MHz. The signal to noise ratio is ~60 dB.

The temperature stability of the carrier frequency was investigated by measuring the beat frequency variation over ~30°C. The resonator was allowed to equilibrate in a fridge at ~5°C and an oven at ~35°C; a higher temperature was not used to avoid the possibility of drying out the index matching oil between the two halves of the directional coupler.

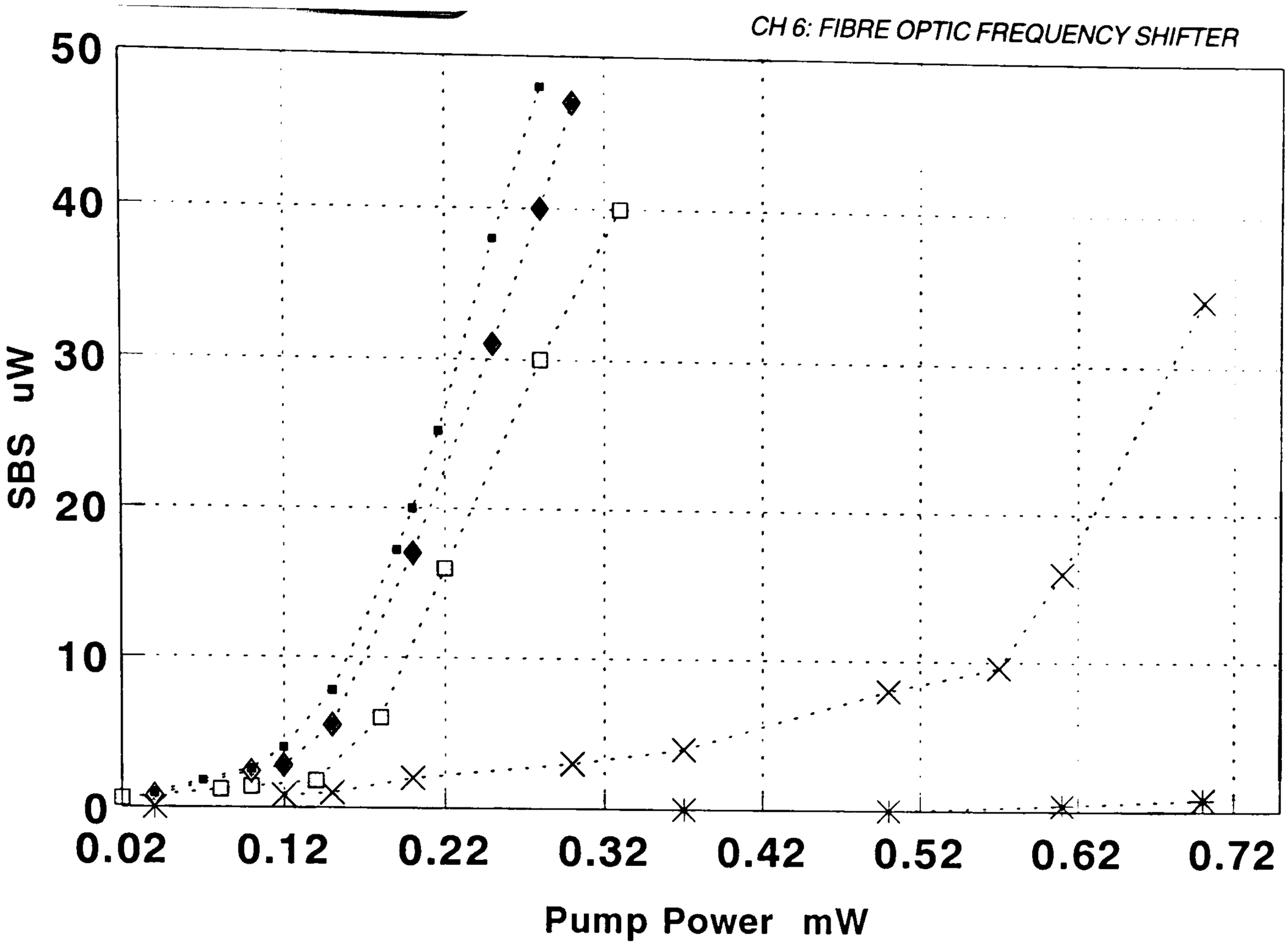

Fig. 6.14(a) Backscattered power for increasing pump power for different finesse (F) values (ring resonator 2)

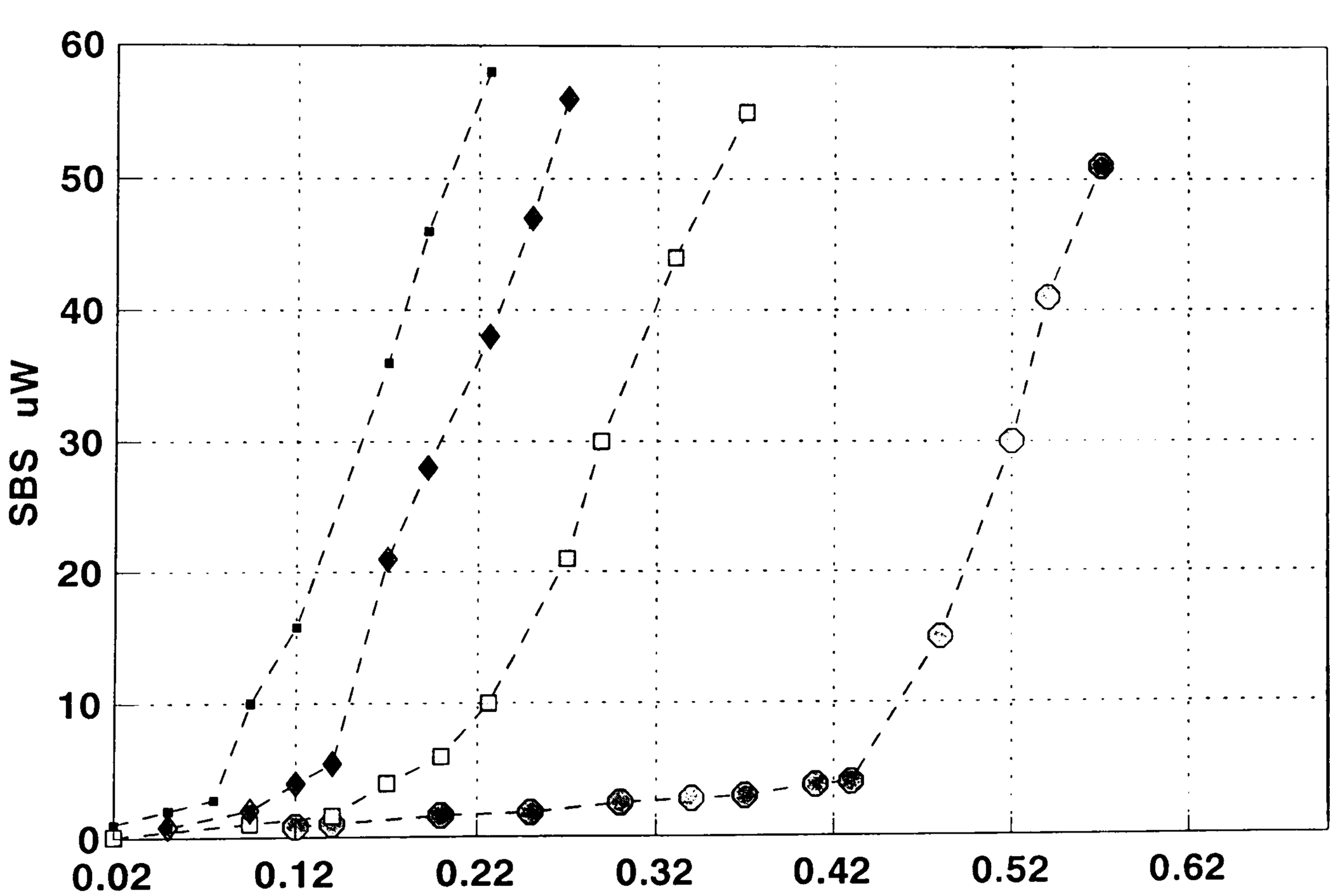

Fig. 6.14(b) Backscattered power for increasing pump power for different finesse (F) values (ring resonator 1).

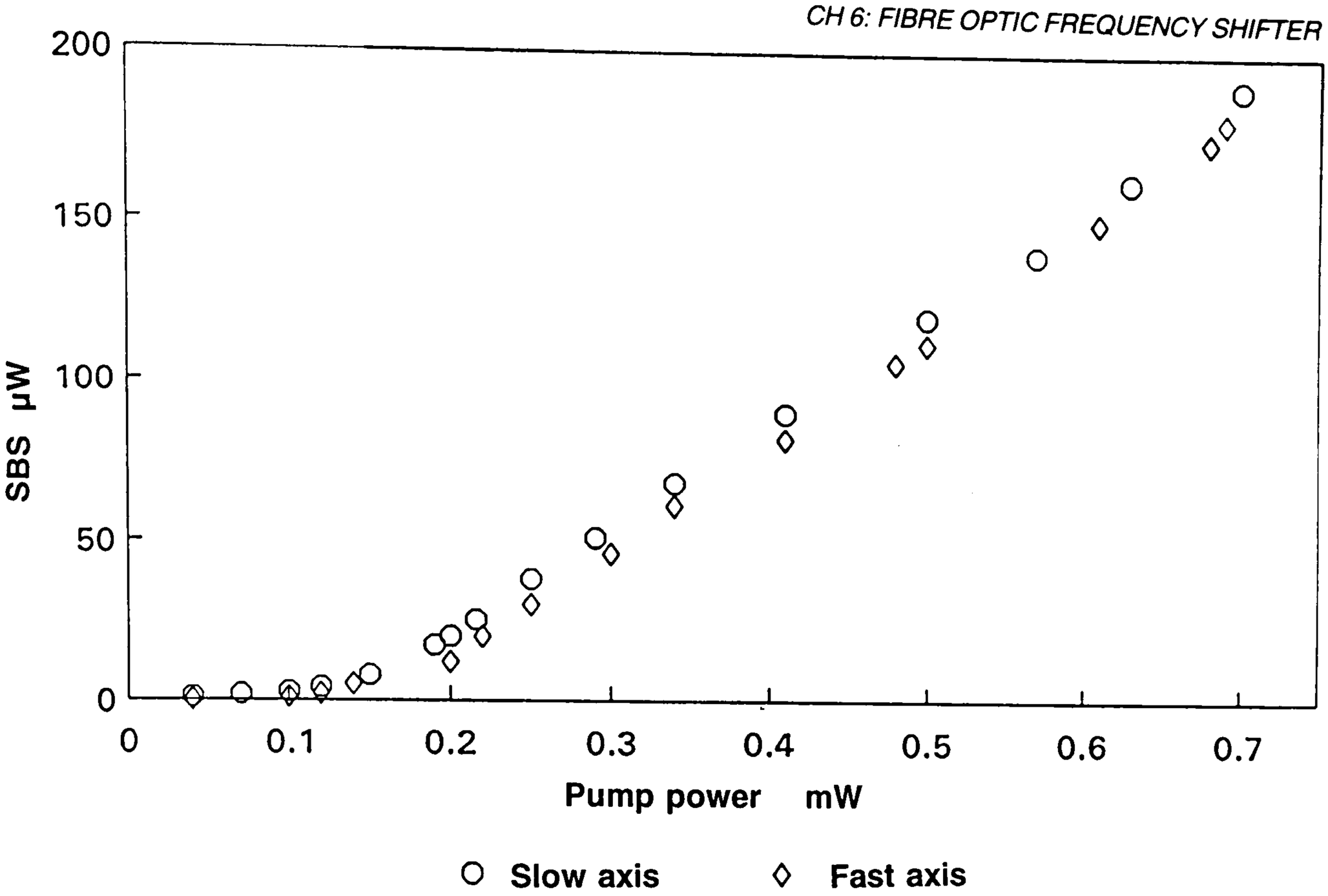

Figure 6.15 Backscattered power for increasing pump power for the fast and slow polarization eigenmodes. The finesse was 71.

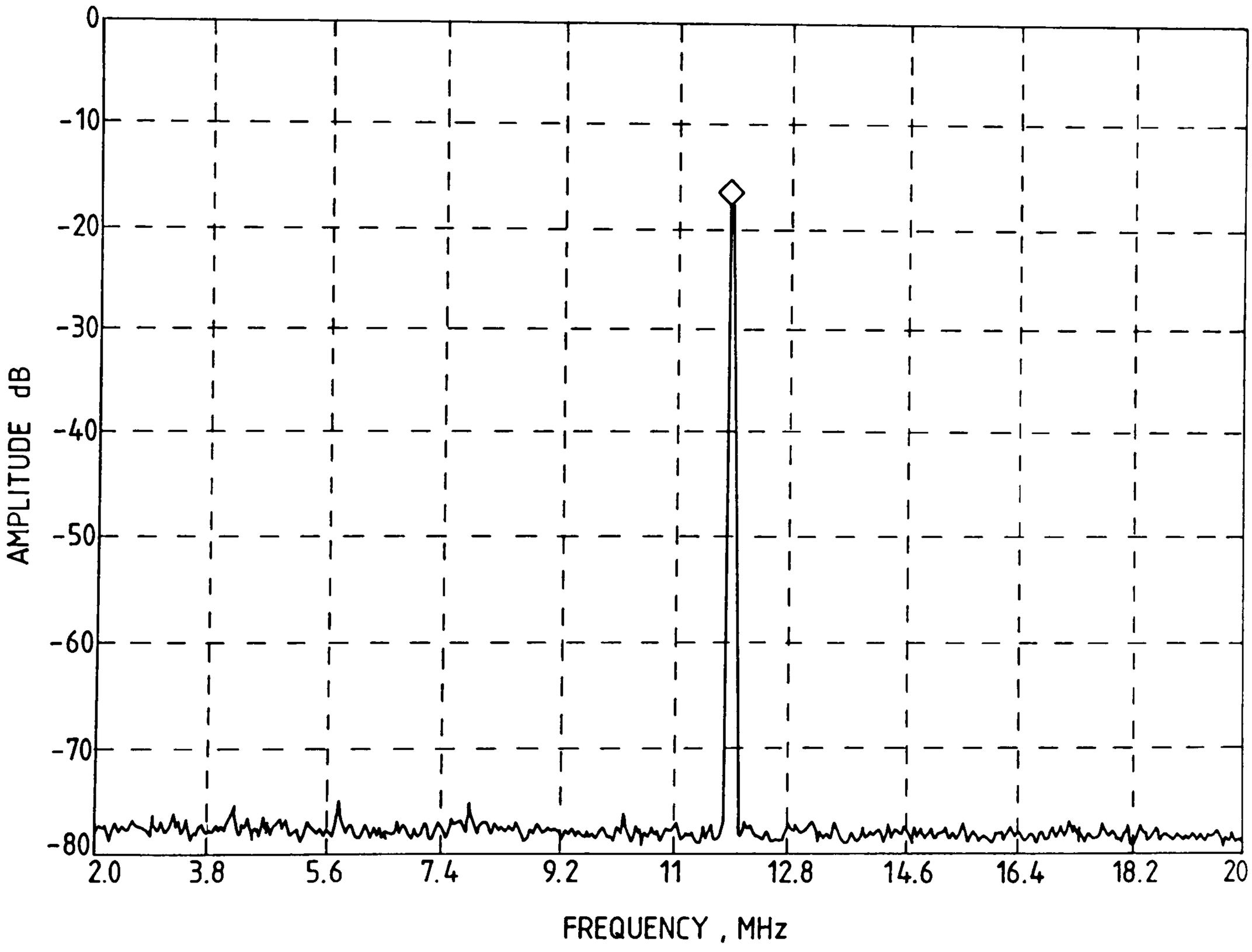

Figure 6.16 Heterodyne beat frequency displayed on electronic spectrum analyzer (single resonator system); the peak is at 11.68 MHz; the resolution bandwidth was 100 kHz.

A coefficient of $d\Delta\nu_{SBS}/dT = 6.7\pm0.5$ kHz/°C was measured. The uncertainty arises from the difficulty of obtaining a constant temperature in the oven over the entire resonator assembly and was estimated to be ±2°C. This coefficient can be obtained theoretically by differentiating equation (6.2), to give

$$\frac{d\nu^{f}_{SBS}}{dT} = \frac{2}{\lambda_p}\left[V_a \frac{d(n^{f})}{dT} + n^{f}\frac{dV_a}{dT}\right] \tag{6.6}$$

and

$$\frac{d\nu^{s}_{SBS}}{dT} = \frac{2}{\lambda_p}\left[V_a \frac{d(n^{s})}{dT} + n^{s}\frac{dV_a}{dT}\right] \tag{6.7}$$

Therefore,

$$\frac{d\Delta\nu_{SBS}}{dT} = \frac{2}{\lambda_p}\left[V_a \frac{d(\Delta n)}{dT} + \Delta n\frac{dV_a}{dT}\right] \tag{6.8}$$

The second term in the above equation, which represents the change in acoustic velocity with temperature, changes by only 7% for a change in temperature of 1600°C [98] and hence $dV_a/dT = 0.24$ ms^{-1}/°C. Δn for the fibre used was quoted by the manufacturer as $5.273\text{x}10^{-4}$. The quantity $d(\Delta n)/dT$ can be obtained by measuring the differential (polarimetric) phase change coefficient, i.e., [99]:

$$\frac{1}{L}\frac{d\phi^{s}}{dT} = \frac{2\pi}{\lambda_p}\left[\frac{1}{L}n^{s}\frac{dL}{dT} + \frac{dn^{s}}{dT}\right] \tag{6.9}$$

$$\frac{1}{L}\frac{d\phi^{f}}{dT} = \frac{2\pi}{\lambda_p}\left[\frac{1}{L}n^{f}\frac{dL}{dT} + \frac{dn^{f}}{dT}\right] \tag{6.10}$$

Therefore

$$\frac{1}{L}\frac{d(\Delta\phi)}{dT} = \frac{2\pi}{\lambda_p}\left[\frac{1}{L}\Delta n\frac{dL}{dT} + \frac{d(\Delta n)}{dT}\right] \qquad (6.11)$$

where $\Delta\phi$ is the difference in optical phase between the fast and slow polarisation eigenaxes. The first term in the bracket is very small ($(1/L)dL/dT$ ~5×10^{-7}/ °C for pure silica [100]. The second term in equation (6.11) was obtained experimentally by launching light into both modes of a short section, ~10 cm, of fibre. The fibre was heated by 40°C and the polarimetric fringes resolved using a linear analyzer. The fibre was then allowed to cool and the number of polarimetric fringes were counted. For this fibre $(1/L)d(\Delta\phi)/dT$ was measured to be 4 ± 0.3 rad $°C^{-1}m^{-1}$ which is comparable to 5 rad $°C^{-1}m^{-1}$ previously reported for York *Bow tie* fibre [101]. The difference is due to the difference in structure of the two fibres, particularly the stress rod location and composition. Hence the predicted value of $d(\Delta\nu_{SBS})/dT = 7.4\pm0.52$ kHz°C^{-1}. The two values are within 9% and indicate that the carrier frequency generated from this technique is very stable to temperature fluctuations compared to a dual resonator or a dual non-interferometric fibre technique. This value is close to that obtained for a conventional Bragg cell, of ~3 kHz^{-1} $°C^{-1}$ [102]. $d(\Delta\nu_{SBS})/dT$ could be reduced further by using fibres with a lower $(1/L)dL/dT$ coefficient, for example Andrews elliptical core fibre for which this has been measured to be a factor of ~5 less than that of the bow tie fibre [103].

In recent studies employing tens to hundreds of meters of birefringent and nominal circular core fibre and an argon ion pump laser at 514.5 nm, the carrier frequency obtained was modulated about its average value by ~$\pm$10 MHz [73,75]. Other features included a broadband spectrum and random pulsed modes. These observations have been associated with non-linear dynamical and possibly chaotic processes occurring in the system due to small non-linear refractive index perturbations in the fibre core, feedback from the

SBS process and the Fresnel reflection of the pump and SBS signal at the fibre-air interface [104]. In this experiment none of the previous characteristics were observed. In addition none of these effects have been reported from previous SBS systems based on two ring resonators. The reasons for this are not fully understood but could be due to a combination of parameters such as reduced photosensitivity at higher pump wavelength, different fibre type and dopant level and reduced reflections and pump-SBS interaction at interfaces due to the unidirectional nature of the resonator configuration. Although the reasons for the non-observation of the effects discussed above in the ring resonator system are not fully understood, and require further investigation, the actual experimental observation that a heterodyne carrier of very stable centre frequency can be generated is important for future development of this technique.

6.8 LASER DIODE BASED FREQUENCY SHIFTER

In the configurations described in the previous sections a single frequency HeNe laser was used as the source as it provides a very stable output with long coherence length making it an ideal choice for the system involving fibre interferometers. However, as far as commercial and industrial feasibility of the device is concerned, laser diodes will provide more versatile rugged pump sources in the long term. The system could be compact and mechanically stable and hence suitable for harsh industrial environments. Problems that have to be taken into account when using these systems are:

- short coherence length; typically 10 cm
- output linewidth very susceptible to external feedback
- output wavelength injection current dependent
- output wavelength temperature dependent.

The short coherence length can be partially overcome by using diode lasers with narrow linewidths of $\leq$ 1MHz ($\geq$ 300 m coherence length).

External feedback effects, caused primarily by reflection at the fibre air interface on launching and by secondary effects from other optical elements in the system, cause unstable operation of the diode output and in general results in a broadening in the laser linewidth. This causes two potential problems. Firstly, to maintain maximum SBS gain the pump linewidth needs to be less than the SBS linewidth. Detailed calculations [11] show that the Brillouin gain under broad band pumping conditions depends on the relative magnitudes of the pump coherence length, defined by $L_{coh} = c/n\Delta\upsilon_p$, and the SBS interaction length L_{int}. If $L_{coh} >> L_{int}$, the SBS process is independent of the mode structure of the pump laser provided the mode spacing exceeds $\Delta\upsilon_B$. On the other hand the Brillouin gain is significantly reduced if $L_{coh} << L_{int}$. The relation between Brillouin gain and the laser linewidth is given by eq. 2.1 (section 2.2.2).

6.8.1 EFFECTIVE FINESSE

For short coherence length sources the observed finesse of the system, called the *effective finesse* is different from the intrinsic finesse of the ring resonator (finesse which is not limited by the linewidth of the source). To calculate the relation between the effective finesse of the resonator and the laser spectral width let us consider a ring resonator with $\Delta\upsilon_r$ as the full width at half maximum point of the resonance notch, illuminated by a low coherence source of spectral width $\Delta\upsilon_l$. Now the resonant characteristic $\Omega_r(\upsilon)$ of the resonator output signal is approximated by the Lorentzian profile [105]:

$$\Omega_r = \frac{\frac{\Gamma}{\pi}}{\Gamma^2 + (\nu - \nu_o)^2} \tag{6.12}$$

where υ_o is the resonant frequency.

$$\Gamma = \frac{c}{2FnL} = \frac{\Delta\nu_r}{2} \tag{6.13}$$

Similarly the power spectral density of the single mode diode laser with spectral width $\Delta\upsilon_l$ is also assumed to have a Lorentzian profile [18] [Yariv]:

$$\Omega_1(\nu) = \frac{\frac{\Psi}{\pi}}{\Psi^2 + \nu^2} \tag{6.14}$$

where

$$\Psi = \frac{\Delta\nu_1}{2} \tag{6.15}$$

The effective finesse *F'* of the ring resonator incorporating the linewidth of the source is given by [105]:

$$F' = \frac{F}{1 + \frac{\Delta\nu_1}{\Delta\nu_r}} = \frac{\Delta\nu_r F}{\Delta\nu_r + \Delta\nu_1} \tag{6.16}$$

As $F = FSR/\Delta\upsilon_r = (c/nL)/\Delta\upsilon_r$ using eqs. (6.15) and (6.17) and eq. (6.18) can be written as:

$$F' = \frac{cF}{FnL\Delta\nu_1 + c} \tag{6.17}$$

A theoretical plot is shown in figure 6.17 , using equation (6.17) which gives a relationship between the effective finesse, of the resonator with a 1 m loop length, and the laser linewidth for different finesse values.

It is important to note that this plot not only provides the value of the effective finesse for a particular $\Delta\upsilon_l$, but it can also be used as an important tool to measure the laser linewidth with the help of the ring resonator transfer function, provided that the intrinsic finesse, *F,* is measured using a narrow linewidth source.

As mentioned earlier, for short coherence length pump sources i.e. laser diodes, the effective finesse *F '* will now determine the threshold power required to generate SBS in the ring resonator. For a resonator with an intrinsic finesse of 100 and fibre refractive index of 1.47, eq. (6.17) can be written as (squaring eq. 6.17 and multiplying by *L*):

$$LF'^2 = \frac{9\times10^{20}}{L\left(147\,\Delta f + \frac{3\times10^8}{L}\right)^2} \tag{6.18}$$

Therefore using eq. 4.44 the threshold power to generate SBS with a system

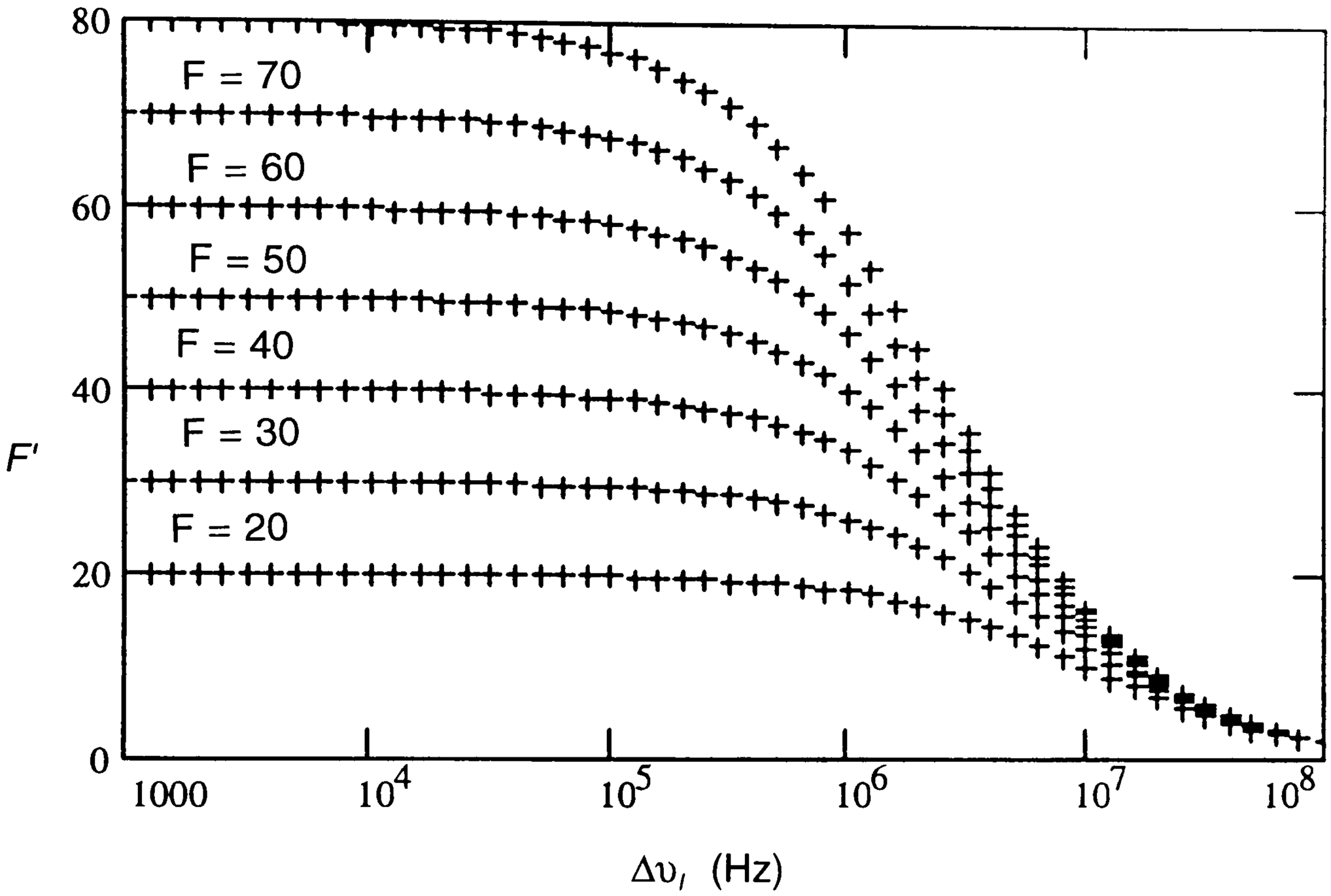

Figure 6.17 Relation between the effective finesse F' and spectral linewidth of laser diode

containing a laser diode is given by:

$$P_{ring} = \frac{2A_{eff}\pi^2}{G_B(\nu_B)\left(\frac{9\times10^{20}}{L(147\Delta f + 3\times10^8/L)^2}\right)} \qquad (6.19)$$

A graphical interpretation of the above equation using different laser linewidths and ring resonator lengths is shown in figure 6.18. A_{eff} and G_B (υ_B) are 25.9×10^{-12} and 3.43×10^{-11} respectively, calculated from eqs. 4.36 & 4.32 respectively. Figure 6.18 demonstrates the importance of a narrow linewidth source to get lower SBS thresholds.

The specifications of the ring resonator, used for the experimental investigation for the laser diode based frequency shifter, are given in table 6.3.

A high power, 100 mW, Spectra Physics SLD-5411-61 laser diode was used to illuminate the ring resonator. Its specifications are tabulated in table 2.2 (section 2.2.2). The high power was intended to compensate for the relatively short coherence length. In order to specify the ring resonator for this system, it was very important to measure the spectral width of the diode.

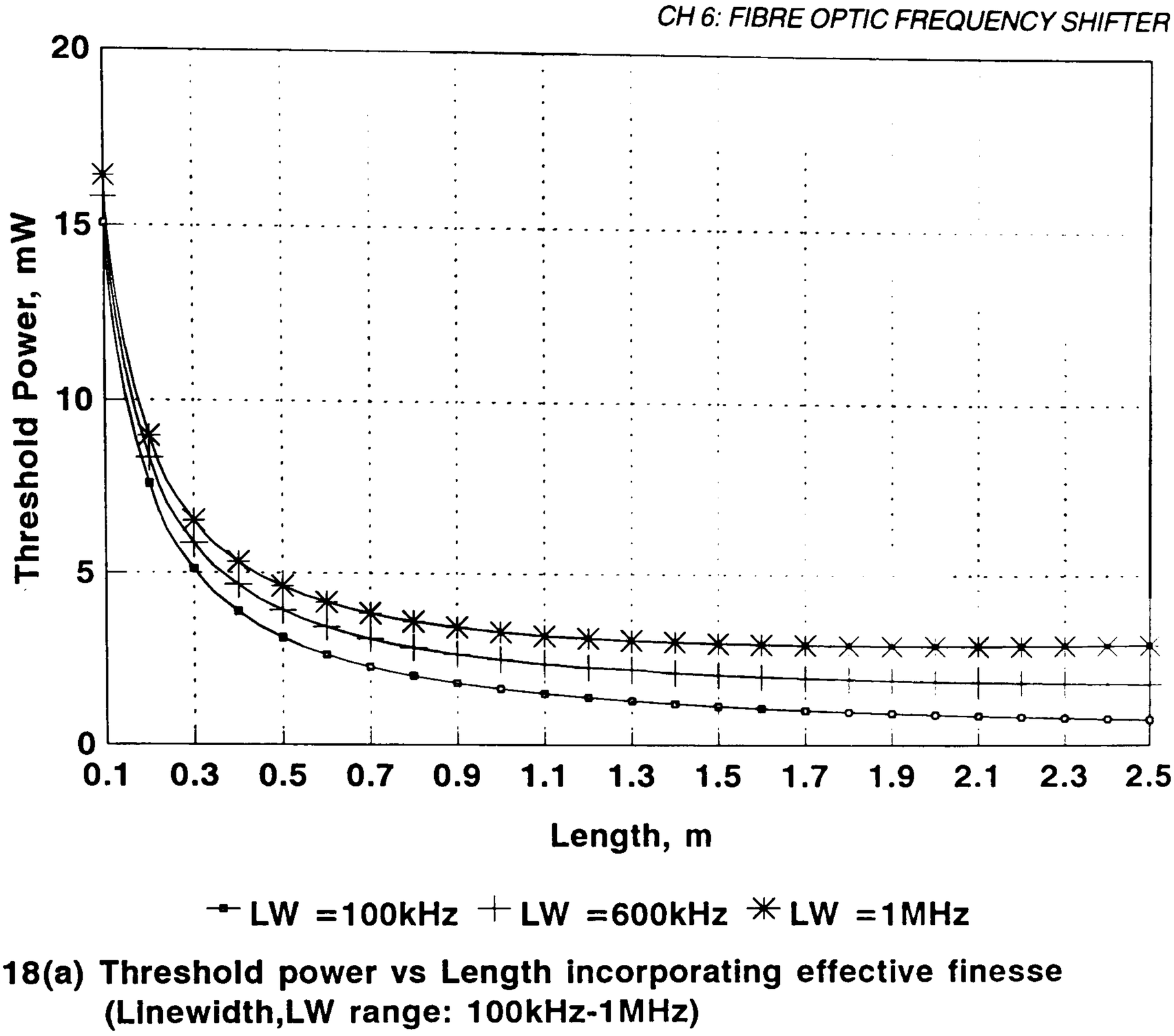

Fig. 6.18(a) Threshold power vs Length incorporating effective finesse (Linewidth,LW range: 100kHz-1MHz)

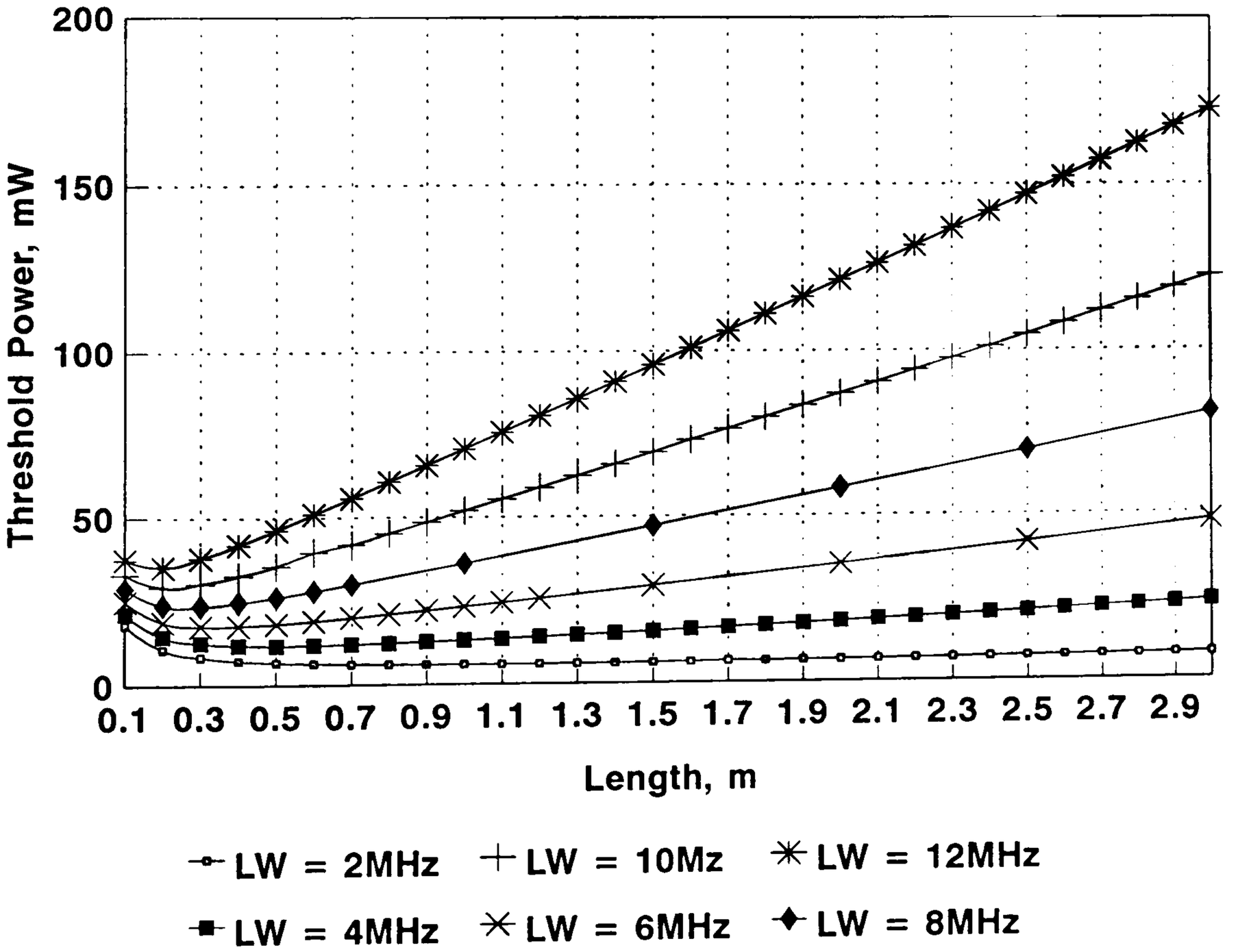

Fig. 6.18(b) Threshold power vs Length incorporating effective finesse (Linewidth, LW range: 2MHz-12MHz)

Loop length	1 m
Fibre type	Fujikura *PANDA*
Fibre loss	3 dB/km
Core diameter	~5.5 μm
Cladding diameter	~125 μm
Cut-off wavelength	800 nm
Numerical aperture	~0.11
Beat length	~1.2 mm

Table 6.3 Specifications of the ring resonator used in the frequency shifter based on a laser diode.

6.8.2 LINEWIDTH MEASUREMENT

The most common method to measure the diode laser linewidth is to use a Fabry-Perot interferometer. The minimum linewidth that can be measured on the Fabry-Perot, available at that time, was limited to 10 MHz. The delayed self-heterodyne technique first proposed by Okoshi *et al* [107] offers better resolution. The experimental arrangement to measure the laser linewidth using this technique is shown in figure 6.19.

The output from the laser was directed through an optical isolator into the interferometer. The isolator is used between the laser and fibre to reduce the

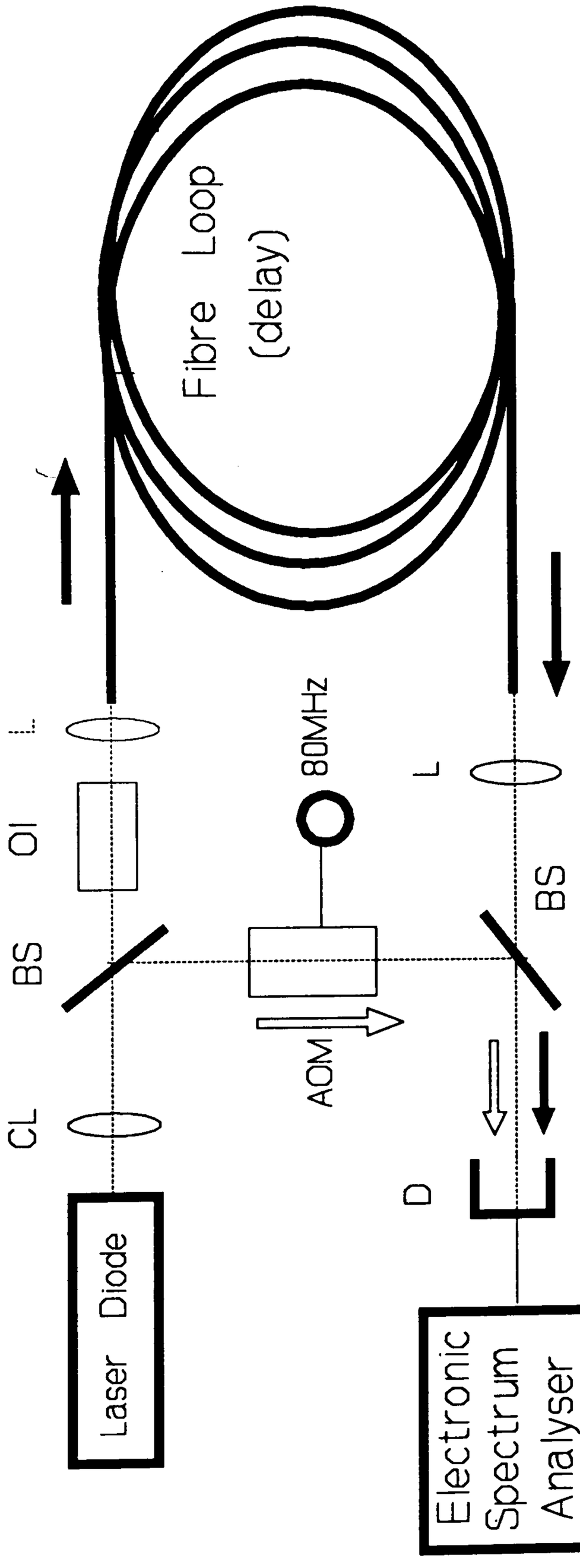

Figure 6.19 Experimental setup for measurement of laser diode output spectrum; CL: collimating lense; BS: beamsplitter; OI: optical isolator; L: lense; AOM: acousto-optic modulator; D: detector

optical feedback from the fibre endface which may cause instabilities in the laser cavity. Immediately following the isolator, the beam was split into two paths by a 50/50 beam splitter. One beam was delayed with respect to the other by 2.2 km of single mode fibre. If the delay is longer than the laser coherence time, the two signals become uncorrelated. A small portion of this beam was constantly monitored with a scanning Fabry-Perot interferometer to ensure that the laser was operating in a single mode. The other beam was directed through an acousto-optic modulator operating at 80 MHz. This process shifts the measured frequency spectrum so that it is centred at the acousto-optic frequency.The first order diffracted beam was mixed with the delayed beam. Thus at the detector we are mixing two uncorrelated signals with the same linewidth and centre frequency. The mixing of these signals in an optical detector causes the resulting photocurrent spectrum to be the autocorrolation of the laser line shape. The measured spectral width will be twice the linewidth of the laser. Figure 6.20 conceptually shows the mixing of the signals at the photodetector.

Light in one of the two arms of the interferometer is frequency shifted to decrease the noise in the measurement, which is concentrated around lower frequencies. Figure 6.21 shows the measured spectrum from the detector with a centre frequency of 80 MHz and 3dB bandwidth of ~12MHz. The optical linewidth in this case would be ~12/2 = 6 MHz. This value is within the linewidth range specified by the manufacturer i.e., 4-12 MHz [6]. According to manufacturer's specifications the range is affected by temperature stability and current noise. Also the current source and the laser were not under any form of temperature control at the time of measurement.

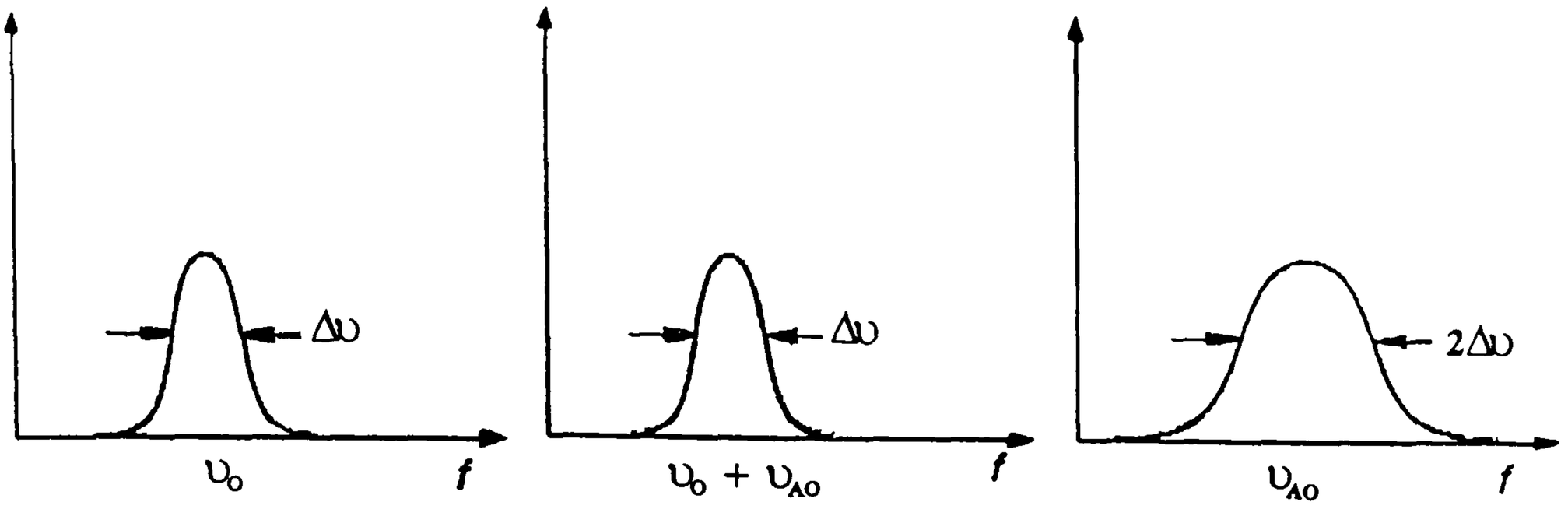

Figure 6.20 The correlation of the signal at the optical frequency υ_o with a signal at the optical pulse acousto-optic frequency ($\upsilon_O + \upsilon_{AO}$) yields a component at the acousto-optic frequency of approximately twice the width.

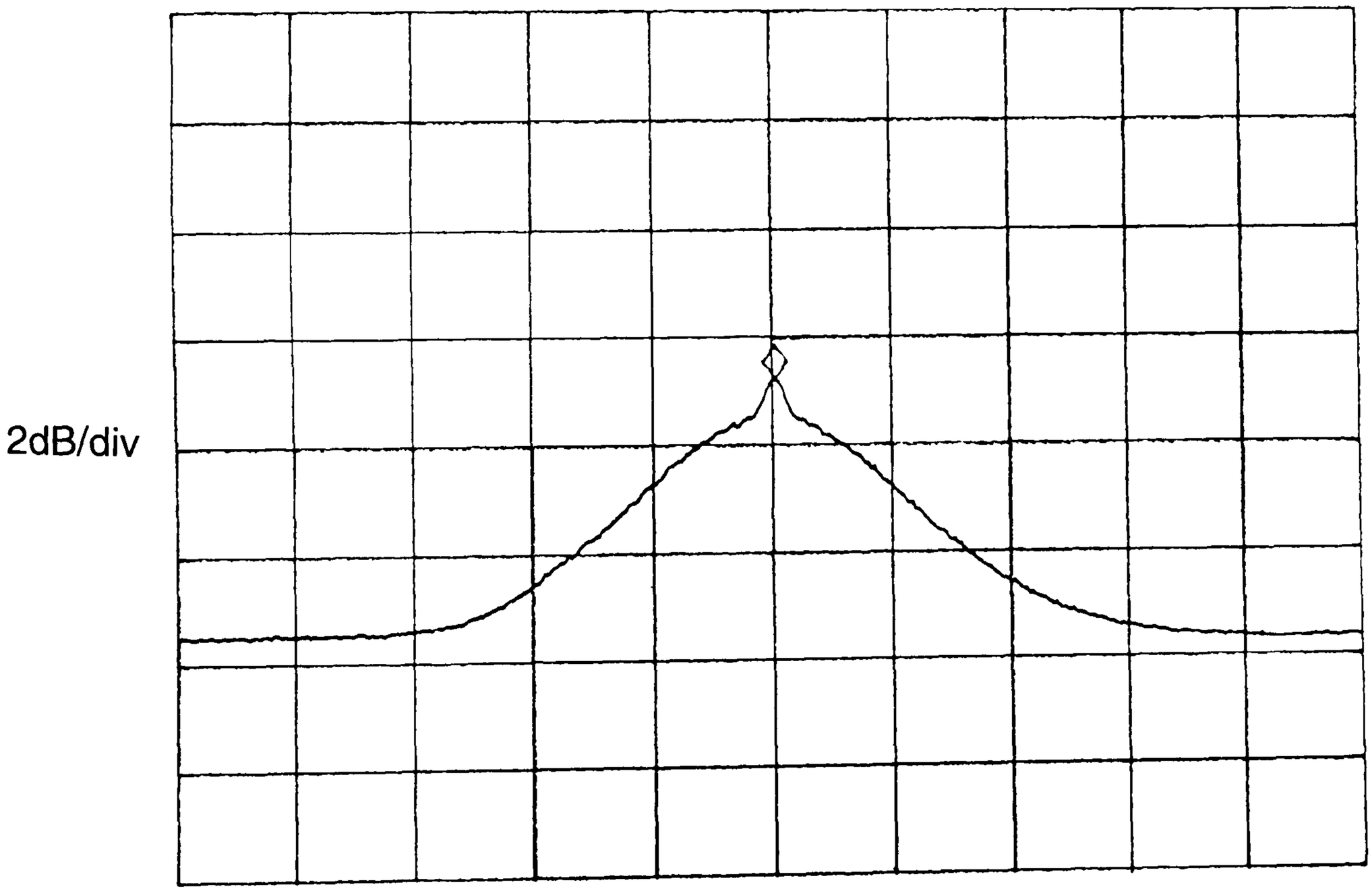

Figure 6.21 Mixer power output spectrum; bandwidth = 100 kHz; span = 40 MHz; laser linewidth = 6 MHz

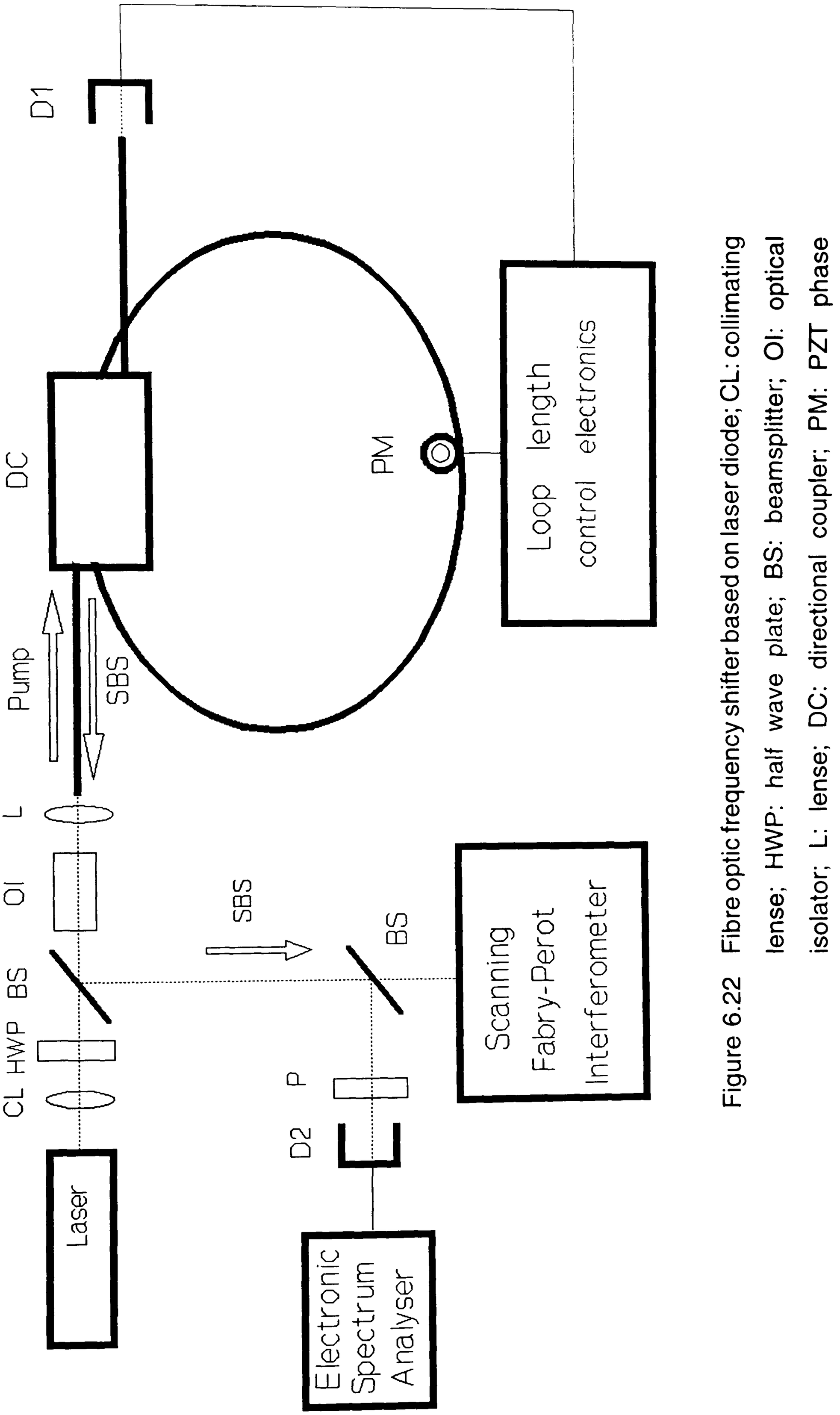

Figure 6.22 Fibre optic frequency shifter based on laser diode; CL: collimating lense; HWP: half wave plate; BS: beamsplitter; OI: optical isolator; L: lense; DC: directional coupler; PM: PZT phase modulator; D1 & D2 : detector-amplifiers; P: polarizer.

6.8.3 THE FREQUENCY SHIFTER

The experimental setup for the frequency shifter using the 100 mW diode, discussed above, is shown in figure 6.22. The resonator was fabricated from 1 m of Fujikura *PANDA* high birefringence fibre with a cut-off wavelength of 800 nm and core radius ~5.5 μm. Light is collimated and launched into one axis of the resonator, via a Farady isolator and a microscope objective. The isolator was used to protect the laser from any feedback from the end of the fibre and other optical components. The beamsplitter has two functions. Firstly, to reflect the light into a Fabry-Perot interferometer, with a finesse of 200 and a free spectral range of 2 GHz, to monitor the spectral width of the laser. Secondly, to monitor the stimulated Brillouin scattering coming out from port 1 of the ring resonator. Figure 6.23 shows the output of the resonator. The average effective finesse was ~22. The output was very noisy and jittery due to the noise in the laser. After passing through the isolator and a 50/50 beamsplitter, ~40 mW of optical power was available for launch. With a launching efficiency of ~30 % only ~2μW of SBS was observed. When light was launched into both axes of the resonator, no beat frequency was observed because the laser coherence length was not long enough to build up SBS gain. The other main reason was that the power launched in the fibre (~12 mW) was slightly less than the theoretical threshold power of ~12.85 mW.

In an effort to make the output spectrum more stable and less noisy, a low noise, battery driven power supply with charging facilities was designed and constructed. Figure 6.24 shows the circuit diagram of the system. The primary aim is to reduce the current noise to the diode and thus reduce the linewidth with a concomitant increase in the coherence length. However no discernable improvement was observed.

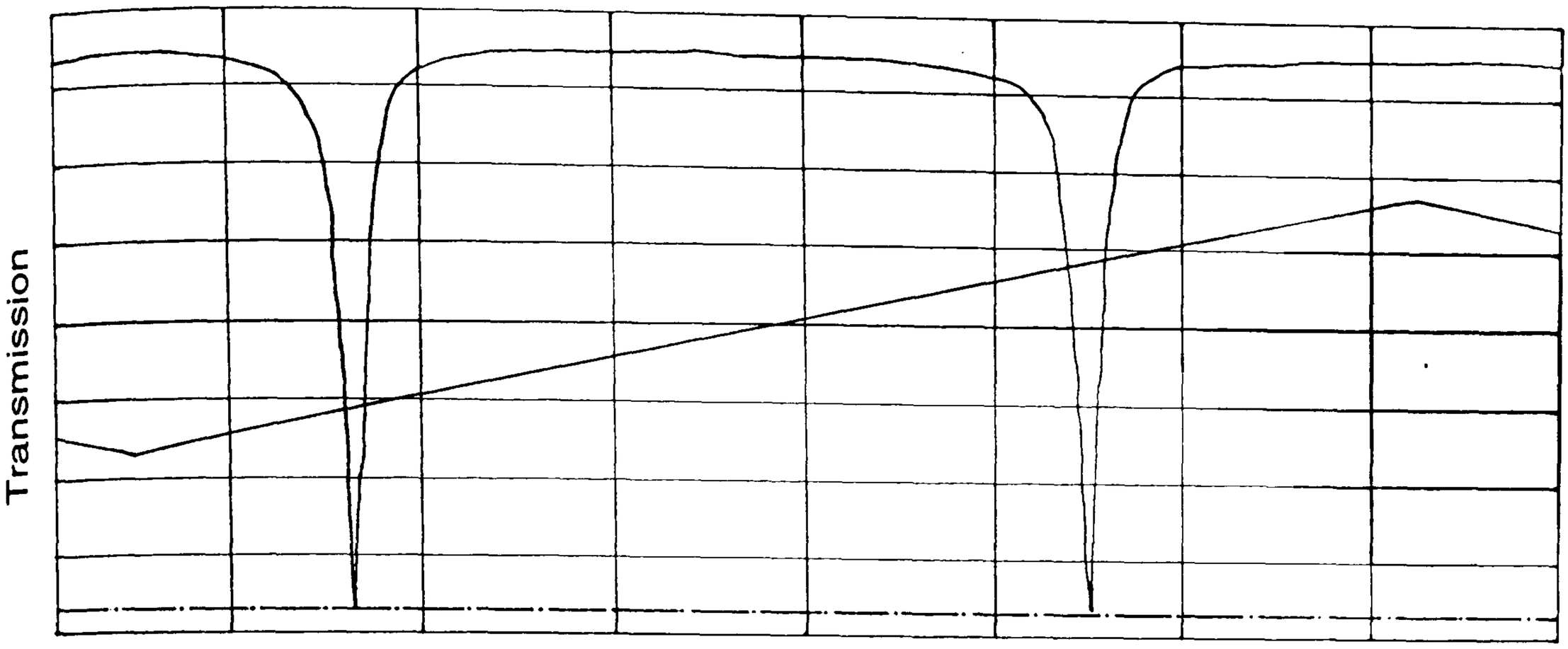

Figure 6.23 Ring resonator output illuminated with a 100 mW laser diode

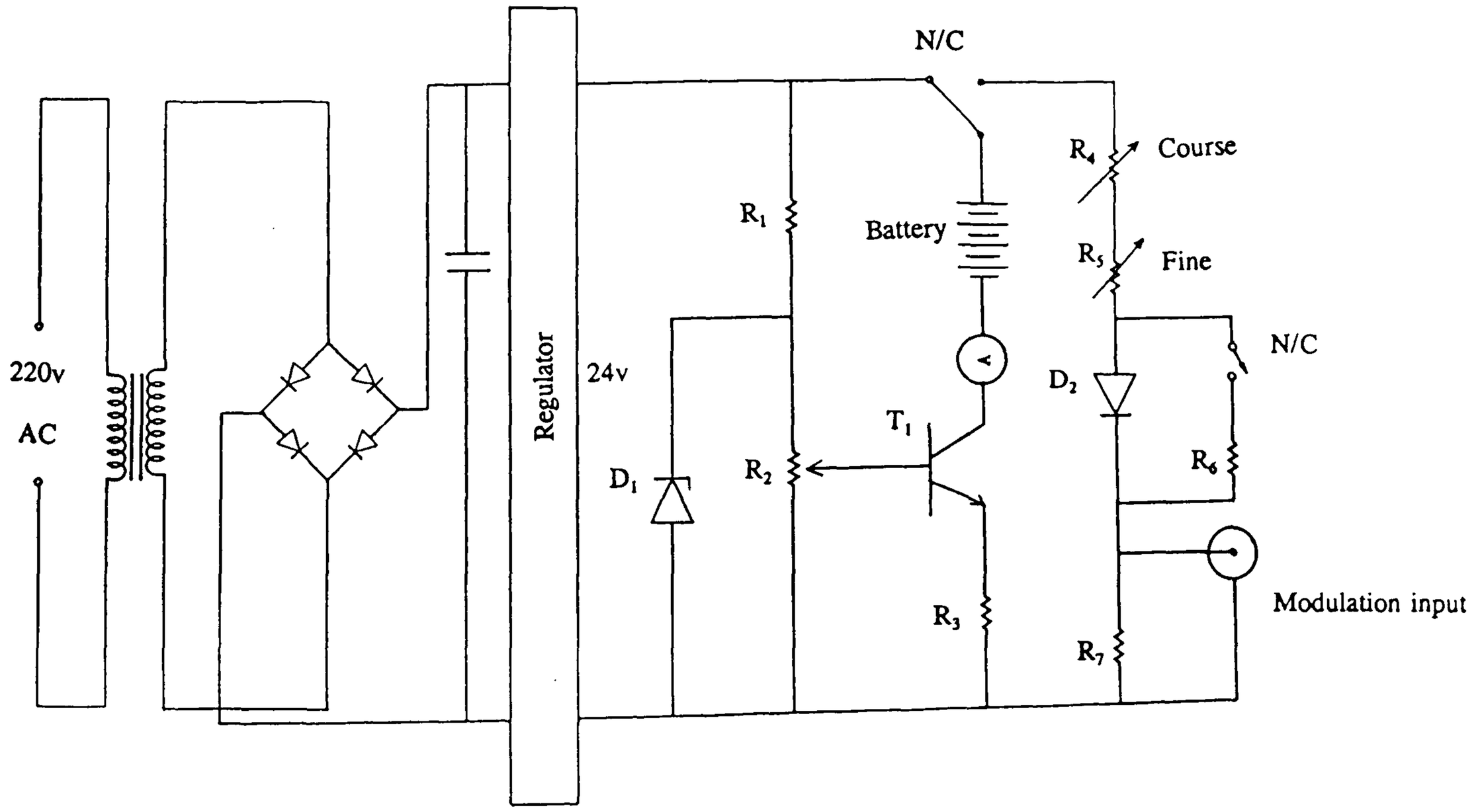

$R_1 = 470\Omega$ $R_2 = 100\Omega$ $R_3 = 5\Omega$ $R_4 = 10k$
$R_5 = 1k$ $R_6 = 18\Omega$ $R_7 = 22\Omega$ $T_1 = 2N3055$

Figure 6.24 Low noise power supply for laser diode with charging facilities

6.8.4 NARROW LINEWIDTH LASER

As the laser discussed in the previous section did not have a coherence length long enough to build up SBS gain, a single frequency narrow linewidth (300 kHz - 1 MHz, according to manufacturer specifications) laser source, Melles Griot 06DSN 503 was used as a source for the frequency shifter. It is important to mention here that this laser diode/driver unit was the first of its kind to be sold anywhere in the world and we experienced many problems in commissioning this laser. Table 6.4 summarizes the specifications of the narrow linewidth laser.

Wavelength	830±15 nm
Output power	11 mW
Output power noise	0.1% p-p, 10kHz bandwidth
Linewidth	300 kHz-1 MHz
Centre frequency drift	2 GHz, p-p
Centre frequency drift rate	900 MHz/hr, maximum
Temperature sensitivity	100 MHz/°C
Beam size	7.5 mm × 2.5 mm, typical
Beam divergence	0.2 mrad × 0.6 mrad, typical
Pointing stability	20 µrad/°C

Table 6. 4 Specifications: 06DSN 503 narrow linewidth laser diode.

This so called narrow linewidth laser consists of a system that uses optical

feedback from a diffraction grating to narrow the linewidth. The assembly top view of the laser is shown in figure 6.25 [108]. The laser system has three basic components, a commercial diode laser LT024ND, a collimating lens,and a diffraction grating. The laser and lens are mounted so that the lens can be carefully positioned relative to the laser to ensure proper collimation. The diffraction grating is mounted in such a configuration that the light diffracted into the first order returns to the laser. As such, the grating serves as one end mirror of a laser cavity, with the back facet of the diode providing the second mirror. This means that the grating must be carefully aligned and very stable. As with any laser, changes in the length of the cavity causes shifts in the laser frequency. Therefore, to obtain a stable output frequency, undesired changes in the length due to mechanical movement or thermal expansion must be avoided.

To reduce the movements due to vibration of the cavity, it is mounted on small soft rubber cushions. To avoid thermal changes, the baseplate is temperature controlled using heaters. In addition to controlling the temperature of the baseplate, the temperature of the laser diode is also independently controlled. Finally, to avoid air currents interfering with the temperature control the entire laser system is enclosed in a small insulated box. In order to finely tune the laser frequency, the length of the laser cavity can be changed using a piezoelectric transducer which moves the grating in response to an applied voltage. The diode driver contains temperature control circuits and a stable low noise current source.

The laser diode demonstrated two major problems. First the output of the laser was emerging at an angle. Therefore, it was very difficult to launch the light into the fibre efficiently. Second the laser output was multimode. Different combinations of drive current and temperature were tried without success. The system was sent back to the USA and fixed by the manufacturer with an

increased output power of ~11 mW. The output beam was collimated but not circularised and has an oblong shape. Approximately 30% of the optical power was lost in the isolator. This time the laser output had a wide spectral linewidth of >10 MHz. The laser did not behave as a single mode for more than a couple of minutes. In an effort to improve the performance, in addition to adjusting drive current and temperature, the grating angle was slightly changed but no improvement was observed. Finally this unit was replaced by a new one which gave a single narrow linewidth output of $\leq$ 1.5 MHz. The laser output spectrum is shown in figure 6.26, obtained from a Melles Griot Fabry-Perot with a finesse of 200 and free spectral range 300 MHz.

6.8.5 THE FREQUENCY SHIFTER

The experimental configuration is the same as shown in figure 6.22. The only difference is the type of laser diode. Due to reasons such as small aperture of the isolator and division of power at the 50/50 beamsplitter, only 3.8 mW of optical power was available to launch in the ring resonator. A low frequency triangular waveform was applied to the piezoelectric phase modulator to scan the output of the resonator. A series of resonance notches was obtained. Figures 6.27(a) show the general cases when the two modes are resonating separately and figure 6.27(b) shows the case when the modes resonate simultaneously.

With a launching efficiency of ~40% , ~5 μW of SBS was obtained. The SBS onset threshold power was ~1.5 mW with a resonator finesse of ~55. No beat frequency was observed on the spectrum analyzer, as this optical power and finesse was not enough to build up SBS in both eigenaxes of the fibre sufficient to produce a detectable beat frequency. It can be seen from

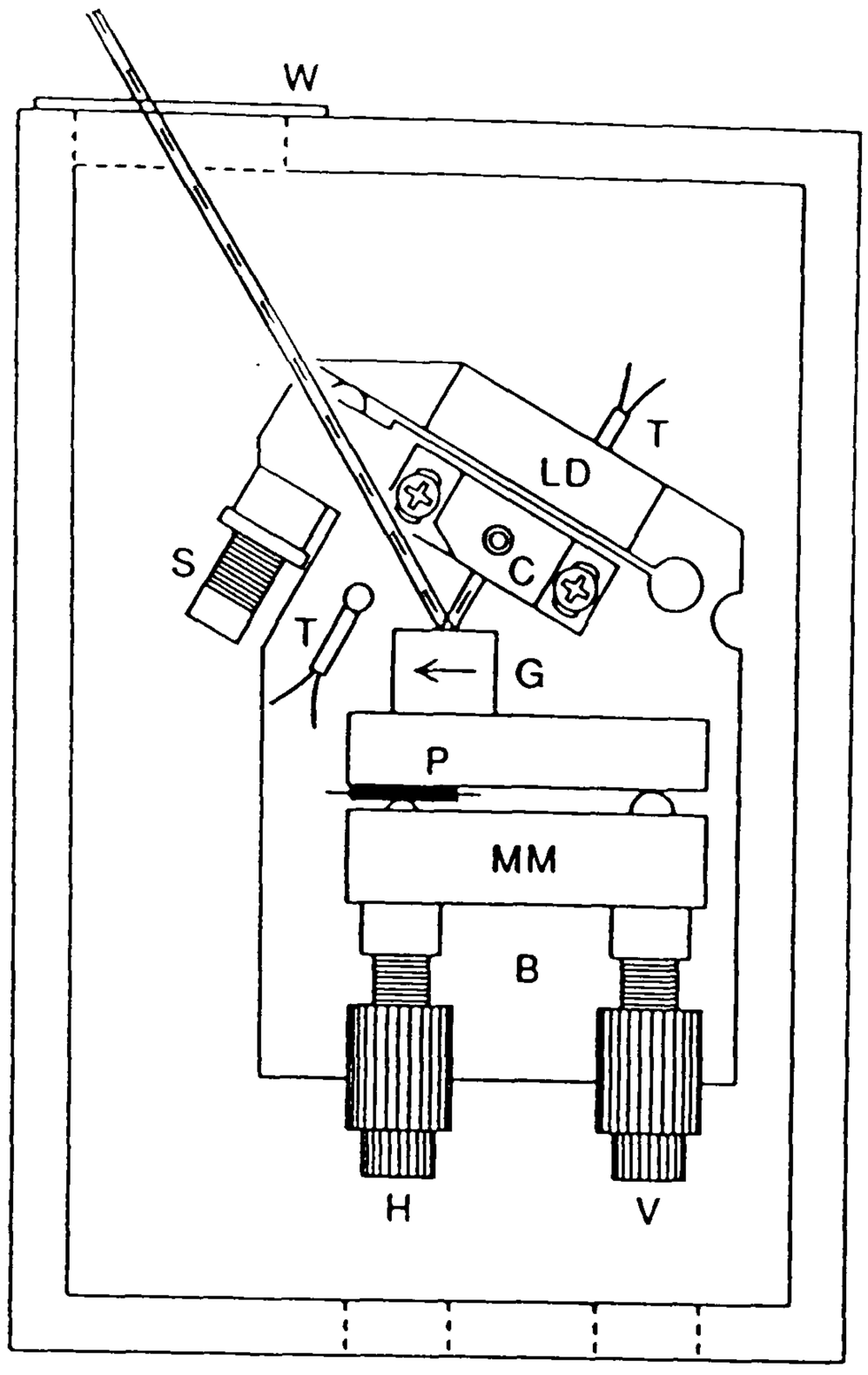

Figure 6.25 Assembly top view of the narrow linewidth laser; T: thermistor; LD: laser diode; C: collimating lense; G: diffraction grating; P: PZT disk; MM: mirror mount; B: base plate; W: window; H & V: MM controls; S: screw.

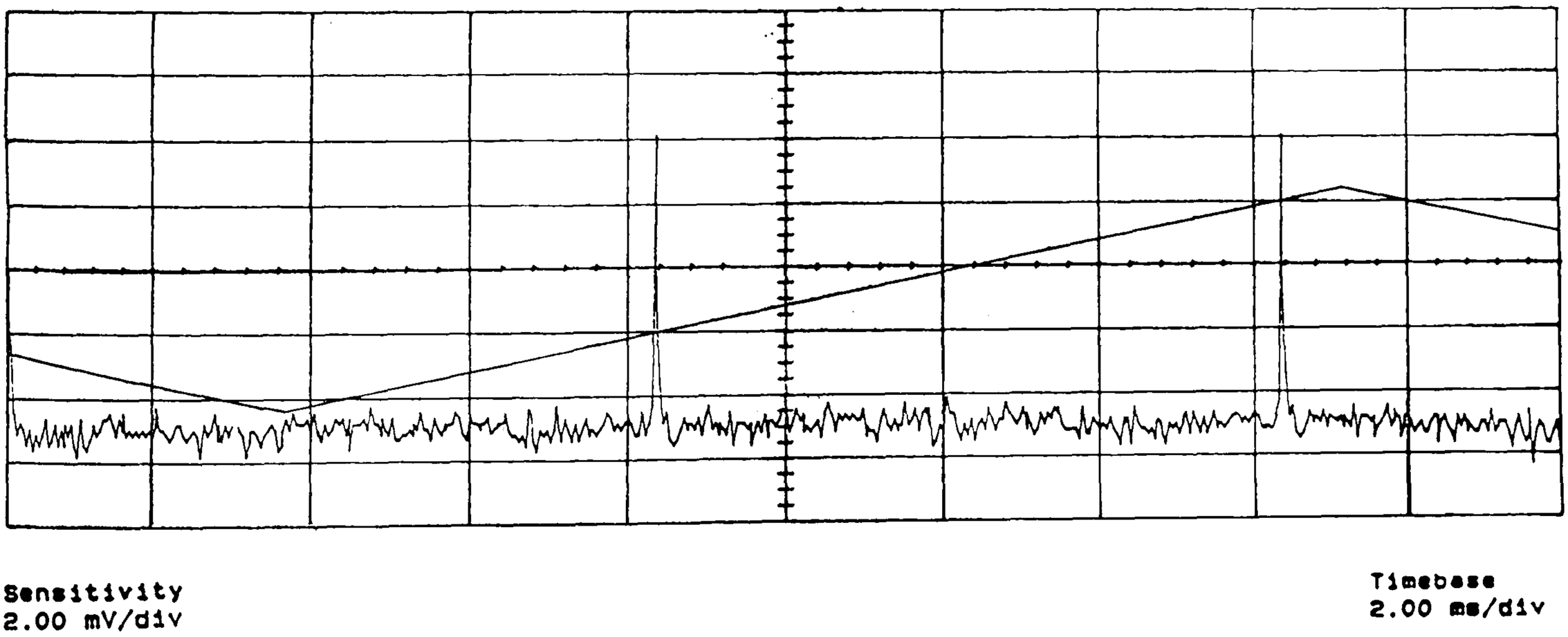

Figure 6.26 Output spectrum of the Melles Griot Narrow linewidth laser diode: linewidth $\leq$ 1.5 MHz.

theoretical modelling (figure 6.18) that even with a finesse of 100, ~3 mW of optical power is required to generate SBS up to the threshold level. It shows that a finesse of >100 is required to observe a beat frequency

At this stage it would be very interesting to compare the results of linewidth measurement of the Spectra Diode Labs laser diode SDL-5411-61 with two different techniques. The first is self heterodyne and the other is using the effective finesse of the resonator. The finesse measured using the narrow linewidth source is the intrinsic or actual finesse of the resonator. The effective finesse F' of the resonator, measured using the Spectra Diode Labs laser diode was ~22. From figure 6.17, which shows the theoretical relation between F' and the laser linewidth, the linewidth of the laser diode is ~5.6 MHz which is very close to the result ~6MHz obtained from the self heterodyne technique.

Although, we did not observe a beat frequency due to the small amount of SBS and limitations on the minimum detectable power of the detector, these observations are very encouraging and a frequency shifter based on a laser diode is, in principle, possible if a laser source with narrow linewidth <1 MHz and a resonator with a higher finesse (~ 100 - 200) is used.

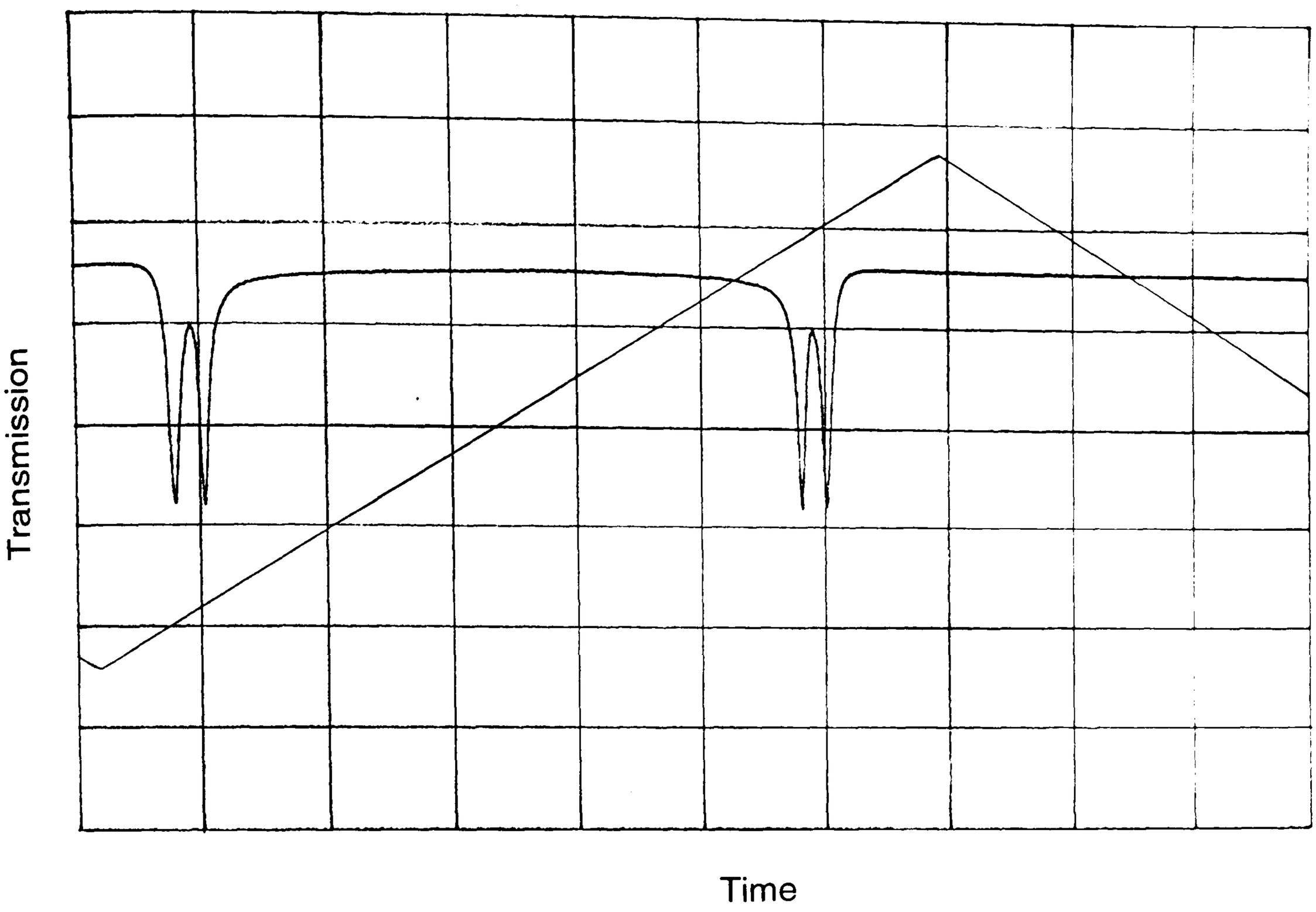

Figure 6.27(a) Orthogonal polarization modes not at resonance

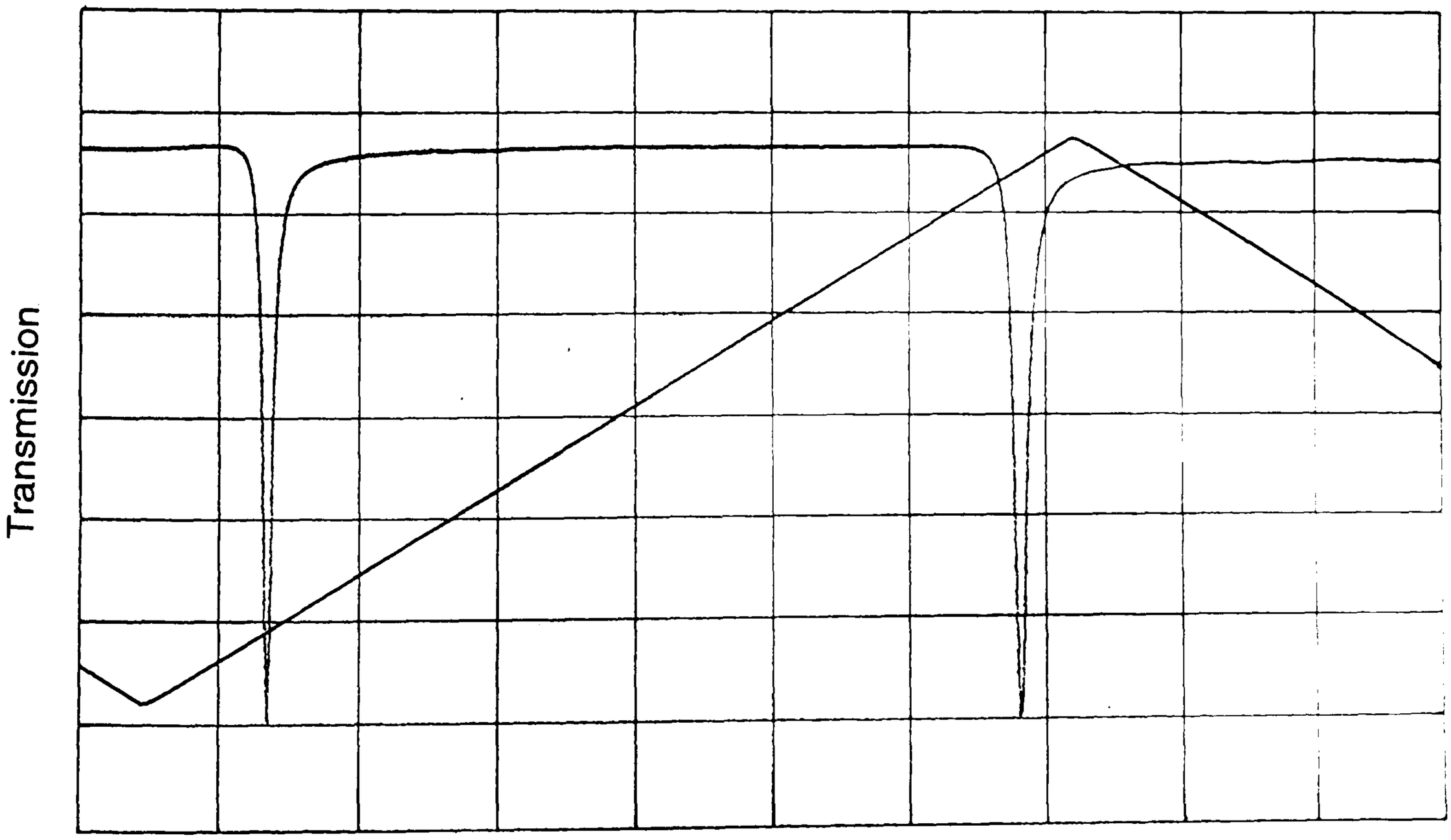

Figure 6.27(b) Orthogonal polarization modes resonating simultaneously

6.9 CONCLUSIONS

This chapter investigated a fibre optic frequency shifter, based on mixing two SBS signals which have slightly different frequencies. Two different configurations were discussed; the first using two separate resonators and the other using a single birefringent resonator. The dependence of carrier frequency on temperature variations was investigated for both configurations. A comparison between the two techniques was presented. The former configuration has the advantage of flexibility in tuning the carrier frequency, while the later is useful where a stable carrier is required. Finally, the use of a laser diode in such a system, the effect of its linewidth on the resonator finesse, its advantages and limitations were described. The linewidth of the laser was measured using two different techniques, i.e., the self heterodyne technique and by observing the transfer function of the ring resonator.

CHAPTER SEVEN

CONCLUSIONS

A fibre optic frequency shifter has been demonstrated that works on the principle of mixing two stimulated Brillouin scattering signals which have slightly different frequencies. Prior to the manifestation of the frequency shifter the behaviour of optical fibre ring resonators was investigated. The SBS shift for Helium Neon laser operating at 632.8 nm was measured as 26$\pm$0.4 GHz. An observable SBS onset for pump powers of ~2-3 μW was obtained from a high birefringent fibre ring resonator with a finesse of ~125. As expected the threshold power was found to decrease for higher finesse and the conversion efficiency was higher for higher finesse. Two different configurations, i.e., dual and single ring resonator have been used. For the dual resonator system a conversion efficiency of ~16 % was obtained. The beat frequency was tunable between 218.4 MHz and 414.6 MHz for a 40°C change in temperature. A temperature coefficient of 5$\pm$ 0.2 $MHzK^{-1}$ was measured.

The single birefringent resonator configuration provides a highly stable carrier frequency with a temperature coefficient of 6.7$\pm$ 0.5 $kHzK^{-1}$. A 20 % conversion efficiency was obtained with this configuration. This demonstrates that this technique offers a practical, fibre efficient, low optical power

requirement method for producing a frequency shifter. One of the main advantages of the system is that no electrical power is required to produce the travelling acoustic waves.

Optical detector-amplifier combinations used in this project, to detect the frequencies generated in the experiments have been characterized using a new technique based on wavelength modulation of a laser diode source via modulation of the injection current in a path length imbalanced two-beam interferometer. A simple robust configuration using birefringent optical fibre has been implemented. Results from direct modulation of the laser intensity and from a circuit simulation using PSpice are shown to be in good agreement with the interferometric technique. A number of detector-amplifier combinations were used to assess the viability of the technique. Agreement between the two experimental methods and the simulation are within a few percent during the linear response regime. As the response rolls off there is greater deviation between the experimental and simulation results due to approximations in the simulation software which lead to deviations between actual and theoretical circuit performance. However, the experimental results presented are the average of many readings resulting in a standard deviation of 6%.

Although the carrier signal produced by the frequency shifter was very stable as far as its frequency is concerned, its amplitude, which fluctuated between $\pm$ 5 dB, needs to be stabilized. One of the main reason for this amplitude variation was that the amount of SBS signal from two polarization eigenaxes was changing due to environmental effects and hence not resonating simultaneously. Improving the thermal and acoustic isolation and the quality of servosystem should improve the simultaneous locking and hence stabilize the amplitude of the beat frequency.

A more advanced type of servosystem could be implemented to improve the

locking system. The idea is that an external dc voltage can be applied to the PZT attached to the fibre to bring two resonating modes to resonate simultaneously. At the same time the output of the resonator should be monitored by the servo system and when the two modes reach the point at which they resonate simultaneously the servo should lock the resonator.

A diode based system offers great potential to develop a rugged and compact system suitable for industrial use. High finesse ($\geq$ 100) ring resonators can allow use of less expensive and ordinary diode lasers.

Finally, the most robust arrangement would utilise a laser diode 'pigtailed' to a high birefringence fibre ring resonator; the pigtail is a non-adjustable optomechanical construction that couples the laser output into the single mode fibre. This implementation would provide a robust technique that could, for example, be utilised for production line testing of devices.

REFERENCES

1. Kobayashi, K., NEC Chairman predicts installation of 10^{10} km of fibre by year 2000, Laser focus world, 16, 1980, p 56.

2. Digonnet, M. J. F., and Shaw, H. J., Analysis of a Tunable single mode optical fibre coupler, IEEE J. Quantum Electron., QE-18, 1982, p 746.

3. Urquhart, P., Review of rare earth doped fibre lasers and amplifiers, IEE proc. 135, 1988, p 385.

4. Khalil, D., Tedjini, S., and Charter G., A simple homodyne technique for the characterization of wideband optical detectors, SPIE 1314, 1990, p 38.

5. Hecht, J., The Laser Guide Book, McGraw Hill, 1976.

6. Data sheet SDL-5411-G1, Spectra Physics Limited.

7. Thompson,G.H.B.,Physics of Semiconductor Laser Devices,Wiley, New York, 1980.

8. Summits,Y., Advances in semiconductor lasers, Phy.Today, 38, 1985, p 32.

9. Laser diode user manual, Sharp Corporation, 1988.

10. Wieman, C. E. and Holberg, L., Using diode lasers for atomic physics. Rev. Sci. Instrum., 62, 1991, p 1.

11. Lichtman, E., and Friesem, A. A., stimulated Brillouin scattering excited by a multimode laser in single mode optical fibers, Opt. Commun. 64,1987, p 544.

12. Edwards, J. B., Cranfield University, private communication.

13. Goldberg,L.,Taylor,H.F.,Dandridge,A.,Weller,J.F.,Miles,R.O.,Spectral characteristics of semiconductor lasers with optical feedback, IEEE J.Quantum Electron.QE-18, 1982, p.555.

14. Hemmati H., Single longitudinal mode operation of semiconductor laser arrays with etalon feedback, Appl. Phys.Lett. 51, 1987, p 224.

15. Dandridge,A.,Miles,R.O., Spectral characteristics of semiconductor laser diodes coupled to optical fibres, Electron. Lett. 17,1981, p 273.

16. Wyatt,R.,Devlin,W.J., 10 kHz linewidth 1.5 μm InGaAsP external cavity laser with 55nm tuning range, Electron.Lett.19, 1983, p110.

17. Favre,F.,LeGuen,D.,Simon,J.C.,Landousies,B., External cavity semiconductor laser with 15nm continuous tuning range, Electron. Lett.22,1986, p 795.

18. Dandridge A.,Goldberg,L., Current induced frequency modulation in diode lasers, Electron.Lett.18,1982, p 302.

19. Gloge, D., Weakly guiding fibres, Appl. Opt. 10,1971, p 2252.

20. Payne, D. N., Barlow, A. J., and Hansen, J. J., Development of low and high birefringence optical fibres, IEEE J. of Quantum Electron. QE18, 1982, p 477.

21. Dyott, R. B., Cozens, J. R., and Morris, D. G., Preservation of polarization in optical fibre waveguides with elliptical cores, Electron. Lett. 15, 1979, p 380.

22. Stolen, R. H., Ramasawamy, V., Kaiser, P., and Pleibel, W., Linear polarization in birefringent single-mode fibres, Appl. Phys. Lett. 33, 1978,p 699.

23. Katsuyama, T., Matsumura, H., and Suganuma, T., Low-loss single-polarization fibres, Electron. Lett. 17,1981, p 473.

24. Hosaka, T., Okomoto, K., Sasaki, Y., and Edahiro, T., Single mode fibres with asymmetrical refractive index pits on both sides of core, Electron. Lett. 17, 1981, p 191.

25. Hosaka, T., Okomoto, K., Miya, T., Sasaki, Y., and Edihiro, T., Low-loss single polarization fibres with asymmetrical strain birefringence, Electron. Lett. 17,1981, p 530.

26. Shibata, N., Sasaki, Y., Okamoto, K., and Hosaka, T., Fabrication of polarization-maintaining and absorption-reducing fibers, J. Lightwave Technol. LT-1, 1983, p 38.

27. Sasaki, Y., Hosaka, T., and Noda, J., Low crosstalk polarization maintaining optical fibre with an 11 km length, Electron. Lett. 20, 1984, p 784.

28. Sasaki, Y., Hosaka, T., and Noda, J., Low-loss polarization maintaining optical fibre with low crosstalk, Electron. Lett. 21, 1985, p156.

29. Birch, R. D., Payne, D. N., and Varnham, M. P., Fabrication of polarization maintaining fibres using gas phase etching, Electron. Lett. 18, 1982, p 1036.

30. Snyder, A. W., and Love, J. D., Optical Waveguide Theory, Chapman and Hall, New York, 1983.

31. Gambling, W. A., and Pool, S. B., Optical fiber sensors, vol. I, Artech House, 1988.

32. Sasaki, Y., Hosaka, T., Takad, K., and Noda, J., 8 km-long polarization maintaining fibre with highly stable polarization state, Electron. Lett., 1983, p 792.

33 . Tomaru, S., Kawachi, M., and Edahiro, T., Fabrication of single-mode fibres by V.A.D., Electron. Lett., 16, 1980.

34. Lafon, P., Private communication, Fujikura Europe Ltd., 1992.

35. Yoshino, T., Kurosawa, K., Itoh, K., and Ose, T., Fiber-Optic Fabry-Perot interferometer and its sensor applications, IEEE J. Quantum Electron. 18, 1982, p 1624.

36. Davies, D. E. N., and Kingsley, S., Method of phase-modulating signals in optical fibres: application to optical-telemetry systems, Electron. Lett., 10, 1974, p 21.

37 . Kingsley, S. A., Optical-fiber phase modulator, Electron. Lett. 11, 1975, p 453.

38. Martini, G., Analysis of a single-mode optical fibre piezoceramic phase modulator, Optical and Quantum Electron. 19, 1987, p179.

39 . Digonnet, M. J. F., Feth, J. R., Stokes, L. F., Shaw, H. J., Measurement of the core proximity in polished fiber substrates and couplers, Opt. Lett. 10, 1985, p 463.

40 . Yu, M. H., and Hall, D. B., Low loss fiber ring resonator, Proc. SPIE-Fiber Optic and Laser Sensors II, 478, 1984, p 104.

41 . Vanclooster, R., and Phariseau, P., The coupling of two parallel dielectric fibers, Parts I and II, Physica, 47, 1970, p 485.

42. Kawachi, M., Kawasaki, B. S, Hill, K. O. and Edahiro, T., Fabrication of single polarization single-mode fibre couplers, Electron. Lett. 18, 1982, p 962.

43. Dyott, R. B., and Bello, J., Polarisation-holding directional coupler made from elliptically cored fibre having a D section, Electron. Lett. 19, 1983, p 601.

44. Nayar, B. K. and Smith, R. D., Monomode-polarization-maintaining fiber directional couplers, Opt. Lett. 8, 1983, p 543.

45. Marcuse, D., The coupling of degenerate modes in two parallel dielectric waveguides, Bell Syst. Tech. J. 50, 1971, p1791.

46. Yariv, A., Coupled-mode theory for guided-wave optics, IEEE J. Quantum Electron. QE-9, 1973, p 919.

47. Snyder, A. W., and Love, J. D., Optical waveguide theory, Chapman and Hall, New York, 1983.

48. Risk, W. P., Youngquist, R. C. Kino, G. S., and Shaw, H. J., Acousto-optic frequency shifting in birefringent fibre, Opt. Lett., 9, 1984, p 309.

49. Pannell, C. N., Tatam, R. P., Jones, J. D. C., and Jackson, D. A., A fibre optic frequency shifter utilizing travelling flexure waves inbirefringent fibre, J. Inst. Electron. and Radio Eng., 58, supplement, 1988, PS92.

50. Heismann, F., and Ulrich, R., Integrated optical frequency translator with strip waveguide, Appl. Phys. Lett. 45, 1984, p 490.

51. Yap, D., and Johnson, L. M., Radiation field coupling in optical waveguide structures with closely spaced abrupt bend and branches, Proc. Soc. Photo-Opt. Instrum. Eng. 517, 1985, p 137.

52. Tatam, R. P., "Optical Modulation Techniques for Fibre Sensors" in Optical Fibre Sensor Technology, Edited by Grattan, K. T. V., and Meggitt, B., Chapman and Hall (to be published).

53. Risk, W. P., Youngquist, R. C., Kino, G. S., and Shaw, H. J., Single sideband frequency shifting in birefringent optical fibre", SPIE Proc., 478, Fiber Optic and Laser Sensors II, 1984, p 91.

54. Youngquist, R. C., Brooks, J. L., and Shaw, H. J., Birefringent-fibre

polarisation coupler, Opt. Lett. 8, 1983, p 656.

55. Risk, W. P., Kino, G. S., and Shaw, H. J., Fibre-optic frequency shifter using surface acoustic wave incident at an oblique angle, Opt. Lett. 11, 1986, p 115.

56. Risk, W. P., and Kino, G. S., Acousto-optic fibre-optic frequency shifter using periodic contact with co-propagating surface acoustic wave, Opt. Lett. 11, 1986, p 336.

57. Greenhalgh, P. A., Foord, A. P., Davies, P. A., Fibre optic frequency shifters, SPIE Proc. 1314, Fibre Optic 90, p 284.

58. Foord, A. P., Greenhalgh, P. A., and Davies, P. A., All-fibre frequency shifters using multiple acoustic transducers, Electron. Lett. 27, 1991, p 1141.

59. Kim, B. Y., Blake, J. N., Engan, H. E., and Shaw, H. J., All-fibre acousto-optic frequency shifter, Opt. Lett.11, 1986, p 389.

60. Patterson, D. B., Digonnet, M. J. F., Liu, A. C., Khuri-Yakuli, B. T., and Kino, G. S., Frequency shifting in optical fiber using a saw horn, Proc. IEEE Ultrasonic Symposium, 1990, p 617.

61. Askautrud, J. O., and Engan, H. E., Fiber-optic frequency shifter with a mode change using cascaded acousto-optic interaction regions, Opt. Lett. 15, 1990, p 649.

62. Sabert, H., Day, L., and P. St: Russell, J., Versatile acousto-optical flexural wave-modulator, filter and frequency shifter in dual-core fibre,

International J. of Optoelectron. 7,1992, p 189.

63. Chu, P. L. and Snyder, A. W., Theory of twin-core optical fibre frequency shifter, Elect. Lett. 23, 1987, p 1101.

64. Smith R. G., Optical power handling capacity of low loss optical fibre as determined by Raman nd Brillouin scattering, Appl. Optic., 11, 1972, p 2489.

65. Stolen, R. H., Nonlinearity in fibre transmission, Proc. IEEE, 68, 1980, p 1232.

66. Cotter, D., stimulated Brillouin scattering in monomode optical fibre, J. Opt. Commun., 4, 1983, p 10.

67. Nye, J. F., Physical properties of crystals, Clarenden press, Oxford 1989.

68. Tang, C. L., Saturation and spectral characteristics of the stokes emission in the stimulated process, J. Appl. Phys., 37, 1966, p 2945.

69. Cotter, D., Observation of stimulated Brillouin scattering in low loss silica fibre at 1.3 μm, Electron Lett. 18, 1982, p 445.

70. Khan, O. S., and Tatam, R. P., A fibre optic frequency shifter based on stimulated Brillouin scattering in a birefringent fibre ring resonator, IOP Proc. Applied Optics and Opto-Electronic Conference, Leeds, 1992, p 239.

71. Labudde, P., Anliker, P., and Weber, H. P., Transmission of narrowband

high power laser radiation through optical fibres, Optics Commun., 32, 1980, p 385.

72. Culverhouse, D., Farahi, F., Pannell, C. N., and Jackson, D. A., Stimulated Brillouin scattering: A means to realise a tunable microwave generator or distributed temperature sensor, Electron Lett., 25, 1989, p 915.

73. Duffy, C. J., and Tatam, R. P., Optical heterodyne carrier generation utilising stimulated Brillouin scattering in birefringent optical fibre, Electron. Lett., 27, 1991, p 2004.

74. Duffy, C. J., and Tatam, R. P., An optical frequency shifter based on stimulated Brillouin scattering in birefringent optical fibre, SPIE Proc. 1511, 1991, p 155.

75. Duffy, C. J., and Tatam, R. P., Optical frequency shifter technique based on stimulate Brillouin scattering in birefringent optical fibre, Appl. Opt. 32, 1993, p 5966.

76. Stokes, L. F., Chodorow, M, and Shaw, H. J., All single mode fibre resonant ring interferometer, J. Lightwave Technol. LT1, 1983, p 110.

77. Smith, S. P., Zarinetchi, F., and Ezekiel, S., Narrow linewidth stimulated Brillouin fibre laser and applications, Opt. Lett. 16, 1991, p 393.

78. Stokes, L. F., Chodorow, M., and Shaw, H. J., All-fibre stimulated Brillouin ring laser with submilliwatt pump threshold, opt. Lett. 7, 1982, p 509.

79. Shupe, D. M., Fibre resonator gyroscope,: Sensitivity and thermal nonreciprocity, Appl. Opt. 20, 1981, p 286.

80. Stokes, L. F., Chodorow,M., and Shaw, H. J., All fibre single mode fibre resonator, Opt. Lett. 7, 1982, p 288.

81. Khan, O. S., Tatam, R. P., Optical frequency shifter based on stimulated Brillouin scattering in a birefringent optical fibre ring resonator, Optics Commun., 103, 1993, p 161.

82. Nayar, B. K., and Smith, D. R., Monomode polarization maintaining fibre directional couplers, Opt. Lett. 4, 1979, p 29.

83. Siegman, A. E., An introduction to Lasers and Masers, McGraw Hill, New York, 1971.

84. Cotter, D., Stimulated Brillouin Scattering in Monomode Optical Fibre., J. Opt. Commun. 4, 1983, p 10.

85. Beals, K. J., and Day, C. R., A review of glass fibres for optical communications, Phys. Chem. Glasses, 21, 1980, p 5.

86. Yariv, A., and Yeh, P., Optical waves in crystals, Wiley, 1984.

87. Shen, Y. R., Principles of nonlinear optics, Wiley, New York, 1984

88. Stolen, R. H., Fibre Raman lasers, Fibre and Integrated Opt. 3, 1980,. p 21.

89. Ippen, E. P., and Stolen, R. H., Stimulated Brillouin Scattering in Optical

Fibre, Appl. Phys. Lett 21, 1972, p 539.

90. Marcuse, D., Gaussian approximation of the fundamental modes of graded-index fibre, J. Opt. Soc. Am., 68, 1978, p 103.

91. Stolen, R.H., Ippen, E. P., Raman gain in glass optical waveguides, Appl. Phys. Lett. 22, 1973, p 276.

92. Andres, M. V., A novel optical fibre technique to calibrate the frequency response of optical detectors. Meas.Sci.Technol. 3, 217, 1992.

93. Yariv, A., Optical Electronics, Holt, Reinhart and Winston, New York, Chapter 15, 1985.

94. Tuinenga, P. W., SPICE - a guide to circuit simulation and analysis using PSpice, Prentice Hall, Coventry, 1988.

95. Jackson, D. A., Priest, P., Dandridge, A., and Tveten, A. B., Elimination of drift in a single-mode optical fiber interferometer using a piezoelectrically stretched coiled fiber, Appl. Opt. 19, 1980, p 2926.

96. Lefevre, H. C.,Single-mode fiber fractional wave devices and polarization controllers,Electron. Lett. 16, 1980, p 778.

97. Ionnidis, Z. K., Radmore, P. M., and Giles, I. P., Phase modulation in all fibre ring resonator sensor, Proc. OFS' 88, ThBB3-1, New Orleans, USA, 1988.

98. Bucaro, J. A., and Drady, H. D., High temperature Brllouin scattering in fused quartz, J. Appl. Phys. 45, 1974,p 5324.

99. Hocker, G. B., Fibre optic sensing of pressure and temperature, Appl. optics, 18, 1979, p 1445.

100. Pinnow, D. P., Electro-optic materials , Handbook of lasers, R. J. Pressley, CRC, Cleveland, Ohio, 1971.

101. Jackson, D. A., and Jones, D. C., "Interferometers" in Optical Fibre Sensors, Artech House, 1989.

102. For example, Data sheet (1988) on D300 Series Acousto-Optic Modulator, Isomet Corporation, USA, quotes a temperature stability of $\pm$ 0.25% from 0° to 60°C.

103. Ford, H. D. and Tatam, R. P., Narrow-band, wavelength-division multiplexers using birefringent optical fibres, Optics Comms. 98, 1993, p 151.

104. Harrison R. G., Uppal, Johnstone A., and Moloney, Phys. Rev. Lett. 69, 1990, p167.

105. Tai, S., Kyuma, K., Hamanaka, K., and Nakayama, T., Application of fibre optic ring resonators using laser diodes, Optica Acta, 33,1986, p 1539.

106. Yariv, A., Quantum Electronics, John Wiley & Sons, 1975.

107. Okoshi, T., Kikuci, K., Nakayama, A., Novel method for high resolution measurement of laser output spectrum, Electron. Lett. 16,1980, p 630.

108. MacAdam, K. B., Steinbach, A., and Wieman C., A narrow-band tunable

diode laser system with grating feedback, and a saturated absorption spectrometer for Cs and Rb, Am. J. Phys. 60, 1992.

APPENDIX A

TRANSFER FUNCTION OF THE RING RESONATOR

In order to drive an expression for the ring resonator transfer function, consider a ring resonator of loop length *L* characterized by an amplitude attenuation coefficient α_o . Let *K* be the intensity coupling coefficient between the two fibres in the coupler and γ_o, the intensity loss coefficient. Applying conservation of energy to the coupler input and output we obtain the following relation (see figure 4.1):

$$|E_3|^2 + |E_4|^2 = (1-\gamma_o)\ (\ |E_1|^2 + |E_2|^2\ ) \qquad \textbf{(A.1)}$$

where E_i is the electric field at *ith* port. The output electric field amplitudes in the fibre after the coupled-mode interaction are related to the incident fields by:

$$E_3 = (1-\gamma_o)^{1/2}\ [\ (1-K)^{1/2} E_1 + j\sqrt{K}\, E_2] \qquad \textbf{(A.2)}$$

$$E_4 = (1-\gamma_o)^{1/2}\ [j\sqrt{K}\, E_1 + (1-K)^{1/2} E_2] \qquad \textbf{(A.3)}$$

Taking into account the attenuation loss in the fibre, E_2 and E_3 are further

related as:

$$E_2 = E_3 e^{j\beta L} e^{-\alpha_o L} \qquad \textbf{(A.4)}$$

where α_o is the amplitude attenuatuin constant of the fibre, $\beta = n\omega/c$ and ω is the optical frequency.

Putting the value of E_2 in Eq.(A.2)

$$E_3 = \sqrt{1-\gamma_o}\,[\sqrt{1-K}E_1 + j\sqrt{K}E_3\, e{-}\alpha_o L\, ej\beta L]$$

$$E_3 - E_3\sqrt{1-\gamma_o}\, j\sqrt{K}\, e^{-\alpha_o L} e^{j\beta L} = \sqrt{1-\gamma_o}\sqrt{1-K}\, E_1$$

$$\frac{E_3}{E_1} = \frac{\sqrt{1-\gamma_o}\sqrt{1-K}}{1-\sqrt{1-\gamma_o}\, j\sqrt{K}\, e^{-\alpha_o L} e^{j\beta L}} \qquad \textbf{(A.5)}$$

$$\left|\frac{E_3}{E_1}\right|^2 = \frac{(1-\gamma_o)\,(1-K)}{|Z|^2} \qquad where\ Z = 1 - j\sqrt{K}\sqrt{1-\gamma_o}\, e^{-\alpha_o L} e^{j\beta L}$$

$$Z = 1 - jA\, e^{j\beta L} \qquad where\ A = \sqrt{K}\sqrt{1-\gamma_o}\, e^{-\alpha_o L}$$

$$Z = 1 - jA(\cos\beta L + j\sin\beta L)$$

$$Z = (1 + A\sin\beta L) - j(A\cos\beta L)$$

$$\Rightarrow |Z|^2 = 1 + A^2 + 2A \sin \beta L$$

$$|Z|^2 = 1 + K(1-\gamma_o)\, e^{-2\alpha_o L} + 2\sqrt{K}\sqrt{1-\gamma_o}\, e^{\alpha_o L} \sin \beta L$$

therefore Eq.(5) becomes:

$$\left|\frac{E_3}{E_1}\right|^2 = \frac{(1-\gamma_o)\,(1-K)}{1 + K(1-\gamma_o)\, e^{-2\alpha_o L} + 2\sqrt{K}\,\sqrt{1-\gamma_o}\, e^{-\alpha_o L} \sin \beta L} \qquad \textbf{(A.6)}$$

As $Sin\ \beta L = -Cos\ (\beta L + \pi/2)$

$= 2Sin^2\ (\beta L/2 + \pi/4) - 1$

$\therefore$ the denominator in eq.A.6 becomes

$$1 + k(1-\gamma)\, e^{-2\alpha_o L} + 2\sqrt{k}\sqrt{1-\gamma_o} e^{-\alpha_o L} [2Sin^2 (\beta \frac{L}{2} + \frac{\pi}{4}) - 1]$$

$$= 1 + k(1-\gamma)\, e^{-2\alpha_o L} + 4\sqrt{k}\sqrt{1-\gamma_o} e^{-\alpha_o L} Sin^2 (\beta \frac{L}{2} + \frac{\pi}{4}) - 2\sqrt{k}\sqrt{1-\gamma_o} e^{-\alpha_o L}$$

$$= [1 + k(1-\gamma)\, e^{-2\alpha_o L} - 2\sqrt{k}\sqrt{1-\gamma_o} e^{-\alpha_o L}] + 4\sqrt{k}\sqrt{1-\gamma_o} e^{-\alpha_o L} Sin^2 (\beta \frac{L}{2} + \frac{\pi}{4})$$

$$= [1^2 - 2(1)\,(\sqrt{k}\sqrt{1-\gamma_o} e^{-\alpha_o L}) + (\sqrt{k}\sqrt{1-\gamma_o} e^{-\alpha_o L})^2 + 4\sqrt{k}\sqrt{1-\gamma_o} e^{-\alpha_o L} Sin^2 (\frac{\beta L}{2} + \frac{\pi}{4})]$$

$$= (1-\sqrt{k}\sqrt{1-\gamma_o}e^{-\alpha_o L})^2 + 4\sqrt{k}\sqrt{1-\gamma o}e^{-\alpha_o L} Sin^2 (\frac{\beta L}{2} + \frac{\pi}{4})$$

∴ Eq. 6 becomes

$$\left|\frac{E_3}{E_1}\right|^2 = \frac{(1-\gamma_o)(1-K)}{(1-\sqrt{K}\sqrt{1-\gamma_o}\,e^{-2\alpha_o L})^2 + 4\sqrt{K}\sqrt{1-\gamma_o}\,e^{-\alpha_o L} Sin^2 (\frac{\beta L}{2} + \frac{\pi}{4})} \qquad (A.7)$$

Equation A.7, periodic in βL with periodicity 2π rad, is the circulating intensity for any value of the coupling constant. Now we will calculate the value of the circulating intensity for the resonant condition, i.e., when the output of the resonator is zero.

Putting the value of E_2 from Eq. A.4 into Eq. A.3

$$E_4 = \sqrt{1-\gamma_o}\,[\,j\sqrt{K}E_1 + \sqrt{1-K}E_3 e^{-\alpha_o L} e^{j\beta L}] \qquad (A.8)$$

Now from Eq. 5

$$E_3 = \frac{\sqrt{1-\gamma_o}\sqrt{1-K}}{1-j\sqrt{K}\sqrt{1-\gamma_o}e^{-\alpha_o L}e^{j\beta L}} E_1$$

Put the value of E_3 in Eq. 8

$$\frac{E_4}{E_1} = \sqrt{1-\gamma_o}\,[j\sqrt{K} + \frac{\sqrt{1-K}\sqrt{1-\gamma_o}\,e^{-\alpha_o L}e^{j\beta L}}{1-j\sqrt{K}\sqrt{1-\gamma_o}\,e^{-\alpha_o L}e^{j\beta L}}] \qquad (A.9)$$

For zero output power we require E_4 to vanish, which gives

$$0 = j\sqrt{K} + \frac{(1-K)\sqrt{1-\gamma_o}\, e^{-\alpha_o L} e^{j\beta L}}{1-j\sqrt{K}\sqrt{1-\gamma_o}\, e^{-\alpha_o L} e^{j\beta L}}$$

$$0 = j\sqrt{K}\,(1-j\sqrt{K}\sqrt{1-\gamma_o}\, e^{-\alpha_o L} e^{j\beta L}) + (1-K)\sqrt{1-\gamma_o}\, e^{-\alpha_o L} e^{j\beta L} \qquad (A.10)$$

$$j\sqrt{K}-j^2K\sqrt{1-\gamma_o}e^{-\alpha_o L}(Cos\beta L+jSin\beta L)+(1-K)\sqrt{1-\gamma_o}e^{-\alpha_o L}(Cos\beta L+jSin\beta L)=0$$

$$j\sqrt{K}+K\sqrt{1-\gamma_o}e^{-\alpha_o L}Cos\beta L+jK\sqrt{1-\gamma_o}Sin\beta Le^{-\alpha_o L}+(1-K)\sqrt{1-\gamma_o}e^{-\alpha_o L}Cos\beta L$$

$$+j(1-K0\sqrt{1-\gamma_o}e^{-\alpha_o L}Sin\beta L=0$$

Now considering the real part

$$K\sqrt{1-\gamma o}e^{-\alpha_o L}Cos\beta L+(1-K)\sqrt{1-\gamma_o}e^{-\alpha_o L}Cos\beta L=0$$

$$K\sqrt{1-\gamma_o}e^{-\alpha_o L}Cos\beta L+\sqrt{1-\gamma_o}e^{-\alpha_o L}Cos\beta L-K\sqrt{1-\gamma_o}e^{-\alpha_o L}Cos\beta L=0$$

$$\sqrt{1-\gamma_o}e^{-\alpha_o L}Cos\beta L=0$$

as γ_o & $e^{-\alpha oL}$ are positive

$Cos\ \beta L = 0$

$\Rightarrow \beta L = \pi/2,\ 3\pi/2,\ ....$

$= (n + 1/2)\pi$

If we take the sin of these angles only two values are possible

$\Rightarrow Sin\ \beta L = \pm 1 \qquad \forall \quad \beta L = (n + 1/2)\pi$

And the Imaginary part is

$$\sqrt{K}+K\sqrt{1-\gamma_o}e^{-\alpha_o L}Sin\beta L+(1-K)\sqrt{1-\gamma_o}e^{-\alpha_o L}Sin\beta L=0$$

$$\sqrt{K}+K\sqrt{1-\gamma_o}e^{-\alpha_o L}Sin\beta L+\sqrt{1-\gamma_o}e^{-\alpha_o L}Sin\beta L-K\sqrt{1-\gamma_o}e^{-\alpha_o L}Sin\beta L=0$$

$$\sqrt{K}+K\sqrt{1-\gamma_o}e^{-\alpha_o L}Sin\beta L=0 \qquad \textbf{(A.10.a)}$$

All values cannot be positive, since ,γ_o K, $e^{-\alpha o L}$ all are positive therefore $Sin\beta L$ must be negative. The relation between K, γ_o, & α_o is required.

Using the assumed relation

$Sin\beta L = -1$

$\beta L = 3\pi/2,\ \ 7\pi/2,\ 11\pi/2....$

$$\beta L = 2\pi n - \pi/2 \qquad (A.11)$$

where n is any integer.

Using $Sin\beta = -1$, the imaginary part of Eq. A.10 further requires that the coupling constant have a certain value for resonance ($E_4 = 0$), denoted by *Kr*, i.e., at resonance a certain value of coupling constant, $K = Kr$

∴ Eq. A.10(a) can be written as

$$\sqrt{K_r}+K_r\sqrt{1-\gamma_o}e^{-\alpha_o L}Sin\beta L=0$$

$$\sqrt{K_r}+K_r\sqrt{1-\gamma_o}e^{-\alpha_o L}(-1)=0$$

$$\sqrt{K_r}=\sqrt{1-\gamma_o}e^{-\alpha_o L}=0$$

$$K_r=(1-\gamma_o)\,e^{-2\alpha_o L}=0 \qquad \textbf{(A.12)}$$

1-Kr is the round-trip intensity loss of the coupler and fibre loop. Equations A.11 & A.12 are two necessary conditions for resonance with zero output power. Using the resonant value of coupling given by eq. A.12, eq. A.7 can be written as:

$$\left|\frac{E_3}{E_1}\right|^2=\frac{(1-\gamma_o)\,(1-K_r)}{(1-\sqrt{K_r}\sqrt{K_r})^2+4\sqrt{K_r}\sqrt{K_r}\sin^2(\beta L/2+\pi/4)}$$

$$\left|\frac{E_3}{E_1}\right|^2=\frac{(1-\gamma_o)\,(1-K_r)}{(1-K_r)^2+4K_r\sin^2(\beta L/2+\pi/4)} \qquad \textbf{(A.13)}$$

Which is the circulating intensity.

OUTPUT INTENSITY

The output intensity can be found by using conservation of energy, given by eq. A.1 & eq.A.4 as follows:

$$|E_2|^2=|E_3|^2e^{-2\alpha_o L}$$

The objective is to calculate $|E_4/E_1|$

Putting the value of $|E_2|^2$ in eq A.1 :

$$|E_3|^2 + |E_4|^2 = (1-\gamma o)\ (|E_1|^2 + |E_3|^2\ e^{-2\alpha_o})$$

$$|E_4|^2 = (1-\gamma_o)\ |E_1|^2 + (1-\gamma_o)\ |E_3|^2 e^{-2\alpha_o L} - |E_3|^2$$

$$\left|\frac{E_4}{E_1}\right|^2 = (1-\gamma_o) + [(1-\gamma_o)\ e^{-2\alpha_o L}-1] \left|\frac{E_3}{E_1}\right|^2 \qquad \textbf{(A.14)}$$

$$\left|\frac{E_4}{E_1}\right|^2 = (1-\gamma_o) - [1 - (1-\gamma_o)\ e^{-2\alpha_o L}] \left|\frac{E_3}{E_1}\right|^2$$

Using eq. A.12:

$$\left|\frac{E_4}{E_1}\right|^2 = (1-\gamma_o) - [1-Kr] \left|\frac{E_3}{E_1}\right|^2$$

Putting the value of $|E_3 / E_1|^2$ from eq. A.13:

$$\left|\frac{E_4}{E_1}\right| = (1-\gamma_o) - \frac{(1-Kr)\ (1-\gamma_o)\ (1-Kr)}{(1-Kr)^2 + 4KrSin^2(\beta L/2 + \pi/4)}$$

$$\left|\frac{E_4}{E_1}\right|^2 = (1-\gamma_o)\ \left[1 - \frac{(1-Kr)^2}{(1-Kr)^2 + 4Kr\ Sin^2\ (\frac{\beta L}{2} + \frac{\pi}{4})}\right] \quad \textbf{(A.15)}$$

$$\left|\frac{E_4}{E_1}\right|^2 = \frac{(1-\gamma_o)\ 4Kr\ Sin^2\ (\frac{\beta L}{2} + \frac{\pi}{4})}{(1-Kr)^2 + 4Kr\ Sin^2\ (\frac{\beta L}{2} + \frac{\pi}{4})} \quad \textbf{(A.16)}$$

which is the output intensity.

At resonance we have:

$$Sin^2\ (\beta\frac{L}{2} + \frac{\pi}{4}) = 0$$

The output intensity (Eq. A.16) is zero and the circulating intensity (Eq. A.13) is given as:

$$\left|\frac{E_3}{E_1}\right|^2_{max} = \frac{(1-\gamma_o)\ (1-Kr)}{(1-Kr)^2}$$

$$\left|\frac{E_3}{E_1}\right|^2_{max} = \frac{1-\gamma_o}{1-Kr} \quad \textbf{(A.17)}$$

APPENDIX B

SBS THRESHOLD POWER

Consider a ring resonator of loop length *L*, illuminated with a laser light source.The relation between the optical power *P* and the fibre attenuation coefficient α_o along the fibre of length *L* is given by:

$$P = P_{input}\, exp(-2\alpha_o L) \qquad \text{(B.1)}$$

where P_{input} is the power launched at the input of the fibre. The round trip transmission experienced by the SBS wave is the product of the fibre transmission, $e^{-2\alpha oL}$ and the net coupler transmission from port 3 to port 2. This transmission (3 to 2) is in fact the coupler power transmission $(1 - \gamma_o)$ multiplied by the coupling coefficient *Kr* because only the fraction *Kr* of the Brillouin wave remains in the fibre ring while the fraction *(1 -Kr)* leaves the ring through port 1.

Therefore the SBS wave round trip transmission is $e^{-2\alpha oL}(1-\gamma_o)Kr$. Putting the value of *Kr* from eq.A.13:

$$\text{Transmission} = e^{-2\alpha oL}(1-\gamma_o)\, e^{-2\alpha oL}(1-\gamma_o) = [e^{-2\alpha oL}(1-\gamma_o)]^2$$

The threshold condition for SBS is:

$$\textit{Transmission X Gain} = 1$$

$$[(1-\gamma_o)\exp(-2\alpha_o L)]^2 \exp[G_B(\upsilon_B)/A_{eff} P_{ct}(0)\, L_{eff}] = 1 \qquad \text{(B.2)}$$

where P_{ct} is the power circulating in the loop.

To a good approximation we have:

$1-\gamma_o = e^{-\gamma o}$, $1-2\alpha_o L \approx e^{-2\alpha o L}$ & $L_{eff} \approx L$ (eq. 4.39). Thus eq. B.2 becomes:

$$(e^{-\gamma_o} e^{-2\alpha_o L})^2 e^{G_B(\nu_B) P_{ct} \frac{L}{A_{eff}}} = 1$$

$$e^{-(\gamma_o + 2\alpha_{oL}) 2 + G_B(\nu_B) P_{ct} \frac{L}{A_{eff}}} = 1$$

$$-(\gamma_o + 2\alpha_o L)\, 2 + G_B(\nu_B)\, P_{ct} \frac{L}{A_{eff}} = 0 \qquad \text{(B.3)}$$

$$\text{Now as} \quad F = \frac{\pi\sqrt{K_r}}{1-K_r}$$

$$\frac{\pi}{F} = \frac{1-K_r}{\sqrt{K_r}} = K_r^{-\frac{1}{2}} - K_r^{+\frac{1}{2}}$$

$$\text{But } K_r = (1-\gamma_o)\, e^{-2\alpha_o L}$$

$$\therefore \frac{\pi}{F} = (1-\gamma_o)^{-\frac{1}{2}} e^{\alpha_o L} - (1-\gamma_o)^{\frac{1}{2}} e^{-\alpha_o L}$$

$$= (1 + \frac{1}{2}\gamma_o)\, e^{\alpha_o L} - (1 - \frac{1}{2}\gamma_o)\, e^{-\alpha_o L}$$

$$= e^{\alpha_o L} + \frac{1}{2}\gamma_o e^{\alpha_o L} - e^{-\alpha_o L} + \frac{1}{2}\gamma_o e^{-\alpha_o L}$$

$$= (e^{\alpha_o L} - e^{-\alpha_o L}) + \frac{1}{2}\gamma_o (e^{\alpha_o L} + e^{-\alpha_o L})$$

$$= [\,(1 + \alpha_o L) - (1 - \alpha_o L)\,] + \frac{1}{2}\gamma_o [1 + \alpha_o L + 1 - \alpha_o L]$$

$$\frac{\pi}{F} = 2\alpha_o L + \gamma_o \qquad \textbf{(B.4)}$$

Putting this value in eq. B.3:

$$P_{ct} = \frac{2A_{eff}}{G_B(\nu_B)\, L}\, \frac{\pi}{F} \qquad \textbf{(B.5)}$$

Now using eq. A.17:

$$\frac{P_{ct}}{P_{input}} = \frac{(1-\gamma_o)}{(1-Kr)} \qquad \textbf{(B.6)}$$

Using eq. B.3.b and B.4 the relation between the threshold power $P_{input,th}$, and SBS gain can be written as:

$$P_{input,th} = \frac{1-Kr}{1-\gamma_o} \cdot \frac{2A}{G_B(\nu_B)\,L}\,(\gamma_o + 2\alpha_o L)$$

$$P_{input,th} = \frac{2A}{G_B(\nu_B)\,L} \cdot \frac{(1-Kr)\,(\gamma_o + 2\alpha_o L)}{(1-\gamma_o)} \qquad \text{(B.7)}$$

Here

$$(1-Kr) = 1-(1-\gamma_o)\,e^{-2\alpha_o L}$$

$$= 1-e^{-2\alpha_o L} + \gamma_o e^{-2\alpha_o L}$$

neglecting higher order terms.

$$(1-K_r) = \gamma_o + 2\alpha_o L - 2\alpha_o L\gamma_o$$

neglecting third term on the left, α_o, γ_o being very small:

$$(1-K_r) = \gamma_o + 2\alpha_o L \qquad \text{(B.8)}$$

Putting the value of *(1 - Kr)* in eq. B.7:

$$P_{input,th} = \frac{2A}{G_B(\nu_B)\,L} \cdot \frac{(\gamma_o + 2\alpha_o L)^2}{(1-\gamma_o)} \qquad \text{(B.9)}$$

Using eq. B.4 and assuming $(1 - \gamma_o) \approx 1$, eq. B.9 becomes:

$$P_{input,th} = \frac{2A}{G_B(\nu_B)\,L} \cdot \frac{\pi^2}{F^2} \qquad \text{(B.10)}$$

APPENDIX C

LIST OF PUBLICATIONS

Publications arising from this work:

1. Omer S. Khan and Ralph P. Tatam, Optical Frequency Shifter based on Stimulated Brillouin Scattering in a Birefringent Optical Fibre Ring Resonator, Optics Commun. vol. 103, 1993, pp 161-168.

2. Omer S. Khan and Ralph P. Tatam, *Heterodyne Signal Processing using a Frequency Shifter based on Stimulated Brillouin Scattering in Ring Resonators*, SPIE Proc., vol. 2003, paper 06, SPIE's 38th International Symposium on Optical Applied Science & Engineering, 1993, San Diego.

3. Omer S. Khan and Ralph P. Tatam, *A Fibre optic frequency shifter based on stimulated Brillouin scattering in a birefringent fibre ring resonator.* IOP Proc. Applied Optics & Opto-Electronics, 92. pp.239-242.

4. Omer S. Khan, Sultan Mahmood, Keith Bowdler and Ralph P. Tatam, *An interferometric technique to characterise optical detectors,* Meas. Sci. Technol., 4, 1993, pp. 1232-1237.

5. Chris J. Duffy, Omer S. Khan and Ralph P. Tatam, *Optical signal processing and sensing techniques exploiting stimulated Brillouin scattering in high birefringence Optical Fibre*, Optical Fibre Sensors conference OFS'9, Firenze, Italy, 1993, pp.7-10.